

ISSN 2712-8970



СИБИРСКИЙ АЭРОКОСМИЧЕСКИЙ ЖУРНАЛ

SIBERIAN AEROSPACE JOURNAL

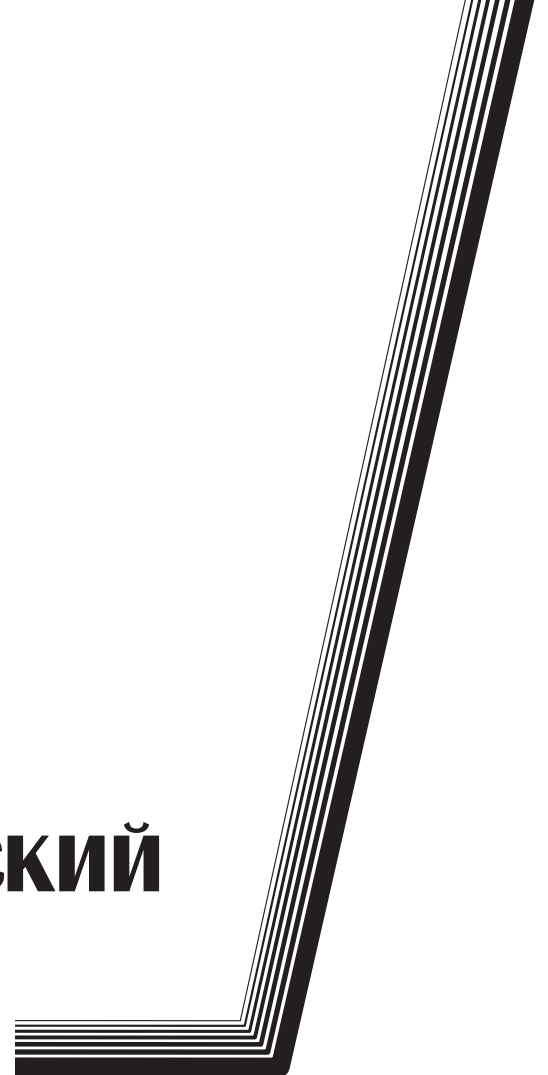
Том
Vol. 24, № 4

КРАСНОЯРСК 2023

СИБИРСКИЙ АЭРОКОСМИЧЕСКИЙ ЖУРНАЛ

Том 24, № 4

Красноярск 2023



СИБИРСКИЙ АЭРОКОСМИЧЕСКИЙ ЖУРНАЛ

Том 24, № 4

Главный редактор

Аплеснин Сергей Степанович, доктор физико-математических наук, профессор
(СибГУ им. М. Ф. Решетнева)

Заместители главного редактора

Логинов Юрий Юрьевич, доктор физико-математических наук, профессор (СибГУ им. М. Ф. Решетнева)

Мурыгин Александр Владимирович, доктор технических наук, профессор, ответственный
за подготовку выпусков журнала, содержащих секретные сведения (СибГУ им. М. Ф. Решетнева)

Сенашов Сергей Иванович, доктор физико-математических наук, профессор (СибГУ им. М. Ф. Решетнева)

РЕДАКЦИОННАЯ КОЛЛЕГИЯ

Галеев Р. Г., доктор технических наук
(АО «НПП «Радиосвязь»)

Головенкин Е. Н., доктор технических наук,
профессор (АО «ИСС»)

Казаковцев Л. А., доктор технических наук,
профессор (СибГУ им. М. Ф. Решетнева)

Левко В. А., доктор технических наук, доцент
(СибГУ им. М. Ф. Решетнева)

Лившиц А. В., доктор технических наук, доцент
(ИрГУПС)

Максимов И. А., доктор технических наук
(АО «ИСС»)

Михеев А. Е., доктор технических наук,
профессор (СибГУ им. М. Ф. Решетнева)

Москвичев В. В., доктор технических наук,
профессор (СКТБ «Наука» ИВТ СО РАН)

Садовский В. М., член-корреспондент РАН,
доктор физико-математических наук, профессор
(ИВМ СО РАН)

Сафонов К. В., доктор физико-математических
наук, доцент (СибГУ им. М. Ф. Решетнева)

Сильченко П. Н., доктор технических наук,
профессор (СФУ)

Смирнов Н. А., доктор технических наук,
профессор (СибГУ им. М. Ф. Решетнева)

Терсков В. А., доктор технических наук,
профессор (КриЖТ ИрГУПС)

Чеботарев В. Е., доктор технических наук,
доцент (АО «ИСС»)

Шайдуров В. В., член-корреспондент РАН,
доктор физико-математических наук, профессор
(ИВМ СО РАН)

РЕДАКЦИОННЫЙ СОВЕТ

Васильев С. Н., академик РАН, доктор физико-
математических наук, профессор (Москва)

Дегерменджи А. Г., академик РАН,
доктор физико-математических наук,
профессор (Красноярск)

Дегтерев А. С., доктор технических наук,
профессор (Красноярск)

Колмыков В. А., кандидат технических наук,
профессор (Химки)

Мионов В. Л., член-корреспондент РАН,
доктор физико-математических наук,
профессор (Красноярск)

Романски Р. П., доктор наук, профессор
(Технический университет Софии, Болгария)

Семенкин Е. С., доктор технических наук,
профессор (Красноярск)

Тестоедов Н. А., академик РАН,
доктор технических наук, профессор
(Железногорск)

Фошнер М., доктор, доцент (Марибор, Словения)

Шабанов В. Ф., академик РАН, доктор физико-
математических наук, профессор (Красноярск)

Швенкер Ф., доктор наук, профессор
(Институт нейроинформатики Университета Ульма,
Германия)

SIBERIAN AEROSPACE JOURNAL

Vol. 24, No 4

Chief Editor:

Aplesnin S. S., Dr.Sc., Professor (Reshetnev University)

Deputy Chief Editors

Loginov Y. Y., Dr.Sc., Professor (Reshetnev University)

Murygin A. V., Dr.Sc., Professor (Reshetnev University)

Senashov S. I., Dr.Sc., Professor (Reshetnev University)

EDITORIAL BOARD

Galeev R. G., Dr.Sc.

(JSC "NPP "Radiosvyaz")

Golovenkin E. N., Dr.Sc., Professor

(ISS-Reshetnev Company)

Kazakovtsev L. A., Dr.Sc., Professor

(Reshetnev University)

Levko V. A., Dr.Sc., Professor

(Reshetnev University)

Livshits A. V., Dr.Sc., Professor

(Irkutsk State Transport University)

Maksimov I. A., Dr.Sc.

(ISS-Reshetnev Company)

Mikheev A. E., Dr.Sc., Professor

(Reshetnev University)

Moskvichev V. V., Dr.Sc., Professor

(SDTB Nauka KSC SB RAS)

Sadovsky V. M., Corresponding Member

of the Russian Academy of Sciences,

Dr.Sc., Professor (ICM SB RAS)

Safonov K. V., Dr.Sc., Professor

(Reshetnev University)

Silchenko P. N., Doctor of Technical

Sciences, Professor (SibFU)

Smirnov N. A., Dr.Sc., Professor

(Reshetnev University)

Terskov V. A., Dr.Sc., Professor

(Irkutsk State Transport University)

Chebotarev V. Y., Dr.Sc., Professor

(ISS-Reshetnev Company)

Shaidurov V. V., Corresponding Member

of the Russian Academy of Sciences,

Dr.Sc., Professor (ICM SB RAS)

EDITORIAL COUNCIL

Vasiliev S. N., Academician of the Russian

Academy of Sciences, Dr.Sc., Professor (Moscow)

Degermendzhi A. G., Academician

of the Russian Academy of Sciences, Dr.Sc.,

Professor (Krasnoyarsk)

Degterev A. S., Dr.Sc., Professor (Krasnoyarsk)

Kolmykov V. A., Cand.Sc., Professor (Khimki)

Mironov V. L., Corresponding Member

of the Russian Academy of Sciences, Dr.Sc.,

Professor (Krasnoyarsk)

Romansky R. P., Dr.Sc., Professor

(Technical University of Sofia, Bulgaria)

Semenkin E. S., Dr.Sc., Professor (Krasnoyarsk)

Testoedov N. A., Academician of the Russian

Academy of Sciences, Dr.Sc., Professor

(Zheleznogorsk)

Fošner M., Ph.D. Associate Professor

(Maribor, Slovenia)

Shabanov V. F., Academician of the Russian

Academy of Sciences, Dr.Sc., Professor (Krasnoyarsk)

Schwenker F., Dr.Sc., Professor (Institute

for Neuroinformatics, University of Ulm, Germany)

«Сибирский аэрокосмический журнал» является научным, производственно-практическим рецензируемым изданием. Свидетельство о регистрации средства массовой информации ПИ № ФС 77-80539 от 01.03.2021 г. выдано Федеральной службой по надзору в сфере связи, информационных технологий и массовых коммуникаций (Роскомнадзор).
ISSN 2712-8970

Подписной индекс в каталоге «Пресса России» — 39263.
Зарегистрирован в Российском индексе научного цитирования (РИНЦ).

Включен в базу данных Ulrich's Periodicals Directory американского издательства Bowker.

Входит в перечень журналов ВАК по следующим научным специальностям:

1.2.2 Математическое моделирование, численные методы и комплексы программ (технические науки);

1.2.2 Математическое моделирование, численные методы и комплексы программ (физико-математические науки);

2.3.1 Системный анализ, управление и обработка информации (технические науки);

2.3.5 Математическое и программное обеспечение вычислительных систем, комплексов и компьютерных сетей (физико-математические науки);

2.3.7 Компьютерное моделирование и автоматизация проектирования (физико-математические науки);

2.3.7 Компьютерное моделирование и автоматизация проектирования (технические науки);

2.5.13 Проектирование, конструкция и производство летательных аппаратов (технические науки);

2.5.15 Тепловые, электроракетные двигатели и энергоустановки летательных аппаратов (технические науки).

Издается с 2000 года. 2000 — «Вестник Сибирской аэрокосмической академии имени академика М. Ф. Решетнева» (Вестник САА); 2002 — «Вестник Сибирского государственного аэрокосмического университета имени академика М. Ф. Решетнева» (Вестник СибГАУ); 2017 — «Сибирский журнал науки и технологий» (СибЖНТ); с 01.03.2021 — «Сибирский аэрокосмический журнал» (САЖ).

Каждый выпуск журнала включает три раздела:

1 раздел. Информатика, вычислительная техника и управление.

2 раздел. Авиационная и ракетно-космическая техника.

3 раздел. Технологические процессы и материалы.

Статьи публикуются бесплатно после обязательного рецензирования и при оформлении их в соответствии с требованиями редакции (www.vestnik.sibsau.ru). Журнал выходит 4 раза в год. Электронная версия журнала представлена на сайте Научной электронной библиотеки (<http://www.elibrary.ru>) и сайте журнала (www.vestnik.sibsau.ru)

При перепечатке или цитировании материалов из журнала «Сибирский аэрокосмический журнал» ссылка обязательна.

Учредитель и издатель

ФГБОУ ВО «Сибирский государственный университет науки и технологий имени академика М. Ф. Решетнева» (СибГУ им. М. Ф. Решетнева)

АДРЕС РЕДАКЦИИ, УЧРЕДИТЕЛЯ И ИЗДАТЕЛЯ:

Сибирский государственный университет науки и технологий имени академика М. Ф. Решетнева, Российская Федерация, 660037, г. Красноярск, проспект имени газеты «Красноярский Рабочий», 31.

Тел. (391) 290-42-31. E-mail: vestnik@sibsau.ru

Редактор Н. Н. ГОЛОСКОКОВА
Ответственный редактор английского текста
Н. А. ШУМАКОВА

Оригинал-макет и верстка Л. В. ЗВОНАРЕВОЙ
Подписано в печать 12.12.2023. Формат 70×108/16.
Бумага офсетная. Печать плоская. Усл. печ. л. 17,2.
Уч.-изд. л. 20,0. Тираж 100 экз. Заказ 3395. С 873/23.

Редакционно-издательский отдел СибГУ им. М.Ф. Решетнева.

Отпечатано в редакционно-издательском центре
СибГУ им. М.Ф. Решетнева.

Российская Федерация, 660037, г. Красноярск,
просп. им. газ. «Красноярский Рабочий», 31.

Дата выхода в свет: 20.12.2023. Свободная цена

Siberian Aerospace Journal is a research, production and practical peer-reviewed journal. Included by the Higher Attestation Commission of the Russian Federation in the Index of Leading Russian Peer-Reviewed Journals and Periodicals, in which significant scientific dissertation results should be published when applying for a Dr.Sc. degree.

The journal is the official periodical of Reshetnev Siberian State University of Science and Technology.

Certificate of Registration as a Mass Media Resource. Certificate: PI No. FC 77-80539, dated 01 March 2021, given by Federal Supervision Agency for Information Technology, Communications and Mass Media. ISSN 2712-8970.

The Journal is included in the following subscription catalogue 39263 — Pressa Rossii.

The journal is registered in the Russian Science Citation Index (RSCI).

The journal is indexed in the database of Ulrich's Periodicals Directory.

The journal was first published in 2000. 2000 — Vestnik Sibirskoy aerokosmicheskoy akademii imeni akademika M. F. Reshetneva (Vestnik SAA); 2002 — Vestnik Sibirskogo gosudarstvennogo aerokosmicheskogo universiteta imeni akademika M. F. Reshetneva (Vestnik SibGAU); 2017 — Siberian Journal of Science and Technology (SZHT); from 01.03.2021 — Siberian Aerospace Journal (SAJ). The Journal is recommended for publishing the main results of research when applying for Cand. Sc. degree and Dr. Sc. degree upon the following specialties:

1.2.2 Mathematical modeling, numerical methods and software packages (technical sciences);

1.2.2 Mathematical modeling, numerical methods and software packages (physical and mathematical sciences);

2.3.1 System analysis, management and information processing (technical sciences);

2.3.5 Mathematical and software support of computer systems, complexes and computer networks (physical and mathematical sciences);

2.3.7 Computer modeling and design automation (physical and mathematical sciences);

2.3.7 Computer modeling and design automation (technical sciences);

2.5.13 Design, construction and production of aircraft (technical sciences);

2.5.15 Thermal, electric rocket engines and power installations of aircraft (technical sciences).

Each issue consists of three parts:

Part 1. Informatics, computer technology and management.

Part 2. Aviation and Spacecraft Engineering.

Part 3. Technological Processes and Material Science.

Papers prepared in accordance with the editorial guidelines (www.vestnik.sibsau.ru) are published free of charge after being peer reviewed.

The journal is published four times a year.

An online version can be viewed at <http://www.elibrary.ru>

Siberian Aerospace Journal should be cited when reprinting or citing materials from the journal.

CONTACTS. Website: www.vestnik.sibsau.ru

Address: Reshetnev Siberian State University of Science and Technology.

31, Krasnoyarskii Rabochii prospekt, Krasnoyarsk, 660037, Russian Federation.

Tel. (391) 290-42-31; e-mail: vestnik@sibsau.ru

Editor N. N. GOLOSOKOVA
Executive editor (English Language) N. A. SHUMAKOVA
Layout original L. V. ZVONAREVA

Signed (for printing): 12.12.2023. Format 70×108/16.
Offset Paper. Print flat. 17,2. Published sheets 20,0.
100 copies. Order 3395. С 873/23.

Printing and Publication Department
Reshetnev University.

Printed in the Department of copying and duplicating
equipment Reshetnev University.

31, Krasnoyarskii Rabochii prospekt, Krasnoyarsk,
660037, Russian Federation.

Date of publication: 20.12.2023. Free price

СОДЕРЖАНИЕ

Раздел 1. ИНФОРМАТИКА, ВЫЧИСЛИТЕЛЬНАЯ ТЕХНИКА И УПРАВЛЕНИЕ

Вайнштейн В. И., Вайнштейн И. И., Сафонов К. В. Решение интегрального уравнения для средней стоимости восстановлений в теории надежности технических систем	628
Гончаров А. Е., Гончарова Е. А. Интерпретация и обработка данных гидролокатора бокового обзора с целью автоматизации данного процесса	639
Каткова В. П., Вяхирев В. А., Кринталь А. Н. Математическое моделирование автокомпенсационных устройств	652
Кононов Д. Д., Исаев С. В. Анализ киберугроз корпоративной сети на основе параллельной обработки данных NETFLOW	663
Кузнецов А. А., Кузнецова А. С., Кишкан В. В. Алгоритм быстрого умножения элементов в 2-группах на основе полиномов Жегалкина	673

Раздел 2. АВИАЦИОННАЯ И РАКЕТНО-КОСМИЧЕСКАЯ ТЕХНИКА

Акбулатов Э. Ш., Назаров В. П., Герасимов Е. В. Исследование характеристик ракетного двигателя малой тяги, изготовленного методом аддитивной SLM-технологии	682
Бакланов А. В. Влияние особенностей конструкции камер сгорания двигателей НК-16СТ, НК-16-18СТ на содержание углекислого газа в продуктах сгорания	697
Гусев Е. В., Заговорчев В. А., Родченко В. В., Садретдинова Э. Р., Шипневская Е. А. Расчёт параметров и характеристик вращающегося лунного реактивного пенетратора	706
Подкопаев И. А., Подкопаев А. В., Должиков В. И. Математическая модель теплофизического нагружения малокалиберного артиллерийского ствола с вариантной дискретизацией полупелых слоев расчетной области	717

Раздел 3. ТЕХНОЛОГИЧЕСКИЕ ПРОЦЕССЫ И МАТЕРИАЛЫ

Серегин Ю. Н., Мурыгин А. В., Курашкин С. О. Моделирование технологических параметров электронно-лучевой сварки для изделий ракетно-космической техники	738
Трифонов С. В., Тихомиров А. А., Мурыгин А. В. Автоматизированная система очистки жидких продуктов переработки отходов для замкнутых экосистем космического назначения	751
Шестаков И. Я., Шестаков В. И., Трифанов И. В., Ремизов И. А. Удельные энергозатраты электро-контактно-химической обработки металлов вибрирующим инструментом в электролите	760

CONTENTS

Part 1. INFORMATICS, COMPUTER TECHNOLOGY AND MANAGEMENT

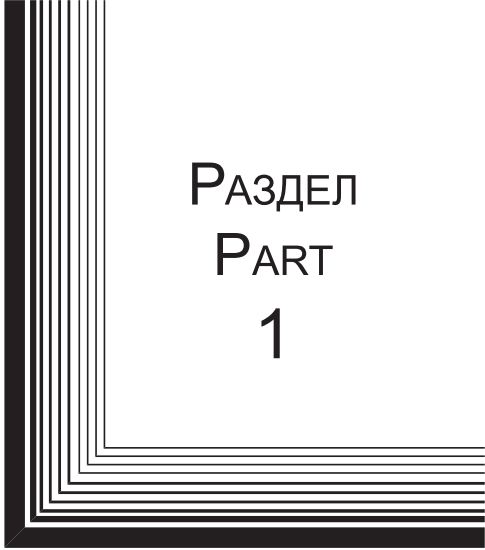
Vainshtein V. I., Vainshtein I. I., Safonov K. V. Solution of the integral equation for the average cost of restoration in the theory of reliability of technical systems	628
Goncharov A. E., Goncharova E. A. Interpreting and processing side-scan sonar data with the objective of further automation	639
Katkova V. P., Vyakhirev V. A., Krintal A. N. Mathematical modeling of autocompensation devices	652
Kononov D. D., Isaev S. V. Analysis of corporate network cyber threats based on parallel processing of Netflow data	663
Kuznetsov A. A., Kuznetsova A. S., Kishkan V. V. An algorithm for fast multiplication of elements in 2-groups based on the Zhegalkin polynomials	673

Part 2. AVIATION AND SPACECRAFT ENGINEERING


Akbulatov E. Sh., Nazarov V. P., Gerasimov E. V. Characteristics research of a low thrust rocket engine manufactured using additive SLM technology	682
Baklanov A. V. Concentration of carbon dioxide in products of combustion of GTE NK-16ST and NK-16-18ST	697
Gusev E. V., Zagovorchev V. A., Rodchenko V. V., Sadretdinova E. R., Shipnevskaya E. A. Calculation of the parameters and characteristics of a rotating lunar jet penetrator	706
Podkopaev I. A., Podkopaev A. V., Dolzhikov V. I. Mathematical model of thermophysical loading of a small-caliber artillery barrel with variant discretization of half-integer layers of the computational domain	717

Part 3. TECHNOLOGICAL PROCESSES AND MATERIAL SCIENCE

Seregin Yu. N., Murygin A. V., Kurashkin S. O. Modeling of technological parameters of electron beam welding for rocket and space technology products	738
Trifonov S. V., Tikhomirov A. A., Murygin A. V. Automated system for cleaning liquid waste products for closed ecosystems for space purposes	751
Shestakov I. Ya., Shestakov V. I., Trifanov I. V., Remizov I. A. Specific energy consumption of electro-contact-chemical treatment of metals with a vibrating tool in the electrolyte	760



РАЗДЕЛ
PART
1



ИНФОРМАТИКА,
ВЫЧИСЛИТЕЛЬНАЯ
ТЕХНИКА И УПРАВЛЕНИЕ

INFORMATICS,
COMPUTER TECHNOLOGY
AND MANAGEMENT



УДК 519.248

Doi: 10.31772/2712-8970-2023-24-4-628-638

Для цитирования: Вайнштейн В. И., Вайнштейн И. И., Сафонов К. В. Решение интегрального уравнения для средней стоимости восстановлений в теории надежности технических систем // Сибирский аэрокосмический журнал. 2023. Т. 24, № 4. С. 628–638. Doi: 10.31772/2712-8970-2023-24-4-628-638.

For citation: Vainshtein V. I., Vainshtein I. I., Safonov K. V. [Solution of the integral equation for the average cost of restoration in the theory of reliability of technical systems]. *Siberian Aerospace Journal*. 2023, Vol. 24, No. 4, P. 628–638. Doi: 10.31772/2712-8970-2023-24-4-628-638.

Решение интегрального уравнения для средней стоимости восстановлений в теории надежности технических систем

В. И. Вайнштейн^{1*}, И. И. Вайнштейн¹, К. В. Сафонов²

¹Сибирский федеральный университет

660041, Российская Федерация, г. Красноярск, просп. Свободный, 79

²Сибирский государственный университет науки и технологий имени академика М. Ф. Решетнева

Российская Федерация, 660037, г. Красноярск, просп. им. газ. «Красноярский Рабочий», 31

*E-mail: vvaynshtyayn@sfu-kras.ru

Отказы элементов при работе технических и многих других систем имеют, как правило, случайный характер. Это приводит к различным моделям процесса восстановления, изучаемым в теории вероятностей и математической теории надежности. В процессе восстановления отказавшие элементы восстанавливаются или заменяются на новые, при этом часто происходит изменение стоимостей и качества восстанавливаемых элементов (функций распределения наработок до отказа).

В работе рассматривается функция затрат (средняя стоимость восстановления) в процессе восстановления порядка (k_1, k_2) , в котором по определенному правилу изменяются стоимости каждого восстановления и функции распределения наработок.

Учитывая, что функция восстановления (среднее число отказов) хорошо изучена в теории надежности, получено решение интегрального уравнения для функции затрат через функцию восстановления рассматриваемой модели.

Для процесса восстановления порядка (k_1, k_2) получена формула вычисления функции затрат через функцию восстановления простого процесса, образованного сверткой всех функций распределения периодической части. Для практического применения получены явные формулы функции затрат при процессе восстановления, у которого периодическая часть распределена по экспоненциальному закону или закону Эрланга порядка t с одним и тем же показателем α .

Полученные формулы могут быть использованы для изучения свойств функции затрат и решения оптимизационных задач в стратегиях проведения процесса восстановления в терминах «цена», «качество», «риск», если, например, за качество принимать среднее число отказов, за цену – среднюю стоимость восстановлений, за риск – дисперсии числа отказов или стоимости восстановлений.

Ключевые слова: модели процесса восстановления, функция восстановления, функция затрат, распределение Эрланга.

Solution of the integral equation for the average cost of restoration in the theory of reliability of technical systems

V. I. Vainshtein^{1*}, I. I. Vainshtein¹, K. V. Safonov²

¹Siberian Federal University

79, Svobodny Av., Krasnoyarsk, 660041, Russian Federation

²Reshetnev Siberian State University of Science and Technology

31, Krasnoyarskii Rabochii prospekt, Krasnoyarsk, 660037, Russian Federation

*E-mail: vvaynshtyayn@sfu-kras.ru

Failures of elements during the operation of technical and many other systems are, as a rule, random in nature. This leads to various models of the recovery process, studied in probability theory and mathematical reliability theory. During the restoration process, failed elements are restored or replaced with new ones, and there is often a change in the costs and quality of the restored elements (time-to-failure distribution functions).

The work examines the cost function (average cost of restoration) in the process of restoration of order (k_1, k_2) , in which, according to a certain rule, the costs of each restoration and the distribution functions of operating time change.

Considering, that the recovery function (average number of failures) is well studied in reliability theory, a solution to the integral equation for the cost function is obtained through the recovery function of the model under consideration.

For the order restoration process (k_1, k_2) , a formula is obtained for calculating the cost function through the restoration function of a simple process formed by the convolution of all distribution functions of the periodic part. For practical application, explicit formulas are obtained for the cost function during the restoration process, in which the periodic part is distributed according to an exponential law or an Erlang law of order m with the same exponent α .

The resulting formulas can be used to study the properties of the cost function and solve optimization problems in strategies for carrying out the restoration process in terms of price, quality, risk, if, for example, the average number of failures is taken as quality, the average cost of restorations as price, the dispersion of the number of failures as the risk, or cost of restoration.

Keywords: recovery process models, recovery function, cost function, Erlang distribution.

Introduction

In the mathematical theory of reliability, when studying recovery processes, the numerical characteristics associated with the random number of failures and the random cost of recovery are first considered, for example, the average and dispersion of the number of failures and the cost of recovery, through which various criteria for the optimality of recovery strategies are determined.

The paper discusses models of the recovery process (X_i, c_i) , $i = 0, 1, \dots$, taking into account the cost of restoration. Where X_i , random operation time with distribution functions $F_i(t)$ elements from $I - 1^{\text{st}}$ to i -th failure, c_i cost of $i - x$ recovery, c_0 - element cost, set at the initial time $t = 0$, $F_0(t) = 0$ for a case $t < 0$, $F_0(t) = 1$ for a case $t \geq 0$ [1-4].

Let $N(t)$ - be the number of failures (recoveries), $C(t)$ be the cost of recovery for the time from 0 to t

$$C(t) = \sum_{i=0}^{N(t)} c_i$$

$$P(N(t) = n) = F^{(n)}(t) - F^{(n+1)}(t),$$

$F^{(n)}(t)$ - n - multiple convolution of distribution functions $F_i(t)$, $i = 1, 2, \dots, n$,

$$F^{(n)}(t) = (F^{(n-1)} * F_n)(t) = \int_0^t F^{(n-1)}(t-x) dF_n(x) \quad F^{(1)}(t) = F_1(t).$$

For [1,2]: $H(t)$ – recovery function (average number of failures)

$$H(t) = E(N(t)) = \sum_{n=1}^{\infty} F^{(n)}(t)$$

$S(t) = E(C(t))$ – cost function (average cost of restorations)

$$S(t) = E(C(t)) = c_0 + \sum_{n=1}^{\infty} c_n F^{(n)}(t).$$

During operation, the quality ($F_i(t)$) of the restored elements and the cost (c_i) of restoration may differ. This leads to different models of the recovery process [1, 3, 5–9].

The work considers the restoration process taking into account the cost of restoration of the order (k_1, k_2) , in which the distribution functions and cost of restoration satisfy the condition: $F_i(t) = F_j(t) \text{ и } c_i = c_j$, if the indices $i, j \geq k_1$ when divided by k_2 give the same excess [1, 3, 8, 9].

In the process under consideration, after the first restorations $k_1 - 1$, a periodic process of the order k_2 begins.

Note, that in the case $k_1 = 1$ we have a periodic process of order restoration k_2 , and if $k_2 = 1$ process of restoring order k_1 .

If $F_i(t)$ coincide ($F_i(t) = F_i(t), i \geq 1$), or coincide starting from number $i = 2$ ($F_i(t) = F_2(t), i \geq 2$), we have simple (ordinary) and general (delayed) recovery processes, well studied in reliability theory.

Note that for the model under consideration, the recovery function $H(t)$ has been well studied. Numerical methods for finding it have been developed, and for many distribution laws characteristic of reliability theory, there are its explicit representations [1, 6].

To find the cost function $S(t)$ there are integral equations [1, 2, 10].

The purpose of the work is to obtain a solution to the integral equation for the cost function $S(t)$ in the form of an integral representation through the restoration function $H(t)$. Such a representation will be convenient for its study and calculation in various theoretical and applied problems of reliability theory.

Representation of the cost function through the recovery function

Let us write the integral equation for the cost function $S(t)$ [1, 2]

$$S(t) = G(t) + \int_0^t S(t-x) d\Phi^{(k_2)}(x) \tag{1}$$

for a case $k_1 > 1$,

$$G(t) = c_0 \left(1 - \Phi^{(k_2)}(t)\right) + \sum_{n=1}^{k_1+k_2-1} c_n F^{(n)}(t) - \sum_{n=1}^{k_1-1} c_n \int_0^t F^{(n)}(t-x) d\Phi^{(k_2)}(x),$$

for a case $k_1 = 1$

$$G(t) = c_0 \left(1 - \Phi^{(k_2)}(t)\right) + \sum_{n=1}^{k_2} c_n F^{(n)}(t)$$

$\Phi^{(k_2)}(t) = (\Phi_1 * \Phi_2 * \dots * \Phi_{k_2})(t)$ –convolution of all distribution functions

$\Phi_i(t) = F_{k_{i-1}+i}(t), i = 1, 2, \dots, k_2$. The functions $\Phi_i(t)$ define the periodic part of the recovery process.

Let $HF(t)$ be the restoration function of a simple process, let $HFG(t)$ be the restoration function of the general process formed by the first distribution function $F(t)$ and the following $G(t)$.

Further [1, 6]

$$HFG(t) = F(t) + \int_0^t HFG(t-x) dG(x) \quad (2)$$

In equation (1) we make the replacement

$$S(t) = V(t) + c_0 + \sum_{n=1}^{k_1-1} c_n F^{(n)}(t) \quad (3)$$

We obtain

$$V(t) + c_0 + \sum_{n=1}^{k_1-1} c_n F^{(n)}(t) = c_0 \left(-\Phi^{(k_2)}(t) \right) + \sum_{n=1}^{k_1-1} c_n F^{(n)}(t) + \sum_{n=k_1}^{k_1+k_2-1} c_n F^{(n)}(t) - \sum_{n=1}^{k_1-1} c_n \int_0^t F^{(n)}(t-x) d\Phi^{(k_2)}(x) + \int_0^t \left(V(t-x) + c_0 + \sum_{n=1}^{k_1-1} c_n F^{(n)}(t-x) \right) d\Phi^{(k_2)}(x).$$

Hence, to find the function $V(t)$, we obtain the integral equation

$$V(t) = \sum_{n=k_1}^{k_1+k_2-1} c_n F^{(n)}(t) + \int_0^t V(t-x) d\Phi^{(k_2)}(x). \quad (4)$$

Let us make a replacement

$$V(t) = \left(\sum_{n=k_1}^{k_1+k_2-1} c_n \right) V_1(t) \quad (5)$$

Equation (4) will be rewritten as

$$V_1(t) = Q(t) + \int_0^t V_1(t-x) d\Phi^{(k_2)}(x), \quad (6)$$

$$Q(t) = \frac{\sum_{n=k_1}^{k_1+k_2-1} c_n F^{(n)}(t)}{\sum_{n=k_1}^{k_1+k_2-1} c_n}. \quad (7)$$

Note, that $\Phi^{(k_2)}(t)$ and $Q(t)$ are distribution functions, $\Phi^{(k_2)}(t)$ – as a convolution of work distribution functions, and $Q(t)$ – mixture of distribution functions.

Comparing equations (6) and (2), we find that equation (6) defines the restoration function $HQ\Phi^{(k_2)}(t)$ of the general process specified by the first distribution function $Q(t)$, of the second and subsequent ones $\Phi^{(k_2)}(t)$.

Thus,

$$V_1(t) = HQ\Phi^{(k_2)}(t), \quad (8)$$

and taking into account (3), (5), (7), (8)

$$S(t) = c_0 + \sum_{n=1}^{k_1-1} c_n F^{(n)}(t) + \left(\sum_{n=k_1}^{k_1+k_2-1} c_n \right) HQ\Phi^{(k_2)}(t). \quad (9)$$

Taking into account (2)

$$HQ\Phi^{(k_2)}(t) = Q(t) + \int_0^t H\Phi^{(k_2)}(t-x)dQ(x), \tag{10}$$

formula (9) will be written in the form

$$S(t) = c_0 + \sum_{n=1}^{k_1-1} c_n F^{(n)}(t) + \sum_{n=k_1}^{k_1+k_2-1} c_n \left(Q(t) + \int_0^t H\Phi^{(k_2)}(t-x)dQ(x) \right),$$

or taking account of (10)

$$S(t) = c_0 + \sum_{n=1}^{k_1+k_2-1} c_n F^{(n)}(t) + \sum_{n=k_1}^{k_1+k_2-1} c_n \int_0^t H\Phi^{(k_2)}(t-x)dF^{(n)}(x). \tag{11}$$

We found that calculating the cost function comes down to calculating the finite number of convolutions of distribution functions and finding the restoration function $H\Phi^{(k_2)}(t)$ of a simple restoration process formed by the distribution function $\Phi^{(k_2)}(t)$, or restoration function $HQ\Phi^{(k_2)}(t)$.

In the practical implementation of the obtained formulas (9), (10), (11), one can use numerical and analytical methods for calculating convolutions and restoration functions, discussed in [1, 11]. We also note that the resulting formulas make it possible to study the properties of the cost function and consider various optimization problems based on strategies for carrying out the restoration process in terms of price, quality, and risk. If, for example, we take the average number of failures as quality, the average cost of restorations as price, and the dispersion of the number of failures or the cost of restorations as the risk [1, 12–15].

This work is a continuation of work [11] and it can be noted that the theorems on the asymptotic behavior of the cost function obtained in [11] are much easier to obtain using the resulting formula for representing the cost function (9).

The cost function for a simple restoration process with exponential distribution. We consider a restoration process in which only the restoration costs c_i change according to the law $c_i = c_j$, if the indices $i, j \geq k_1$ when divided by k_2 , give the same excess. This corresponds to the common case where failures result in full restorations, but the costs of restorations change, for example, only the price of the element changes.

Let the operating time of the elements be distributed according to the exponential law $F(t) = 1 - e^{-\alpha t}$, $t \geq 0$. For this case, we obtain calculation formulas for calculating the cost function.

Taking into account, that n – multiple convolution of the distribution functions of independent random variables is a function of the distribution of their sum, and that the Erlang order distribution n is the distribution of the sum of random variables n distributed according to the exponential law, we conclude that for the case under consideration

$$F^{(n)}(t) = F_{e,n}(t) = 1 - e^{-\alpha t} \sum_{i=0}^{n-1} \frac{(\alpha t)^i}{i!} \quad dF^{(n)}(x) = dF_{e,n}(x) = e^{-\alpha x} \alpha \frac{(\alpha x)^{n-1}}{(n-1)!} dx,$$

$$\Phi^{(k_2)}(t) = F_{e,k_2}(t), \quad H\Phi^{(k_2)}(t) = HF_{e,k_2}(t),$$

$F_{e,n}(t)$ – Erlang order distribution n , and [1,6]

$$HF_{e,k_2}(t) = \frac{1}{k_2} \left(\alpha t + \sum_{k=1}^{k_2-1} \frac{c^k}{1-c^k} \left(-e^{-\alpha t(1-c^k)} \right) \right), \quad c = e^{\frac{2\pi}{k_2}} = \cos\left(\frac{2\pi}{k_2}\right) + i \sin\left(\frac{2\pi}{k_2}\right), \tag{12}$$

$$HF_{e,k_2}(t) = \frac{1}{k_2} \left(\alpha t - \frac{k_2-1}{2} + \frac{1}{2} \sum_{k=1}^{k_2-1} \frac{e^{-\alpha t \left(1 - \cos\left(\frac{2\pi}{k_2} k\right)\right)} \sin\left(\alpha t \sin\left(\frac{2\pi}{k_2} k\right) + \frac{\pi}{k_2} k\right)}{\sin\left(\frac{\pi}{k_2} k\right)} \right)$$

Now, according to (11)

$$S(t) = c_0 + \sum_{n=1}^{k_1+k_2-1} c_n F_{e,n}(t) + \sum_{n=k_1}^{k_1+k_2-1} c_n \frac{\alpha^n}{(n-1)!} \int_0^t HF_{e,k_2}(t-x) e^{-\alpha x} x^{n-1} dx \quad (13)$$

Taking into account (12), when calculating $S(t)$, the integrals included in formula (13) are calculated explicitly. For example [16]

$$\int e^{\beta x} x^n dx = \frac{e^{\beta t}}{\beta} t^n + \sum_{j=1}^n \left((-1)^j \frac{n(n-1)\dots(n-j+1)}{\beta^j} t^{n-j} \right) + C.$$

When substituting

$$I(\beta, n)(t) = \int_0^t e^{\beta x} x^n dx = \frac{e^{\beta t}}{\beta} t^n + \sum_{j=1}^n \left((-1)^j \frac{n(n-1)\dots(n-j+1)}{\beta^j} t^{n-j} \right) + (-1)^{n+1} \frac{n!}{\beta^{n+1}}$$

in (13), we obtain

$$\begin{aligned} S(t) &= c_0 + \sum_{n=1}^{k_1+k_2-1} c_n F_{e,n}(t) + \\ &+ \frac{1}{k_2} \sum_{n=k_1}^{k_1+k_2-1} c_n \frac{\alpha^n}{(n-1)!} \alpha t I(-\alpha, n-1)(t) - \alpha I(-\alpha, n)(t) + \\ &+ \sum_{k=1}^{k_2-1} \frac{c^k}{1-c^k} \left(I(-\alpha, n-1)(t) - e^{-\alpha(1-c^k)t} I(-\alpha c^k, n-1)(t) \right). \end{aligned} \quad (14)$$

We select the real part in (14):

$$\begin{aligned} 1-c^k &= -2ie^{\frac{\pi k}{k_2}i} \sin\left(\frac{\pi k}{k_2}\right), \sum_{k=1}^{k_2-1} \frac{c^k}{1-c^k} = \frac{i}{2} \sum_{k=1}^{k_2-1} \operatorname{ctg}\left(\frac{\pi}{k_2}k\right) - \frac{k_2-1}{2} \\ \operatorname{Re} \sum_{k=1}^{k_2-1} \frac{c^k}{1-c^k} &= \operatorname{Re} \sum_{k=1}^{k_2-1} \frac{e^{\frac{2\pi ki}{k_2}} e^{-\frac{\pi ki}{k_2}}}{-2i \sin \frac{\pi k}{k_2}} = \frac{1-k_2}{2} \\ \sum_{k=1}^{k_2-1} \frac{c^k}{1-c^k} e^{-\alpha(1-c^k)t} I(-\alpha c^k, n-1)(t) &= \\ &= \sum_{k=1}^{k_2-1} \left(\frac{c^k}{1-c^k} e^{-\alpha(1-c^k)t} \frac{e^{-\alpha c^k t}}{-\alpha c^k} (t^{n-1} + \right. \\ &+ \left. \sum_{j=1}^{n-1} (-1)^j \frac{(n-1)\dots(n-j)}{(-\alpha)^j c^{kj}} t^{n-1-j} \right) + \left((-1)^n \frac{(n-1)!}{(-\alpha)^n c^{kn}} \right) = \\ &= -\frac{1}{\alpha} \sum_{k=1}^{k_2-1} \frac{e^{-\alpha t}}{1-c^k} \left(t^{n-1} + \sum_{j=1}^{n-1} \frac{(n-1)\dots(n-j)}{\alpha^j} e^{-\frac{2\pi i}{k_2}kj} t^{n-1-j} \right) + \\ &+ \frac{(n-1)!}{\alpha^n} \sum_{k=1}^{k_2-1} \frac{c^{-k(n-1)} e^{-\alpha(1-c^k)t}}{1-c^k} = \\ &= -\frac{i}{2\alpha} \sum_{k=1}^{k_2-1} \frac{e^{-\alpha t} e^{-\frac{\pi ki}{k_2}}}{\sin \frac{\pi k}{k_2}} \left(t^{n-1} + \sum_{j=1}^{n-1} \frac{(n-1)\dots(n-j)}{\alpha^j} e^{-\frac{2\pi i}{k_2}kj} t^{n-1-j} \right) + \end{aligned}$$

$$\begin{aligned}
 & + \frac{(n-1)!i}{2\alpha^n} \sum_{k=1}^{k_2-1} \frac{e^{-\frac{\pi k}{k_2}i}}{\sin \frac{\pi k}{k_2}} e^{-\frac{2\pi k(n-1)}{k_2}i} e^{-\alpha t} e^{\alpha t \cos \frac{2\pi k}{k_2}} e^{\alpha t \sin \frac{2\pi k}{k_2}i} = \\
 & = -\frac{i}{2\alpha} \sum_{k=1}^{k_2-1} \frac{e^{-\alpha t} e^{\frac{\pi k}{k_2}i}}{\sin \frac{\pi k}{k_2}} \left(t^{n-1} + \sum_{j=1}^{n-1} \frac{(n-1)\dots(n-j)}{\alpha^j} e^{-\frac{2\pi i}{k_2}kj} t^{n-1-j} \right) + \\
 & + \frac{(n-1)!i}{2\alpha^n} \sum_{k=1}^{k_2-1} \frac{e^{-\alpha t \left(1 - \cos \frac{2\pi k}{k_2}\right)} e^{\left(\alpha t \sin \frac{2\pi k}{k_2} - \frac{\pi k(2n-1)}{k_2}\right)i}}{\sin \frac{\pi k}{k_2}}
 \end{aligned}$$

Therefore

$$\begin{aligned}
 & \operatorname{Re} \left(\sum_{k=1}^{k_2-1} \frac{c^k}{1-c^k} e^{-\alpha(1-c^k)t} I(-\alpha c^k, n-1)(t) \right) = \\
 & = -\frac{1}{2\alpha} \sum_{k=1}^{k_2-1} e^{-\alpha t} t^{n-1} - \frac{e^{-\alpha t}}{2\alpha} \sum_{k=1}^{k_2-1} \frac{1}{\sin \left(\frac{\pi k}{k_2} \right)} \sum_{j=1}^{n-1} \frac{(n-1)\dots(n-j)}{\alpha^j} \sin \left(\frac{\pi k(2j+1)}{k_2} \right) t^{n-1-j} - \\
 & - \frac{(n-1)!}{2\alpha^n} \sum_{k=1}^{k_2-1} \frac{e^{-\alpha t \left(1 - \cos \left(\frac{2\pi k}{k_2} \right) \right)} \sin \left(\alpha t \sin \left(\frac{2\pi k}{k_2} \right) - \frac{\pi k(2n-1)}{k_2} \right)}{\sin \left(\frac{\pi k}{k_2} \right)}
 \end{aligned}$$

Let us write down the formula for the cost function

$$\begin{aligned}
 S(t) & = c_0 + \sum_{n=1}^{k_1+k_2-1} c_n F_{e,n}(t) + \\
 & + \frac{1}{k_2} \sum_{n=k_1}^{k_1+k_2-1} \epsilon_n \frac{\alpha^n}{(n-1)!} \left(\alpha t + \frac{1-k_2}{2} \right) I(-\alpha, n-1)(t) - \alpha I(-\alpha, n)(t) + \\
 & + \frac{1}{2\alpha} \sum_{k=1}^{k_2-1} e^{-\alpha t} t^{n-1} + \frac{e^{-\alpha t}}{2\alpha} \sum_{k=1}^{k_2-1} \frac{1}{\sin \left(\frac{\pi k}{k_2} \right)} \sum_{j=1}^{n-1} \frac{(n-1)\dots(n-j)}{\alpha^j} \sin \left(\frac{\pi k(2j+1)}{k_2} \right) t^{n-1-j} + \\
 & + \frac{(n-1)!}{2\alpha^n} \sum_{k=1}^{k_2-1} \frac{e^{-\alpha t \left(1 - \cos \left(\frac{2\pi k}{k_2} \right) \right)} \sin \left(\alpha t \sin \left(\frac{2\pi k}{k_2} \right) + \frac{\pi k(2n-1)}{k_2} \right)}{\sin \left(\frac{\pi k}{k_2} \right)}.
 \end{aligned}$$

We also consider the cost function during the process of restoring order (k_1, k_2) , when the operating time of the periodic part of the process is distributed according to the Erlang law of order m with a parameter α .

Let $\Phi_j(t) = F_{e,m,\alpha}(t)$. We find $H\Phi^{(k_2)}(t)$. Let us write down the integral equations for $HF_{e,m,\alpha}(t)$, $H\Phi^{(k_2)}(t)$

$$HF_{e,m,\alpha}(t) = F_{e,m,\alpha}(t) + \int_0^t HF_{e,m,\alpha}(t-x) dF_{e,m,\alpha}(x) \tag{15}$$

$$H\Phi^{(k_2)}(t) = \Phi^{(k_2)}(t) + \int_0^t H\Phi^{(k_2)}(t-x) d\Phi^{(k_2)}(x). \tag{16}$$

Let there be given

$$F^*(s) = \int_0^\infty e^{-st} dF(x)$$

Laplace-Stieltjes transform function $F(x)$ [1,6]. Considering $F_{e,m,\alpha}^*(s) = (\frac{\alpha}{s+\alpha})^m$, $(F_i^*F_j^*)^*(s) = F_i^*(s)F_j^*(s)$, from (15),(16) we obtain

$$H^*F_{e,m,\alpha}(s) = (\frac{\alpha}{s+\alpha})^m + H^*F_{e,m,\alpha}(s)(\frac{\alpha}{s+\alpha})^m, \tag{17}$$

$$H^*\Phi^{(k_2)}(s) = (\frac{\alpha}{s+\alpha})^{mk_2} + H^*\Phi^{(k_2)}(s)(\frac{\alpha}{s+\alpha})^{mk_2}. \tag{18}$$

Comparing (17), (18), we conclude that

$$H\Phi^{(k_2)}(t) = HF_{e,mk_2,\alpha}(t).$$

We found that the restoration function of a simple restoration process formed by k_2 multiple convolution of Erlang order m distributions with the parameter α is the restoration function of a simple restoration process formed by an Erlang order mk_2 distribution with the same parameter α .

We have

$$HF_{e,mk_2,\alpha}(t) = \frac{1}{mk_2} (\alpha t + \sum_{k=1}^{mk_2-1} \frac{c^k}{1-c^k} (-e^{-\alpha t(1-c^k)})),$$

$$c = e^{\frac{2\pi i}{mk_2}} = \cos\left(\frac{2\pi}{mk_2}\right) + i \sin\left(\frac{2\pi}{mk_2}\right),$$

$$HF_{e,mk_2,\alpha}(t) = \frac{1}{mk_2} \left(\alpha t - \frac{mk_2-1}{2} + \frac{1}{2} \sum_{k=1}^{mk_2-1} \frac{e^{-\alpha t(1-\cos(\frac{2\pi}{mk_2}k))} \sin\left(\alpha t \sin\left(\frac{2\pi}{mk_2}k\right) + \frac{\pi}{mk_2}k\right)}{\sin\left(\frac{\pi}{mk_2}k\right)} \right)$$

Now in accordance with (11)

$$S(t) = c_0 + \sum_{n=1}^{k_1-1} c_n F^{(n)}(t) + \sum_{n=k_1}^{k_1+k_2-1} c_n \int_0^t F^{(k_1-1)}(t-x) dF_{e,mn,\alpha}(x) +$$

$$+ \sum_{n=k_1}^{k_1+k_2-1} c_n \int_0^t HF_{e,mk_2,\alpha}(t-x) e^{-\alpha x} \alpha \frac{(\alpha x)^{mn-1}}{(mn-1)!} dx \tag{19}$$

Integral

$$\int_0^t HF_{e,mk_2,\alpha}(t-x) e^{-\alpha x} \alpha \frac{(\alpha x)^{mn-1}}{(mn-1)!} dx$$

in (19) it is calculated similarly to the previous example with replacing k_2 by mk_2 and n by mn .

We also note that if additionally $F_i(t) = F_{e,l,\beta}(t)$, $i=1,2,\dots, k_1-1$, then $F^{(n)}(t) = F_{e,nl,\beta}(t)$, $n=1,2,\dots, k_1-1$ and in accordance with (19)

$$S(t) = c_0 + \sum_{n=1}^{k_1-1} c_n F_{e,nl,\beta}(t) + \sum_{n=k_1}^{k_1+k_2-1} c_n \int_0^t F_{e,(k_1-1)l,\beta}(t-x) dF_{e,mn,\alpha}(x) +$$

$$+ \sum_{n=k_1}^{k_1+k_2-1} c_n \int_0^t HF_{e, mk_2, \alpha}(t-x) e^{-\alpha x} \alpha \frac{(\alpha x)^{mn-1}}{(mn-1)!} dx$$

Conclusion

The most important performance indicators of technical and many other systems are random variables [17]. These are, for example, the operating time of the restored elements before failure, the number of failures and the cost of restoration during the restoration process. In the mathematical theory of reliability, when studying restoration processes, the numerical characteristics of these quantities are first considered, for example, the average and dispersion of the number of failures and the cost of restoration, through which various criteria for the optimality of restoration strategies are determined.

Considering that the recovery function for the model under consideration is well studied, the work obtained a solution to the integral equation for the cost function through the recovery function of a simple process specified by the convolution of all distribution functions of the periodic part. As a practical example, explicit formulas for the cost function are obtained for the restoration process, in which the periodic part is distributed according to an exponential law or Erlang law of order m with the same property α .

Note that the resulting formulas make it possible to study the properties of the cost function and consider various optimization problems in strategies for carrying out the restoration process in terms of price, quality, and risk. If, for example, we take the average number of failures as quality, the average cost of restorations as price, and the variance of the number of failures or the cost of restorations as risk.

We also note that, along with the obtained formulas for calculating the cost function, limit theorems for the cost of restorations (as a random variable), similar to those for the number of failures [3], as well as finding the dispersion of the cost of restorations in the models under consideration will also be important.

Библиографические ссылки

1. Вайнштейн И. И. Процессы и стратегии восстановления с изменяющимися функциями распределения в теории надежности. Красноярск : СФУ, 2016. 189 с.
2. Шмидт О. О. Обобщенная модель процесса восстановления в теории надежности использования информационных технологий : дис. ... канд. ф.-м. н. Красноярск. 2008. 125 с.
3. Булинская Е. В., Соколова А. И. Асимптотическое поведение некоторых стохастических систем хранения // Современные проблемы математики и механики. 2015. Т. 10, вып. 3. С. 37–62.
4. Боровков А. А. Обобщенные процессы восстановления. М. : РАН, 2020. 455 с.
5. Кокс Д. Р., Смит В. Л. Теория восстановления. М. : Советское радио. 1967. 300 с.
6. Байхельт Ф., Франкен П. Надежность и техническое обслуживание. Математический подход. М. : Радио и связь, 1988. 189 с.
7. Боровков А. А. Теория вероятностей. М. : Либроком, 2009. 652 с.
8. Bulinskaya E. V. Limit theorems for generalized renewal processes // Theory of Probability and its Applications. 2018. Vol. 62, No. 1. P. 35–54.
9. Вайнштейн И. И., Вайнштейн В. И., Вейсов Е. А. О моделях процессов восстановления в теории надежности // Вопросы математического анализа : сб. науч. тр. Красноярск, 2003. С. 78–84.
10. Вайнштейн В. И., Вайнштейн И. И., Сафонов К. В. Асимптотика поведения средней стоимости восстановлений в моделях процессов восстановления // Сибирский аэрокосмический журнал. 2022. Т. 23, №4. С. 582–592.
11. Вайнштейн В. И. Функция восстановления при распределении элементов технических систем как смесь функций распределения // Современные наукоемкие технологии. 2018. № 6. С. 48–49.
12. Вайнштейн В. И., Вайнштейн И. И. Дисперсия стоимости восстановлений и оптимизационные задачи в процессах восстановления технических и информационных систем // Моде-

лирование, оптимизация и информационные технологии. 2021. Т. 9, № 2 (33) [Электронный ресурс]. URL: <https://moitvvt.ru/ru/journal/pdf?id=931>. DOI: 10.26102/2310-6018/2021.33.2.001.

13. Vainshtein V. I., Vainshtein I. I. Optimization problems in forming a mixture of distribution functions of operating times to failure of elements of technical systems // *Journal of Machinery Manufacture and Reliability*. 2021. Т. 50, № 3. С. 274–279.

14. Каштанов В. А., Медведев А. И. Теория надежности сложных систем. М. : Физматлит, 2010. 608 с.

15. Песчанский А. И. Полумарковские модели профилактики ненадежной одноканальной системы обслуживания с потерями. Сер. Научная мысль, 2022. 267 с.

16. Градштейн И. С., Рыжик И. М. Таблицы интегралов, сумм, рядов и произведений. М., 1963. 1108 с.

17. Надежность технических систем / Е. В. Сугак, Н. В. Василенко, Г. Г. Назаров и др. Красноярск : МГП «Раско», 2001. 608 с.

References

1. Vainshtein I. I. *Protsessy i strategii vosstanovleniia s izmeniaiushchimisia funktsiiami raspredeleniia v teorii nadezhnosti* [Processes and recovery strategies with changing distribution functions in reliability theory]. Krasnoiar'sk, 2016, 189 p.

2. Shmidt O. O. *Obobshchennaia model' protsessa vosstanovleniia v teorii nadezhnosti ispol'zovaniia informatsionnykh tekhologii. Dis. kand.* [Generalized model of the recovery process in the theory of reliability of using information technologies. Diss. cand.]. Krasnoiar'sk. 2008. 125 с.

3. Bulinskaya E. V., Sokolova A. I. [Asymptotic behavior of some stochastic storage systems]. *Sovremennye problemy matematiki i mekhaniki*. 2015, Vol. 10, No. 3, P. 37–62 (In Russ.).

4. Borovkov A. A. *Obobshchennye protsessy vosstanovleniia* [Generalized recovery processes]. Moscow, RAS Publ., 2020, 455 p.

5. Cox D. R., Smith V. L. *Teoriia vosstanovleniia* [Theory of restoration]. Moscow, Sovetskoe radio Publ., 1967, 189 p.

6. Baikhel't F., Franken P. *Nadezhnost' i tekhnicheskoe obsluzhivanie. Matematicheskii podkhod* [Reliability and maintenance. Mathematical approach]. Moscow, Radio i sviaz' Publ., 1988, 189 p.

7. Borovkov A. A. *Teoriia veroiatnosteni* [Theory of Probability]. Moscow, Librocom Publ., 2009, 652 p.

8. Bulinskaya E. V. Limit theorems for generalized renewal processes. *Theory of Probability and its Applications*. 2018, Vol. 62, No. 1, P. 35–54.

9. Vainshtein I. I., Vainshtein V. I., Veysov E. A. [On models of recovery processes in reliability theory]. *Voprosy matematicheskogo analiza. Sbornik nauchnykh trudov*. Krasnoiar'sk, 2003, P. 78–84 (In Russ.).

10. Vainshtein V. I., Vainshtein I. I., Safonov K. V. [Asymptotic behavior of the average cost of restoration in models of restoration processes]. *Siberian Aerospace Journal*. 2022, Vol. 23, No. 4. P. 582–592 (In Russ.).

11. Vainshtein V. I. [Reconstruction function for the distribution of elements of technical systems as a mixture of distribution functions]. *Sovremennye naukoemkie tekhnologii*. 2018, No. 6, P. 48–49 (In Russ.).

12. Vainshtein V. I. [Modeling, optimization and information technologies]. *Modelirovanie, optimizatsiia i informatsionnye tekhnologii*. 2021, Vol. 9, No. 2(33). Available at: <https://moitvvt.ru/ru/journal/pdf?id=931>. DOI: 10.26102/2310-6018/2021.33.2.001 (In Russ.).

13. Vainshtein V. I., Vainshtein I. I. Optimization problems in forming a mixture of distribution functions of operating times to failure of elements of technical systems. *Journal of Machinery Manufacture and Reliability*. 2021, Vol. 50, No. 3, P. 274–279.

14. Kashtanov V. A., Medvedev A. I. *Teoriia nadezhnosti slozhnykh sistem* [Theory of reliability of complex systems]. Moscow, Fizmatlit Publ., 2010, 608 p.
15. Peschanskii A. I. *Polumarkovskie modeli profilaktiki nenadezhnoi odnokanal'noi sistemy obsluzhivaniia s poteriami* [Semi-Markov models for the prevention of an unreliable single-channel service system with losses]. 2022, 267 p.
16. Gradshtein I. S., Ryzhik I. M. *Tablitsy integralov, summ, riadov i proizvedenii* [Tables of integrals, sums, series and products]. Moscow, 1963, 1108 p.
17. Sugak E. V. et al. *Nadezhnost' tekhnicheskikh sistem* [Reliability of technical systems]. Krasnoyarsk, Rasko Publ., 2001, 608 p.

© Vainshtein V. I., Vainshtein I. I., Safonov K. V., 2023

Вайнштейн Виталий Исаакович – кандидат физико-математических наук, доцент, заведующий кафедрой информационной безопасности; Сибирский федеральный университет. E-mail: vvaynshtyaun@sfu-kras.ru.

Вайнштейн Исаак Иосифович – кандидат физико-математических наук, доцент, профессор кафедры ПМиКБ; Сибирский федеральный университет. E-mail: isvain@mail.ru.

Сафонов Константин Владимирович – доктор физико-математических наук, профессор, заведующий кафедрой прикладной математики; Сибирский государственный университет науки и технологий имени академика М. Ф. Решетнева. E-mail: safonovkv@rambler.ru.

Vainshtein Vitaly Isaakovich – Cand. Sc., associate professor, Head of the Department of Information Security; Siberian Federal University. E-mail: vvaynshtyaun@sfu-kras.ru.

Vainshtein Isaak Iosifovich – Cand. Sc., professor, Department of Applied Mathematics and Computer Security; Siberian Federal University. E-mail: isvain@mail.ru.

Safonov Konstantin Vladimirovich – Dr. Sc., Associate Professor, Head of the Department of Applied Mathematics; Reshetnev Siberian State University of Science and Technology. E-mail: safonovkv@rambler.ru.

УДК 556

Doi: 10.31772/2712-8970-2023-24-4-639-651

Для цитирования: Гончаров А. Е., Гончарова Е. А. Интерпретация и обработка данных гидролокатора бокового обзора с целью автоматизации данного процесса // Сибирский аэрокосмический журнал. 2023. Т. 24, № 4. С. 639–651. Doi: 10.31772/2712-8970-2023-24-4-639-651.

For citation: Goncharov A. E., Goncharova E. A. [Interpreting and processing side-scan sonar data with the objective of further automation of the process]. *Siberian Aerospace Journal*. 2023, Vol. 24, No. 4, P. 639–651. Doi: 10.31772/2712-8970-2023-24-4-639-651.

Интерпретация и обработка данных гидролокатора бокового обзора с целью автоматизации данного процесса

А. Е. Гончаров, Е. А. Гончарова

Сибирский государственный университет науки и технологий имени академика М. Ф. Решетнева
Российская Федерация, 660037, г. Красноярск, просп. им. газ. «Красноярский Рабочий», 31
*E-mail: goncharovae@sibsau.ru

Одним из наиболее эффективных средств дистанционного зондирования и визуализации подводных объектов являются гидроакустические приборы, в частности гидролокатор бокового обзора (ГБО). В последнее время, во многом, благодаря появлению доступных бюджетных образцов, география и сфера применения данного прибора существенно расширилась. Однако, несмотря на достигнутые успехи в части совершенствования и минимизации аппаратной части ГБО, используемые программные средства остаются, в целом, на базовом уровне, обеспечивая, главным образом, простую визуализацию донной среды и ее запись с целью дальнейшей постобработки. Опыт эксплуатации ГБО показывает, что основная проблема интерпретации акустических изображений заключается в самих физических особенностях их получения. Следует признать бесперспективными попытки осуществления автоматизированной интерпретации образов методами, применяемыми для оптических сред. В настоящей работе рассматриваются теоретические и прикладные аспекты процесса интерпретации и обработки данных ГБО с целью дальнейшей автоматизации данного процесса. С учетом условий эксплуатации данного прибора, в частности обширные площади акваторий – поисковых зон, настоящая проблема является одной из ключевых для операторов ГБО. Проблема автоматизации обработки данных напрямую связана с проблемой интерпретации данных дистанционного зондирования, в том числе космоснимков, геометрического искажения образов, вызванного физическими особенностями прибора и среды его эксплуатации, а также привязки полученных данных к системе спутниковых координат.

Ключевые слова: гидролокатор бокового обзора, автоматизация, распознавание образов, спутниковые системы позиционирования, геометрическое искажение.

Interpreting and processing side-scan sonar data with the objective of further automation of the process

A. E. Goncharov, E. A. Goncharova

Reshetnev Siberian State University of Science and Technology
31, Krasnoyarskii Rabochii prospekt, Krasnoyarsk, 660037, Russian Federation
*E-mail: goncharovae@sibsau.ru

One of the most effective tools of remote sensing and visualization of underwater surfaces and objects are acoustic devices, in particular side-scan sonars (SSSs). Recently, largely due to the emergence of affordable devices, the geography and scope of application of SSSs has been significantly expanded. Meanwhile, despite certain progress achieved in terms of improving and minimizing the SSS hardware, the software used remains, in general, at a basic level, providing the operator mainly with a simple tool for visualizing benthic environments and data recording for further post-processing. Existing experience in SSS exploitation reveals that the key problem of interpreting acoustic images lies in the physical peculiarities of their acquisition. Arguably, attempts to implement methods of automated interpretation of optical images have no perspective. Hence, the objective of this paper is to provide a theoretical and practical background of SSS data interpretation and processing with the objective of further automation of this process. Taking into account the operating conditions of the SSS, in particular the vast areas of water areas - search zones, this problem is one of the key ones for SSS operators. The problem of automating data processing is directly related to the problem of interpreting remote sensing data, including satellite images, geometric distortion of images caused by the physical characteristics of the device and its operating environment, as well as referencing the obtained data to the satellite coordinate system.

Keywords: side-scan sonar, automation, image recognition, satellite target localization, geometric distortion.

Introduction

A side-scan sonar (SSS) is an effective means of underwater remote sensing, providing a high degree of visualization of the benthic surface of various reservoirs. It is significantly superior to optical means. This device is used to conduct a wide range of hydrological studies, from geomorphological to archaeological ones, as well as to perform applied tasks in the field of hydrography, hydraulic design and construction, search and fixation of underwater objects. The development of SSS technologies and the production of compact and at the same time affordable models have significantly expanded its operational characteristics in terms of increasing the number of users and expanding the conditions for its use. The miniaturization of SSSs has made it possible to include them as one of the components of amateur echo sounders available on the market of recreational devices: they can be successfully used even by one operator on board a small vessel (special works are devoted to the issue of using this SSS subtype [1–4]).

In the scientific literature, the problem of developing software for SSS systems has received significantly less attention than their hardware. For example, the fundamental work of the British scientist Phillip Blondel [5] is almost entirely devoted to the physical features of the operation and application of SSSs. It is explained by the fact that it is the physical parameters of the device (the higher the frequency, the more detailed the visualization) that are responsible for the quality of data. In addition, for the correct interpretation of images, it is necessary to take into account the propagation of sound waves in water, the reflective abilities of benthic objects and other hydroacoustic phenomena. Thus, a trained operator knows, for example, that dark areas of the image are softer, dispersed surfaces, and light areas, on the contrary, are hard and dense, giving a stronger reflective signal. Therefore, equipment users are often focused on improving the SSS hardware, rather than its software. It should be noted that the software installed by default fully meets the requirements of the majority of users of this device: searching for objects and studying the area are carried out mainly *in situ*, which is quite acceptable in small water areas. Proprietary programs (Scanline Starfish, Reefmaster, Humminbird, etc.) quite satisfy the user with the capabilities of viewing images in real time, recording, as well as built-in post-processing functions.

At the same time, it should be pointed out that there is no effective and accessible software on the market that allows for the automated identification of detected underwater objects, their classification and cataloging, as well as the automated calculation of telemetric data coming from the device. The solution to these issues is the focus of this paper.

The problem of visualizing SSS sonograms is considered in [2–6], but in these works the main attention is paid not so much to the issues of creating new software, but to using existing one. Thus,

visualization of field material was carried out according to the method proposed in [3–5] for sonograms obtained by recreational SSSs.

Due to its physical characteristics, the data obtained by SSSs cannot be parsed within the framework of existing pattern recognition algorithms for optical images. The operating principle of SSSs, as well as other acoustic imaging devices, is to process reflected sound rays from the surface of objects (Fig. 1). While at nadir, the transducer studies a thin acoustic beam directed towards the bottom of the reservoir, then receives the reflected echo. The data processing unit processes the received signal and displays it as an image on the operator's monitor. At the same time, the physical identity of this principle of working with ultrasonic medical devices, as well as non-destructive testing devices, should not create a misleading impression about the possibility of using their data processing methods in hydro-acoustics. This is due, first of all, to completely different operating conditions of this technology. The above devices are used in direct contact with the object being studied, while SSSs can be operated in ranges from one meter to several thousand meters. The features and nature of the objects being studied within the framework of diagnostics are relatively known, while at the bottom of reservoirs there can be a variety of sometimes unpredictable objects of both natural and anthropogenic origin. Finally, the amount of data generated by SSSs is significant.

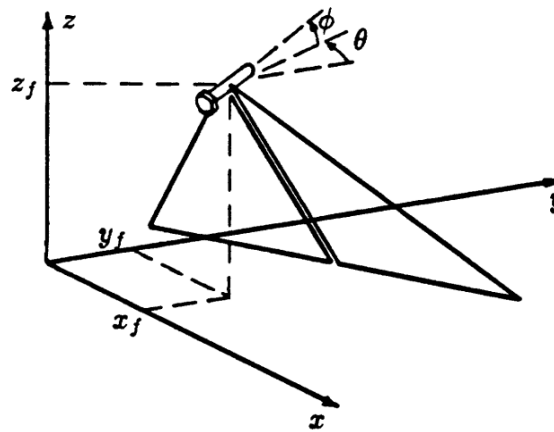


Рис. 1. Принцип формирования ГБО изображения и положение трансдьюсера (x_f, y_f, z_f) : ϕ – угол атаки; θ – угол рыскания. Сост. по [7]

Fig. 1. Principles of SSS image formation. The position of transducer is denoted by (x_f, y_f, z_f) : its pitch angle by ϕ , its yaw angle by θ . Based on [7]

The problem of visualizing SSS data

SSS systems make it possible to obtain an image of the aquatic environment by converting the amplitude values of the own acoustic signal reflected from objects into successive rows of pixels that make up the image of the bottom of the reservoir. Thus, this system, measuring the amplitude of the signal, converts the values into the tone of pixels of the future image. Hard and dense objects reflect more sonar signal than soft and loose objects. Therefore, based on the tone or color of the pixel, one can make assumptions about the underlying object. There are other factors that influence the tonality of pixels in the final image: characteristics of the water body itself (water composition, its density, temperature), scanning parameters - scanning range (scanning bandwidth) and frequency of the emitted sound signal, survey route, the speed of movement of the transducer and other sources, the occurrence and influence of which is not always possible to foresee and prevent, for example, different speeds of water flows on the surface and under water, thermoclines, meteorological conditions (precipitation, atmospheric pressure) and other factors.

Considering that the stability of the hydrosphere depends on a set of fixed factors of both natural and anthropogenic origin [8], the accumulation of information about the state of the bottom of water bodies is the most important task not only for developing a strategy for the economic exploitation of

water resources, but also for creating geographical information systems using SSS data. Thus, the interpretation of SSS images by a human operator is based on a combination of knowledge of factors and their causes that influence the operation of the device, personal experience, as well as parameters and settings of the equipment.

Let us consider, as an example, a fragment of a survey of several sections of the Yenisei River in the upper and lower reaches (depths 3–15 m). During the work, a Starfish 990F SSS (manufactured by Tritech) was used, operating at a constant frequency of 1 MHz and intended for work at depths of up to 30 m. Figure 2 shows underwater objects, as well as the characteristics of the water space.

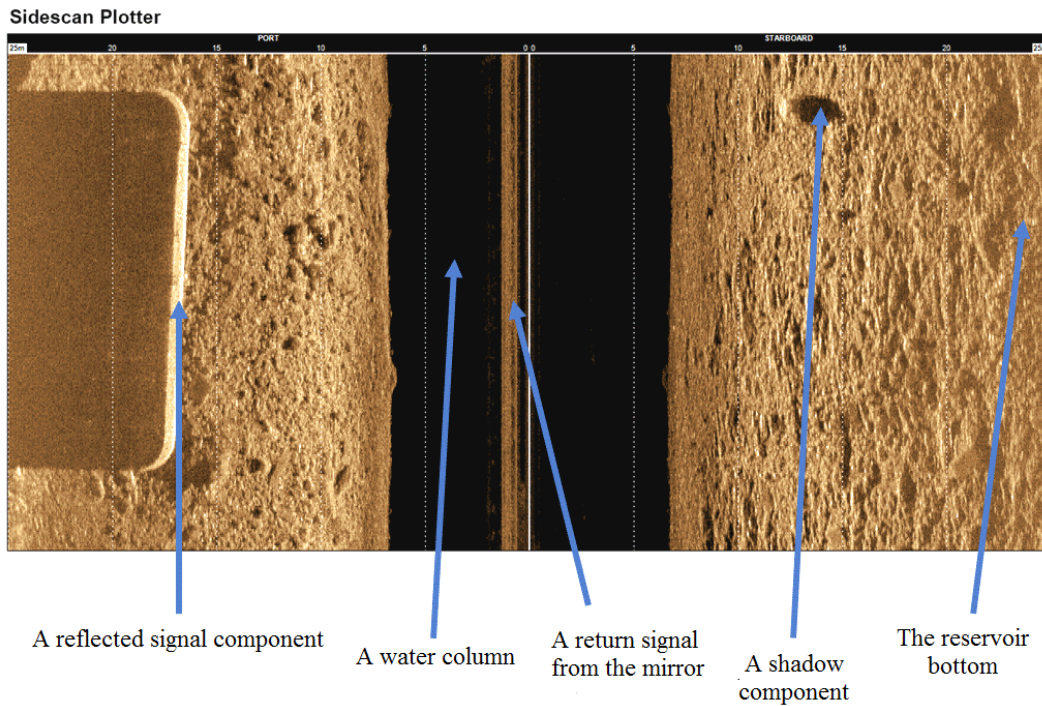


Рис. 2. Фрагмент отснятого прохода ГБО (ширина прохода 50 м) района поиска с элементами снимка

Fig. 2. A fragment of the SSS scanline (overall breadth of 50 m) showing the main elements of the image

There is no shoreline in the image because the passage was made more than 25 m from the shore. The left half of the image shows the clear geometric shape of a reinforced concrete hydraulic structure, with an acoustic beam passing through the structure, which is about 5 m thick. The image is clear and bright. This is ensured by the uniformity of the passage (tack), as well as the presence of a rocky and pebble bottom, which provides the strongest return signal. Large boulders and fragments of building materials are clearly visible at the bottom. In the middle of the image, traces of the sound wave reflected from the mirror of the reservoir are clearly visible. This effect occurs when the signal is reflected twice, first from the bottom of the reservoir, then from the mirror, which is due to the choice of acute angles of the signal pitch at shallow depths of the reservoir. As depth values increase, the data in the image becomes less clear. Although SSSs do not determine depth, it can be calculated from the width of the shadow area in the center of the image, representing the water column below the transducer. There may be fish, floating debris, and various suspended matter. Thus, it is possible to make a rough assessment of the level of water contamination with large particles. Changes in depths along the entire survey route are significant - both small areas with a depth of up to 2 m and large depressions with a depth of more than 8 m are observed. For the most part, the bottom material is homogeneous, presumably fine stone. At the very edge of the water, the stone formations increase in size.

Based on the above, it is clear that with a small area of water at shallow depths (up to 10 m), as well as with the ability to build a correct, uniform trajectory of movement, one can obtain images of high quality, amenable to simple interpretation, and not requiring automation. However, due to their physical characteristics, SSS sonograms are subject to distortion in any case, be it distortions in the intensity of the SSS signal (caused by deviations in the ideal linear relationship between image intensity and signal backscatter) or geometric distortions (caused by inconsistencies between the relative location of properties in the image and the true position of the object on the bottom) [7].

Geometric distortions of benthic objects

One of the key problems is the geometric distortion of underwater objects. The SSS image is a monochrome digital image with return acoustic signals reflected from benthic objects applied to it. For a mathematical description of this transformation, it is necessary to introduce a three-dimensional rectangular coordinate system (x, y, z) of the benthic surface and a two-dimensional rectangular coordinate system (m, n) on the sonogram. The main problem of image formation is the instability of the transducer position, which can change the direction of movement in different planes. Changes in the speed of transducer movement, sudden deepening or ascent, fluctuations in pitch and yaw angles lead to significant distortion of the image. So, in Fig. 3, curvature of all objects to the right side of the image is observed, which is caused by a sharp change in the movement of the transducer tack. The man-made structure on the left side is distorted and has acquired a typical “twisted” shape.

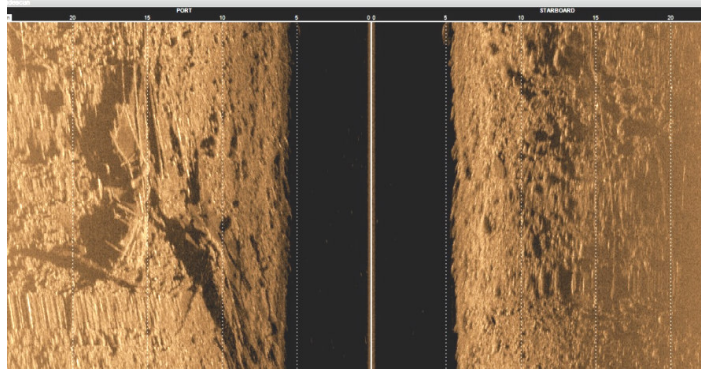


Рис. 3. Пример геометрических искажений донных объектов

Fig. 3. An example of SSS geometric distortion caused by irregularity of vessel movement

One of the most effective ways to solve the problem of geometric distortion is a set of methods based on a combination of the least squares method (extended and recursive identifier) and the use of an effective recursive filter, for example, the Kalman filter, presented in [7; 9]. The main merit of the developers of this approach is the ability to perform automatic image correction without additional navigation or field data. The proposed method is suitable for images with high resolution (frequencies 100 KHz and higher), which is fully consistent with our examples. This approach does not require navigation information and does not rely on image correction by slant range determination.

Let us consider one of the mathematical models of geometric distortions proposed in [7]. Let us imagine the absolute position of the benthic surface points $(x_s[m, n], y_s[m, n])$ as a function of the values of the transducer position parameters relative to fixed coordinates (x, y, z) (see Fig. 1). If the values of the measured parameters could be obtained directly from sensors installed on the transducer, it would be enough to substitute them into a known set of equations to obtain the coordinates of the benthic points, and then correct geometric distortions to obtain the correct image. Unfortunately, for the reasons stated above, it is not possible to directly reference underwater objects to the GNSS system. To assess changes in the positioning parameters of the towed transducer, it is necessary to extract some values of geometric distortions from the sonogram.

Assessing the geometric distortion of images requires making a number of assumptions about it. The basic assumption to obtain the size of the geometric distortion is that the 2D backscattering function is an arbitrary process with an isotropic autocorrelation function. The assumption about the constancy of the backscattering function may turn out to be erroneous in the presence of significant diversity in the benthic surface topography and its geomorphology. However, this technique can well be used to correct hydroacoustic images if the surface under study is first divided into homogeneous areas according to their morphology. In this case, a certain degree of constancy can be assumed. At the same time, the assumption of isotropy is valid in the absence of a systematic direction of benthic objects (direction of current, geology, prevailing direction of waves, etc.).

Thus, assuming that the backscattering function is constant and its autocorrelation function is isotropic, the degree of geometric distortion of a hydroacoustic image can be calculated by measuring changes in the shape of an autocorrelation sequence sample of small sections of the image. Estimation of local geometric transducers can be performed for two images using the method presented in [10]. Due to the fact that the medium under study is not isotropic, the parameters will be determined at the local level. After performing the analysis of SSS images, automatic compensation of the data acquisition speed occurs. Thus, the speed factor (the main distortion factor) is no longer needed to perform running scanning. In the case of using this method, the geometric transformation of a certain object in the scalar factor is equal to zero at a zero rotation angle for each identified object.

Image adjustments can be made during surveys. Thus, the real distance to the benthic object from the transducer can be calculated using a simple formula

$$x = \sqrt{y^2 - h^2},$$

where x is the actual distance to the object; y is the distance indicated on the SSS image; h is the transducer height at nadir. Although this problem is more relevant for towed transducers, it should also be taken into account when operating fixed devices, since each point on the sonogram is conditionally referenced to a geographic coordinate system, calculated depending on the distance of the point from the onboard GNSS receiver.

When processing sonograms, the acoustic shadow area can be removed using graphic editing programs, thus connecting the visible areas on both sides of the vessel into one image. In this case, the width of the shadow along one side represents the conditional distance from the bottom point of the transducer to the bottom of the reservoir.

The choice of the trajectory of a hydrographic vessel is also important. There are several standard methods for covering a given water area, but the meander type performed by a sequence of reciprocal parallel tacks is suitable for SSSs [11].

The results of image correction based on the methods presented above can be seen in Fig. 4.

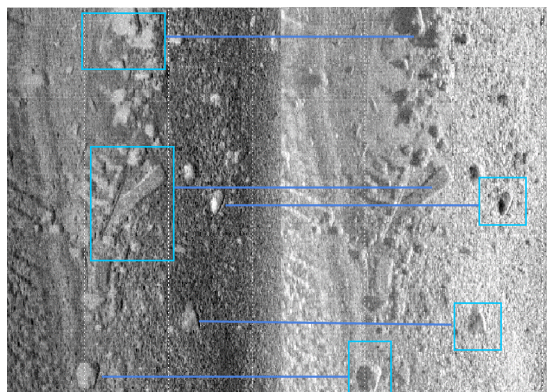


Рис. 4. Результаты коррекции изображения с ГБО

Fig. 4. Results of a corrected SSS image

Construction of an SSS mosaic and recognition of acoustic images

A sonogram and its description are not the final product of hydroacoustic study. A sonogram can be used as the main source when compiling maps of water bodies or as an additional source of information in the case of studying a specific object located in the water column or lying at the bottom of a reservoir. An example of constructing a SSS mosaic for images is presented in works [2–4; 6], however, they were performed using recreational echo sounders, for which commercial mapping software exists. Starfish Scanline does not have the function of constructing a route track, as well as its further plotting on the map. In [12], we referenced the SSS sonogram to the Landsat-8 satellite image (Fig. 5). The work was performed in the Quantum GIS software package.

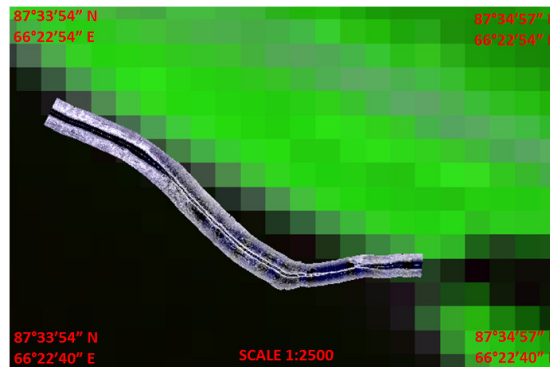


Рис. 5. Построение ГБО мозаики, наложенной на космический снимок Landsat-8

Fig. 5. SSS mosaic transferred to a Landsat-8 satellite image

The sonar sonogram is a file with a LogDoc extension, a standard file format for StarFish, which is visualized by the instrument manufacturer's Starfish Scanline software. The software offers several ways to extract data - directly the finished sonogram and the so-called “raw data”, which is a table with parameters entered into it. We used the function to extract the finished sonogram. Thus, the sonogram file was divided into 43 uniform fragments, representing the details of a large mosaic. For each element, the coordinates of 15 points were recorded in the table. It is necessary for carrying out the procedure of georeferencing each element; in addition, this number of points is sufficient to transform the display of sonograms by a second-order polynomial, which will increase the accuracy of the work. Thus, georeferencing gave the data a natural location in space for each sonogram, not in the form of a “straight line”, but along the trajectory of the watercraft with filming equipment with all the turns along the route during research work. As the georeferencing proceeds, the elements are joined to each other one by one, making up a single mosaic.

The problem when carrying out georeferencing was the so-called “corner fragments” (fragments located in areas of the vessel). Special attention was paid to them. Since it is not always possible to shoot on straight lines, sharp bends are visible in the images, which can lead to severe distortion of the sonogram, which, in turn, negatively affects the clarity of the image and the referencing accuracy. In our work there is a fragment of a sharp turn (Fig. 6). One can see how much the shape of the fragment has changed after spatial referencing and transformation of the image. It is also necessary to note that a “tear” has formed on the outer corner of the sonogram - this is the lack of data in this place due to a sharp turn [13].

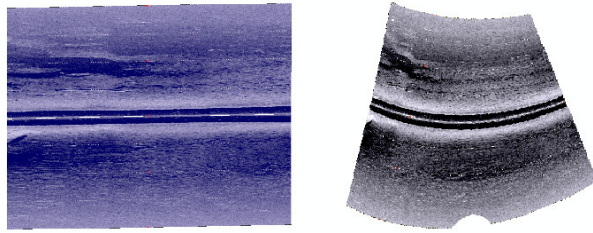


Рис. 6. Изменение угловой сонограммы после географической привязки и трансформирования полиномом второго порядка

Fig. 6. Correction of an angular sonogram after georeferencing and transformation by a second-degree polynomial

After completing the mosaic, we add a layer of satellite imagery from Landsat-8. Combining the image and sonar data allows one to accurately determine the position of objects in the water column and at the bottom of the reservoir relative to the shoreline and, in general, for correct visual perception (Fig. 7).

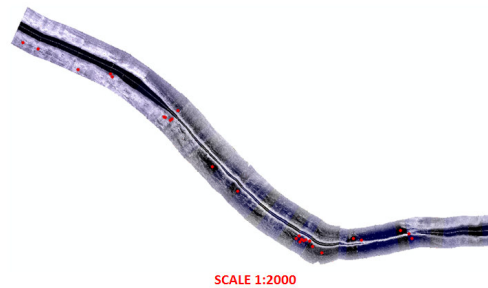


Рис. 7. Построенная ГБО мозаика с точечным слоем обнаруженных объектов и явлений

Fig. 7. A SSS mosaic with a point layer showing detected objects and artifacts

The discovered phenomena and objects can be divided into several groups. The objects themselves stand out against the background of a relatively flat surface of the river bottom, regarding which it can be assumed that they are fragments of a woody nature, since they have a characteristic elongated rectangular shape, and their volume is determined by the falling shadow. It was also noted that these objects have average reflected sound signal values (20–30 dB). The second group consists of areas with distortions (including geometric ones) and fading of the reflected sound signal, which ultimately leads to data loss. Such areas must be determined by knowing the coordinates and locations of such “dark spots” on the map in order to re-explore this area. Note that this problem has so far been solved only partially due to a significant error in referencing satellite coordinates to the sonogram. In areas where the trajectory deviates from a given meander, geometric distortion (stretching) of the raster image occurs, which subsequently affects the work on object recognition. Taking into account the location of these sections, it will also be possible to avoid distortions or minimize the turning radius.

All identified objects were presented on the map (Fig. 7) by creating and overlaying a new layer that stored information about the location, the order of the sonogram (a mosaic fragment), as well as a brief descriptive characteristic. This data is located in the attribute table of the layer.

This method of presenting information made it possible to detect some characteristics of objects that were not so obvious in the original form of the SSS data. For example, at the junction of two sonograms, a vertical object was discovered with a high degree of sound reflection and a characteristic elongated sound shadow. This may indicate a large object. Also, in the vicinity of the object, other

sources of high reflection were discovered, having a characteristic rectangular shape and their own shadow (Fig. 8–9).

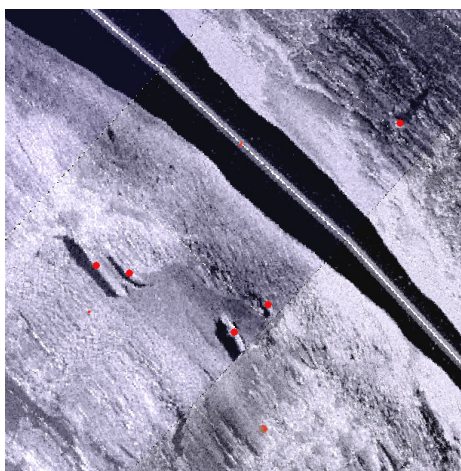


Рис. 8. Фрагмент построенной ГБО мозаики с обнаруженным вытянутым вертикально залегающим объектом на стыке мозаики

Fig. 8. A SSS mosaic fragment showing distorted (elongated) object at mosaic join

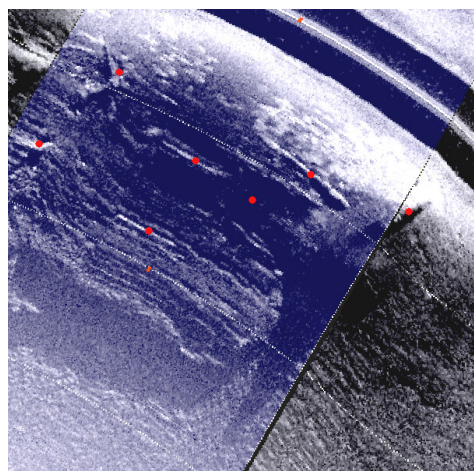


Рис. 9. Фрагмент построенной ГБО мозаики с обнаруженным вытянутым горизонтально залегающим объектом

Fig. 9. A SSS mosaic fragment showing a horizontal object distorted by stretching

The problem of automating the process of processing and interpreting SSS data

It should be noted that, despite the fact that the issue of creating a system that allows excluding the human operator from the process of processing SSS data was considered by a number of researchers, including [5; 14–15], they achieved very modest results. Thus, in work [15], by constructing a complex neural network, it was possible, according to the authors, to create a system that makes it possible to automatically identify boulders (Fig. 10).

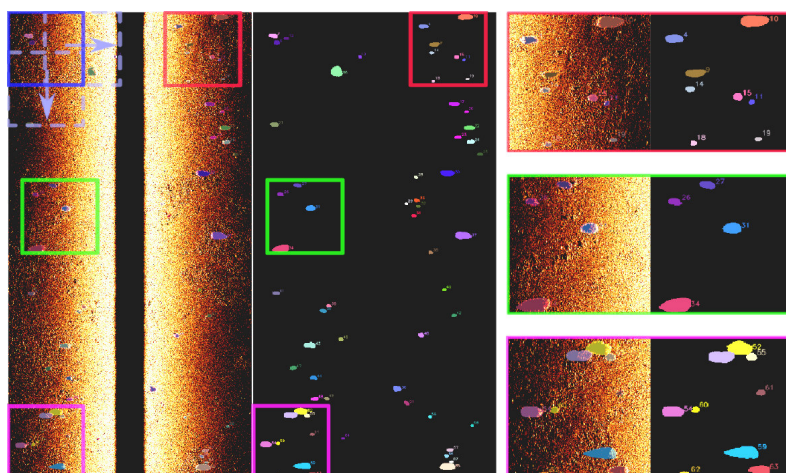


Рис. 10. Результаты работы системы по автоматизированному распознаванию валунов (выделенные объекты) [15]

Fig. 10. The results of the work of a system for automatic identification of boulders (seen as highlighted shapes) [15]

As it can be seen from the image, the results are very modest and can hardly claim further development. It should be noted that objects such as large stones and other rocks can be quite easily recog-

nized by the strength of the return signal (more than 30 dB), and not by their graphical appearance, which in conditions of geometric distortion can be very deceptive. Thus, the use of various methods of information processing and its automation, including methods such as machine learning algorithms [10], can be considered effective (the impossibility of fully implementing high-precision determination of final objects, as well as the limitations of time determination models) only on condition that the problems of object distortion will be taken into account, as well as taking into account acoustic parameters. Attempts to apply these methods to SSS images in the optical data recognition paradigm cannot be of practical significance.

In this sense, work [16] compares favorably, in which the authors describe the process of classification of SSS images, and also identify problems such as the inapplicability of most extractor programs, since they are created for optical images.

The recognition and classification process for SSS images traditionally contains three main steps:

- data preprocessing (grey tone correction);
- feature extraction (image segmentation);
- classification (performed by a human operator on the basis of segmentation).

The authors of [16] proposed to solve the problem of automated recognition of underwater objects using an algorithm built on the basis of a neural network with spatial pyramidal convolution and referencing to network databases of hydroacoustic images. In the proposed method, five different neural networks were used in data preprocessing for object recognition. Then, spatial pyramidal convolution and network SSS databases were introduced into this system. Then a comparative analysis of the results obtained by the networks before and after the inclusion of additional components was carried out. This approach is in many ways identical to the principle of *n*-version programming, according to which the optimal software or individual component is selected based on a voting algorithm. Note that the data preprocessing within the proposed method was limited to improving image quality.

Conclusion

Taking into account the above, we can conclude that, despite a fairly large number of studies in the field of recognition, correction and automated interpretation of underwater objects visualized using SSS, currently there is no effective way to implement this process. In this regard, we were the first to propose combining methods for correcting geometric distortions of underwater objects with modern methods of information processing proposed in recent scientific research. In our opinion, image correction using effective recursive filters, as well as a set of mathematical methods presented in [7; 9], is promising. The use of more accurate satellite imagery data, as well as correction of the motion trajectory (meander) using satellite coordinates, makes it possible to correct distortions in the planes of movement of the transducer. As post-processing methods, both image correction using the proposed methods and image fragmentation turned out to be effective, which provided the possibility of detailed elaboration of each fragment and implementation of georeferencing at 15 points with subsequent transformation by a second-order polynomial.

It can be affirmed that mathematical methods can quite effectively solve problems of geometric distortion of images obtained from SSSs. This area of research has promise in terms of creating new methods for image correction, as well as transferring them to solving similar problems in the field of earth remote sensing (ERS).

Based on all of the above, we can conclude that creating a list of detected objects using SSSs is an important step in processing the received data. However, such data analysis today cannot be made without participation of a human operator, despite the availability of experimental automation methods. Human participation makes it possible to rationally conduct repeated observations (if

necessary), to further use data for more easy determining objects and phenomena, identifying patterns or general characteristics of the area under study.

Automated SSS image recognition systems must include all of the above elements of image distortion, and also rely on the physical features of the images themselves, obtained by processing acoustic rather than optical signals. This issue needs to be paid attention to in the further development of this topic.

Библиографические ссылки

1. Фирсов Ю. Г. Основы гидроакустики и использование гидрографических сонаров. СПб. : Нестор-История, 2010. 348 с.
2. Hamill D., Wheaton J. M., Buscombe D., Grams P.E., Melis T.S. Bed texture mapping in large rivers using recreational-grade sidescan sonar // River Flow 2016: Eighth International Conference on Fluvial Hydraulics (11–14 July 2016, Iowa City, IL) / Constantinescu, G. & H. (Eds). London: Taylor & Francis Group, 2017. P. 306–312. DOI: 10.1201/9781315644479-51.
3. Halmai Á.; Gradwohl-Valkay A.; Czigány S.; Ficsor J.; Liptay Z.Á.; Kiss K.; Lóczy D.; Pirkhofer E. Applicability of a Recreational-Grade Interferometric Sonar for the Bathymetric Survey and Monitoring of the Drava River // ISPRS Int. J. Geo-Inf., 2020, No. 9(3), P. 149. DOI: 10.3390/ijgi9030149
4. Hamill D., Buscombe D., Wheaton J.M. Alluvial substrate mapping by automated texture segmentation of recreational-grade side scan sonar imagery // PLoS ONE. 2018. No. 13(3). P. e0194373. DOI: 10.1371/journal.pone.0194373.
5. Blondel P. The handbook of sidescan sonar. Springer – PraxisPublishing, 2009. 316 p.
6. Kaeser A., Litts T. An Illustrated Guide to Low-Cost Sonar Habitat Mapping v1.0. 2014 [Электронный ресурс]. URL: <https://www.fws.gov/panamacity/resources/An%20Illustrated%20Guide%20to%20Low-Cost%20Sonar%20Habitat%20Mapping%20v1.1.pdf> (дата обращения: 22.08.2023).
7. Cobra D. T. Q. Estimation and correction of geometric distortions in side-scan sonar images // RLE Technical Report. 1990. No. 5561990. 142 p.
8. Аузина Л. И. Опыт использования метода конечных разностей при моделировании изменения уровня грунтовых вод в пластах на наклонном водоупоре // Вестник ИргТУ. 2011. № 8(55). С. 28–33.
9. Cobra D. T., Oppenheim A. V., Jaffe J. S. Geometric distortions in side-scan sonar images: a procedure for their estimation and correction // IEEE Journal of Oceanic Engineering. 1992. Vol. 17, No. 3. P. 252–268. DOI: 10.1109/48.153442.
10. Daniel S., Le Léanec F., Roux C., Solaiman B., Maillard E. P. Side-Scan Sonar Image Matching // IEEE Journal of Oceanic Engineering, 1998, Vol. 23(3), P. 245–259.
11. Багницкий А. В., Инзарцев А. В. Автоматизация подготовки миссии для автономного необитаемого подводного аппарата в задачах обследования акваторий // Подводные исследования и робототехника. 2010. № 2(10). С. 17–24.
12. Бабий И. А., Галимзянов О. А., Гончаров А. Е. Обработка изображений с гидролокатора бокового обзора на примере одного участка нижнего течения реки Енисей // Российская Арктика. 2020. № 11. С. 16–23.
13. Kaeser A. J., Litts T. L., Tracy T. W. Using low-cost side-scan sonar for benthic mapping throughout the Lower Flint River, Georgia, USA // River Res. Applic., 2013. No. 29. P 634–644. DOI: 10.1002/rra.2556/.
14. Einsidler D., Dhanak M. R. Beaujean P-P. J. A Deep Learning Approach to Target Recognition in Side-Scan Sonar Imagery // OCEANS 2018: MTS/IEEE Charleston (22–25 October 2018, Charleston SC). IEEE, 2018. P. 1–4. DOI: 10.1109/OCEANS.2018.8604879

15. Christensen J. H., Mogensen L. V., Ravn O. Side-scan sonar imaging: Automatic boulder identification // OCEANS 2021: San Diego–Porto (20–23 September 2021, San Diego, CA). IEEE, 2021. P. 1–6. DOI: 10.23919/OCEANS44145.2021.9705713

16. Improved neural network with spatial pyramid pooling and online datasets preprocessing for underwater target detection based on side scan sonar imagery / J. Li, L. Chen, J. Shen et al. // Remote Sensing. 2023. No. 15. P. 440. DOI: <https://doi.org/10.3390/rs15020440>.

References

1. Firsov Iu. G. *Osnovy gidroakustiki i ispol'zovanie gigrograficheskikh sonarov* [The Fundamentals of Water Acoustics and Hydrographic Sonar Application]. St. Petersburg, Nestor-Istoriia Publ., 2010, 348 p.

2. Hamill D., Wheaton J. M., Buscombe D., Grams P.E., Melis T.S. Bed texture mapping in large rivers using recreational-grade sidescan sonar. *River Flow 2016: Eighth International Conference on Fluvial Hydraulics* (11–14 July 2016, Iowa City, IL), Constantinescu G. & H. (Eds). London: Taylor & Francis Group, 2017. P. 306–312. DOI: 10.1201/9781315644479-51.

3. Halmai Á.; Gradwohl-Valkay A.; Czigány S.; Ficsor J.; Liptay Z.Á.; Kiss K.; Lóczy D.; Pirkhofer E. Applicability of a Recreational-Grade Interferometric Sonar for the Bathymetric Survey and Monitoring of the Drava River. *ISPRS Int. J. Geo-Inf.*, 2020, No. 9(3), P. 149. DOI: 10.3390/ijgi9030149.

4. Hamill D., Buscombe D., Wheaton J. M. Alluvial substrate mapping by automated texture segmentation of recreational-grade side scan sonar imagery. *PLoS ONE*. 2018, No. 13(3), P. e0194373. DOI: 10.1371/journal.pone.0194373.

5. Blondel P. The handbook of sidescan sonar. Springer – PraxisPublishing, 2009. 316 p.

6. Kaeser A., Litts T. An Illustrated Guide to Low-Cost Sonar Habitat Mapping v1.0. 2014. Available at URL: <https://www.fws.gov/panamacity/resources/An%20Illustrated%20Guide%20to%20Low-Cost%20Sonar%20Habitat%20Mapping%20v1.1.pdf> (accessed: 22.08.2023).

7. Auzina L. I. [Experience in using the finite difference method in modeling changes in groundwater levels in layers on an inclined aquitard]. *Vestnik IrGTU*. 2011, No. 8(55), P. 28–33 (In Russ.).

8. Cobra D. T. Q. Estimation and correction of geometric distortions in side-scan sonar images. *RLE Technical Report*. 1990, No. 5561990, 142 p.

9. Cobra D. T., Oppenheim A. V., Jaffe J. S. Geometric distortions in side-scan sonar images: a procedure for their estimation and correction. *IEEE Journal of Oceanic Engineering*. 1992, Vol. 17, No. 3, P. 252–268. DOI: 10.1109/48.153442.

10. Daniel S., Le Léannec F., Roux C., Solaiman B., Maillard E. P. Side-Scan Sonar Image Matching. *IEEE Journal of Oceanic Engineering*. 1998, Vol. 23 (3), P. 245–259.

11. Bagnitskii A. V., Inzartsev A. V. [Automatizing mission preparation for an ROV for an aquatic study area]. *Podvodnye issledovaniia i robototekhnika*. 2010, No. 2(10), P. 17–24 (In Russ.).

12. Babiya I. A., Galimzyanov O. A., Goncharov A. E. [Visualizing And Processing Side-Scan Sonar Images: a Case of the Lower Reaches of the Enisei River]. *Russian Arctic*. 2020, No. 11, P. 16–23 (In Russ.).

13. Kaeser A. J., Litts T. L., Tracy T. W. Using low-cost side-scan sonar for benthic mapping throughout the Lower Flint River, Georgia, USA. *River Res. Applic.*, 2013, No. 29, P. 634–644. DOI:10.1002/rra.2556/.

14. Einsidler D., Dhanak M. R. Beaujean P-P. J. A Deep Learning Approach to Target Recognition in Side-Scan Sonar Imagery. *OCEANS 2018: MTS/IEEE Charleston* (22–25 October 2018, Charleston SC). IEEE, 2018, P. 1–4. DOI: 10.1109/OCEANS.2018.8604879

15. Christensen J. H., Mogensen L. V., Ravn O. Side-scan sonar imaging: Automatic boulder identification. *OCEANS 2021: San Diego–Porto* (20–23 September 2021, San Diego, CA). IEEE, 2021, P. 1–6. DOI: 10.23919/OCEANS44145.2021.9705713
16. Li J., Chen L., Shen J. et al. Improved neural network with spatial pyramid pooling and online datasets preprocessing for underwater target detection based on side scan sonar imagery. *Remote Sensing*, 2023, No. 15, P. 440. DOI: 10.3390/rs15020440.

© Goncharov A. E., Goncharova E. A., 2023

Гончаров Александр Евгеньевич – доцент; Сибирский государственный университет науки и технологий имени академика М. Ф. Решетнева. E-mail: goncharovae@sibsau.ru.

Гончарова Екатерина Александровна – магистрант; Сибирский государственный университет науки и технологий имени академика М. Ф. Решетнева. E-mail: kate-jane-bande@mail.ru.

Goncharov Alexander Evgen'evich is an associate professor; Reshetnev Siberian State University of Science and Technology. E-mail: goncharovae@sibsau.ru.

Goncharova Ekaterina Aleksandrovna is a graduate student; Reshetnev Siberian State University of Science and Technology. E-mail: kate-jane-bande@mail.ru.

УДК 621.396.962.38

Doi: 10.31772/2712-8970-2023-24-4-652-662

Для цитирования: Каткова В. П., Вяхирев В. А., Кринталь А. Н. Математическое моделирование автокомпенсационных устройств // Сибирский аэрокосмический журнал. 2023. Т. 24, № 4. С. 652–662. Doi: 10.31772/2712-8970-2023-24-4-652-662.

For citation: Katkova V. P., Vyakhirev V. A., Krintal A. N. [Mathematical modeling of autocompensation devices]. *Siberian Aerospace Journal*. 2023, Vol. 24, No. 4, P. 652–662. Doi: 10.31772/2712-8970-2023-24-4-652-662.

Математическое моделирование автокомпенсационных устройств

В. П. Каткова^{1*}, В. А. Вяхирев², А. Н. Кринталь²

¹Войсковая часть 58133-5

Российская Федерация, 659300, Алтайский край, г. Бийск

²Сибирский федеральный университет, Военно-Инженерный институт
Российская Федерация, 660036, г. Красноярск, ул. Академгородок, 13а

*E-mail: Lesoedova.2011@mail.ru

Статья посвящена порядку разработки и описанию математических моделей автокомпенсационных устройств радиолокационных станций кругового обзора. Разработка алгоритмов пространственной обработки сигналов в радиолокационных системах с фазированными антенными решетками является важным этапом проектирования радиолокационных станций. В данной статье будет рассмотрен порядок создания математических моделей автокомпенсационных устройств, которые разнятся способами реализации, а именно: количеством компенсационных каналов, положением основного и компенсационных (дополнительных) каналов радиолокационной станции (стационарное или динамическое), амплитудно-фазовым распределением основной и дополнительных антенн, представлением фазированной антенной решетки, алгоритмами нахождения вектора весового коэффициента. Адекватность работы моделей проверена методом вычислительного эксперимента и результатами, сравнимыми с реализованными автокомпенсаторами в радиолокационных станциях. Результаты вычислительного эксперимента, представленные в виде графиков сигнала на выходе автокомпенсационного устройства, а также прохождения согласованного фильтра, показывают, насколько эффективен алгоритм вычисления вектора весового коэффициента, позволяют наглядно, быстро и экономично сравнить эффективность работы автокомпенсационных устройств в зависимости от способа их реализации. В статье рассматривается алгоритм непосредственного формирования вектора весового коэффициента и алгоритм формирования вектора весового коэффициента через обратную корреляционную переобеляющую матрицу. Математические модели автокомпенсационных устройств и результаты вычислительного эксперимента могут применяться для обучения будущих специалистов, разрабатывающих и эксплуатирующих радиолокационные станции.

Ключевые слова: математическая модель, активная шумовая помеха, корреляционный автокомпенсатор, вектор весового коэффициента, быстроедействие.

Mathematical modeling of autocompensation devices

V. P. Katkova^{1*}, V. A. Vyakhirev², A. N. Krintal²

¹Military unit 58133-5

Altai Territory, Biysk, 659300, Russian Federation

²Siberian Federal University, Military Engineering Institute
13a, Akademgorodok St., Krasnoyarsk, 660036, Russian Federation

*E-mail: Lesoedova.2011@mail.ru

The article studies the order of developing and describing mathematical models of automatic compensation devices of all-round radar stations. The development of algorithms for spatial processing of signals in radar systems with phased antenna arrays is an important stage in the design of radar stations. This article considers the procedure to create mathematical models of automatic compensation devices that differ in implementation methods, namely: the number of compensation channels, the position of the main and compensation (additional) channels of the radar station (stationary or dynamic), the amplitude-phase distribution of the main and additional antennas, the representation phased antenna array, algorithms for finding the weight vector. The method of computational experiment verifies the adequacy of the operation of the models and the results are comparable with the implemented automatic compensation devices in radar stations. Presented in the form of graphs of the signal at the output of the automatic compensation device as well as the passage of the matched filter, the results of the computational experiment show effectiveness of the algorithm to calculate the weight vector; they permit to visually, quickly and economically compare the efficiency of the automatic compensation devices, depending on the method of their implementation. The article discusses the algorithm for the direct formation of the weight vector and the algorithm for the formation of the weight vector through the inverse correlation whitening matrix. Mathematical models of automatic compensation devices and the results of a computational experiment can be used to train future specialists who develop and operate radar stations.

Keywords: mathematical model, active noise interference, correlation automatic compensation, weight coefficient vector, speed.

Introduction

The issue of detecting air objects and accurately determining their characteristics has been and remains significant [1]. Radar stations (RS) of all-round coverage, designed to deal with this issue, perform information tasks under the conditions of exposure to external interference. Interference sources conceal or imitate signals and make it difficult to extract useful information. A significant influence on the detection and correct determination of the plane coordinates of an airborne object is exerted by response pulse interference (RPI) and active noise interference (ANI) [2].

The impact on the operation of ANI RS is currently caused by the rapid development of methods and techniques of radio countermeasures, as well as a variety of types of intentional radio interference that reduce the efficiency of isolating useful signals [3]. RPI negatively affects the quality of reception of the useful signal, affecting the side lobes of the antenna pattern of the main channel. That is why one of the most important tasks in radar is the development of devices designed to compensate for various noise and interference when receiving a useful signal [4]. To solve this problem, radars use automatic compensation systems that implement algorithms for ANI compensation and RPI suppression along the side lobes of the main channel antenna radiation pattern.

Mathematical modeling is a powerful tool for studying complex technical systems, such as automatic interference compensation systems, which has got a number of advantages over other research methods [5]. The development of various mathematical models of algorithms and systems is currently an urgent task [6].

The purpose of this work is to consider the procedure for modeling the autocompensator and the response suppression algorithm adopted by the side lobes of the main channel antenna radiation pattern.

The automatic compensator (AC) is designed to reduce the influence of ANI affecting the receiving channel of the radar. The main idea of side-lobe ANI compensation is to add in antiphase the signals received by the antenna of the main channel with signals from additional channels, multiplied by a weighting factor. With an accurate and fast calculated weight coefficient, ANI is successfully suppressed without significantly weakening the useful signal [7]. To successfully suppress ANI, accurate and fast calculation of the weighting coefficient vector is necessary.

The algorithm for suppressing RPI based on the side lobes of the main channel radiation pattern consists of subtracting the signals received by the additional antenna from the signals of the main antenna. In this case, the level of signals received by the additional antenna in the direction of the side

lobes of the antenna pattern of the main channel exceeds the signals received by the main antenna in the direction of the main lobe.

The procedure for creating a mathematical model of autocompensation devices

Fig. 1 presents the block diagram of the autocompensation system.

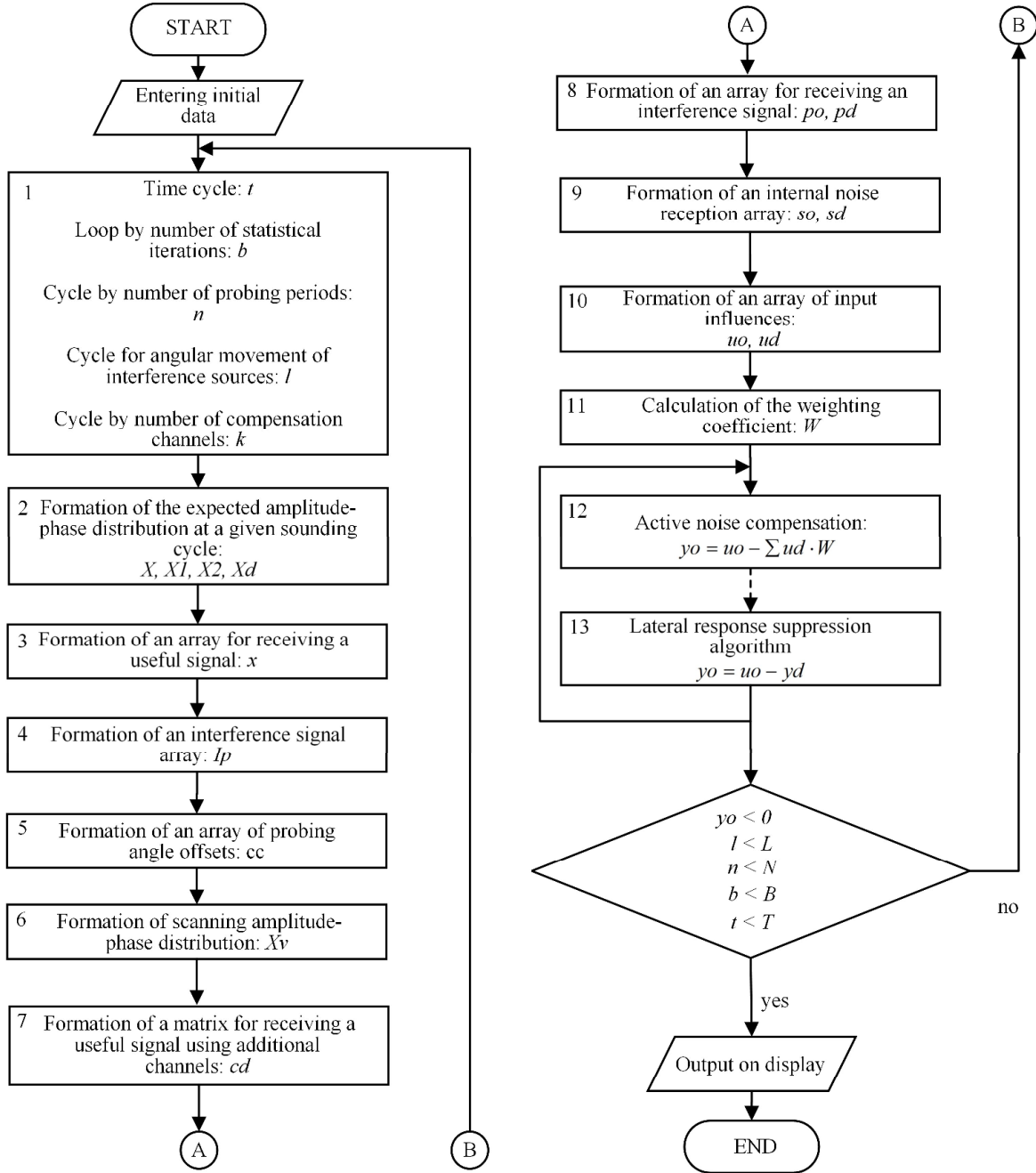


Рис. 1. Блок-схема системы автокомпенсации

Fig. 1. Block diagram of the autocompensation system

To start modeling auto-compensation systems, it is necessary to set the initial data, as well as the cycles indicated by block 1 in Fig. 1.

Modeling of the autocompensation system begins with the formation of amplitude-phase distributions of the antennae of the main and compensation channels (block 2 in Fig. 1). The amplitude-phase

distribution of the main channel antenna, depending on the type of main channel antenna, is formed according to the expression [8]

$$X(m, l) = e^{-i(2(m+1)-M-1) \cdot L(l) \cdot \frac{\pi}{M}} \cdot d(m), \quad (1)$$

where m – sequence number of the antenna element of the main channel array; M – quantity of non-directional antenna array elements; l – sequence number of the angular parameter of interference sources; L – reference number of the angular parameter; $d(m)$ – component of the amplitude-phase distribution of the antenna depending on the type of antenna.

The formation of an array of amplitude-phase distribution of compensation channels is carried out based on the expression

$$X1(ml, l) = e^{-i(2(m+1)-M1-1) \cdot L(l) \cdot \frac{\pi}{M1 \cdot p}},$$

where ml – sequence number of the antenna element of the compensation channel array, $M1$ – quantity of non-directional elements of the compensation channel antenna array, p – coefficient of normalization of the antenna radiation pattern by azimuth.

Further, an array of useful reception (x) is formed (block 3 in Fig. 1) [9]

$$x(m, t) = A \cdot e^{-i(2(m+1)-M-1) \cdot a \cdot \frac{\pi}{M \cdot p}} \cdot e^{-i(\omega t + \varphi_0 + \varphi)},$$

where A – useful signal amplitude; a – direction of the useful signal arrival; ω – signal frequency; φ_0 – initial signal phase; φ – inter-period signal phase shift.

The amplitude of the useful signal can be constant, rapidly or slowly fluctuating due to one of the known laws [10].

Formation of an interference signal array (Ip) (block 4 in Fig. 1)

$$ap(n, t) = ip \cdot rnorm(1, 0, 1)_0,$$

$$fp(n, t) = rnd(2\pi),$$

$$Ip(n, t) = ap(n, t) \cdot (\cos(fp(n, t)) + i \cdot \sin(fp(n, t))),$$

where ip – interference intensity; n – sequence number of the sounding period; t – sequence number of time reference.

Next, the rotation of the main antenna is simulated, that is, the displacement array is formed (block 5 in Fig 1),

$$cc(m, n) = e^{-i(2(m+1)-M-1) \cdot aa(n) \cdot \frac{\pi}{M \cdot p}}, \quad (2)$$

where aa – antenna rotation step during the sounding period.

Multiplying (1) and (2) gives the scanning result (nc).

Based on the scanning expression, an array of scanning amplitude-phase distribution (Xv) is formed (block 6 in Fig. 1)

$$Xv_n^{(l)} = X^{(l)} \cdot \left(nc^{(n)} \right)_l.$$

The notation (l) indicates that the values of the matrix column vector are considered.

Modeling the rotation of antennas of additional channels depends on the radar stations. Their position can be stationary, or the compensation channels can rotate along with the main channel antenna. The formation of the amplitude-phase distribution (APD) for each compensation channel during their rotation (this article provides an example for two compensation channels) is carried out according to the expressions [11; 12]

$$X1(m1, l) = e^{-i \cdot (2 \cdot (m1+1) - M1-1) \cdot (L(l)+a1) \cdot \frac{\pi}{M1 \cdot p}},$$

$$X2(m1, l) = e^{-i \cdot (2 \cdot (m1+1) - M1-1) \cdot (L(l)-a1) \cdot \frac{\pi}{M1 \cdot p}},$$

where $a1$ – correction for the separation of antenna electrical centers.

Based on the obtained amplitude-phase distributions for each channel, the amplitude-phase distribution of the system of additional antennae is formed:

$$Xd = [X1 \ X2]^T.$$

where T – transposition operation.

Further, an array is formed for receiving the useful signal by compensation channels according to the expression (block 7 in Fig. 1)

$$cd(m1, t) = Yc(m1) \cdot A \cdot e^{-i \cdot (2 \cdot (m1+1) - M1-1) \cdot (a \pm a1) \cdot \frac{\pi}{M1 \cdot p}} \cdot e^{-i \cdot (\omega \cdot t + \varphi_0)}.$$

where Yc – amplitude-phase multiplier for the received useful signal by additional channels; k – sequence number of an additional channel.

Taking into account the errors in the amplitude-phase distribution of the antenna caused by various components and the movement of the antenna of the main channel, resulting in the formation of an interference matrix of the main and additional channels (po, pd) (block 8 in Fig. 1),

$$po(m, t) = Ip(n, t) \cdot e^{-1i \cdot (2 \cdot (m+1) - M-1) \cdot np \cdot \frac{\pi}{M \cdot p}},$$

where np – direction of the interfering signal arrival.

$$pd(t, m1) = \left(YN^{(k)} \right)_{m1} \cdot Ip(n, t) \cdot e^{-1i \cdot (2 \cdot (m1+1) - M1-1) \cdot (np \pm a1) \cdot \frac{\pi}{M1 \cdot p}},$$

where $YN^{(k)}$ – amplitude-phase multiplier for the received interference signal of additional channels.

The internal noise matrix of the main channel so is formed according to the expression (block 9 in Fig. 1)

$$so(m, t) = as(m, t) \cdot (\cos(fs(m, t)) + i \cdot \sin(fs(m, t))), \quad (3)$$

where as and fs – random amplitude and phase of internal noise, respectively, are formed in a similar way to ap and fp . The noise matrix $sd(m1, t)$ of the additional channel is formed similarly (3).

From arrays of useful signal, interference and self-noise, an additive mixture of input influences arriving at the input of the antennae of the main and compensation channels (uo, ud) is formed (block 10 in Fig. 1), which is a mixture of noise recalculated to the input of the antenna array, useful signal and interference. In the case of rotation of the compensation channels, expression (4) will take a different form (5)

$$uo(n) = po(n) + so(n) + x(n),$$

$$ud(n, k) = pd(n, k) + sd(n, k) + cd(n, k), \quad (4)$$

$$ud := [ud1 \ ud2]^T, \quad (5)$$

where $ud1, ud2$ – additive mixture of input influences arriving at the input of the antennas of two compensation channels, formed similarly to ud .

When forming a flat antenna array, the number of array elements in the a ($M1$) plane, the number of array elements in the b ($M2$) plane, the direction of the useful signal source in the a (a) plane, the direction of the useful signal source in the b (b) plane will be added to the initial data; quantitative pa-

parameter reading in a (LL) plane, quantitative parameter reading in plane b (KK), as well as errors in the positions of elements in a , b ($r1$, $r2$) plane, random component to the amplitude of the useful signal (AA).

An array of errors is formed caused by the delay in the arrival of the useful signal due to the location of the elements normal to the antenna ($r3$).

Then an array of useful signal (x) is formed

$$x(m1, m2) = e^{-i(2(m1+1)-M1-1) \cdot a \cdot \frac{\pi}{M1}} \cdot e^{-i(2(m2+1)-M2-1) \cdot a \cdot \frac{\pi}{M2}} \cdot e^{-i(r3(n))_{m1, m2}}.$$

Next, an array of the random component of the signal amplitude (An) is formed.

Further, an array of signal distribution in the time domain is formed, taking into account the random amplitude component (xt)

$$xt(t, m1, m2) = e^{-i \cdot t \cdot \psi} \cdot An(n) \cdot (x(n))_{m1, m2},$$

where ψ – frequency multiplier; An – amplitude of a useful signal with a random component.

Expressions for the formation of the amplitude-phase distribution for each of the planes will take the following form in plane a ($X1$):

$$X1(m1, l) = e^{-i(2(m1+r1(n, m1)+1)-M1-1) \cdot L(l) \cdot \frac{\pi}{M1}}. \quad (6)$$

For plane b , expression (6) will take a similar form, with the exception of the components $M1$, $r1$, L , which will be replaced by $M2$, $r2$, K similar to them.

Then we set the direction of arrival of the interference signal in plane a ($N1$), the direction of arrival of the useful signal in plane b ($N2$), and the number of counts in the direction of arrival of the interference signal (r).

Based on $N1$ and $N2$, a matrix of directions of interference sources is formed for two planes (np)

$$np(m1, m2) = e^{-i(2(m1+1)-M1-1) \cdot N1(r) \cdot \frac{\pi}{M1}} \cdot e^{-i(2(m2+1)-M2-1) \cdot N2(r) \cdot \frac{\pi}{M2}} \cdot e^{-i(r3(n))_{m1, m2}}.$$

There are many methods for finding the weight vector. We consider some of them, namely: the direct formation of a weight coefficient vector and the formation of a weight coefficient vector through an inverse correlation re-whitening matrix.

In practice, as a rule, the ANI parameters and spatial correlation matrix are unknown. Moreover, they change in time due to the movement of the noise sources and the radar space survey. Therefore, it is not possible to protect the main radar channel with pre-selected fixed parameters [13; 14].

That is why the ability to adapt to a constantly changing interference environment is of great importance for auto-compensation systems. The most important parameter of the quality of adaptive systems is their speed [14].

The performance of the auto-compensation system largely depends on the speed of calculating the weight coefficient vector. The additive mixture of useful signal and noise is multiplied by a vector of weighting coefficients and the summation of the signal coming from the main channel and the signals received by additional channels and multiplied by the vector of weighting coefficients occurs. At the output of the auto-compensator we receive a signal with compensated ANI. Based on this signal, the vector of weighting coefficients is calculated again, which ensures an increase in the signal/(noise + interference) ratio.

Direct formation of the weight coefficient vector is carried out due to the expression (block 11 in Fig. 1) [15]

$$W_k(n, k) = \frac{1}{T} \sum_{t=0}^{T-1} \left((y o_{n-1})_t \cdot \left(u d_{n-1, k}^{(t)} \cdot \overline{X1} \right) \right), \quad (7)$$

where $y o_{n-1}$ – reaction coefficient; T – number of time counts; $\overline{}$ – complex conjugation operation.

Expression (7) is applicable for the case when the main channel antenna rotation is disabled. When rotation is enabled, expression (7) will take the following form:

$$W(n, k) = \frac{1}{T} \sum_{t=0}^{T-1} \left(\left(\frac{1}{1 + y B_{n-1}} \right)_t \cdot \left(\left(\left((u d_b)_{n-1, k} \right)^{(t)} \right)^T \cdot \overline{X1_n^{(k)}} \right) \right),$$

where yB – the result of the difference between the signals of the main and compensation channels.

The algorithm for directly finding the weight coefficient vector (W) is in the summation over time of the product of the reaction coefficient in the previous sounding period by the additive mixture of input influences arriving at the input of the antennae of additional channels and the expected complex conjugate amplitude-phase distribution of additional channels.

Forming the weight coefficient vector through the inverse correlation whitening matrix is carried out according to the expression [10]:

$$W_k(n, k) = \frac{1}{T} \sum_{t=0}^{T-1} \left(\frac{1}{1 + (y o_{n-1})_t} \cdot \left((u d_{n-1, k}^{(t)})^T \cdot \overline{X1^{(Nc)}} \right) \right), \quad (8)$$

where Nc – quantitative counting of the direction of arrival of the useful signal.

When rotation is enabled, expression (8) will take the following form:

$$W_k(n, k) = \frac{1}{T} \sum_{t=0}^{T-1} \left(I - \frac{1}{1 + (u d^{(t)})^T \cdot \overline{u d^{(t)}}} \cdot u d^{(t)} \cdot \overline{u d^{(t)}}^T \right), \quad (9)$$

where I – identity matrix; $u d(k, t) = \left((u d_b)_{n-1, k} \right)^{(t)} \cdot \overline{X1_{n-1}^{(k)}}$.

At the second and subsequent sounding periods, expression (9) will take the following form:

$$W_k(n) = \frac{1}{T} \sum_{t=0}^{T-1} \left(W_k(n-1) - \frac{1}{1 + (u d^{(t)})^T \cdot \overline{u d^{(t)}}} \cdot u d^{(t)} \cdot \overline{u d^{(t)}}^T \right).$$

Unlike the algorithm for directly finding the weight coefficient vector, the correlation matrix of noise is estimated.

After calculating the weight coefficient vector (W) at the zero iteration step, the array of input influences is multiplied by the weight coefficient vector (W), which is calculated depending on the algorithm used. It is calculated in such a way that after summing the signals coming from the compensation channels, ANI compensation occurs (block 12 in Fig. 1)

$$y o(n) = u o(n) \cdot X v - \sum (u d \cdot X d \cdot W).$$

Suppression of RPI occurs according to the algorithm (block 13 in Fig. 1)

$$y o(n) = |u o(n) \cdot X v| - \sum |u d \cdot X d|.$$

If the sum of the values of the signals arriving at the antennas of the compensation channels is greater than the signal arriving at the main channel, then we can assume that $y o(n) = 0$. Therefore, RPI is suppressed.

Simulation results

The simulation results are presented in the form of graphs. Figure 2 demonstrates the simulation result with the autocompensator disabled. There is a lack of useful signal. It should be taken into account that Fig. 2 and 3 reflect the amplitude of the additive mixture of the useful signal, interference and intrinsic noise is normalized to the standard deviation of the noise.

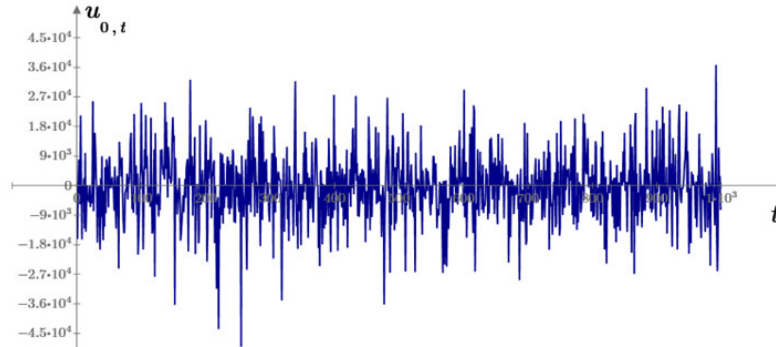


Рис. 2. Сигнал на выходе антенны основного канала при выключенном автокомпенсаторе

Fig. 2. The signal at the output of the antenna of the main channel when the automatic compensation devices is disabled

Figure 3 presents a graph of the signal at the output of the autocompensator and after passing through a matched filter for two algorithms for finding the weight coefficient vector. From the results of the computational experiment, we can conclude that the algorithm for finding the weight coefficient vector through the inverse correlation whitening matrix compensates for ANI faster.

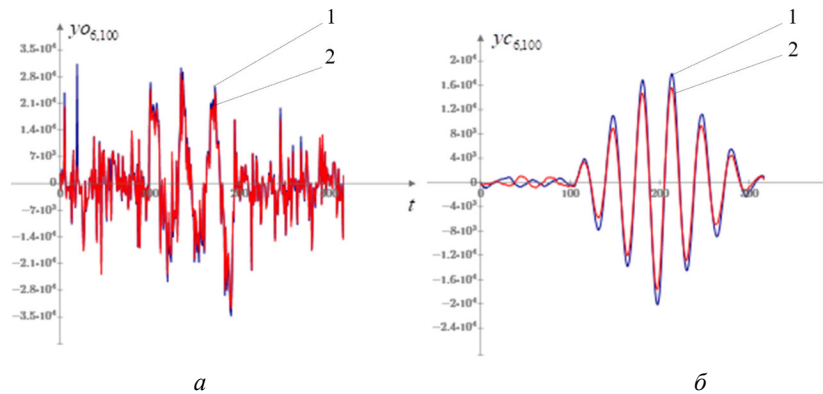


Рис. 3. График сигнала:

a – на выходе автокомпенсатора; *б* – после прохождения согласованного фильтра для двух алгоритмов. 1 – алгоритм непосредственного формирования вектора весового коэффициента; 2 – алгоритм вычисления вектора весового коэффициента через обратную корреляционную переобеляющую матрицу

Fig. 3. The graph of the signal:

a – at the output of the automatic compensation devices; *b* – the graph of the signal after passing the matched filter for two algorithms. In 1 – the algorithm for the direct formation of the vector of the weighting coefficient; 2 – the algorithm for calculating the vector of the weighting coefficient through the inverse correlation re-whitewashing matrix

Conclusion

The article discusses the mathematical model of the autocompensator and the algorithm for suppressing RPI along the side lobes. The results of computational experiments are presented in the form of graphs. The developed model makes it possible to conduct computational experiments depending on:

- from the selected adaptation algorithms to interference signals according to the criteria: maximum signal-to-noise ratio and speed of adaptation to interference;
- operation of the main antenna rotation system: rotation disabled or rotation enabled;
- position of compensation channels (dynamic or stationary);
- algorithm implemented in the radar for calculating the weight coefficient vector.

A mathematical model of an auto-compensator and an algorithm for suppressing RPI along the side lobes of the radiation pattern of the main channel antenna allows to better understand the principle of operation of auto-compensation devices and therefore can be used to train future specialists operating radars.

Библиографические ссылки

1. Синтез обобщенного алгоритма обработки и формирования данных по отраженным сигналам от сложных целей / Х. В. Сунг, К. Н. Трунг, Б. Н. Фунг, Х. Д. Куанг // Изв. вузов России. Радиоэлектроника. 2023. Т. 26. № 1. С. 44–57. Doi: 10.32603/1993-8985-2023-26-1-44-57.
2. Рябуха В. П., Семеняка А. В., Катюшин Е. А. Математические модели взаимнокоррелированных и некоррелированных гауссовых шумовых помех от внешних источников // Изв. Вузов. Радиоэлектроника. 2021. Т. 64. № 3. С. 172–180. Doi: 10.20535/S0021347021030043.
3. Ширман Я. Д., Манжос В. Н. Теория и техника обработки радиолокационной информации на фоне помех. М. : Радио и связь, 1981. 416 с.
4. Чухломин И. Е., Файзулин Н. А., Павлик В. В. Анализ межпериодной обработки при нестационарном влиянии пассивных гауссовских помех // Вестник Южно-Уральского гос. ун-та. Серия: компьютерные технологии, автоматическое управление и радиоэлектроника. 2020. № 20. С. 79–88. Doi: 10.14529/ctcr200108.
5. Шеннон Р., Масловский Е. К. Имитационное моделирование систем – искусство и наука. М. : Мир, 1978. 411 с.
6. Дятко А. А. Моделирование пассивных помех в виде отражений от облаков дипольных отражателей // Информационные технологии : материалы 86-й науч.-техн.й конф. профес.-препод. сост., науч. сотруд. и аспирантов. Минск, 31 января – 12 февраля 2022 г. Минск : БГТУ, 2022. С. 115–117.
7. Елагина К. А. Адаптивные алгоритмы обнаружения и разрешения ЧМ сигналов в РЛС обзора при сложном помеховом воздействии: дис. ... канд. техн. наук. Красноярск, 2017. 157 с.
8. Ботов М. И., Вяхирев В. А. Основы теории радиолокационных систем и комплексов. Красноярск : СФУ, 2013. 530 с.
9. Бородин М. А. Моделирование формы эхосигнала радиовысотомера // Известия вузов России. Радиоэлектроника. 2022. Т. 25. № 4. С. 52–62. Doi: 10.32603/1993-8985-2022-25-4-52-62.
10. Моделирование информационных систем на основе законов распределения случайных величин: Монография / Ю. Ю. Громов, И. Г. Карпов, И. Н. Ищук и др. Тамбов : Нобелистика, 2019. 202 с.
11. Свид. о гос. рег. программы для ЭВМ. РФ. Математическая модель вращения антенны основного канала РЛС / Вяхирев В. А., Лесоедова В. П., Соболева М. А. № 2021665483, заявл. 20.09.2021; опубли. 27.09.2021.
12. Свид. о гос. рег. программы для ЭВМ. РФ. Математическая модель двухканального автокомпенсатора РЛС с разнесённым положением компенсационных каналов / Вяхирев В. А., Каткова В. П., Кринталь А. Н. № 2022661902, заявл. 14.07.2022; опубли. 28.07.2022.
13. Рябуха В. П., Адаптивные системы защиты РЛС от шумовых помех. 1. Корреляционные автокомпенсаторы на основе стохастических градиентных алгоритмов адаптации // Прикладная радиоэлектроника. 2016. Т. 15, № 1. С. 11–25.
14. Защита когерентно-импульсных РЛС от комбинированных помех. 3. Цифровая адаптивная система последовательной защиты РЛС программного обзора от комбинированных помех

на основе АРФ / В. П. Рябуха, А. В. Семяника, Е. А. Катюшин, Д. В. Атаманский // Известия вузов России. Радиоэлектроника. 2022. Т. 65, № 2. С. 84–94. Doi: 10.20535/S0021347022020029.

15. Свид. о гос. рег. программы для ЭВМ. РФ. Математическая модель алгоритма оценки переобеленной корреляционной матрицы помех / Вяхирев В. А., Каткова В. П. № 2022615816, заявл. 16.03.2022; опублик. 04.04.2022.

References

1. Sung Kh. V., Trung K. N., Fung B. N., Kuang Kh. D. [Synthesis of a generalized algorithm for processing and generating data on reflected signals from simple targets]. *Izv. vuzov Rossii. Radioelektronika*. 2023, Vol. 26, No. 1, P. 44–57. Doi: 10.32603/1993-8985-2023-26-1-44-57 (In Russ.).

2. Ryabukha V. P., Semenyaka A. V., Katyushin E. A. [Mathematical models of cross-correlated and uncorrelated Gaussian noise interference from external sources]. *Izv. Vuzov. Radioelektronika*. 2021, Vol. 64. No. 3, P. 172–180. Doi: 10.20535/S0021347021030043 (In Russ.).

3. Shirman Ya. D., Manzhos V. N. *Teoriya i tekhnika obrabotki radiolokatsionnoy informatsii na fone pomekh* [Theory and technique of processing radar information against the background of interference]. Moscow, Radio i svyaz' Publ., 1981, 416 p.

4. Chukhlomin I. E., Fayzulin N. A., Pavlik V. V. [Analysis of interperiod processing under non-stationary influence of passive Gaussian noise]. *Vestnik Yuzhno-Ural'skogo gosudarstvennogo universiteta. Seriya: kompyuternye tekhnologii, avtomaticheskoe upravlenie i radioelektronika*. 2020, No. 20, P. 79–88. Doi: 10.14529/ctcr200108 (In Russ.).

5. Shannon R. *Imitatsionnoe modelirovanie sistem – iskusstvo i nauka* [Simulation modeling of systems – art and science]. Moscow, Mir Publ., 1978, 411 p.

6. Dyatko A. A. [Modeling passive interference in the form of reflections from clouds of dipole reflectors]. *Informatsionnye tekhnologii : materialy 86-y nauchno-tekhnicheskoy konferentsii professorско-prepodavatel'skogo sostava, nauchnykh sotrudnikov i aspirantov* [Information technologies: materials of the 86th scientific and technical conference of faculty, researchers and graduate students]. Minsk, 2022, P. 115–117 (In Russ.).

7. Elagina K. A. *Adaptivnye algoritmy obnaruzheniya i razresheniya ChM signalov v RLS obzora pri slozhnom pomekhovom vozdeystvii* [Adaptive algorithms for detecting and resolving FM signals in surveillance radar under complex interference]. Krasnoyarsk, 2017, 157 p.

8. Botov M. I., Vyakhirev V. A. *Osnovy teorii radiolokatsionnykh sistem i kompleksov* [Fundamentals of the theory of radar systems and complexes]. Krasnoyarsk, Sibirskiy federal'nyy universitet, 2013, 530 p.

9. Borodin M. A. [Modeling the form of the echo signal of a radio altimeter]. *Izvestiya vuzov Rossii. Radioelektronika*. 2022, Vol. 25, No. 4, P. 52–62. Doi: 10.32603/1993-8985-2022-25-4-52-62 (In Russ.).

10. Gromov Yu. Yu., Karpov I. G., Ishchuk I. N., Minin Yu. V., Ivanov O. G., Tyutyunnik V. M. *Modelirovanie informatsionnykh sistem na osnove zakonov raspredeleniya sluchaynykh velichin* [Modeling of information systems based on the laws of distribution of random variables]. Tambov, Nobelistika Publ., 2019, 202 p.

11. Vyakhirev V. A., Lesoedova V. P., Soboleva M. A. *Matematicheskaya model' vrashcheniya anteny osnovnogo kanala RLS* [Mathematical model of rotation of the antenna of the main channel of the radar]. Certificate of state registration of the computer program RF, No. 2021665483, 2021.

12. Vyakhirev V. A., Katkova V. P., Krintal' A.N. *Matematicheskaya model' dvukhkanal'nogo avtokompensatora RLS s raznesennym polozheniem kompensatsionnykh kanalov* [Mathematical model of a two-channel auto-compensator radar with a spaced position of compensation channels]. Certificate of state registration of the computer program RF, No. 2022661902, 2022.

13. Ryabukha V. P. [Adaptive systems for protecting radar from noise interference. 1. Correlation autocompensators based on stochastic gradient adaptation algorithms]. *Prikladnaya radioelektronika*. 2016, Vol. 15, No. 1, P. 11–25 (In Russ.).

14. Ryabukha V. P., Semyanika A. V., Katyushin E. A., Atamanskiy D. V. [Protection of coherent-pulse radars from combined interference. 3. Digital adaptive system for sequential protection of the radar of a program review from combined interference based on an active notch filter]. *Izvestiya vysshikh uchebnykh zavedeniy Rossii. Radioelektronika*. 2022, Vol. 65, No. 2, P. 84–94. Doi: 10.20535/S0021347022020029 (In Russ.).

15. Vyakhirev V. A., Katkova V. P. *Matematicheskaya model' algoritma otsenki pereobelyayushchey korrelyatsionnoy matritsy pomekh* [Mathematical model of the algorithm for estimating the whitening correlation matrix of interference]. Certificate of state registration of the computer program RF, No. 2022615816, 2022.

© Katkova V. P., Vyakhirev V. A., Krintal A. N., 2023

Каткова Вера Павловна – инженер, войсковая часть 58133-5. E-mail: Lesoedova.2011@mail.ru.

Вяхирев Виктор Александрович – кандидат технических наук, доцент, профессор Военного учебного центра; Сибирский федеральный университет. E-mail: vyakhirev@yandex.ru.

Кринталь Андрей Николаевич – студент; Сибирский федеральный университет. E-mail: Andrey-krintal@yandex.ru.

Katkova Vera Pavlovna – engineer, military unit 58133-5. E-mail: Lesoedova.2011@mail.ru.

Vyakhirev Viktor Aleksandrovich – Cand. Sc., associate professor, professor of the Military Training Center; Siberian Federal University. E-mail: vyakhirev@yandex.ru.

Krintal Andrey Nikolaevich – student; Siberian Federal University. E-mail: Andrey-krintal@yandex.ru.

УДК 004.056

Doi: 10.31772/2712-8970-2023-24-4-663-672

Для цитирования: Кононов Д. Д., Исаев С. В. Анализ киберугроз корпоративной сети на основе параллельной обработки данных Netflow // Сибирский аэрокосмический журнал. 2023. Т. 24, № 4. С. 663–672. Doi: 10.31772/2712-8970-2023-24-4-663-672.

For citation: Kononov D. D., Isaev S. V. [Analysis of corporate network cyber threats based on parallel processing of Netflow data]. *Siberian Aerospace Journal*. 2023, Vol. 24, No. 4, P. 663–672. Doi: 10.31772/2712-8970-2023-24-4-663-672.

Анализ киберугроз корпоративной сети на основе параллельной обработки данных Netflow

Д. Д. Кононов*, С. В. Исаев

Институт вычислительного моделирования СО РАН
Российская Федерация, 660036, г. Красноярск, ул. Академгородок, 50/44
*E-mail: ddk@icm.krasn.ru

Публичные сервисы различных организаций подвергаются постоянным кибератакам, что повышает риски информационной безопасности. Анализ сетевого трафика является важной задачей для обеспечения безопасного функционирования сетевой инфраструктуры, в том числе корпоративных сетей. В данной работе представлен обзор основных подходов для анализа сетевого трафика, приведены смежные работы, указаны недостатки существующих работ. Одним из методов является анализ данных сетевого трафика с использованием протокола Netflow, который позволяет сохранять данные о трафике на уровне L3 модели OSI. Особенностью исследования является использование длительных периодов наблюдения. При сохранении данных на длительных временных интервалах журналы имеют большой объем, что требует распараллеливания для первичной обработки данных. Авторами разработан кросс-платформенный программный комплекс распределенной обработки журналов сетевой активности, который использовался для анализа сетевой активности корпоративной сети Красноярского научного центра за 2021–2022 гг. Показана схема программного комплекса, описаны его возможности и особенности функционирования. Приведены источники данных для анализа и методика обработки. В работе были сформулированы и формализованы эвристические критерии аномальности сетевого трафика, которые сигнализируют о наличии возможных атак на сеть, также выделены датасеты по сетевой активности различных протоколов прикладного уровня. Для полученных наборов данных были рассчитаны статистические показатели, на основе которых получена информация об аномальной сетевой активности в течение двух лет. В работе проверен предложенный ранее авторами метод сравнения рисков киберугроз для различных временных интервалов, показавший существенное увеличение рисков для 50 % показателей в 2022 г. Сравнение месячных интервалов за различные годы показало аналогичное увеличение риска. Таким образом, метод доказал свою работоспособность и может применяться в других областях, в которых существуют группы критериев независимых показателей. Авторы привели планы по дальнейшему развитию методики анализа сетевой активности.

Ключевые слова: интернет, сетевая безопасность, анализ сетевого трафика, киберугрозы, корпоративная сеть.

Analysis of corporate network cyber threats based on parallel processing of Netflow data

D. D. Kononov^{*}, S. V. Isaev

Institute of Computational Modelling of SB RAS
50/44, Akademgorodok St., Krasnoyarsk, 660036, Russian Federation
^{*}E-mail: ddk@icm.krasn.ru

Public services of various organizations are subject to constant cyber attacks, which increases information security risks. Network traffic analysis is an important task to ensure the safe operation of network infrastructure, including corporate networks. This paper provides an overview of the main approaches for analyzing network traffic, it provides the related work and points out the shortcomings of the existing work. Here is a method is to analyze network traffic data using the Netflow protocol, which allows traffic data to be stored at the L3 layer of the OSI model. A feature of the study is the use of long observation periods. When storing data over long time intervals, the logs become large, which requires parallelization for primary data processing. The authors developed a cross-platform software package for distributed processing of network activity logs, which was used to analyze the network activity of the corporate network of the Krasnoyarsk Scientific Center for 2021–2022. A diagram of the software package is shown, its capabilities and operating features are described. Data sources for analysis and processing methods are provided. In this paper the authors formulated and formalized heuristic criteria for the anomaly of network traffic, which identify the presence of possible network attacks, and extracted datasets on the network activity of various application-level protocols. For the obtained data sets, statistical indicators were calculated, information about anomalous network activity was obtained for two years. In this research, we tested the previously proposed method for comparing the cyber threats risks for different time intervals, which showed a significant increase in risks for 50% of indicators in 2022. Comparisons of monthly intervals over different years showed similar increases in risk. Therefore, the method has shown its efficiency and can be used in other areas in which there are groups of criteria for independent indicators. The authors have proposed plans for further development of methods for analyzing network activity.

Keywords: Internet, network security, network traffic analysis, risk assessment, cyber threats, corporate network.

Introduction

Currently information technology are used everywhere to organize the work of various services, including corporate ones. Publicly available services are subject to information security risks, which requires to organize comprehensive measures to protect information. One of the important parts ensuring information security is to monitor and analyse network activity (NTA - Network traffic analysis), it allows to detect anomalies in network operation, identify the cause (external or internal) and take appropriate measures. Analysis of network activity is a significant task and is used in various fields. For example, analyzing the network activity of IoT devices permits to identify their type [1] and identify security problems [2]. Fragmented standards and methods for collecting and analyzing network traffic do not often contribute to reproducing the results. Some authors are making attempts to develop universal formats and software for traffic analysis [3]. In spite of automating traffic processing and analysis processes can reduce the number of routine operations, identifying anomalies with the help of a human operator is a problem due to the large volume of data. Machine learning techniques presents the interest to identify anomalies in network activity [4; 5]. Using various techniques to analyse and identify traffic features is applied for mobile devices [6], in particular, the analysis of encrypted traffic allows to determine the mobile applications being used with high accuracy [7]. Therefore, analysis of network activity makes it possible to obtain much useful information that can be used to improve the performance and security of information systems, including corporate network services.

An important part of ensuring information security is assessing the risks of cyber threats. Applying various techniques to analyse network traffic affords to identify anomalies in network activity, which results in assessing the risks of cyber threats to which the network infrastructure is exposed. Risk assessments can be carried out at different time intervals, so it is necessary to be able to assess the dynamics of changes in cyber threat risks.

Related research

Network traffic analysis allows to identify anomalies in the operation of the network infrastructure. Methods to detect network traffic anomalies can be divided into three categories: unsupervised, supervised, and partially supervised. Unsupervised methods are quite common and do not require preliminary data preparation. The normal data are assumed to be found in datasets more often than anomalous ones [8]. Supervised methods involve building models by dividing data into two categories: normal and abnormal. The analyzed data are compared due to two models, and a conclusion is made about whether the data belongs to a certain category [9]. Partially supervised methods involve building a model only for normal data [10] and are simpler and more common than supervised models.

Cluster analysis and classification methods are the most common. Cluster analysis involves dividing the properties and attributes of data into clusters, from which normal and anomalous behavior are distinguished [11]. In general, large clusters are normal and small clusters are abnormal. Classification methods are used to divide data into previously known categories, they can be distributed into the following types: support vector machine (SVM), neural networks, decision tree, statistical methods. One type of classification using supervised learning is the support vector machine (SVM), which is used for training and testing a large amount of data. [12] uses the SVM method to analyze traffic, and high matching accuracy is achieved. Neural network methods use a model of neurons with connections that convert an input signal into an output signal. The method is widespread and used, for example, to identify malicious traffic [13] and build intrusion detection systems (IDS) [14]. Decision tree methods result in constructing a tree consisting of leaves, nodes and edges, which can be used for multi-stage data classification. Research [15] shows its high efficiency in analyzing malicious traffic of IoT devices. Statistical methods are based on Bayes theorem: if the class is known, it is possible to predict the attributes; if the class is unknown, the rules can determine the class based on the available attributes. In [16], a Bayesian network is used to analyze traffic and ensure the security of cloud services.

An important component in protecting information systems and data networks is to assess the risks of cyber threats. Risk assessment methods can be quantitative and qualitative [17]. Quantitative methods operate with numerical indicators, while qualitative methods use fixed categories of “high risk”, “medium risk”, “low risk”. Typically, qualitative methods are subjective and rely on expert judgment, while quantitative methods are objective and enable results to be reproduced. There are various methods to assess the risk of cyber threats [18]. In [19], the authors use various models of a quantitative method for assessing cloud computing cybersecurity risks. Hybrid risk assessment models are also used, combining different approaches [20]. Information security risk assessment is used in various areas: industrial networks [21], Supervisory Control and Data Acquisition (SCADA) management systems [22], Internet of Things (IoT) devices [23]. Some researchers consider risk assessment as a complex task that includes functional safety, physical safety and cybersecurity [24].

The existing research applies different approaches to traffic analysis and cyber threat risk assessment. For example, the authors develop a new technique and use standard test datasets, which does not allow to assess the effectiveness of the method on a real network infrastructure. Other authors apply real data with short time intervals, which does not result in a deep analysis and identification of the dynamics of ongoing processes.

The current research studies the security of the corporate network of the Krasnoyarsk Scientific Center (Federal Research Center KSC SB RAS) based on analyzing Netflow network traffic. The pa-

per describes the use of a statistical method for comparing the risks of cyber threats proposed earlier by the authors [25]. Unlike the existing research, the method uses long time intervals when analyzing real network traffic and enables to compare the risks of cyber threats at arbitrary intervals.

Data source and processing methodology

The data source to be analyzed is the Netflow network activity data of the edge router and proxy server of the corporate network of the Krasnoyarsk Scientific Center for 2021–2022 period (volume of 680 GB, 19.5 billion records). Data processing is carried out in several stages: 1) collecting statistics of network interfaces using nfcapd agents; 2) extracting data with the nfdump utility; 3) filtering and aggregating the required fields based on specified rules; 4) saving the obtained data for the analysis; 5) applying statistical analysis.

Data processing is performed using the GNetProc software package for distributed processing of network activity developed by the authors in the Go language. The software package consists of several parts: a client, a message broker, and a computing cluster (Fig. 1).

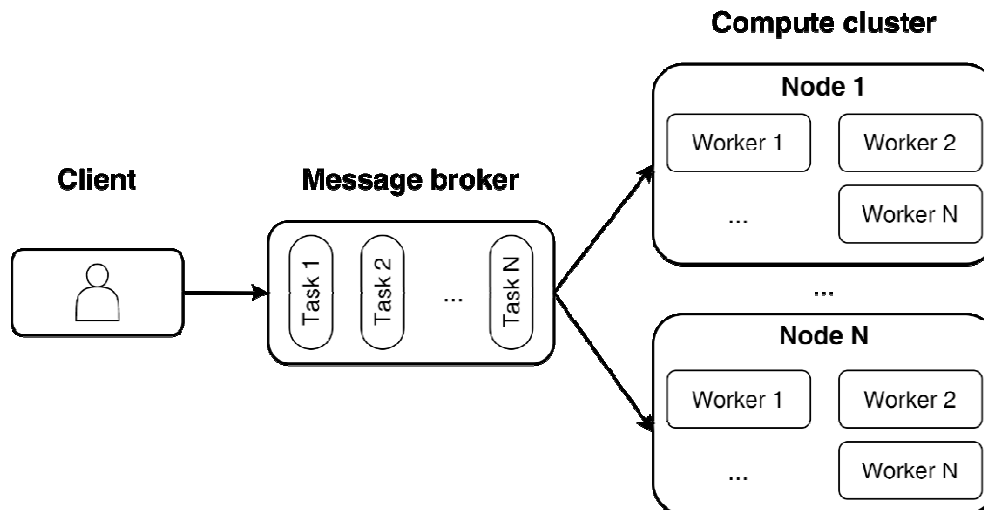


Рис. 1. Архитектура GNetProc

Fig. 1. GNetProc software architecture

The client part interacts with the message broker and allows to send assignments for processing to a common assignment queue, the server part retrieves the assignment from the queue and starts processing using workers. The server part consists of many nodes of a computing cluster; each node can run several workers in parallel, which ensures parallel data processing and reduces assignment execution time. The worker contacts the message broker, receives a new assignment, starts it for execution, saves the processing results, then receives a new assignment. The worker contacts the message broker, receives a new assignment, starts it for execution, saves the processing results, then receives a new assignment. An assignment consists of a list of <name, value> elements that include the data source, data sink, assignment type, aggregation parameters, start and end time intervals, filter, and data selector. A filter, using a special language, allows to specify a set of rules for filtering data. The selector specifies a list of fields that, after filtering and aggregation, will be retrieved and recorded as the result of the assignment. The message broker uses the Redis DBMS to process the assignment queue. YAML is used to describe assignments. The software package is cross-platform and supports work in heterogeneous configurations with Linux, *BSD, and Windows operating systems.

Data analysis

To assess the level of risk of cyber threats based on the principles of normal functioning of various protocols, heuristic criteria for traffic anomaly were formulated:

1. Incoming TCP flows with less than 4 packets indicate that the TCP connection was not completed in a controlled manner. Suspicion of a DoS attack.
2. Incoming TCP flows with a duration of 0 indicate that a TCP connection was not established. Suspicion of a DoS attack.
3. A large number of incoming UDP flows is a suspicion of a DDoS attack.
4. An excess of incoming UDP flows over outgoing ones is a suspicion of a DoS attack.
5. An excess of the number of incoming TCP flows over outgoing ones is a suspicion of a DoS attack.
6. Incoming TCP and UDP flows to unused but routable addresses are suspected of vulnerability scanning (Unused).
7. Incoming TCP flows to common services (MSSQL, MySQL, RDP, SMB, SMTP, SSH, Telnet) – unauthorized login attempts.

These criteria were formalized as rules for the primary traffic processing system according to a given syntax. Having processed the primary data using the created software, the aggregated data were obtained for further analysis. Each data set is a collection of pairs <time label, integral characteristic>. A typical yearly data set consists of 105 thousand records (the number of five-minute intervals in a year) and can be processed using desktop systems such as MS Excel. Figure 2 presents a diagram of the number of streams of zero duration for 2022. Anomalous values do not have a pronounced periodicity, they are several orders of magnitude higher than the average value (35256), due to which their identification can be automated.

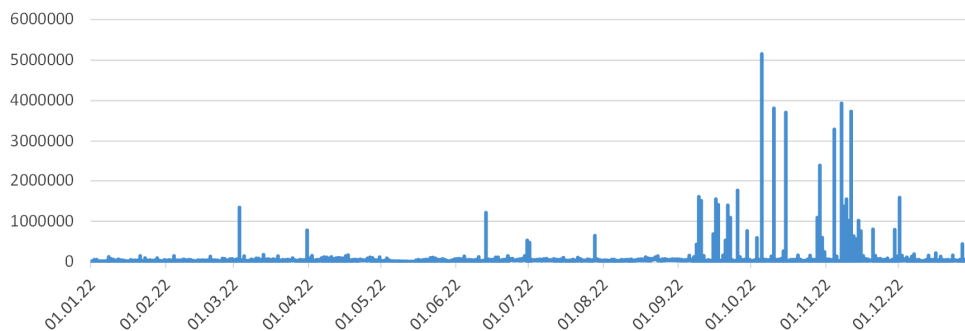


Рис. 2. Количество TCP-потоков нулевой длительностью

Fig. 2. Number of TCP flows with zero duration

The resulting distribution has a clearly expressed right asymmetry, that meets the following condition:

$$Mode < Median < Mean.$$

Figure 3 shows a histogram of the frequency distribution of TCP flows with a duration 0 s. More than 99 % of the sample is contained in the interval $[\mu - 3\sigma, \mu + 3\sigma]$, which makes it possible to identify cyber threats based on outlier data.

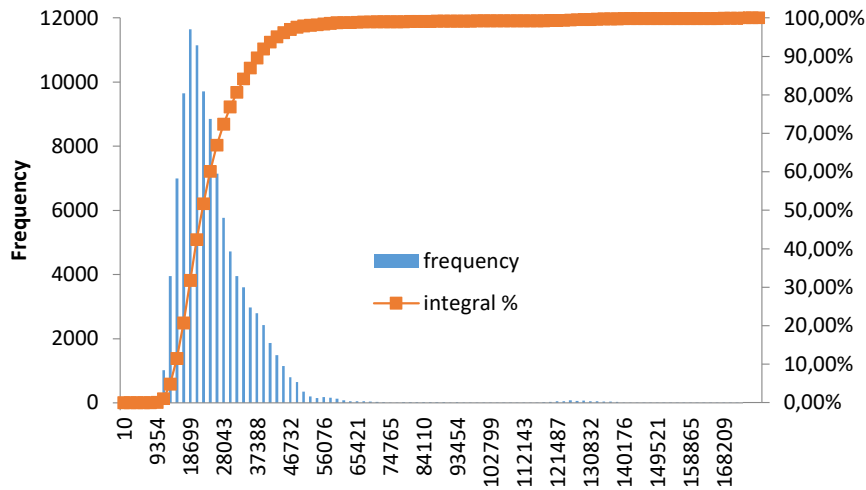


Рис. 3. Гистограмма распределения частот TCP-потоков длительностью 0

Fig. 3. Histogram of frequency distribution of TCP flows with zero duration

For all obtained data sets, the following indicators were calculated: mean, mode, median, standard deviation and percentage of outliers with values greater than 3 standard deviations from the mean. Additionally, the relative increase in the standard deviation of indicators was calculated in 2022 compared to 2021. The findings are in the table: Mean – sample average μ ; S – standard deviation σ ; Me – sample median; Mo – sample mode; P – percentage of data outside the range $[\mu - 3\sigma, \mu + 3\sigma]$; ΔS – average increase in S in 2022 relatively to 2021.

Indicator results calculated using traffic anomaly criteria

Название	2021 г.					2022 г.					$\Delta S, \%$
	Mean	S	Me	Mo	P, %	Mean	S	Me	Mo	P, %	
TCP-flows, duration 0	25205	8343	22079	18975	2.15	35257	14301	29059	22951	1.13	71
TCP-packages < 4 packages	34906	11608	30188	27535	2.35	45287	17732	37461	35331	1.02	53
UDP-flows	15071	5809	13541	13217	2.62	17221	6069	15589	13965	2.95	4
UDP (input-output)	1878	2114	1678	1532	2.08	3511	2428	3175	1325	1.90	15
TCP (input-output)	16759	8751	14846	12540	2.06	26087	11707	21363	16602	1.42	34
Unused TCP	20615	6357	18662	15287	2.30	22035	6736	20457	15148	0.98	6
Unused UDP	965	500	762	376	1.82	1519	1184	862	454	4.24	137
MSSQL	128	63	93	87	7.01	96	30	82	82	3.93	-52
MySQL	21	19	10	3	2.93	32	31	13	5	4.25	63
RDP	105	66	78	39	3.97	120	80	84	40	4.27	21
SMB	367	267	190	128	3.33	224	128	154	129	7.84	-52
SMTP	190	80	166	139	3.88	195	95	162	104	2.98	19
SSH	281	160	197	141	4.19	494	389	270	226	4.02	143
Telnet	405	70	384	363	4.10	922	259	953	1151	0.17	270

All distributions except Telnet 2022 demonstrate right asymmetry. The Telnet 2022 data set has two histogram maxima, which is due to reconfiguration of the data acquisition equipment. Figure 4 shows histograms for 2021 and 2022.

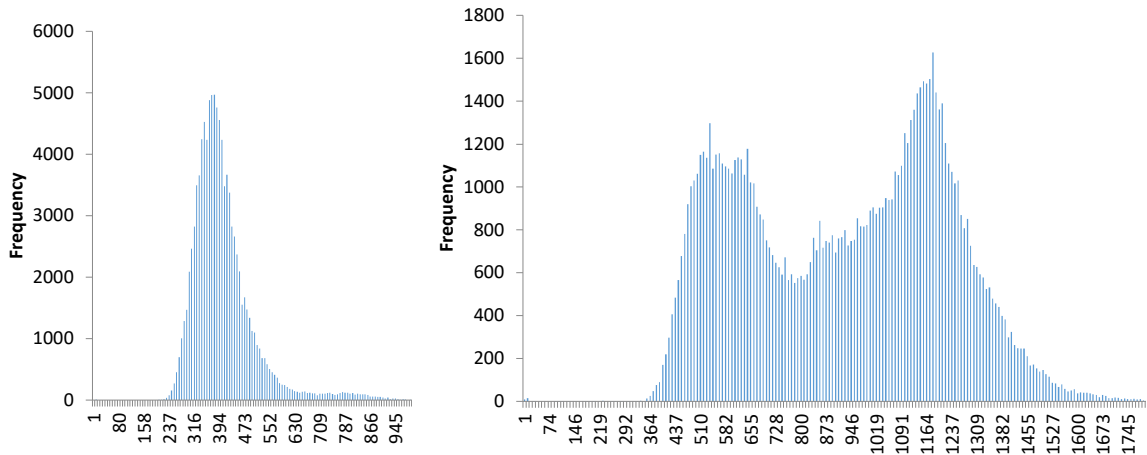


Рис. 4. Гистограмма наборов Telnet за 2021 и 2022 гг.

Fig. 4. Histogram of Telnet datasets for 2021 and 2022

The standard deviation for most data sets for 2022 has a significant increase compared to 2021, indicating an increase in the measure of uncertainty in the occurrence of various computer attacks. Using the risk comparison method described in [25] for the 2021 (V_1) and 2022 (V_2) samples, we calculate the R function for assessing risk changes:

$$R(V_1, V_2) = \frac{1}{N} * \sum_{i=1}^N K_i,$$

$$\text{where } K_i = \begin{cases} 1, & \text{if } \mu_{2i} > \mu_{1i} + 0,6745 * \sigma_{1i}, \\ 0, & \text{if } \mu_{1i} - 0,6745 * \sigma_{1i} \leq \mu_{2i} \leq \mu_{1i} + 0,6745 * \sigma_{1i}, \quad \mu_{ji} - \text{sample mean of } i\text{-th sample char-} \\ -1, & \text{if } \mu_{2i} < \mu_{1i} - 0,6745 * \sigma_{1i}; \end{cases}$$

acteristic V_j ; σ_{ji} – standard deviation of the sample V_j of the i -th sample characteristic.

Half of the studied indicators add up to 1, the rest add up to 0, resulting in $R(2021, 2022) = 0.5$. This can be interpreted as follows: the risk within the framework of the studied criteria as a whole in 2022 compared to 2021 increased significantly - by 50% of the indicators. When comparing March, 2021 and March, 2022 intervals, we get an R value of 0.43. Therefore, the proposed method makes it possible to compare risks both over long time intervals (a year) and over medium ones, provided there are sufficient samples.

Conclusion

The paper examined the risks of cyber attacks based on Internet traffic data from the network of the Krasnoyarsk Scientific Center SB RAS for 2021 and 2022. The cross-platform software for processing large volumes of data was developed, which had scaling capabilities through parallel processing and can perform data analysis in real time. Heuristic criteria for anomalous Internet traffic were formulated and formalized, signaling possible attacks on the network. Statistical indicators were calculated for the obtained data sets, based on them the conclusions were drawn about the shape of the distributions and the dynamics of attacks. The method proposed by the authors for comparing the risks of cyber threats for annual and monthly intervals was tested, which showed a similar increase in risks. Since the method does not depend on the time intervals and sample sizes being compared, it can be used in other areas in which groups of criteria for independent indicators exist. The next task is to expand the analysis criteria taking into account TCP connection flags and application level protocols, taking into ac-

count the logic of their operation. The developed software are planned to use while creating data sets for machine learning methods when solving problems of identifying cyber threats.

Библиографические ссылки

1. Shahid M. R., Blanc G., Zhang Z., and Debar H. IoT Devices Recognition Through Network Traffic Analysis // 2018 IEEE International Conference on Big Data (Big Data). 2018. P. 5187–5192.
2. Sairam R., Bhunia S. S., Thangavelu V., Gurusamy M. NETRA: Enhancing IoT security using NFV-based edge traffic analysis // IEEE Sensors Journal. 2019. No. 19(12). P. 4660–4671.
3. Towards Reproducible Network Traffic Analysis / J. Holland, P. Schmitt, P. Mittal, N. Feamster // arXiv preprint arXiv:2203.2022. 12410 p.
4. Alqudah N., Yaseen Q. Machine learning for traffic analysis: a review // Procedia Computer Science. 2020. Vol. 170. P. 911–916.
5. Abbasi M., Shahraki A., Taherkordi A. Deep learning for network traffic monitoring and analysis (NTMA): A survey // Computer Communications. 2021. Vol. 170. P. 19–41.
6. The dark side (-channel) of mobile devices: A survey on network traffic analysis / M. Conti, Q. Q. Li, A. Maragno, R. Spolaor // IEEE communications surveys & tutorials. 2018. No. 20(4). P. 2658–2713.
7. Robust smartphone app identification via encrypted network traffic analysis / V. F. Taylor, R. Spolaor, M. Conti, I. Martinovic // IEEE Transactions on Information Forensics and Security. 2017. Vol. 13(1). P. 63–78.
8. Goldstein M., Uchida S. A comparative evaluation of unsupervised anomaly detection algorithms for multivariate data // PloS one. 2016. Vol. 11(4). P.e0152173.
9. Garg R., Mukherjee S. A comparative study using supervised learning for anomaly detection in network traffic // Journal of Physics: Conference Series. 2022. Vol. 2161, No. 1. P. 012030.
10. Comparison of supervised, semi-supervised and unsupervised learning methods in network intrusion detection system (NIDS) application / N. S. Arunraj, R. Hable, M. Fernandes et al. // Anwendungen und Konzepte der Wirtschaftsinformatik. 2017. No. 6. P. 10–19.
11. Zhang P., Ma W., Qian S. Cluster analysis of day-to-day traffic data in networks // Transportation Research Part C: Emerging Technologies. 2022. Vol. 144. P. 103882.
12. Retracted: Traffic identification and traffic analysis based on support vector machine / W. Zhongsheng, W. Jianguo, Y. Sen, G. Jiaqiong // Concurrency and Computation: Practice and Experience. 2020. Vol. 32(2). P. e5292.
13. Malicious network traffic detection based on deep neural networks and association analysis / M. Gao, L. Ma, H. Liu et al. // Sensors. 2020. Vol. 20(5). P. 1452.
14. Vinayakumar R., Soman K. P., Poornachandran P. Evaluation of recurrent neural network and its variants for intrusion detection system (IDS) // International Journal of Information System Modeling and Design (IJISMD). 2017. Vol. 8(3). P. 43–63.
15. Comparing Malware Attack Detection using Machine Learning Techniques in IoT Network Traffic / Y. Z. Wei, M. Md-Arshad, A. A. Samad, N. Ithnin // International Journal of Innovative Computing. 2023. Vol. 13(1). P. 21–27.
16. Nie L., Jiang D., Lv Z. Modeling network traffic for traffic matrix estimation and anomaly detection based on Bayesian network in cloud computing networks // Annals of Telecommunications. 2017. Vol. 72. P. 297–305.
17. Landoll D. The security risk assessment handbook: A complete guide for performing security risk assessments // CRC Press. 2021.
18. Macek D., Magdalenic I., Redep N. B. A systematic literature review on the application of multicriteria decision making methods for information security risk assessment // International Journal of Safety and Security Engineering. 2020. Vol. 10, No. 2. P. 161–174.

19. Jouini M., Rabai L. B. A. Comparative study of information security risk assessment models for cloud computing systems // *Procedia Computer Science*. 2016. Vol. 83. P. 1084–1089.
20. Haji S., Tan Q., Costa R. S. A hybrid model for information security risk assessment // *Int. j. adv. trends comput. sci. eng.* 2019. ART-2019-111611.
21. Summary of research on IT network and industrial control network security assessment / L. Hu, H. Li, Z. Wei et al. // 2019 IEEE 3rd information technology, networking, electronic and automation control conference (ITNEC). 2019. P. 1203–1210.
22. A review of cyber security risk assessment methods for SCADA systems / Y. Cherdantseva, P. Burnap, A. Blyth et al. // *Computers & security*. 2016. Vol. 56. P. 1–27.
23. Mahak M., Singh Y. Threat modelling and risk assessment in internet of things: A review // *Proceedings of Second International Conference on Computing, Communications, and Cyber-Security: IC4S 2020*, 2021. Springer Singapore. P. 293–305.
24. Lyu X., Ding Y., Yang S. H. Safety and security risk assessment in cyber-physical systems // *IET Cyber-Physical Systems: Theory & Applications*, 2019. Vol. 4(3). P. 221–232.
25. Исаев С. В., Кононов Д. Д. Исследование динамики и классификация атак на веб-сервисы корпоративной сети // *Сибирский аэрокосмический журнал*. 2022. Т. 23, № 4. С. 593–600.

References

1. Shahid M. R., Blanc G., Zhang Z., Debar H. IoT Devices Recognition Through Network Traffic Analysis. *2018 IEEE International Conference on Big Data (Big Data)*. 2018, P. 5187–5192.
2. Sairam R., Bhunia S. S., Thangavelu V., Gurusamy M. NETRA: Enhancing IoT security using NFV-based edge traffic analysis. *IEEE Sensors Journal*. 2019, Vol. 19(12), P. 4660–4671.
3. Holland J., Schmitt P., Mittal P., Feamster N. Towards Reproducible Network Traffic Analysis. *arXiv preprint arXiv:2203.2022*, P. 12410.
4. Alqudah N., Yaseen Q. Machine learning for traffic analysis: a review. *Procedia Computer Science*. 2020, Vol. 170, P. 911–916.
5. Abbasi M., Shahraki A., and Taherkordi A. Deep learning for network traffic monitoring and analysis (NTMA): A survey. *Computer Communications*. 2021, Vol. 170, P. 19–41.
6. Conti M., Li Q. Q., Maragno A., Spolaor R. The dark side (-channel) of mobile devices: A survey on network traffic analysis. *IEEE communications surveys & tutorials*. 2018, Vol. 20(4), P. 2658–2713.
7. Taylor V. F., Spolaor R., Conti M., Martinovic I. Robust smartphone app identification via encrypted network traffic analysis. *IEEE Transactions on Information Forensics and Security*. 2017, Vol. 13(1), P. 63–78.
8. Goldstein M., and Uchida S. A comparative evaluation of unsupervised anomaly detection algorithms for multivariate data. *PloS one*. 2016, Vol. 11(4), P. e0152173.
9. Garg R., Mukherjee S. A comparative study using supervised learning for anomaly detection in network traffic. *Journal of Physics: Conference Series*. 2022, Vol. 2161, No. 1, P. 012030.
10. Arunraj N. S., Hable R., Fernandes M., Leidl K., Heigl M. Comparison of supervised, semi-supervised and unsupervised learning methods in network intrusion detection system (NIDS) application. *Anwendungen und Konzepte der Wirtschaftsinformatik*. 2017, No. 6, P. 10–19.
11. Zhang P., Ma W., Qian S. Cluster analysis of day-to-day traffic data in networks. *Transportation Research Part C: Emerging Technologies*. 2022, Vol. 144, P. 103882.
12. Zhongsheng W., Jianguo W., Sen Y., Jiaqiong G. Retracted: Traffic identification and traffic analysis based on support vector machine. *Concurrency and Computation: Practice and Experience*. 2020, Vol. 32(2), P. e5292.
13. Gao M., Ma L., Liu H., Zhang Z., Ning Z., Xu J. Malicious network traffic detection based on deep neural networks and association analysis. *Sensors*. 2020, Vol. 20(5), P. 1452.

14. Vinayakumar R., Soman K. P., Poornachandran P. Evaluation of recurrent neural network and its variants for intrusion detection system (IDS). *International Journal of Information System Modeling and Design (IJISMD)*. 2017, Vol. 8(3), P. 43–63.
15. Wei Y. Z., Md-Arshad M., Samad A. A., Ithnin N. Comparing Malware Attack Detection using Machine Learning Techniques in IoT Network Traffic. *International Journal of Innovative Computing*. 2023, Vol. 13(1), P. 21–27.
16. Nie L., Jiang D., Lv Z. Modeling network traffic for traffic matrix estimation and anomaly detection based on Bayesian network in cloud computing networks. *Annals of Telecommunications*. 2017, Vol. 72, P. 297–305.
17. Landoll D. The security risk assessment handbook: A complete guide for performing security risk assessments. *CRC Press*, 2021.
18. Macek D., Magdalenic I., Redep N. B. A systematic literature review on the application of multicriteria decision making methods for information security risk assessment. *International Journal of Safety and Security Engineering*. 2020, Vol. 10, No. 2, P. 161–174.
19. Jouini M., Rabai L. B. A. Comparative study of information security risk assessment models for cloud computing systems. *Procedia Computer Science*. 2016, 83, P. 1084–1089.
20. Haji S., Tan Q., Costa R.S. A hybrid model for information security risk assessment. *Int. j. adv. trends comput. sci. eng.* 2019, ART-2019-111611.
21. Hu L., Li H., Wei Z., Dong S., Zhang Z. Summary of research on IT network and industrial control network security assessment. *2019 IEEE 3rd information technology, networking, electronic and automation control conference (ITNEC)*. 2019, P. 1203–1210.
22. Cherdantseva Y., Burnap P., Blyth A., Eden P., Jones K., Soulsby H., Stoddart K. A review of cyber security risk assessment methods for SCADA systems. *Computers & security*. 2016, Vol. 56, P. 1–27.
23. Mahak M., Singh Y. Threat modelling and risk assessment in internet of things: A review. *Proceedings of Second International Conference on Computing, Communications, and Cyber-Security: IC4S 2020*. 2021, Springer Singapore, P. 293–305.
24. Lyu X., Ding Y., Yang S. H. Safety and security risk assessment in cyber-physical systems. *IET Cyber-Physical Systems: Theory & Applications*. 2019, Vol. 4(3), P. 221–232.
25. Isaev S. V., Kononov D. D. A study of dynamics and classification of attacks on corporate network web services. *Siberian Aerospace Journal*. 2022, Vol. 23, No. 4, P. 593–601.

© Kononov D. D., Isaev S. V., 2023

Кононов Дмитрий Дмитриевич – научный сотрудник; Институт вычислительного моделирования СО РАН. E-mail: ddk@icm.krasn.ru.

Исаев Сергей Владиславович – кандидат технических наук, доцент, заведующий отделом информационно-телекоммуникационных технологий; Институт вычислительного моделирования СО РАН. E-mail: si@icm.krasn.ru.

Kononov Dmitry Dmitrievich – scientific researcher; Institute of Computational Modelling SB RAS. E-mail: ddk@icm.krasn.ru.

Isaev Sergey Vladislavovich – Cand. Sc., associate professor, head of the Department of Information and Telecommunication Technologies; Institute of Computational Modelling SB RAS. E-mail: si@icm.krasn.ru.

УДК 519.6

Doi: 10.31772/2712-8970-2023-24-4-673-680

Для цитирования: Кузнецов А. А., Кузнецова А. С., Кишкан В. В. Алгоритм быстрого умножения элементов в 2-группах на основе полиномов Жегалкина // Сибирский аэрокосмический журнал. 2023. Т. 24, № 4. С. 673–680. Doi: 10.31772/2712-8970-2023-24-4-673-680.

For citation: Kuznetsov A. A., Kuznetsova A. S., Kishkan V. V. [An algorithm for fast multiplication of elements in 2-groups based on the Zhegalkin polynomials]. *Siberian Aerospace Journal*. 2023, Vol. 24, No. 4, P. 673–680. Doi: 10.31772/2712-8970-2023-24-4-673-680.

Алгоритм быстрого умножения элементов в 2-группах на основе полиномов Жегалкина

А. А. Кузнецов*, А. С. Кузнецова, В. В. Кишкан

Сибирский государственный университет науки и технологий имени академика М. Ф. Решетнева
Российская Федерация, 660037, г. Красноярск, просп. им. газ. «Красноярский Рабочий», 31

*E-mail: alex_kuznetsov80@mail.ru

Проектирование сети многопроцессорной вычислительной системы или дата-центра представляет собой важную проблему, в рамках которой осуществляется поиск моделей графов, обладающих привлекательными топологическими свойствами и позволяющих применять эффективные алгоритмы маршрутизации. Указанными свойствами, в частности такими, как высокая симметрия, иерархическая структура, рекурсивная конструкция, высокая связность и отказоустойчивость, обладают графы Кэли. Например, такие базовые топологии сети, как «кольцо», «гиперкуб» и «тор», являются графами Кэли.

Определение графа Кэли подразумевает, что вершины графа являются элементами некоторой алгебраической группы. Выбор группы и ее порождающих элементов позволяет получить граф, отвечающий необходимым требованиям по диаметру, степени вершин, количеству узлов и т. д. Решению данной задачи посвящено большое количество научных статей и монографий.

Для исследования графов Кэли, в первую очередь, необходимо разработать быстрые алгоритмы умножения элементов в данных группах. Такие алгоритмы помогают осуществлять эффективную маршрутизацию на соответствующих графах Кэли.

Цель настоящей работы – создать алгоритм быстрого умножения элементов в конечных 2-группах, т. е. в группах периода 2^n .

В первом разделе статьи дано теоретическое обоснование алгоритма. Показано, что элементы данных групп могут быть представлены в виде битовых строк, а их умножение осуществляется на основе полиномов Жегалкина.

Во втором разделе представлен псевдокод алгоритма, на основе которого вычисляются полиномы Жегалкина. На первом этапе алгоритма вычисляется rs -представление группы, на основе которого получают полиномы Холла. На заключительном этапе полиномы Холла преобразуются в полиномы Жегалкина.

В третьем разделе продемонстрирован пример получения полиномов Жегалкина для двупорожденной группы периода 4.

В заключении рассматриваются перспективы применения алгоритма на реальных вычислительных устройствах. Отмечается, что предложенное представление элементов группы в форме битовых векторов позволяет применять их даже на самых примитивных микроконтроллерах.

Ключевые слова: 2-группа, граф Кэли, полином Жегалкина.

An algorithm for fast multiplication of elements in 2-groups based on the Zhegalkin polynomials

A. A. Kuznetsov*, A. S. Kuznetsova, V. V. Kishkan

Reshetnev Siberian State University of Science and Technology
31, Krasnoyarskii Rabochii prospekt, Krasnoyarsk, 660037, Russian Federation

*E-mail: alex_kuznetsov80@mail.ru

Network design for a multiprocessor computing system or data center is an important problem where the search for graph models that have attractive topological properties and allow the use of efficient routing algorithms is carried out. Cayley graphs have the indicated properties, in particular such as high symmetry, hierarchical structure, recursive design, high connectivity and fault tolerance.

The definition of the Cayley graph implies that the vertices of the graph are elements of some algebraic group. Selecting a group and its generating elements allows us to obtain a graph that meets the necessary requirements for diameter, degree of vertices, number of nodes, etc. A large number of scientific articles and monographs are devoted to solving this problem.

The goal of this work is to create an algorithm for fast multiplication of elements in finite 2-groups whose exponent is 2^n .

The first section of the article provides a theoretical justification for the algorithm for fast multiplication in finite 2-groups. It is shown that elements of these groups can be represented in the form of bit strings, and their multiplication is carried out based on the Zhegalkin polynomials.

The second section presents the pseudocode of the algorithm on the basis of which the Zhegalkin polynomials are calculated.

The third section demonstrates an example of obtaining the Zhegalkin polynomials for a two-generated group of exponent 4.

In conclusion, the prospects for using the algorithm on the real hardware are discussed.

Keywords: 2-group, the Cayley graph, the Zhegalkin polynomial.

Introduction

Designing a network of a multiprocessor computing system (MCS) or a data center is an important problem in which graph models are searched for that have attractive topological properties and allow the use of effective routing algorithms. Cayley graphs possess these properties, in particular such as high symmetry, hierarchical structure, recursive construction, high connectivity and fault tolerance [1]. For example, such basic network topologies as "ring", "hypercube" and "torus" are Cayley graphs.

The definition of a Cayley graph implies that the vertices of the graph are elements of some algebraic group. The choice of the group and its generating elements allows us to obtain a graph [2] that meets the necessary requirements in diameter, degree of vertices, number of nodes, etc. A large number of scientific articles and monographs have been devoted to solving this problem, among which we highlight the works [3–15].

As it was said, one of the widely used MCS topologies is the k -dimensional hypercube. This graph is given by the k -generated Burnside group of exponent 2. This group has a simple structure and is equal to the direct product of k instances of a cyclic 2-group. A generalization of the hypercube is an n -dimensional torus, which is generated by the direct multiplication of n instances of cyclic subgroups whose orders may not coincide. In articles [16–19], Cayley graphs of Burnside groups of exponents 3, 4, 5 and 7 are studied.

To study Cayley graphs generated by groups of higher exponents, first of all, it is necessary to develop fast algorithms for multiplying elements in these groups. Such algorithms help to implement efficient routing on the corresponding Cayley graphs.

The purpose of this work is to create an algorithm for fast multiplication of elements in finite 2-groups, i.e. in groups of exponent 2^n .

The first section of the article provides a theoretical justification for the algorithm of fast multiplication in finite 2-groups. It is shown that the elements of these groups can be represented as bit strings, and their multiplication is carried out on the basis of Zhegalkin polynomials.

The second section presents the pseudocode of the algorithm on the basis of which the Zhegalkin polynomials are calculated.

In the third section, an example of obtaining Zhegalkin polynomials for a two-generated group of exponent 4 is demonstrated.

In conclusion, the prospects of using the algorithm on real computing devices are considered.

1. Proof of the main result

The theorem. *Let G be an arbitrary finite group 2-a group whose order is equal to 2^n . Then the following statements will be true:*

1. $\forall x \in G \Rightarrow x = (x_1, \dots, x_n) \in \mathbb{Z}_2^n$.
2. $\forall x, y, z \in G: x \cdot y = z \Rightarrow z_i = f_i(x, y) \in \mathbb{Z}_2$, where $f_i(x, y)$ are some Zhegalkin polynomials.

Proof. Any finite 2-group G has a pc-presentation (power commutator presentation [3; 4]):

$$G = \{a_1, \dots, a_n \mid a_i^2 = v_{ii}, 1 \leq i \leq n, [a_k, a_j] = v_{jk}, 1 \leq j < k \leq n\},$$

where the word v_{jk} at is $1 \leq j \leq k \leq n$ expressed in terms of as a_{k+1}, \dots, a_n follows:

$$v_{jk} = a_{k+1}^{x_{k+1}} \dots a_n^{x_n}, x_i \in \mathbb{Z}_2.$$

In this case

$$\forall x \in G \Rightarrow x = a_1^{x_1} \dots a_n^{x_n}, x_i \in \mathbb{Z}_2.$$

Each element of the group x is uniquely defined in terms of degrees x_1, \dots, x_n , so we can write the elements of the group as follows:

$$\forall x \in G \Rightarrow x = (x_1, \dots, x_n) \in \mathbb{Z}_2^n.$$

Thus, we can naturally represent the elements of the group in the form of Boolean (bit) vectors of dimension n .

Let $x = (x_1, \dots, x_n)$ and $y = (y_1, \dots, y_n)$ be two arbitrary elements of the group G , consider their multiplication $x \cdot y = z = (z_1, \dots, z_n)$.

The calculation of degrees is z_i traditionally carried out on the basis of the collective Hall process [3; 4]. However, there is a more efficient way to multiply elements based on Hall polynomials [20]. In this case

$$z_i = x_i + y_i + p_i(x_1, \dots, x_{i-1}, y_1, \dots, y_{i-1}), x_i, y_i, z_i \in \mathbb{Z}_2.$$

Note that the multiplication and addition operations in the field are \mathbb{Z}_2 identical to the Boolean operations "and", as well as the exclusive "or", respectively. By performing the specified substitution of operations in Hall polynomials, we obtain Zhegalkin polynomials [21]. Thus,

$$\forall x, y, z \in G: x \cdot y = z \Rightarrow z_i = f_i(x, y) \in \mathbb{Z}_2,$$

where $f_i(x, y)$ are some Zhegalkin polynomials.

2. Algorithm for calculating Zhegalkin polynomials

In this section, we consider an algorithm for calculating Zhegalkin polynomials for a finite 2-group G . The input algorithm knows such parameters of the group as the number of generating

elements, the order of G and its exponent. Also, the nilpotence level of the group may appear as an input data.

The pseudocode of the algorithm is shown below.

Input: G – finite group 2-group G

Output: Zhegalkin polynomials for group G

1. $pc = pq(G)$ – we calculate the pc-presentation of the group using the p -quotient algorithm [3, 4].

Note that this algorithm has already been implemented in computer algebra systems such as GAP and Magma.

2. $H = \text{Hall}(pc)$ – based on the pc-presentation, we calculate the Hall polynomials using the algorithm from [22].

3. $F = \text{Zhegalkin}(H)$ – we obtain Zhegalkin polynomials from Hall polynomials by replacing the multiplication and summing operations in the field with \mathbb{Z}_2 identical Boolean operations "and", as well as the exclusive "or", respectively.

3. An example

As an example, consider the maximum two - generated finite $G = \langle a_1, a_2 \rangle$ period group $2^2 = 4$, which is usually denoted by $B(2,4)$ or $B_2(4)$. The order of this group is equal 2^{12} , and for each element of G there is a unique pc-presentation of the form $a_1^{x_1} \dots a_{12}^{x_{12}}$, where $x_i \in \mathbb{Z}_2$, $i = 1, 2, \dots, 12$. Here a_1 and a_2 are the generating elements G , a_3, \dots, a_{12} calculated recursively through a_1 and a_2 .

We obtain a GAP pc-presentation of this group in the computer algebra system.

For brevity, trivial commutator relations are not given (for example, such as $[a_4, a_1] = 1$, etc.).

$a_1^2 = a_4$, $a_2^2 = a_5$, $a_3^2 = a_8 a_9 a_{10} a_{11} a_{12}$, $a_4^2 = 1$, $a_5^2 = 1$, $a_6^2 = a_{11}$, $a_7^2 = a_{11} a_{12}$, $a_i^2 = 1$ ($8 \leq i \leq 12$),
 $[a_3, a_1] = a_6$, $[a_3, a_2] = a_7$, $[a_4, a_2] = a_6 a_8 a_9 a_{10} a_{12}$, $[a_4, a_3] = a_8 a_{11}$, $[a_5, a_1] = a_7 a_8 a_9 a_{10}$,
 $[a_5, a_3] = a_{10} a_{11} a_{12}$, $[a_5, a_4] = a_9 a_{11}$, $[a_6, a_1] = a_8$, $[a_6, a_2] = a_9$, $[a_6, a_3] = a_{11}$, $[a_6, a_4] = a_{11}$,
 $[a_6, a_5] = a_{11}$, $[a_7, a_1] = a_9 a_{12}$, $[a_7, a_2] = a_{10}$, $[a_7, a_3] = a_{11} a_{12}$, $[a_7, a_4] = a_{11} a_{12}$, $[a_7, a_5] = a_{11} a_{12}$,
 $[a_8, a_1] = a_{11}$, $[a_8, a_2] = a_{12}$, $[a_9, a_1] = a_{11} a_{12}$, $[a_9, a_2] = a_{11}$, $[a_{10}, a_1] = a_{12}$, $[a_{10}, a_2] = a_{11} a_{12}$.

Calculate the Hall polynomials of group G for generating elements a_1 and a_2 based on the algorithm from [22]:

1) $a_1 \cdot a_1^{y_1} \dots a_{12}^{y_{12}} = a_1^{z_1} \dots a_{12}^{z_{12}}$, where

- $z_1 = y_1 + 1$,
- $z_2 = y_2$,
- $z_3 = y_3$,
- $z_4 = y_1 + y_4$,
- $z_5 = y_5$,
- $z_6 = y_6 + y_1 y_2$,
- $z_7 = y_7$,
- $z_8 = y_8 + y_1 y_2 + y_1 y_3$,
- $z_9 = y_9 + y_1 y_2$,
- $z_{10} = y_{10} + y_1 y_2$,
- $z_{11} = y_{11} + y_1 y_3 + y_1 y_2 y_3 + y_1 y_2 y_4 + y_1 y_2 y_5 + y_1 y_2 y_6$,
- $z_{12} = y_{12} + y_1 y_2$;

2) $a_2 \cdot a_1^{y_1} \dots a_{12}^{y_{12}} = a_1^{z_1} \dots a_{12}^{z_{12}}$, where

$$z_1 = y_1,$$

$$z_2 = y_2 + 1,$$

$$z_3 = y_1 + y_3,$$

$$z_4 = y_4,$$

$$z_5 = y_2 + y_5,$$

$$z_6 = y_6,$$

$$z_7 = y_7 + y_1 y_2,$$

$$z_8 = y_8 + y_1 y_3,$$

$$z_9 = y_9 + y_1 y_3 + y_2 y_4,$$

$$z_{10} = y_{10} + y_1 y_2 + y_1 y_3 + y_2 y_3,$$

$$z_{11} = y_{11} + y_1 y_2 + y_1 y_3 + y_2 y_3 + y_2 y_4 + y_1 y_2 y_3 + y_1 y_2 y_4 + y_1 y_2 y_5 + y_1 y_2 y_7,$$

$$z_{12} = y_{12} + y_1 y_2 + y_1 y_3 + y_2 y_3 + y_1 y_2 y_3 + y_1 y_2 y_4 + y_1 y_2 y_5 + y_1 y_2 y_7.$$

Replace the multiplication and summing operations with the Boolean operations "and", as well as the exclusive "or", respectively. As a result, we obtain the Zhegalkin polynomials.

Each element of the group is a bit string $(z_1, z_2, \dots, z_{12})$. Thus, it will $B(2, 4)$ take 12 bits to encode one element in. In general, if the order of the group is equal 2^n , then it will take n bits to store one element.

Conclusion

In conclusion, we say that in tasks requiring the calculation of a large number of multiplications of group elements, the method described in this paper will dramatically reduce the running time of computer programs. For example, one of these problems is the task of finding the shortest routes on Cayley graphs, which are often used in the design of topologies for interprocessor connection networks in supercomputers, as well as data centers.

In addition, it should be noted that the proposed presentation of the group elements in the form of bit vectors allows them to be used even on the most primitive microcontrollers.

Библиографические ссылки

1. Heydemann M. Cayley graphs and interconnection networks, in Graph symmetry: algebraic methods and applications (Editors: Hahn and Sabidussi) // Dordrecht: Kluwer Academic Publishers. 1997. P. 167–226.
2. Loz E. New record graphs in the degree-diameter problem // Australasian Journal of Combinatorics. 2008. Vol. 41. P. 63–80.
3. Sims C. Computation with Finitely Presented Groups. Cambridge: Cambridge University Press, 1994. 628 p.
4. Holt D., Eick B., O'Brien E. Handbook of computational group theory. Boca Raton: Chapman & Hall/CRC Press, 2005. 514 p.
5. Schibell S., Stafford R. Processor interconnection networks and Cayley graphs // Discrete Applied Mathematics. 1992. Vol. 40. P. 337–357.
6. Stamoulis G., Tsitsiklis J. Efficient routing Scheme for Multiple Broadcasts in Hypercubes // IEEE Trans. on Parallel and Distributed Systems. 1993. Vol. 4(7). P. 725–739.

7. Stamoulis G., Tsitsiklis J. The Efficiency of Greedy Routing in Hypercubes and Butterflies // IEEE Transaction on Communication. 1994. Vol. 42(11). P. 3051–3061.
8. Kiasari A., Sarbazi-Azad H. Analytic performance comparison of hypercubes and star graphs with implementation constraints // Journal of Computer and System Sciences. 2008. No. 6. P. 1000–1012.
9. Akers S., Krishnamurthy B. A group theoretic model for symmetric interconnection networks // Proceedings of the International Conference on Parallel Processing. 1986. P. 216–223.
10. Tang K., Arden B. Vertex-transitivity and routing for Cayley graphs in GCR representations // Proceedings of ACM Symposium on Applied Computing SAC. 1992. P. 1180–1187.
11. Wang L., Tang K. Topology-Based Routing for Xmesh in Wireless Sensor Networks // Lecture Notes in Electrical Engineering. 2009. Vol. 44. P. 229–239.
12. Ryu J., Noel E., Tang K. Fault-tolerant Routing on Borel Cayley Graph // IEEE ICC Next Generation Networking Symposium. 2012. P. 2872–2877.
13. On the feasibility of completely wireless datacenters / J. Shin, E. Sirer, H. Weatherspoon, D. Kirovski // IEEE/ACM Transaction On Networking. 2013. Vol. 21(5). P. 1666–1679.
14. Кузнецов А. А., Кузнецова А. С. Параллельный алгоритм для исследования графов Кэли групп подстановок // Вестник СибГАУ. 2014. № 1(53). С. 34–39.
15. Efficient Routing in Data Center with Underlying Cayley Graph / M. Camelo, D. Papadimitriou, L. Fabrega, P. Vila // Proceedings of the 5th Workshop on Complex Networks CompleNet. 2014. P. 189–197.
16. Кузнецов А. А. Графы Кэли бернсайдовых групп периода 3 // Сибирские электронные математические известия. 2015. Т. 12. С. 248–254.
17. Кузнецов А. А., Кузнецова А. С. Перспективные топологии многопроцессорных вычислительных систем, основанные на графах Кэли, заданных группами периода 4 // Вестник СибГАУ. 2016. № 3(17). С. 575–578.
18. Кузнецов А. А. Об одном алгоритме вычисления функций роста в конечных двупорожденных группах периода пять // Прикладная дискретная математика. 2016. № 3(33). С. 116–125.
19. Kuznetsov A. A., Kishkan V. V. The Cayley graphs of finite two-generator burnside groups of exponent 7 // Siberian Journal of Science and Technology. 2018. № 2. P. 217–222.
20. Hall P. Nilpotent groups, Notes of lectures given at the Canadian Mathematical Congress 1957 Summer Seminar, in The collected works of Philip Hall. Oxford: Clarendon Press, 1988. P. 415–462.
21. Яблонский С. В. Введение в дискретную математику. М. : Наука, 1986. 384 с.
22. Кузнецов А. А., Кузнецова А. С. Быстрое умножение элементов в конечных двупорожденных группах периода пять // Прикладная дискретная математика. 2013. № 1 (18). С. 110–116.

References

1. Heydemann M. Cayley graphs and interconnection networks, in Graph symmetry: algebraic methods and applications (Editors: Hahnand Sabidussi). Dordrecht: Kluwer Academic Publishers. 1997, P. 167–226.
2. Loz E. New record graphs in the degree-diameter problem. Australasian Journal of Combinatorics. 2008, Vol. 41, P.63–80.
3. Sims C. Computation with Finitely Presented Groups. Cambridge: Cambridge University Press, 1994, 628 p.
4. Holt D., Eick B., O'Brien E. Handbook of computational group theory. Boca Raton: Chapman & Hall/CRC Press, 2005, 514 p.
5. Schibell S., Stafford R. Processor interconnection networks and Cayley graphs. Discrete Applied Mathematics. 1992, Vol. 40, P. 337–357.

6. Stamoulis G., Tsitsiklis J. Efficient routing Scheme for Multiple Broadcasts in Hypercubes. *IEEE Trans. on Parallel and Distributed Systems*. 1993, Vol. 4(7), P. 725–739.
7. Stamoulis G., Tsitsiklis J. The Efficiency of Greedy Routing in Hypercubes and Butteries. *IEEE Transaction on Communication*. 1994, Vol. 42(11), P. 3051–3061.
8. Kiasari A., Sarbazi-Azad H. Analytic performance comparison of hypercubes and star graphs with implementation constraints. *Journal of Computer and System Sciences*. 2008, No. 6, P. 1000–1012.
9. Akers S., Krishnamurthy B. A group theoretic model for symmetric interconnection networks. *Proceedings of the International Conference on Parallel Processing*. 1986, P. 216–223.
10. Tang K., Arden B. Vertex-transitivity and routing for Cayley graphs in GCR representations. *Proceedings of ACM Symposium on Applied Computing SAC*. 1992, P. 1180–1187.
11. Wang L., Tang K. Topology-Based Routing for Xmesh in Wireless Sensor Networks. *Lecture Notes in Electrical Engineering*. 2009. Vol.44. P. 229–239.
12. Ryu J., Noel E., and Tang K. Fault-tolerant Routing on Borel Cayley Graph // *IEEE ICC Next Generation Networking Symposium*. 2012, P. 2872–2877.
13. Shin J., Simer E., Weatherspoon H., Kirovski D. On the feasibility of completely wireless datacenters. *EEE/ACM Transaction On Networking*. 2013, Vol. 21(5), P. 1666–1679.
14. Kuznetsov A. A., Kuznetsova A. S. [A parallel algorithm for study of the Cayley graphs of permutation groups]. *Vestnik SibGAU*. 2014, No. 1(53), P. 34–39 (In Russ.).
15. Camelo M., Papadimitriou D., Fabrega L., Vila P. Efficient Routing in Data Center with Underlying Cayley Graph. *Proceedings of the 5th Workshop on Complex Networks CompleNet*. 2014. P. 189–197.
16. Kuznetsov A. A. [The Cayley graphs of Burnside groups of exponent 3]. *Siberian Electronic Mathematical Reports*. 2015, Vol. 12, P. 248–254 (In Russ.).
17. Kuznetsov A. A., Kuznetsova A. S. [Perspective topologies of multiprocessor computing systems based on the Cayley graphs of groups of period 4]. *Vestnik SibGAU*. 2016, No. 3 (17), P. 575–578 (In Russ.).
18. Kuznetsov A. A. [An algorithm of computation of the growth functions in finite two-generated groups of exponent five]. *Prikladnaya Diskretnaya Matematika*. 2016, No. 3 (33), P. 116–125 (In Russ.).
19. Kuznetsov A. A., Kishkan V. V. The Cayley graphs of finite two-generator burnside groups of exponent 7. *Siberian Journal of Science and Technology*. 2018. No. 2, P. 217–222 (In Russ.).
20. Hall P. Nilpotent groups, Notes of lectures given at the Canadian Mathematical Congress 1957 Summer Seminar, in The collected works of Philip Hall. Oxford: Clarendon Press, 1988. P. 415–462.
21. Yablonsky S. V. *Vvedeniye v diskretnuyu matematiku* [Introduction to discrete mathematics]. Moscow, Nauka Publ., 1989, 384 p.
22. Kuznetsov A. A., Kuznetsova A. S. [Fast multiplication in finite two-generated groups of exponent five]. *Prikladnaya Diskretnaya Matematika*. 2013, No. 1 (18), P. 110–1116 (In Russ.).

© Kuznetsov A. A., Kuznetsova A. S., Kishkan V. V., 2023

Кузнецов Александр Алексеевич – доктор физико-математических наук, профессор, директор НОЦ «Институт космических исследований и высоких технологий»; Сибирский государственный университет науки и технологий имени академика М. Ф. Решетнева. E-mail: alex_kuznetsov80@mail.ru.

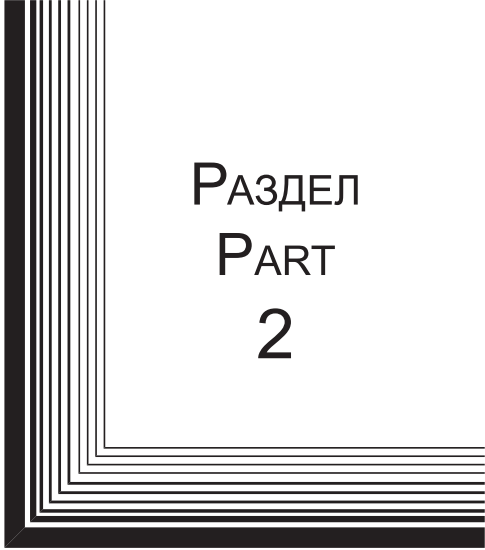
Кузнецова Александра Сергеевна – кандидат физико-математических наук, доцент кафедры прикладной математики; Сибирский государственный университет науки и технологий имени академика М. Ф. Решетнева. E-mail: alexakuznetsova85@gmail.com.

Кишкан Владимир Владимирович – кандидат физико-математических наук, доцент кафедры информатики и вычислительной техники; Сибирский государственный университет науки и технологий имени академика М. Ф. Решетнева. E-mail: kishkan@mail.ru.


Kuznetsov Alexander Alexeevich – Dr. Sc., Professor, Head of Institute of Space Research and High Technologies; Reshetnev Siberian State University of Science and Technology. E-mail: alex_kuznetsov80@mail.ru.

Kuznetsova Alexandra Sergeevna – Cand. Sc., Associate Professor of the Department of Applied Mathematics; Reshetnev Siberian State University of Science and Technology. E-mail: alexakuznetsova85@gmail.com.

Kishkan Vladimir Vladimirovich – Cand. Sc., Associate Professor of the Department of Informatics and Computer Science; Reshetnev Siberian State University of Science and Technology. E-mail: kishkan@mail.ru.



РАЗДЕЛ
PART
2



АВИАЦИОННАЯ
И РАКЕТНО-
КОСМИЧЕСКАЯ ТЕХНИКА

AVIATION
AND SPACECRAFT
ENGINEERING



УДК 621.454

Doi: 10.31772/2712-8970-2023-24-4-682-696

Для цитирования: Акбулатов Э. Ш., Назаров В. П., Герасимов Е. В. Исследование характеристик ракетного двигателя малой тяги, изготовленного методом аддитивной SLM-технологии // Сибирский аэрокосмический журнал. 2023. Т. 24, № 4. С. 682–696. Doi: 10.31772/2712-8970-2023-24-4-682-696.

For citation: Akbulatov E. Sh., Nazarov V. P., Gerasimov E. V. [Characteristics research of a low thrust rocket engine manufactured using additive SLM technology]. *Siberian Aerospace Journal*. 2023, Vol. 24, No. 4, P. 682–696. Doi: 10.31772/2712-8970-2023-24-4-682-696.

Исследование характеристик ракетного двигателя малой тяги, изготовленного методом аддитивной SLM-технологии

Э. Ш. Акбулатов¹, В. П. Назаров^{1*}, Е. В. Герасимов²

¹Сибирский государственный университет науки и технологий имени академика М. Ф. Решетнева
Российская Федерация, 660037, г. Красноярск, просп. им. газ. «Красноярский Рабочий», 31

²ООО «Полихром»

Российская Федерация, 660049, г. Красноярск, ул. Дубровинского, 58

*E-mail: nazarov@sibsau.ru

Развитие и совершенствование ракетно-космической техники в значительной степени обусловлено применением производственных технологий, обеспечивающих изготовление изделий с высокими характеристиками надежности и энергетической эффективности при одновременном снижении показателей материалоемкости и уменьшении длительности производственного цикла. К таким прогрессивным технологиям следует отнести аддитивные технологии, физическая сущность которых заключается в получении деталей методом послойного плавления материала на основе компьютерной 3D-модели изделия в камере специального 3D-принтера, оснащенного лазерным устройством. Применение аддитивных технологий в ракетном двигателестроении требует проведения большого объема научно-исследовательских и экспериментальных работ для подтверждения соответствия нормативным критериям и правилам, установленным в отрасли, а также обязательной сертификации на государственном уровне. В соответствии с программой приоритетных научно-исследовательских работ, в СибГУ им. М. Ф. Решетнева совместно с промышленным партнером ООО «Полихром» проводится комплекс экспериментальных работ по апробации и отработке режимов 3D-печати образца камеры-демонстратора ракетного двигателя малой тяги (РДМТ).

Разработана конструкция РДМТ, работающего на экологически безопасных газообразных компонентах топлива, адаптированная для 3D-печати на принтере ASTRA 420. Рассмотрены параметры и характеристики принтера. Приведена последовательность экспериментальных работ по подбору режимов печати корпуса камеры и смесительной головки. Установлена принципиальная возможность корректировки режимов лазерного плавления материала и формообразования детали.

Представлены основные технологические этапы послепечатной обработки деталей камеры РДМТ. Дано описание оборудования для термообработки и электрохимического полирования деталей. Изложена последовательность исследования структуры материала, приведены результаты металлографического и рентгенографического анализа внутреннего состояния металла.

Показано значение стендовых испытаний ракетных двигателей при разработке инновационных конструктивных решений и внедрении инновационных технологий производства. Представлено описание и состав систем испытательного стенда СибГУ им. М. Ф. Решетнева. Результаты стендовых огневых испытаний свидетельствуют о принципиальной возможности изготовления РДМТ методом аддитивных технологий селективного лазерного плавления из жаростойких легированных сплавов.

Ключевые слова: аддитивные технологии, ракетный двигатель малой тяги, Инконель 718, послепечатная обработка, виброиспытания, испытания на прочность и герметичность, стендовые огневые испытания.

Characteristics research of a low thrust rocket engine manufactured using additive SLM technology

E. Sh. Akbulatov¹, V. P. Nazarov^{1*}, E. V. Gerasimov²

¹Reshetnev Siberian State University of Science and Technology
31, Krasnoyarskii Rabochii prospekt, Krasnoyarsk, 660037, Russian Federation

²LLC "Polychrome"
58, Dubrovinskogo, Krasnoyarsk, 660049, Russian Federation
*E-mail: nazarov@sibsau.ru

The development and improvement of rocket and space technology are largely determined by the application of manufacturing technologies that enable the production of high-reliability products with energy efficiency, while simultaneously reducing material intensity and shortening the production cycle. Among these progressive technologies, additive technologies should be mentioned. The essence of these technologies lies in obtaining parts through layer-by-layer melting of material based on a computer 3D model of the product in a chamber of a specialized 3D printer equipped with a laser device.

The application of additive technologies in rocket engine construction requires extensive scientific research and experimental work to confirm compliance with industry standards, rules, and mandatory certification at the state level. In accordance with the program of priority research at SibSU, in collaboration with the industrial partner "Polychrome" LLC a complex of experimental work is being carried out to test and refine the 3D printing modes of a demonstrator model of a low thrust rocket engine (LTRE).

The design of the LTRE, operating on environmentally friendly gaseous fuel components, has been developed and adapted for 3D printing on the ASTRA 420 printer. The parameters and characteristics of the printer are considered, and the sequence of experimental work on selecting printing modes for the engine chamber housing and mixing head is outlined. The fundamental possibility of adjusting the modes of laser material melting and forming of the part has been established.

The main technological stages of post-printing processing of LTRE chamber parts are presented. A description of the equipment for heat treatment and electrochemical polishing of parts is provided. The sequence of material structure research is outlined, and the results of metallographic and X-ray analysis of the internal state of the metal are presented.

The importance of stand tests of rocket engines in the development of innovative design solutions and the implementation of innovative production technologies is demonstrated. A description and composition of the testing stand system at SibSU are presented. The results of stand firing tests indicate the fundamental possibility of manufacturing LTRE using selective laser melting of heat-resistant alloy.

Keywords: additive technologies, low thrust rocket engine, Inconel 718, post-printing processing, vibration testing, strength and tightness tests, bench fire tests.

Introduction

The Russian aerospace industry has high innovative potential and is one of the main priorities of the country's economic development strategy. Its importance is currently determined by the special tasks of strengthening the defense capability of the state and the ability to ensure an accelerated pace of modernization of industrial production technological base. The practical results of space activities should be used to truly improve the quality of life of people and the development of all spheres of the economy. In the aerospace industry, extensive technical re-equipment of production, reconstruction of industrial facilities, and development of advanced world-class technologies are underway.

These include additive technologies (AF – Additive Fabrication from the term additivity – addition) [1–3], which represent a sequential layer-by-layer build-up of material and synthesis of a production object using component 3D application programs. The joining of layers of the source material can be carried out in various ways: by fusion, sintering, gluing, polymerization, depending on the

physical and chemical properties of the material, the characteristics of the technological equipment and the intended purpose of the product.

The most promising type of additive technologies for use in the rocket and space industry is considered to be SLM 3D printing technology [4]. SLM (Selective laser melting) is an innovative technology for the production of complex products by laser melting of metal powder using mathematical CAD models (3D metal printing). This process consists of sequential layer-by-layer melting of powder material using powerful laser radiation. Using SLM technology, they create both precision metal parts for use as components and assemblies, as well as non-separable structures that ensure increased reliability of products.

Compared to traditional technologies currently used, selective laser melting technology has a number of advantages [5]:

- solving complex technological problems; – reduction of the cycle of research and development work, construction of complex parts without the use of equipment;
- reduction of the final mass of the product due to optimization of the design, taking into account the distribution of forces on the internal partitions and stiffeners of the product;
- lower consumption of final material through topological optimization at the product design stage.

At the same time, the use of SLM technology must be accompanied by a certain amount of post-printing processing, since the manufactured parts have increased roughness parameters, traces of technological supports, and unevenness on surfaces mating with the surfaces of other parts of the assembly unit. Porosity on the end surfaces of parts does not always provide a high-quality hermetic connection of metals by welding.

The purpose of the research

At enterprises and research organizations of the rocket and space industry, work is being carried out to create a system for the implementation and practical testing of additive technologies with their subsequent certification at the industry level. Due to this the issue of organizing advanced training of specialists in the field of additive technologies, taking into account the long-term interest and needs of enterprises of industrial partners is of relevance both for the Reshetnev Siberian State University of Science and Technology at the new stage of its development as a flagship university of the region and rocket and space engineering in general.

As part of the “Priority 2030” program, the Reshetnev Siberian State University of Science and Technology is implementing a scientific and educational project “Development, production by selective (additive) laser melting and testing of a low-thrust demonstrator rocket engine running on environmentally friendly fuel.”

A low-thrust rocket engine (LTRE) was chosen as the subject and the object of the research. Since the functional purpose of this demonstrator engine is to conduct model bench tests without simulating space conditions, the use of environmentally friendly fuel components is provided: oxygen gas O₂ (oxidizer) and methane gas CH₄ (fuel).

Currently, LTREs are the main executive bodies in the control system of spacecraft. They serve to orient, stabilize and correct the aircraft in space. The purpose of LTREs and the conditions of their operation impose a number of specific requirements on them, in particular the following:

- multi-mode, due to continuous operation (duration up to $\tau_b > 10^3$ s) and various pulse modes with a minimum switching time of 0.03 s or less ;
- long service life in terms of total operating time - up to 50,000 s or more ;
- large resource in terms of total number of inclusions - up to 10⁶.

Meeting the above requirements causes significant difficulties in the design of an LTRE, the organization of mixture formation and the working process in its combustion chamber, due to the following factors:

- low fuel consumption ;
- small number of nozzle head elements ;

- the impossibility of creating regenerative cooling;
- the difficulty of ensuring uniform distribution of mixed fuel throughout the volume of the combustion chamber.

Research object characteristics

It is known that the creation of LTRE is largely based on the results of experimental testing of prototype engines and empirical interpretation of the theoretical laws of fluid dynamics and chemical kinetics. The design, thermodynamic and gas-dynamic calculations of the demonstrator engine chamber were carried out according to the educational methods of the Department of Aircraft Engines at Reshetnev Siberian State University of Science and Technology and the recommendations of JSC “Design Bureau of Chemical Engineering named after Alexey Mikhailovich Isaev” using SolidWorks application programs, Mathcad.

The developed demonstrator engine has the following technical characteristics:

- thrust $P = 200 \text{ H}$;
- oxidizer O_2 (oxygen – gas, $T = 298 \text{ K}$);
- fuel CH_4 (methane - gas, $T = 298 \text{ K}$);
- oxidizer mass flow $\dot{m}_o = 0,04316 \text{ kg/s}$;
- mass fuel consumption $\dot{m}_r = 0,02439 \text{ kg/s}$;
- combustion chamber pressure $p_k = 1 \text{ MPa}$;
- nozzle exit pressure $p_a = 0,00085 \text{ MPa}$;
- engine specific impulse $J_y = 2960 \text{ m/s}$.

The design of the engine chamber is made in the form of two monoblocks – the mixing head and the chamber body (Fig. 1), connected to each other by argon arc welding. The capabilities of SLM technology made it possible to carry out a complex design of the mixing head without making assembly units – nozzles, the topological optimization of which made it possible to additively print them in the form of holes with jet and tangential (centrifugal) supply of components to the zone of atomization and mixture formation.

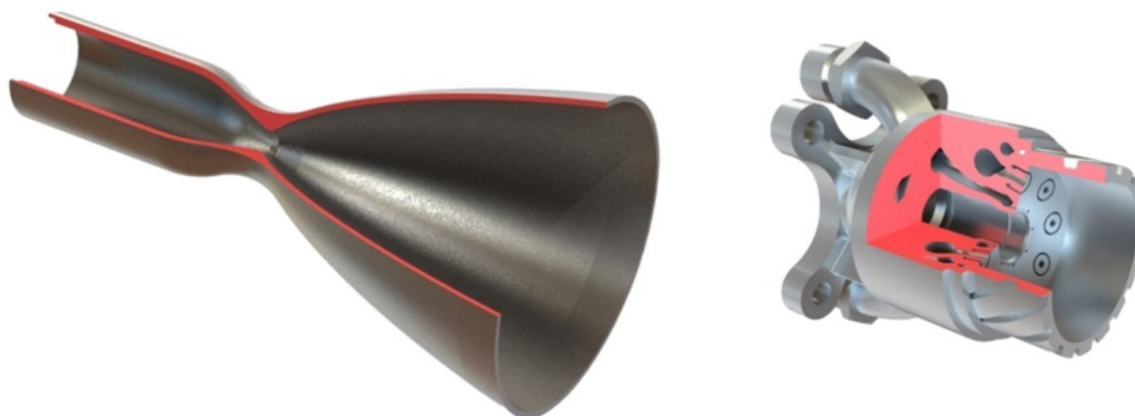


Рис. 1. 3D-модели корпуса камеры и смесительной головки

Fig. 1. 3D models of the chamber body and mixing unit

3D printing equipment

The production of the engine using 3D printing technology was carried out by the industrial partner of the university, Polychrome LLC, on an ASTRA 420 printer, which was developed and manufactured at this enterprise (Fig. 2).

A special feature of the ASTRA 420 printer is the implementation of innovative solutions in dynamic modulation of the laser spot with the ability to adjust the laser power, which allows you to achieve high speeds for building parts. The ASTRA 420 3D printer can be used to solve complex production problems, in the manufacture of 3D parts and conducting research work [6; 7].

The ASTRA 420 3D printer has the following technical specifications.

Build chamber options:

- build chamber size – 420×420×280 mm;
- working stroke of the vertical movement table – 280 mm;
- table moving step – 1 mkm;
- repeatability per table stroke – ±5 mkm;
- applying a layer of powder on the construction table – from 20 mkm (with a step 1 mkm).

Laser and optical system parameters:

- continuous IR laser, wavelength – 1080 nm;
- laser radiation power – 500 W ;
- positioning accuracy of the galvanic scanner (at the edges) – no more 10 mkm;
- exposure speed – 20–2000 m/s ;
- laser spot modulation – from 40 mkm to 2 mm ;
- laser spot modulation speed – less than 0.2 s .

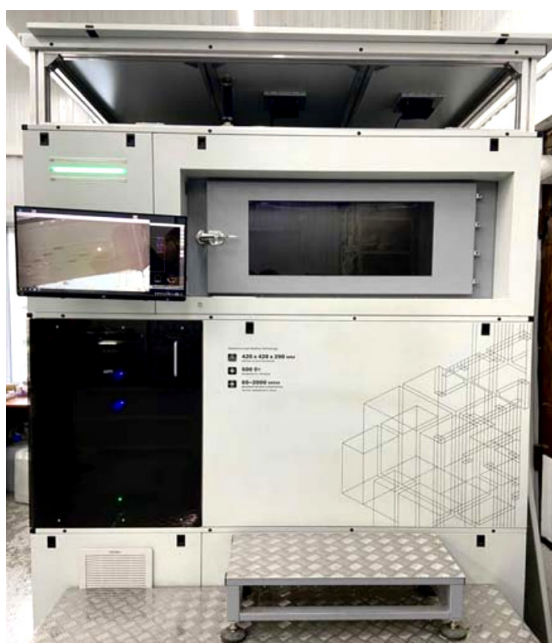


Рис. 2. 3D-принтер ASTRA 420. Внешний вид

Fig. 2. 3D printer ASTRA 420. Appearance

The software includes a control program and a task preparation program. The first allows you to set technological parameters for completing a task, control all processes associated with the operation of the printer, and set movement trajectories laser spot, its modulation, control the task being performed and video record the process of building the part. The second includes software for processing STL files (geometry optimization, construction of support elements, cutting into layers).

The technical capabilities of the printer allow you to perform high-quality 3D printing CAD models using layer-by-layer selective laser melting from powders of non-ferrous metals, all types of steels, titanium, nickel, cobalt-chromium alloys and other metal materials [8].

Development of 3D printing technology

On order to increase the practical orientation of the scientific and educational project, bringing it closer to the requirements of real production, the main design, production and technological activities of the project were carried out taking into account the recommendations of the “Technological support system for the development and production of products”, which is accepted in the aerospace industry. In particular, the general methodology for technological preparation of production was used, set out in Application standard 92-4718-86 “Organization of technological development and launching of new

products production” and Application standard 92-4928-90 “Basic provisions for the organization and management of technological preparation of production process”.

The SLM process belongs to the class of powder technologies [9]. The basic principle of SLM technology is to apply a thin layer of powder (20–80 microns) onto the construction table, followed by melting of a programmatically selected part of the layer of the part being built with a laser beam spot. Next, the construction table is lowered to a given height and the next layer of powder is applied to it. The selective melting process is then repeated. The process of constructing large-sized parts using SLM technology in automatic continuous printer operation mode can take up to 300 hours, depending on the size and configuration of the parts.

At the first stage of the project, in accordance with the logic of scientific research, a set of experimental work was carried out to test the manufacturing modes on an ASTRA 420 3D printer of an RDMT camera from the model powder material Silumin RS-300. The choice of this material is explained by its plasticity, low melting point and low cost. The manufactured copies of the demonstrator camera were subjected to various types of research and testing in laboratory and production conditions.

As a result, it was established that the technical characteristics of the printer ensure the implementation of innovative solutions and dynamic modulation of the laser spot with the ability to adjust the laser power, which allows you to achieve high speeds for building parts and, therefore, begin printing a chamber from the heat-resistant austenitic alloy Inconel 718.

Inconel 718 powder was selected for the chamber body and LTRE mixing head. It is known that this material was developed and patented in the USA by the author Eiselstein in 1962 [10] and is currently widely used in the aerospace and mechanical engineering industries of foreign countries. In the domestic industry, PR-08XH53БМТУ powder is used for additive technologies Material specification (MS) 1479-704-5689-2016, which in its chemical composition is an analogue of the Inconel 718 alloy. The powder is produced by spraying the melt with an inert gas – high-pressure nitrogen. The shape of the powder particles is predominantly spherical. Manufacturer LLC "Grankom".

Previously, research work was carried out to study the melting characteristics of this powder and select printing modes. Selected modes for printing single tracks and continuous printing of samples .

The selection of modes began with a series of printing 48 samples of hollow cells in single tracks to determine the optimal combination of laser beam spot diameter, scanning speed and laser power. In the first batch of 12 samples, the spot diameter and scanning speed remained static while the laser power was varied in 15 W increments. In the second batch the speed was changed, in the third the spot diameter was changed. In the final batch, all three parameters were changed proportionally in small increments in order to determine the optimal printing mode. The results were studied using an Insein Li Fung microscope with a magnification of x10-300. The track thickness, its integrity, stability and strength were visually assessed.

The next stage of the experiments was printing three-dimensional images. The pattern (geography of filling) of the laser beam, idle speed, internal distance from the contour and step between tracks were added to the parameters established in previous experiments. The orientation of the sample in space is also important, but when working with small samples this can be neglected. The results were recorded using a microscope, and strength and porosity were assessed visually. Experiments have shown that a layer spacing of 150 μm provides the best filling and low porosity.

Balancing all of the above parameters is a primary task in SLM printing. Deviation of the mode in any direction will lead to an insufficient amount of energy supplied to the working surface and, consequently, to lack of fusion and increased porosity. The parameters can be selected based on the volume of the part: thin areas, with a small scanning area per layer, can be printed relatively quickly without the risk of porosity, and for areas of large accumulation of material, a suitable pattern is selected that will not cause overheating at the same speed. Regardless of the geometry of the part, in order to avoid the accumulation of internal residual stress, the scanning direction on each layer changes by 90° relative to the previous one.

The mixing head differs from the combustion chamber body in its massiveness and large accumulation of material throughout the entire volume. To print such a product, it was decided to manually segment it into components that would be printed sequentially in a prescribed order. This method prevents overheating on the surface while maintaining print speed. The LTRE combustion chamber was also segmented – the top and bottom of the combustion chamber were a thin-walled cylinder and cone that were printed as normal. The area that requires changing the parameters is the critical section, located at the junction of two chamber zones. This area was printed using an alternate print pattern as described above to avoid overheating. It was decided to install both models vertically, since this orientation provided the least amount of internal vertical surfaces. Supports were installed from the table to the lower surface of the parts in combination with heat sinks for reliable fixation

Thus, the parameters for printing the first LTRE sample and the mixing head were obtained, presented in the table.

Printing operating modes of LTRE combustion chamber and mixing head

The combustion chamber						
Segment	P, W	V, mm/s	D, mkm	Step, mkm	Idle speed, mm/s	Pattern
Before the critical section	300	600	190	150	600	Bidirectional optimized
Critical section						Unidirectional
After the critical section						Bidirectional optimized
Mixing head						
Segment	P, W	V, mm/s	D, mkm	Step, mkm	Idle speed, mm/s	Pattern
Outer layer (1.5 mm)	300	600	190	150	600	Unidirectional optimized
Inner layer						Cells

Testing of the first sample revealed the presence of porosity and leakage in the critical section area. Before printing the second sample, a series of additional experiments were undertaken to select the optimal mode for printing the critical section separately. As a result, this segment was once again divided into two equal parts, which were printed with two different patterns. The use of this approach when printing a working sample showed positive results. Porosity decreased significantly throughout the entire volume of the sample.

The above technique was applied to print the mixing head. Segmentation and delamination of the model showed a positive result; the sample had low porosity. At this stage of work, optimization of printing time was not carried out. Printing time for the camera body – 3 days, mixing head – 2 days.

Post-press technology

The shaping of chamber parts is the initial and at the same time the most critical stage of the overall technological process of manufacturing LTRE. According to some information, based on the experience of producing experimental rocket and space technology products, including the experience of the authors of this article, post-printing costs can account for more than one third of the total amount of labor costs for the production of 3D printed parts and assembly units.

Post-printing technology is developed taking into account the physico-chemical, mechanical, technological and other properties of the source material Inconel 718.

The manufacturer of the powdered material recommends heat treatment of parts made by 3D printing - hardening in a vacuum, followed by cooling in an oven while maintaining a vacuum environment and further blowing with argon. Printed chamber bodies, mixing heads and plate samples were subjected to heat treatment.

Heat treatment was carried out in a vacuum furnace SECO/WARWICK 10 VPT-4050/48 HV (Fig. 3) of the partner enterprise JSC “Kras mash”. The vacuum oven is certified to perform similar types of heat treatment.

The heat treatment modes are as follows :

- residual pressure (vacuum) in the furnace $P = 10^{-2}$ kg/sm²;
- heating speed – 20 degrees/min (~50 min);
- heat treatment temperature $t = 1060$ °C ;
- exposure – 60 min .



Рис. 3. Вакуумная печь SECO/WARWICK 10 VPT-4050/48 HV

Fig. 3. Vacuum furnace SECO/WARWICK 10 VPT-4050/48 HV

After cooling the parts to a standard room temperature $t = 20$ °C, they were subjected to abrasive treatment (sandblasting) using artificial abrasive – F-120 electrocorundum at an air-abrasive mixture pressure $P = 4$ kg/cm² for 5–8 minutes.

A study was conducted of the influence of the 3D printing process on the chemical composition of the source material. Non-heat-treated and heat-treated printed samples were studied. The study was carried out in the mass spectrometry laboratory of JSC Kras mash using a 67A1053 HITACHI PMI-MASTER UVR spectrometer. As a result of the research, it was established that the chemical composition of the samples meets the requirements stated by the manufacturer in the certificate of the Inconel 718 material,

and also meets the requirements of the foreign standard AMS 5663M. Thus we can conclude that the process of selective laser melting and subsequent high-temperature heat treatment does not affect the chemical composition of the material and does not lead to a change in the balance of alloying elements of the alloy.



Рис. 4. Микроструктура материала без термообработки

Fig. 4. Material microstructure without heat treatment

Metallographic analysis was carried out by viewing microsections of heat-treated and non-heat-treated samples after etching in a special reagent on a NICON ECLIPSE MA200 microscope at a magnification of 50 to 1000 times in a research laboratory. skom center of JSC “Kras mash”.

It was established that the structure of the microstructure of the material without heat treatment in some areas has structural banding (Fig. 4), due to the

manufacturing method by layer-by-layer laser fusion. The microstructure of the samples is austenite with precipitates of intermetallic compounds (such as the γ' -phase). In the microstructure of samples without heat treatment, grain boundaries are not detected. The grain sizes of heat-treated samples correspond to those for alloyed austenitic steels and alloys. In the non-heat-treated material, single local discontinuities with spherical particles are observed, there are defects in the form of oxide films with a length of 0.06–0.35 mm and areas of pore accumulation with a size of 0.015–0.085 mm. In heat-treated samples, such defects are not clearly visible, but microporosity is preserved (in smaller sizes). The results of metallographic analysis are in sufficient agreement with the studies of other authors [11–13].

In order to more accurately identify spatial defects in the material of printed products, radiographic inspection of engine chamber housings was carried out. The studies were carried out in areas accessible for control using a YXLON MG-103 X-ray machine. At the same time, discontinuities in the form of individual point voids with dimensions 0.3–1 mm and ring discontinuities with an intensity of 0.1–0.2 mm elongated along the printed layers with a deterioration in print quality in the zone of the critical section of the nozzle and an increase in porosity in areas measuring 0.5–2 mm [14].

The roughness control of the internal and external surfaces of the camera body was carried out using a SurfTest SJ-201 device, which has a verification certificate from the State Regional Center for Standardization, Metrology and Testing. Due to the lack of a standard technique and special devices for measuring actual roughness values, the most characteristic areas were identified on the internal surfaces of the supersonic part of the nozzle and the cylindrical part of the combustion chamber. A total of 7 areas are allocated, accessible for control using universal means included in the device. As a result measurements, actual roughness values were obtained in the range $R_a = 14.4\text{--}23.84 \mu\text{m}$, which significantly exceed the roughness parameters of the internal surfaces of liquid-propellant rocket engine chambers accepted in rocket engine construction ($R_a = 2.5\text{--}3.6 \mu\text{m}$). Thus, the next task in developing the optimal finishing technology for the LTRE camera is choosing a method to improve the quality of product surfaces.

One of the effective and proven methods in the mass production of shells of rocket engine chambers is electrochemical polishing (hereinafter referred to as electropolishing), which is based on the intensive dissolution of microprotrusions of surface roughness and the slow dissolution of cavities [15; 16]. The processing process was carried out in a cathode-anode bath with a solution of sulfuric acid (H_2SO_4), phosphoric acid (H_3PO_4) and chromic anhydride (CrO_3) in a certain concentration of each substance. Processing modes have been experimentally selected for chamber bodies and mixing heads:

- voltage $V = 8,8 \text{ V}$;
- current magnitude $I = 90\text{--}40 \text{ A}$;
- time of processing $t = 4\text{--}6 \text{ min}$.

Next, washing operations were carried out in cascade baths with cold and hot water, clarification in a solution of nitric acid (HNO_3), and neutralization in a solution of calcium carbonate (Na_2CO_3). Roughness control was carried out by comparison with a standard (roughness sample) and showed acceptable convergence of actual roughness parameters to the requirements of the drawing.

In accordance with the research program, the physical and mechanical parameters and characteristics of printed products were determined (breaking point σ_B , yield $\sigma_{0,2}$, modulus of rigidity E etc.), hardness measurements on samples, vibration tests, strength and tightness tests. A description of the methods and these studies results analysis is not provided in this article. Separately, it should be noted that during leak testing of the first of the printed samples of the cam-



Рис. 5. Камера РДМТ в сборе

Fig. 5. LTRE chamber assembly

era body, a leak was detected in the critical section area. This confirms the conclusions about the developed porosity of the material of this sample during X-ray inspection. As shown in one of the previous sections of the article, adjustments were made to the printing modes, ensuring the tightness of the products printed further.

At the end of the technological process of post-printing processing, mechanical preparation of the joining surfaces and manual argon arc welding of the camera body and mixing head were carried out. Welding was performed with a non-consumable tungsten electrode with a filler wire with a diameter $\varnothing 1,5$ mm, printed from Inconel 718 powder on 3D printer. Due to the lack of recommendations in the industry's regulatory and technological documentation for welding printed parts made of this material, welding modes were tested on printed flat and cylindrical simulator samples.

Figure 5 shows the assembled LTRE chamber: threaded fittings for supplying fuel components are installed and welded onto the mixing head. The quality of welded joints is checked by leak testing using the "aquarium" method. A socket is installed on the lower cylindrical section of the combustion chamber to secure the thermoelectric sensor. A spark plug is installed in the central hole of the mixing head using a threaded connection with a metal seal. .

LTRE Bench Tests

When creating new designs of rocket engines, developing and implementing innovative technologies for their industrial production, bench fire tests are carried out, which are the main means of checking the validity of the adopted design and technological decisions, monitoring the specified design parameters and characteristics of the work process, assessing the performance and reliability of products [17; 18].

For this purpose, during the implementation of the project, a test bench complex was developed and manufactured on the territory of the "Ustanovo" suburban testing ground (Fig. 6). The test bench includes the following systems:

- fuel component supply system. It consists of two parts: an oxidizer supply system and a fuel supply system. Structurally, these systems are made separately in the oxidizer and fuel compartments. The compartments are subject to requirements for the tightness of the systems, the use of materials that do not react with fuel components and prevent sparking during the operation of the stand. The system includes two high-pressure cylinders with oxygen gas and methane gas, lines for supplying fuel components made of stainless steel, and gas reducers;

- ignition system of fuel components in the combustion chamber. Consists of power supply unit and spark plug 6213 NGK SILMAR9A9S;

- measurement system. This system is the most important when conducting bench tests, since it is from the results of measuring a wide range of parameters of the propulsion system that both the conditions for conducting bench tests and the operation of the engine are determined. It includes a draft measuring device, pressure and flow sensors of components. In this regard, the measurement system must perform the function of visual monitoring of the main parameters of the engine and the stand, remote measurement according to a given program, storing information on media, and also ensure high accuracy and safety of measuring instruments and have high noise immunity of its measuring instruments;

- control system. Designed for automatic starting, changing operating and stopping modes, automatic control of some basic engine parameters. When critical values are reached, it gives a signal and also provides, if necessary, an emergency stop, automatic control of pipeline valves and maintenance of specified pressures. When performing preparatory and final operations, manual control of the stand elements is used;

- safety system. Explosion and fire safety of the stand consists of dividing the stand into compartments of a chamber, oxygen cylinders, methane cylinders, control lines, fire extinguishing equipment, as well as emergency stop control .



Рис. 6. Общий вид рабочей зоны стендового испытательного комплекса

Fig. 6. General view of the bench testing complex working area

The first fire bench tests of a low-thrust rocket engine manufactured using additive technologies (code name: LTRE “Fakel-1”) took place on September 15, 2023 (Fig. 7). In accordance with the developed and approved test cyclogram, five starts were carried out with a working cycle duration of 1.5 s, followed by purging of the lines with air for 180–300 s. A stable appearance of a torch at the nozzle exit, a stable cut-off of the supply of fuel components and the cessation of combustion of the mixture of components in the combustion chamber were recorded. The thrust measuring device measured the engine thrust, which approximately corresponds to the calculated value $P = 200 \text{ H}$ (20 kg). In order to guarantee the safety of personnel and test bench equipment, the supply pressure of gaseous components at the engine inlet was reduced by 35–40% compared to the design pressure in the combustion chamber ($p_k = 1 \text{ MPa}$). In this case, the achieved thrust value at reduced pressure should be explained by the operation of the nozzle in the overexpansion mode, since the ambient barometric pressure (conditionally $p_H = 0,1 \text{ MPa}$) significantly exceeds the calculated pressure of the gas flow at the nozzle exit ($p_a = 0,00085 \text{ MPa}$).



Рис. 7. Огневые испытания РДМТ

Fig. 7. LTRE fire test

After dismantling, a visual inspection of the condition of the engine surfaces was carried out (visual defect detection of the product – according to industry terminology). During an external inspection of the external and internal surfaces of the engine (in accessible places) using local illumination and a

standard technical magnifying glass of four times magnification, no surface damage was found that would prevent repeated testing.

Conclusion

In the process of implementing the scientific and educational project “Development, production by selective (additive) laser alloying and testing of a low-thrust demonstrator rocket engine operating on environmentally friendly fuel,” a significant amount of research, development, and educational and laboratory work was carried out to study and the practical application of innovative additive technologies, which have great potential for the accelerated development of the rocket and space industry.

Project participants, including students from Reshetnev University, gained new knowledge and skills in conducting practical work in the field of mechanical engineering and metallurgical production, metrology, assembly and installation operations, laser, electrochemical and other technologies used in rocket engine construction. New professional competencies were obtained that contribute to the intellectual development of Reshetnev University students – future specialists of aerospace industry enterprises.

At the same time, it should be concluded that the use of additive 3D printing technologies in the manufacture of complex and highly loaded rocket and space technology products requires a large complex of scientific research and production and technological tests to confirm the stability of characteristics and reliability indicators with subsequent certification of the innovative technology for compliance with the requirements.

Благодарности

Реализация научно-исследовательского проекта осуществляется при поддержке благотворительного фонда известного государственного и общественного деятеля, предпринимателя, почетного гражданина Красноярского края Х. М. Совмена.

Поддержку проекту оказывали также промышленные партнеры СибГУ им. М. Ф. Решетнева: ООО «Полихром», АО «Красмаш», АО «КБХиммаш им. А. М. Исаева», ООО «Вариант 999», АО «ОКБ Зенит».

Acknowledgements

The implementation of the research project is carried out with the support of the charitable foundation of the famous statesman and public figure, entrepreneur, honorary citizen of the Krasnoyarsk Territory Kh. M. Sovmen.

The project was also supported by industrial partners of Siberian State University: “Polychrome” LLC, “Kras mash” JSC, “KBkhimmash named after A.M. Isaev” JSC, “Variant 999” LLC, “OKB Zenith” JSC.

Библиографические ссылки

1. Логачева А. И. Аддитивные технологии изделий ракетно-космической техники : перспективы и проблемы применения // Технология легких сплавов. 2015, № 3. С. 39–44.
2. NASA tests limits of 3D-printing with powerful rocket engine check [Электронный ресурс]. URL: <http://nasa.gov> (дата обращения: 15.11.2023).
3. Перспективы применения аддитивных технологии в производстве сложных деталей газотурбинных двигателей из металлических материалов / С. В. Белов, С. А. Волков, Л. А. Магеррамова [и др.] // Аддитивные технологии в российской промышленности : сб. науч. тр. М. : ВИАМ, 2015. С. 101–102.
4. Аддитивные технологии / Терехов М. В., Филиппова Л. Б., Мартыненко А. А. [и др.]. М. : ФЛИНТА, 2018. 74 с.

5. ГОСТ Р 59036–2020. Аддитивные технологии. Производство на основе селективного лазерного сплавления металлических порошков. Общие положения. М. : Стандартинформ, 2020. 22 с.
6. ГОСТ Р 59184–2020. Аддитивные технологии. Оборудование для лазерного сплавления. Общие требования. М. : Стандартинформ, 2020. 18 с.
7. Преображенская Е. В., Боровик Т. Н., Баранова Н. С. Технологии, материалы и оборудование аддитивных производств. М. : РТУ МИРЭА, 2021. 173 с.
8. Gu D. D., Meiners W., Wissenbach K., Poprawe R. Laser additive manufacturing of metallic components: Materials, processes and mechanisms // *International Materials Reviews*, 2012. No. 57 (3). P. 133–164.
9. Additive Manufacturing. With Amperprint for 3D-Printing you Have the Powder to Create [Электронный ресурс]. URL: <https://www.hoganas.com/en/powder-technologies/additive-manufacturing/3d-printingpowders/> (дата обращения: 15.11.2023).
10. Пат. 3046108А US. Age-hardenable nickel alloy / Eiselstein H. L. № US773702А ; заявл. 13.11.1958 ; опубл. 24.07.1962. 10 с.
11. Металлографический анализ камеры, изготовленной методом 3D-печати / Е. Е. Жигурова, К. Е. Мумбер, Р. А. Казаков [и др.] // Решетневские чтения : материалы XXVI Международной научно-практической конференции (Красноярск, 09–11 ноября 2022 года) ; СибГУ им. М. Ф. Решетнева. Красноярск, 2022. Ч. 1. С. 175–177.
12. Назаров Е. Г., Масленков С. Б. Термическая обработка аустенитных жаропрочных сталей и сплавов // *Металловедение и термическая обработка металлов*. 1970, № 3. С. 63–72.
13. Педаш А. А., Лысенко Н. А. [и др.]. Структура и свойства образцов из сплава Inconel 718 полученных по технологии селективного лазерного плавления // *Авиационно-космическая техника и технология*. 2017. № 8. С. 46–54.
14. Анализ результатов рентгенографических исследований изделий РКТ изготовленных методом SLM-печати / Э. С. Манохина, М. А. Шикарев, А. П. Рубайло [и др.] // Решетневские чтения : материалы XXVI Международной научно-практической конференции. Красноярск, 2022. С. 186–187.
15. Краснова Е. В., Саушкин Б. П., Слюсарь И. А., Смяян С. В. Электрохимическая обработка изделий аддитивного производства из металлов и сплавов // *Аддитивные технологии*. 2023, № 2. С. 49–57.
16. Zhao C., Qu N., Tang X. Removal of adhesive powders from additive manufactured internal surface via electrochemical machining with flexible cathode // *Precision Engineering*, 2021. Vol. 67, P. 438–452. DOI: 10.1016/j.precisioneng.2020.11.003.
17. Яцуненко В. Г., Назаров В. П., Коломенцев А. И. Стендовые испытания жидкостных ракетных двигателей ; Сиб. гос. аэрокосмич. ун-т. Красноярск, 2016. 248 с.
18. Имитационное моделирование условий стендовых испытаний жидкостных ракетных двигателей малой тяги / В. П. Назаров, В. Ю. Пиунов, К. Ф. Голиковская, Л. П. Назарова // Решетневские чтения : материалы XXVI Международной научно-практической конференции. Красноярск, 2022. С. 191–192.

References

1. Logacheva A. I. [Additive technologies for rocket and space technology products: prospects and problems of application]. *Tekhnologiya legkikh splavov*. 2015, No. 3, P. 39–44 (In Russ.).
2. NASA tests limits of 3D-printing with powerfull rocket engine check. Available at: <http://nasa.gov> (accessed: 15.11.2023).
3. Belov S. V., Volkov S. A., Magerramova L. A., et. al. [Prospects for the use of additive technologies in the production of complex parts of gas turbine engines from metal materials]. *Sbornik nauchnykh trudov nauchn. konf. "Addivnye tekhnologii v rossiyskoy promyshlennosti"* [Collection of

scientific papers Scientific. Conf. “Additive technologies in Russian industry”]. Moscow, 2015, P. 101–102 (In Russ.).

4. Terekhov M. V., Filippova L. B., Martynenko A. A., et. al. *Additivnye tekhnologii* [Additive technologies]. Moscow, FLINTA Publ., 2018, 74 p.

5. *GOST R 59036–2020. Additivnye tekhnologii. Proizvodstvo na osnove selektivnogo lazernogo splavleniya metallicheskih poroshkov. Obshchie polozheniya* [State Standard R 59036-2020. Additive technologies. Production based on selective laser melting of metal powders. General provisions]. Moscow, Standartinform Publ., 2020. 22 p.

6. *GOST R 59184–2020. Additivnye tekhnologii. Oborudovanie dlya lazernogo splavleniya. Obshchie trebovaniya* [State Standard R 59184-2020. Additive technologies. Equipment for laser melting. General requirements]. Moscow, Standartinform Publ., 2020. 18 p.

7. Preobrazhenskaya E. V., Borovik T. N., Baranova N. S. *Tekhnologii, materialy i oborudovanie additivnykh proizvodstv* [Technologies, materials and equipment for additive manufacturing]. Moscow, RTU MIREA Publ., 2021, 173 p.

8. Gu D. D., Meiners W., Wissenbach K., Poprawe R. Laser additive manufacturing of metallic components: Materials, processes and mechanisms. *International Materials Reviews*, 2012, No. 57 (3), P. 133–164.

9. Additive Manufacturing. With Amperprint for 3D-Printing you Have the Powder to Create. Available at: <https://www.hoganas.com/en/powder-technologies/additive-manufacturing/3d-printingpowders/> (accessed: 15.11.2023).

10. Eiselstein H. L. Age-hardenable nickel alloy. Patent US, no. 3046108A, 1962.

11. Zhigurova E. E., Mumber K. E., Kazakov R. A., et. al. [Metallographic analysis of a 3D printed chamber]. *Materialy XXVI Mezhdunar. nauch. konf. “Reshetnevskie chteniya”* [Materials XXVI Intern. Scientific. Conf “Reshetnev reading”]. Krasnoyarsk, 2022, P. 175–177 (In Russ.).

12. Nazarov E. G., Maslennikov S. B. [Heat treatment of austenitic heat-resistant steels and alloys]. *Metallovedenie i termicheskaya obrabotka metallov*. 1970, No. 3, P. 63–72 (In Russ.).

13. Pedash A. A., Lysenko N. A., et. al. [Structure and properties of samples from Inconel 718 alloy obtained using selective laser melting technology]. *Aviatsionno-kosmicheskaya tekhnika i tekhnologiya*. 2017, No. 8, P. 46–54 (In Russ.).

14. Manokhina E. S., Shikarev M. A., Rubaylo A. P., et. al. [Analysis of the results of x-ray studies of RCT products manufactured by SLM printing]. *Materialy XXVI Mezhdunar. nauch. konf. “Reshetnevskie chteniya”* [Materials XXVI Intern. Scientific. Conf. “Reshetnev reading”]. Krasnoyarsk, 2022, P. 186–187 (In Russ.).

15. Krasnova E. V., Saushkin B. P., Slyusar' I. A., Smeyan S. V. [Electrochemical processing of additive manufacturing products from metals and alloys]. *Additivnye tekhnologii*. 2023, No. 2, P. 49–57 (In Russ.).

16. Zhao C., Qu N., Tang X. Removal of adhesive powders from additive manufactured internal surface via electrochemical machining with flexible cathode. *Precision Engineering*, 2021, Vol. 67, P. 438–452. DOI: 10.1016/j.precisioneng.2020.11.003.

17. Yatsunenko V. G., Nazarov V. P., Kolomentsev A. I. *Stendovye ispytaniya zhidkostnykh raketnykh dvigateley* [Bench testing of liquid-propellant rocket engines]. Krasnoyarsk, Sib. St. Univ. Publ., 2016, 248 p.

18. Nazarov V. P., Piunov V. Yu., Golikovskaya K. F., Nazarova L. P. [Simulation modeling of bench test conditions of liquid rocket engines of low-thrust]. *Materialy XXVI Mezhdunar. nauch. konf. “Reshetnevskie chteniya”* [Materials XXVI Intern. Scientific. Conf “Reshetnev reading”]. Krasnoyarsk, 2022, P. 191–192 (In Russ.).

Акбулатов Эдхам Шукриевич – кандидат технических наук, доцент, ректор; Сибирский государственный университет науки и технологий имени академика М. Ф. Решетнева. E-mail: rector@sibsau.ru.

Назаров Владимир Павлович – кандидат технических наук, профессор кафедры двигателей летательных аппаратов; Сибирский государственный университет науки и технологий имени академика М. Ф. Решетнева. E-mail: nazarov@sibsau.ru.

Герасимов Евгений Витальевич – инженер-конструктор ООО «Полихром». E-mail: gerasimov24rus@mail.ru.

Akbulatov Edkham Shukrievich – Cand. Sc., associate professor, rector; Reshetnev Siberian State University of Science and Technology. E-mail: rector@sibsau.ru.

Nazarov Vladimir Pavlovich – Cand. Sc., Professor of the Department of Aircraft Engines; Reshetnev Siberian State University of Science and Technology. E-mail: nazarov@sibsau.ru.

Gerasimov Evgeny Vitalievich – design engineer at “Polychrome” LLC. E-mail: gerasimov24rus@mail.ru.

УДК 621.43.056

Doi: 10.31772/2712-8970-2023-24-4-697-705

Для цитирования: Бакланов А. В. Влияние особенностей конструкции камер сгорания двигателей НК-16СТ, НК-16-18СТ на содержание углекислого газа в продуктах сгорания // Сибирский аэрокосмический журнал. 2023. Т. 24, № 4. С. 697–705. Doi: 10.31772/2712-8970-2023-24-4-697-705.

For citation: Baklanov A. V. [Concentration of carbon dioxide in products of combustion of GTE NK-16ST and NK-16-18ST]. *Siberian Aerospace Journal*. 2023, Vol. 24, No. 4, P. 697–705. Doi: 10.31772/2712-8970-2023-24-4-697-705.

Влияние особенностей конструкции камер сгорания двигателей НК-16СТ, НК-16-18СТ на содержание углекислого газа в продуктах сгорания

А. В. Бакланов

АО «Казанское моторостроительное производственное объединение»
Российская Федерация, 420036, г. Казань, ул. Дементьева, 1
E-mail: andreymbaklanov@bk.ru

В данной работе рассмотрена конструкция двух камер сгорания газотурбинного двигателя, работающего на природном газе. В одной камере сгорания имеется 32 горелки, в другой – 136 форсунок, расположенных в два яруса во фронтальном устройстве.

Основным фактором, влияющим на глобальное потепление, считаются значительные объемы выбросов парниковых газов, в первую очередь углекислого (CO_2), выделяющихся в том числе при работе газотурбинных двигателей и энергетических установок. Снижение уровня CO_2 путем формирования набора конструктивных мероприятий в камере сгорания – одна из актуальных задач двигателестроения, которую необходимо решить для удовлетворения современных экологических требований, предъявляемых к газотурбинным двигателям, служащим приводами нагнетателей газоперекачивающих агрегатов. Представленное исследование посвящено анализу влияния изменения конструкции камеры сгорания на снижение уровня CO_2 в выхлопных газах газотурбинного двигателя НК-16СТ. Рассмотрено две модификации. Первый вариант – серийная камера сгорания с организацией диффузионного горения, второй – модернизированная с измененным фронтальным устройством. Каждая из рассмотренных камер была испытана в составе двигателя. Во время исследования непосредственно в шахте выхлопа производился отбор продуктов сгорания и определялись их концентрации, в том числе содержание CO_2 . В результате проведенных работ была подтверждена возможность уменьшения уровня концентрации CO_2 в продуктах сгорания двигателя до 20 % без ухудшения его параметров. Такого эффекта удалось достигнуть за счет снижения полноты сгорания топлива в камере сгорания. Полученные данные по изменению концентрации CO_2 могут быть полезны при выборе наиболее подходящего режима работы двигателя во время его эксплуатации, а представленные подходы к организации процессов горения – использованы разработчиками при проектировании камер сгорания газотурбинных двигателей на природном газе.

Ключевые слова: выброс углекислого газа, камера сгорания, газотурбинный двигатель, продукт сгорания, газоперекачивающий агрегат.

Concentration of carbon dioxide in products of combustion of GTE NK-16ST and NK-16-18ST

A. V. Baklanov

JSC "Kazan motor production association"
1, Dementieva St., Kazan, 420036, Russian Federation
E-mail: andreybaklanov@bk.ru

This paper considers the design of two combustion chambers of a gas turbine engine running on natural gas. One combustion chamber has 32 burners, and the other has 136 nozzles located in two rows in the flame tube head.

A major contributor to global warming is considered to be the significant emissions of greenhouse gases, primarily CO₂, including those emitted by gas turbine engines and power plants. The reduction of carbon dioxide levels by developing a set of structural measures in the combustion chamber is one of the urgent tasks of engine construction which requires a solution in order to meet modern environmental requirements for gas turbine engines serving as blower drives for gas compressor units. The presented research is dedicated to the analysis of influence of changes in combustion chamber design on reduction of CO₂ level in exhaust gases of gas turbine engine NK-16ST. Two modifications of the combustion chamber are considered. The first one was a serial combustion chamber with diffusion combustion; the second one was a modernized combustion chamber with a modified front device. Each of the chambers considered was tested as part of the engine. During the study, combustion products were sampled directly in the exhaust tower and their concentrations, including the CO₂ content, were determined. As a result of this work, it was confirmed that there is a possibility to reduce the concentration of CO₂ in the engine combustion products up to 20 % without affecting the engine parameters. This reduction in carbon dioxide content was made possible by reducing the completeness of fuel combustion in the combustion chamber. The obtained data on changes in CO₂ concentration can be useful in selecting the most suitable mode of engine operation, and the presented approaches to combustion processes organization can be used by developers in designing combustion chambers of natural gas-fired gas turbine engines.

Keywords: carbon dioxide emission, combustion chamber, gas turbine engine, combustion product, gas compressor unit.

Introduction

A combustion chamber is one of the main elements that determine the reliability and efficiency of gas turbine engines (GTE). The operating process of a combustion chamber of a GTE is very complex and is determined by many factors: aerodynamics of air and gas flows, nature of fuel supply and its mixing with air and vaporisation, ignition, flame stabilisation, mass and heat exchange conditions, combustion patterns along the length of a combustion chamber. Despite significant differences in the general layout and great diversity in the design of individual elements of combustion chambers of various engines, they are based on common principles of the organisation of the working process [1].

A peculiarity of the combustion process in a gas turbine engine is that the total composition of the fuel-air mixture lies outside the flammability limits, and the cycle temperature is below the instantaneous ignition temperature of any hydrocarbon fuels. Combustion in the engine occurs in the air flow, the velocity of which is much higher than the flame propagation velocity of hydrocarbon fuels. The flow velocity in combustion chambers of stationary engines is 30-80 m/s, aviation engines is up to 50-120 m/s. In addition, combustion must occur in a very limited volume, therefore with a high rate of heat release at rapid mixing and combustion processes. Irrespective of these limitations, the engine must ensure stable combustion, high combustion completeness, flammability and low toxic emissions.

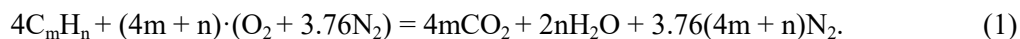
At present, the issues of reducing greenhouse gases, in particular, CO₂ emissions in the exhaust gases of GTEs are relevant for power engineering and gas transport industries. Of particular interest is

the influence of combustion process in the combustion chamber on CO₂ formation depending on GTE operation modes [2].

Modern gaseous fuels are a mixture of various hydrocarbon compounds. The conditional chemical formula of such fuels can be represented as follows: C_mH_n; for the methane $m \sim 1$, $n \sim 4$.

In technical calculations atmospheric air is taken as a mixture of nitrogen and oxygen, then the conventional chemical formula of air can be represented by the ratio (O₂ + 3.76N₂). The ratio 3.76 shows that the air contains approximately 3.76 nitrogen molecules per 1 oxygen molecule.

The chemical reaction of hydrocarbon fuel oxidation in air can be written symbolically as a stoichiometric equation



The stoichiometric equation is written under the assumption of complete conversion of fuel into the main products of combustion and complete chemical inertness of atmospheric nitrogen. The stoichiometric equation provides a macroscopic description of the fuel oxidation process and makes it possible to determine such important characteristics as the stoichiometric ratio for the fuel L₀ and the composition of the products of complete combustion, namely:

$$L_0 = \frac{(4m + n)(\mu_{O_2} + 3.76 \cdot \mu_{N_2})}{4(m \cdot \mu_C + n \cdot \mu_H)} = \frac{34.32(4m + n)}{12m + n} \frac{\text{kg of air}}{\text{kg of fuel}}, \quad (2)$$

where μ is molecular weight of the respective substance,

$$C_{CO_2} = \frac{4m \cdot 100}{4m + 2n + 3.76(4m + n)} \%, \quad (3)$$

$$C_{H_2O} = \frac{2n \cdot 100}{4m + 2n + 3.76(4m + n)} \%, \quad (4)$$

$$C_{N_2} = \frac{3.76(4m + n) \cdot 100}{4m + 2n + 3.76(4m + n)} \%. \quad (5)$$

For the methane $m = 1$, $n = 4$, then

$$L_0 \approx 17.2; C_{CO_2} \approx 9.5; C_{H_2O} \approx 19; C_{N_2} \approx 71.5 \%$$

In the process of oxidation of carbon-containing fuels, carbon monoxide CO is formed as an intermediate substance. The conversion of CO into CO₂ is determined to a greater extent by the elementary reaction [3]



Since this reaction is the only one that determines the conversion of CO into CO₂, it can be concluded that all the carbon originally contained in the fuel is converted into CO₂. It follows that the content of CO₂ in the combustion products will be determined by the completeness or incompleteness of its oxidation reaction.

Study object

To determine the influence of combustion chamber design on the CO₂ content in the combustion products, two types of combustion chambers are being considered in this paper. One is a serial one for the NK-16ST engine, the other is for the NK-16-18ST engine.

The diffusion principle of fuel combustion is organised in the serial combustion chamber of the NK-16ST GTE. The chamber (Fig. 1) consists of outer 1 and inner 2 casings, collector 3, pipelines 4

for fuel supply from the collector to the nozzles 5, flame tube 6 including casings 7 with applied holes 8 and mixer nozzles 9. The annular front device 10 accommodates 32 swirl burners 11. The flame tube (annular) consists of annular sections, between which an annular channel for supplying cooling air is formed, which provides convective-film cooling of the walls [4].

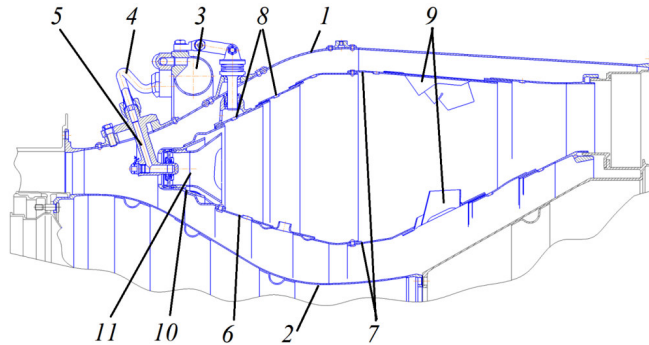


Рис. 1. Камера сгорания двигателя НК-16СТ

Fig. 1. Combustion Chamber of the Gas-turbine Engine NK-16ST

In each swirl burner, an individual fuel gas supply is carried out by means of nozzles providing a jet gas supply [5].

The flame tube front device of the NK-16-18ST GTE (Fig. 2) contains an annular head 1 including an outer and inner fuel manifold 2. On the wall of the outer fuel manifold four inlets are evenly located, necessary for gas feeding into the inner cavity of the manifolds. The cavities of the manifolds are connected by means of channels 3 arranged in the front device. There are also staggered shaped windows 4 with a central hole and nozzle mounting posts 5 [6; 7].

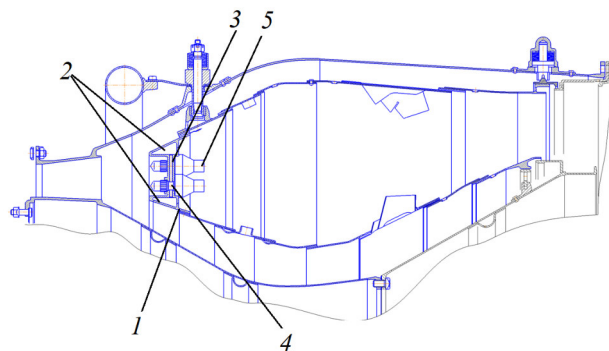


Рис. 2. Камера сгорания двигателя НК-16-18СТ

Fig. 2. Combustion Chamber of the NK-16-18ST Gas-turbine Engine

Each chamber was tested as part of a gas turbine engine. The stand (Fig. 3), where the engine was installed, consists of an air inlet equalising pipe, the inlet of which is protected by a protective mesh. It is necessary to prevent the ingress of foreign particles into the the engine block. In order to transport the exhaust gases to the exhaust tower, an exhaust unit is installed in the exhaust part of the engine. An air compressor (pneumatic brake) was used as a loading device of the free turbine [8].

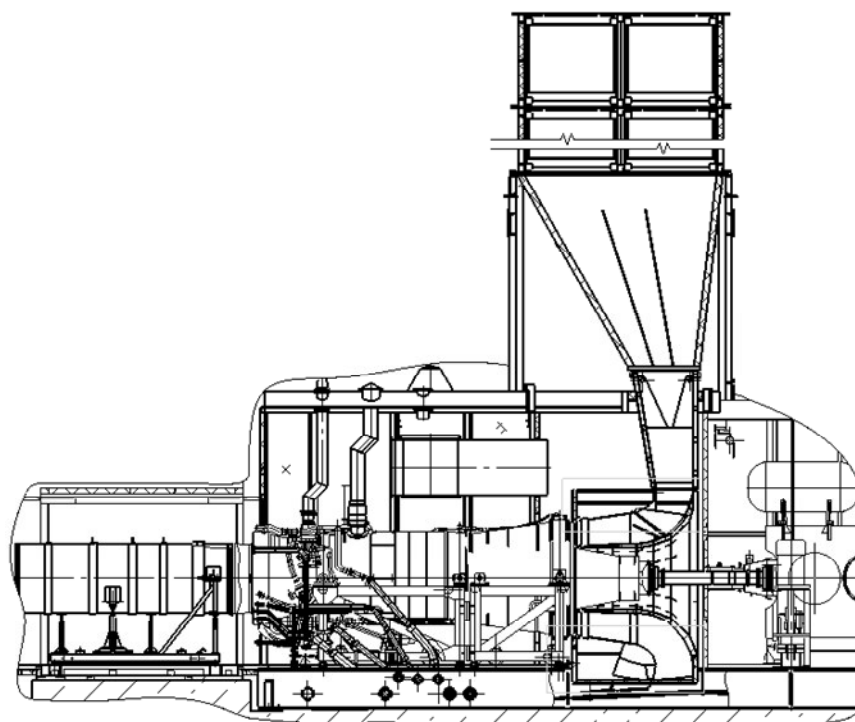


Рис. 3. Схема стенда

Fig. 3. Scheme of the Stand

The stand is equipped with necessary measuring instruments. It has an oil system for lubrication of engine supports and units during testing. To ensure starting and fuel gas supply to the fuel supply elements, the stand contains a gas system. The engine parameters are monitored and its operation modes are adjusted from the control panel equipped with the monitors on which the measured parameters are displayed [9].

Test results

During the tests, the engines were started and reached the modes necessary for building the throttle characteristic. At modes higher than 10 MW, in accordance with the standard [10], combustion products were sampled in the exhaust tower and the concentrations of toxic substances in them were determined.

A gas sampling probe immersed in a special window made in the wall of the exhaust tower was used for sampling, and the Testo 350 gas analyser was used to determine the concentration of toxic components in the combustion products. The measured value of oxygen (O_2) concentration in the combustion products is used to calculate the CO_2 content:

$$c(CO_2) = \frac{c(CO_{2max})(21 - c(O_2))}{21}, \quad (7)$$

where $c(CO_{2max})$ is a maximum concentration value CO_2 , %; 21 is O_2 concentration in the air, %; $c(O_2)$ is measured O_2 concentration in combustion products, %.

According to the high speed of the instrument, the time of one measurement was 40 seconds. The data processed by the gas analyser were displayed on the screen and also recorded using a printing device embedded into the gas analyser [11].

To convert mass concentrations of CO_2 from % to g/m^3 , a number of conditions are assumed: the temperature of exhaust gases is 618.15 K, the pressure of exhaust gases is equal to atmospheric pressure under normal conditions and corresponds to 101 325 Pa.

The volume of one mole of carbon dioxide at a temperature of 618.15 K is calculated using the following formula

$$V_{mCO_2T_G} = V_{mCO_2T_N} \left(\frac{T_G}{T_N} \right) \quad (8)$$

and it is 50.69 litres, where $T_G = 618.15$ K, $T_N = 273.15$ K, $V_{mCO_2T_N} = 22.40$ litres is the volume of one mole of CO_2 at a temperature of 273.15 K.

Since the mass of one mole of CO_2 M_{mCO_2} is 44 grams, the mass of 1 litre will be calculated according to the ratio $M_{mCO_2}/V_{mCO_2T_G}$ and it will be 0.868 g/l. The volume of 1% of 1 m^3 is 10 litres. It follows that the mass of 1% of 1 m^3 is 10 litres \cdot 0.868 g/l and equals 8.68 g [12].

The data on CO_2 content in combustion products in % and g/m^3 depending on the engine operation mode are summarised in the table.

Fig. 4 shows that with increasing engine operation mode, the content of CO_2 in the exhaust gases rises, which is associated with an increase in fuel and air consumption with power gain, and consequently with an increase in the consumption of combustion products.

In exhaust gases of the NK-16ST engine the level of CO_2 carbon dioxide content is lower by $\approx 20\%$ compared to the NK-16-18ST engine.

If we adhere to the earlier assumption that the only mechanism of CO_2 reduction is incomplete oxidation reaction, then CO_2 reduction should lead to an increase in CO emissions, which is confirmed by the measurement data (Fig. 5).

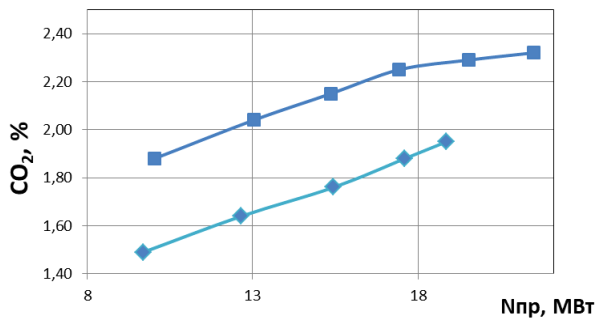


Рис. 4. Содержание углекислого газа CO_2 в продуктах сгорания:
◆ – двигатель НК-16СТ и ■ – двигатель НК-16-18СТ

Fig. 4. Content of CO_2 carbon dioxide in combustion products:
◆ – engine NK-16CT and ■ – engine NK-16-18CT

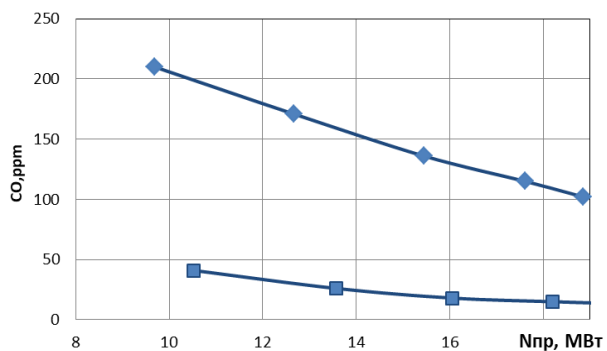


Рис. 5. Содержание оксидов углерода CO в продуктах сгорания:
◆ – двигатель НК-16СТ и ■ – двигатель НК-16-18СТ

Fig. 5. Content of carbon oxides in combustion products:
◆ – engine NK-16CT and ■ – engine NK-16-18CT

For the further analysis, the CO_2 mass concentrations for each operating mode of NK-16-18ST and NK-16ST engines are presented and converted into g/m^3 using the previously derived ratio of 1% = 8.68 g/m^3 .

CO_2 content depending on engine operation mode

NK-16-18ST					
	n_{LPC}	N_c	CO, ppm	CO_2 , %	CO_2 , g/m^3
1	4900	10.515	41	1.71	14.84
2	5100	13.577	26	1.89	16.41
3	5250	16.064	18	2.00	17.36
4	5350	18.201	15	2.10	18.22
5	5450	20.133	13	2.20	19.09
6	max	22.011	13	2.25	19.53

NK-16ST					
	N_{LPC}	N_c	CO, ppm	CO ₂ , %	CO ₂ , g/m ³
1	4900	9.69	210	1.49	12.93
2	5100	12.66	171	1.64	14.24
3	5250	15.451	136	1.76	15.28
4	5350	17.61	115	1.88	16.32
5	max	18.864	102	1.95	16.93

From Fig. 4 and the table it can be seen that the NK-16ST engine with a commercially available combustion chamber has a lower CO₂ concentration level than the NK-16-18ST engine with a combustion chamber having a multi-nozzle front device [13].

To calculate the completeness of fuel combustion the following dependence was used [14]:

$$\eta_G = 1 - (0.20175 \cdot EI_{CO} + EI_{CH_4}) \cdot 10^{-3}, \quad (9)$$

where EI_{CO} is a carbon monoxide emission index; EI_{CH_4} is a methane emission index; the value 0.20175 is a coefficient that takes into account the ratio of the net calorific value of carbon monoxide Q_N^{CO} to the lower calorific value of methane $Q_N^{CH_4}$, which are $Q_N^{CO} = 10096$ kJ/kg and $Q_N^{CH_4} = 50042$ kJ/kg.

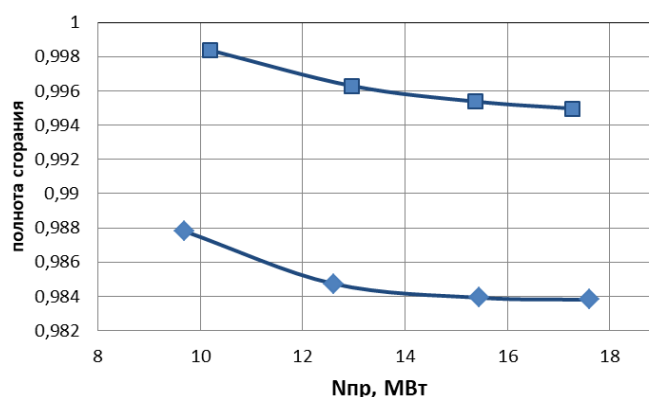


Рис. 6. Полнота сгорания топлива на различных режимах:
 ◆ – двигатель НК-16СТ, ■ – двигатель НК-16-18СТ

Fig. 6. Completeness of Combustion of Fuel on various power setting:
 ◆ – engine NK-16СТ and ■ – engine NK-16-18СТ

The emission indices EI_i for carbon monoxide and methane are calculated using the equation

$$EI_i = \frac{\mu_i}{\mu_a} (1 - \alpha_i \cdot L_0) \cdot \chi_i \cdot 10^{-3}, \quad (10)$$

where $L_0 = 17.2$ is a previously calculated stoichiometric methane combustion coefficient (kg of air/kg of fuel); α_i is a total or local air excess ratio; μ_i is a molar mass of the toxic substance to be determined (CO, CH₄), g/mole; μ_a is a molar mass of the air, g/mole; χ_i is a volume fraction of toxic substance, ppm.

The variation of combustion completeness is characterised by insignificant decrease within 0.5 % in the power range from 10 to 17 MW, thus at the 16 MW mode the average completeness for the NK-16ST engine was $\eta = 0.985$, for the NK-16-18ST engine - $\eta = 0.996$ (Fig. 6).

Conclusion

The possibility of reducing the level of CO₂ concentration in the engine combustion products up to 20 % by reducing the completeness of fuel combustion in the combustion chamber was confirmed.

The data obtained on the change of CO₂ concentration with the change of engine operation mode can be useful in selecting the most appropriate mode to minimise CO₂ during operation.

The presented approaches to the organisation of combustion processes can be used by developers when designing combustion chambers of gas turbine engines operating on natural gas to minimise CO₂ emissions while ensuring CO optimum and combustion completeness.

Библиографические ссылки

1. Lefebvre A. H. Fuel effects on gas turbine combustion-ignition, stability, and combustion efficiency // Am. Soc. Mech. Eng. 1984. Vol. 84, No. CONF-840611.
2. Бакланов А. В. Влияние изменения конструкции камеры сгорания на уровень CO₂ в выхлопных газах газотурбинного двигателя НК-16СТ // Газовая промышленность. 2022. № 6 (834). С. 80–88.
3. Маркушин А. Н., Бакланов А. В. Исследование рабочего процесса камер сгорания в составе ГТД // Вестник Самарского ун-та. Аэрокосмическая техника, технологии и машиностроение. 2016. Т. 15, № 3. С. 81–89.
4. Некоторые вопросы проектирования авиационных газотурбинных двигателей / Е. А. Гриценко, В. П. Данильченко, С. В. Лукачев и др. Самара : СНЦ РАН, 2002. 527 с.
5. Бакланов А. В. Влияние геометрии горелки на характеристики камеры сгорания газотурбинного двигателя // Вестник Москов. авиац. ин-та. 2021. Т. 28, № 2. С. 86–95.
6. Features of commissioning a gas turbine unit with a low-emission combustion chamber / I. E. Vorotyntsev, D. D. Tyulkin, D. G. Fedorchenko, Yu. I. Tsybizov // Journal of Physics: Conference Series. 2021. Vol. 1891. P. 012002.
7. Бакланов А. В. Управление процессом сжигания топлива путем изменения конструкции горелки в камере сгорания газотурбинного двигателя // Вестник Москов. авиац. ин-та. 2018. Т. 25, № 2. С. 73–85.
8. Бакланов А. В. Малоэмиссионная камера сгорания диффузионного типа с микропламенным горением для конвертированного авиационного газотурбинного двигателя // Вестник Москов. авиац. ин-та. 2017. Т. 24, № 2. С. 57–68.
9. ГОСТ 28775–90. Агрегаты газоперекачивающие с газотурбинным приводом. Общие технические условия. М. : Стандартиформ, 2005. 12 с.
10. Energy Efficient Engine Combustor Test Hardware–Detailed Design Report / D. L. Burrus, C. A. Charour, H. L. Foltz et al. NASA CR-168301.
11. Dodds W. J., Ekstedt E. E. Broad Specification Fuel Combustion Technology Program. Phase II, Final Report, 1989.
12. Lefebvre A. H. Influence of Fuel Properties on Gas Turbine Combustion Performance. AFWAL-TR-84-2104, 1985.
13. Анализ применимости моделей горения для расчёта многофорсуночной камеры сгорания ГТД / Б. Г. Мингазов, В. Б. Явкин, А. Н. Сабирзянов, А. В. Бакланов // Вестник Самарского гос. аэрокосмич. ун-та им. акад. С. П. Королёва (нац. исслед. ун-та). 2011. № 5 (29). С. 208–214.
14. Канило П. М. Энергетические и экологические характеристики ГТД при использовании углеводородных топлив и водорода. Киев : Наук. думка, 1987. 224 с.

References

1. Lefebvre A. H. [Fuel effects on gas turbine combustion-ignition, stability, and combustion efficiency]. Am. Soc. Mech. Eng. 1984, Vol. 84, No. CONF-840611.

2. Baklanov A. V. [Impact of changing the combustion chamber design on the CO₂ concentration in the exhaust gases of the NK-16ST gas turbine engine]. *Gas industry*. 2022, No. 6 (834), P. 80–88 (In Russ.).
3. Markushin A. N., Baklanov A. V. [Investigation of the gas turbine engine combustion chamber workflow]. *Bulletin of the Samara university. Space equipment, technologies and mechanical engineering*. 2016, Vol. 15, No. 3, P. 81–89 (In Russ.).
4. Gritsenko E. A., Danilchenko V. P., Lukachev S. V. *Nekotoryye voprosy proyektirovaniya aviatsionnykh gazoturbinnnykh dvigateley* [Some issues of the design of aircraft gas turbine engines]. Samara, 2002, 527 p.
5. Baklanov A. V. [Burner geometry impact of gas turbine engine combustion chamber characteristics]. *Vestnik moskovskogo aviatsionnogo instituta*. 2021, Vol. 28, No. 1, P. 86–95 (In Russ.).
6. Vorotyntsev I. E., Tyulkin D. D., Fedorchenko D. G., Tsybizov Yu. I. [Features of commissioning a gas turbine unit with a low-emission combustion chamber]. *Journal of Physics: Conference Series*. 2021, Vol. 1891, P. 012002.
7. Baklanov A. V. [Controlling fuel combustion process by burner design change in gas turbine engine combustion chamber]. *Vestnik moskovskogo aviatsionnogo instituta*. 2018, Vol. 25, No. 2, P. 73–85 (In Russ.).
8. Baklanov A. V. [Low-emission combustion chamber of diffusion type employing micro flame burning process for converted aircraft gas turbine engine]. *Vestnik moskovskogo aviatsionnogo instituta*. 2017, Vol. 24, No. 2, P. 57–68 (In Russ.).
9. STO Gazprom 2-3.5-038-2005 Instructions for conducting control measurements of harmful emissions of gas turbine plants at compressor stations. Chelyabinsk, Center for Work Safety, 2005, 13 p.
10. Burrus D. L., Charour C. A., Foltz H. L. et al. Energy Efficient Engine Combustor Test Hardware—Detailed Design Report. NASA CR-168301.
11. Dodds W. J., Ekstedt E. E. Broad Specification Fuel Combustion Technology Program. Phase II, Final Report, 1989.
12. Lefebvre A. H. Influence of Fuel Properties on Gas Turbine Combustion Performance. AFWAL-TR-84-2104, 1985.
13. Mingazov B. G., Yavkin V. B., Sabirzyanov A. N., Baklanov A. V. [The analysis of applicability of models of burning for calculation of the GTD mnogoforsunochny combustion chamber]. *Bulletin of Samara State Aerospace University of the academician S.P. Korolyov (national research university)*. 2011, No. 5 (29), P. 208–214 (In Russ.).
14. Canilo P. M. *Energeticheskiye i ekologicheskiye kharakteristiki GTD pri ispol'zovanii uglevodородnykh topliv i vodoroda* [Energy and environmental performance of gas turbine engines when using hydrocarbon fuels and hydrogen]. Kiev, Nauk. Dumka, 1987, 224 p.

© Baklanov A. V., 2023

Бакланов Андрей Владимирович – заместитель главного конструктора; АО «Казанское моторостроительное производственное объединение». E-mail: andreybaklanov@bk.ru.

Baklanov Andrey Vladimirovich – deputy chief designer; Joint-Stock Company “Kazan motor production association”. E-mail: andreybaklanov@bk.ru.

УДК 629.785

Doi: 10.31772/2712-8970-2023-24-4-706-716

Для цитирования: Расчёт параметров и характеристик вращающегося лунного реактивного пенетратора / Е. В. Гусев, В. А. Заговорчев, В. В. Родченко и др. // Сибирский аэрокосмический журнал. 2023. Т. 24, № 4. С. 706–716. Doi: 10.31772/2712-8970-2023-24-4-706-716.

For citation: Gusev E. V., Zagovorchev V. A., Rodchenko V. V. et al. [Calculation of the parameters and characteristics of a rotating lunar jet penetrator]. *Siberian Aerospace Journal*. 2023, Vol. 24, No. 4, P. 706–716. Doi: 10.31772/2712-8970-2023-24-4-706-716.

Расчёт параметров и характеристик вращающегося лунного реактивного пенетратора

Е. В. Гусев*, В. А. Заговорчев, В. В. Родченко, Э. Р. Садретдинова,
Е. А. Шипневская

Московский авиационный институт (национальный исследовательский университет)
Российская Федерация, 125993, г. Москва, А-80, ГСП-3, Волоколамское шоссе, 4
*E-mail: ccg-gus@mail.ru

Целью работы является определение параметров внутренней баллистики реактивного двигателя твёрдого топлива, установленного на реактивном пенетраторе, входящем в грунт с высокой скоростью вращения вокруг собственной оси. Методы исследования: для определения величины давления в камере вращающегося двигателя обычно используют известные уравнения баланса прихода и расхода газа, что и в случае невращающегося реактивного двигателя твёрдого топлива. Отличие внутренней баллистики вращающегося реактивного двигателя твёрдого топлива состоит в том, что влияние вращения на рабочий процесс учитывается коэффициентом расхода газов из камеры вращающегося двигателя, изменением скорости эрозионного горения твёрдого топлива при вращении реактивного двигателя твёрдого топлива, коэффициентом тепловых потерь. Результаты: установлено, что на параметры внутренней баллистики вращающихся реактивных двигателей твёрдого топлива основное влияние оказывают коэффициент расхода газов из камеры вращающегося двигателя, эффект эрозионного горения твёрдого топлива и изменение коэффициента тепловых потерь. Приведены основные расчетные зависимости для определения давления в камере сгорания вращающегося двигателя твёрдого топлива для периодов выхода давления на стационарный режим работы двигателя, работа двигателя на стационарном режиме и в период свободного истечения газов из камеры реактивного двигателя твёрдого топлива. Представлена методика выбора линейных и угловых размеров сопла вращающегося двигателя. Приведена оценка силы тяги для одинарного сопла, вращающегося реактивного двигателя твёрдого топлива. Установлено, что величина силы тяги вращающихся двигателей (при прочих одинаковых условиях в камере сгорания) в 1,1–1,36 раза меньше, чем у невращающихся реактивных двигателей твёрдого топлива. Проведённые опыты показали уменьшение степени закрутки газового потока вращающихся двигателей твёрдого топлива при увеличении количества топливных шашек в заряде двигателя. Заключение: результаты, изложенные в статье, могут быть полезны для научных работников, аспирантов и инженеров, занятых созданием и эксплуатацией авиационной и ракетно-космической техники, а также студентов технических вузов, обучающихся по соответствующим специальностям.

Ключевые слова: пенетратор, параметры и характеристики, вращение вокруг оси.

Calculation of the parameters and characteristics of a rotating lunar jet penetrator

E. V. Gusev^{*}, V. A. Zagovorchev, V. V. Rodchenko,
E. R. Sadretdinova, E. A. Shipnevskaya

Moscow Aviation Institute (National Research University)
4, Volokolamskoe highway, Moscow, 125993, Russian Federation
^{*}E-mail: ccg-gus@mail.ru

The purpose of the work is to determine the parameters of the internal ballistics of a solid propellant jet engine mounted on a jet penetrator entering the ground at a high rotation speed around its own axis. Research methods: to determine the pressure in the chamber of a rotating engine, the known equations for the balance of gas inflow and consumption are usually used, as in the case of a non-rotating solid propellant jet engine. The difference between the internal ballistics of a rotating solid propellant jet engine is that the effect of rotation on the operating process is taken into account by the coefficient of gas flow from the chamber of the rotating engine; a change in the rate of erosive combustion of solid propellant during rotation of a solid propellant jet engine; heat loss coefficient. Results: it was found that the parameters of the internal ballistics of rotating jet engines of solid propellant are mainly influenced by the coefficient of gas flow from the chamber of the rotating engine; effect of erosive combustion of solid propellant and change in heat loss coefficient. The main calculated dependencies for determining the pressure in the combustion chamber of a rotating solid propellant engine are presented for periods when the pressure reaches a stationary mode of operation of the engine, operation of the engine in a stationary mode and during the period of free flow of gases from the chamber of a solid propellant jet engine. A method for selecting the linear and angular dimensions of a rotating engine nozzle is presented. An estimate of the thrust force for a single nozzle rotating solid propellant jet engine is given. It has been established that the magnitude of the thrust force of rotating engines (under other identical conditions in the combustion chamber) is 1.1–1.36 times less than that of non-rotating solid propellant jet engines. The experiments carried out showed a decrease in the degree of swirl of the gas flow of rotating solid propellant engines with an increase in the number of propellant pellets in the engine charge. Conclusion: the results presented in the article can be useful for scientists, graduate students and engineers involved in the creation and operation of aviation and rocket and space technology, and can also be useful for students of technical universities studying in relevant specialties.

Keywords: penetrator, parameters and characteristics, rotation around an axis.

Introduction

Theoretical and experimental studies on embedding solid bodies into the ground at the expense of kinetic energy accumulated outside the ground section of the trajectory show that the section of motion in the ground sometimes has a noticeable curvilinear character, in which a significant departure from rectilinear motion is possible, up to a complete turn of the penetrating body and movement of its bottom part forward. The character of motion is significantly influenced by forces, which in turn depend both on the shape of the body and on the initial conditions of penetration, determined by the presence of the angle between the velocity vector and the axis of symmetry, as well as the angular velocities of precession, nutation and proper rotation.

When a jet penetrator with a running engine is embedded in the ground, its stability is affected (in addition to the above-mentioned factors) by such factors as the thrust magnitude, its eccentricity and the possibility of swirling motion.

The purpose of this paper is to determine the internal ballistics parameters of a solid propellant jet engine mounted on a jet penetrator entering the ground with a high rotational velocity around its own axis.

To determine the pressure value in the chamber of a rotating engine, the well-known equations of the balance of gas inflow and outflow are usually used, as in the case of a non-rotating solid propellant jet engine. The difference between the internal ballistics of a rotating solid propellant jet engine is that the effect of rotation on the working process is taken into account [1]:

– by the flow coefficient of gases from the rotating engine chamber

$$A_{rot} = A_0 \left(\frac{1}{1 + \frac{k}{k+1} \alpha_{cr}^2} \right)^{\frac{1}{1-\nu}} ; \quad (1)$$

– by change in the rate of erosive combustion of solid propellant during the rotation of a solid propellant jet engine

$$\varepsilon_{rot} = 1 + Bn^{0.5}; \quad (2)$$

– by the heat loss coefficient

$$\chi_{rot} = \frac{1 - 0.16 \left(1 + \tan^2 \alpha_{cr} \right)^{0.4}}{1 + 2\psi}, \quad (3)$$

where A_0 is a flow coefficient of gases from the combustion chamber of a non-rotating solid propellant jet engine.

The value of the gas flow coefficient is determined according to the following dependence

$$A_0 = \frac{\dot{M}_0}{\dot{M}_T} \leq 1, \quad (4)$$

where \dot{M}_0 is a real (experimental) mass flow rate, taking into account all possible types of losses that reduce the gas flow rate through the nozzle; $\dot{M}_m = \frac{p_{cr} f_{cr}}{\sqrt{\chi RT_0}}$ is theoretical gas flow rate through the nozzle;

p_{cr} is braking pressure at the nozzle inlet; f_{cr} is a critical cross-sectional area of the nozzle; χ

is a coefficient of heat loss; RT_0 is a reduced force of solid propellant; $B = 3.7 \cdot 10^{-6}$ at $n \leq 10^3 \frac{rot}{min}$;

k is an adiabatic value; α_{cr} is angle of swirl of gas flow in the critical section of the engine nozzle;

n is a number of revolutions of the rotating ground jet penetrator; ν is a degree exponent in the propellant combustion rate law; ψ is a relative fraction of burnt charge.

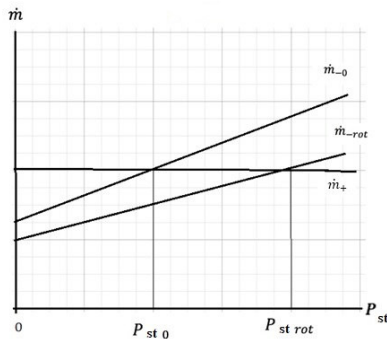


Рис. 1. График, иллюстрирующий принцип стационарности

Fig. 1. Graph illustrating the principle of stationarity

The algorithm for determining the pressure in the combustion chamber of a rotating solid propellant engine

1. Steady-state pressure at the stationary operation section of the solid propellant jet engine.

Fig. 1 graphically depicts the principle of stationarity of the operation of the rotating solid propellant jet engine.

Here \dot{m}_+ is gas supply into the combustion chamber of the solid propellant jet engine; \dot{m}_0 and \dot{m}_{rot} are gas flow rate of the non-rotating and rotating engine, respectively.

The graph shows that a decrease in the gas flow rate of a rotating engine leads to an increase in the steady-state pressure in its combustion chamber, i.e. $P_{strot} \geq P_0$.

In this case the following equation is used for the calculation of P_{strot}

$$P_{strot} = \left(\frac{1}{N_1} \right)^{\frac{1}{1-\nu}}, \quad (5)$$

where $N_1 = \frac{N}{\varepsilon}$; $\varepsilon = \frac{P}{\rho_m \chi_{rot} RT_0}$; $\chi_{rot}(\alpha)$ is from (3); $N = \frac{\Phi_2 A_{rot} p_k f_{cr}}{S_g U_m \rho_m \sqrt{\chi_{rot} RT_0}}$;

$U_m = f_1(T_3) f_2(p_c) f_3(\alpha_{cr}) f_4(\chi_0)$ – $U_m = f_1 f_2 f_3 f_4$ is solid propellant burning speed depending on the charging temperature ($f(T_3)$), pressure in the combustion chamber $f_2(p_c)$, degree of swirl $f_3(\alpha_{cr})$ of gas flow and the Pobedonostsev criterion $f_4(\chi_0)$ [2; 3].

Fig. 2 shows the dependence of the steady-state pressure in the chamber of a rotating solid propellant jet engine on the degree of swirl of the gas flow.

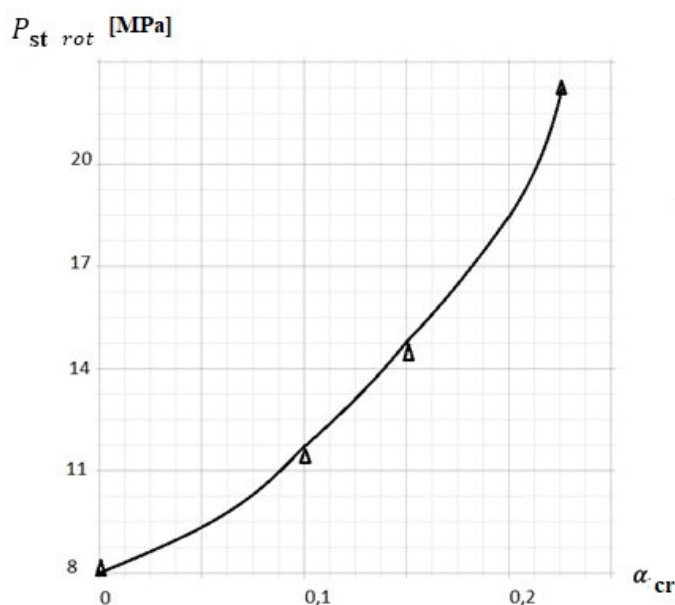


Рис. 2. Зависимость величины установившегося давления в камере сгорания от степени закрутки газового потока

Fig. 2. Dependence of the steady-state pressure in the combustion chamber on the degree of swirl of the gas flow

The calculations P_{strot} were performed for a real engine of a 40 mm diameter model ground jet. Here Δ marks are used to indicate experimental values of steady-state pressure. A good agreement between the calculated and experimental data can be seen.

Thus, the steady-state pressure in the chamber of solid propellant jet engine varies depending on the speed of its rotation around its own axis. In this case, with the increase in the degree of swirl of the gas flow, the value of the steady-state pressure increases, the rate of pressure build-up in the process of the engine entering the steady-state mode of operation decreases, and at a given propellant mass, the engine operation time decreases (Fig. 3).

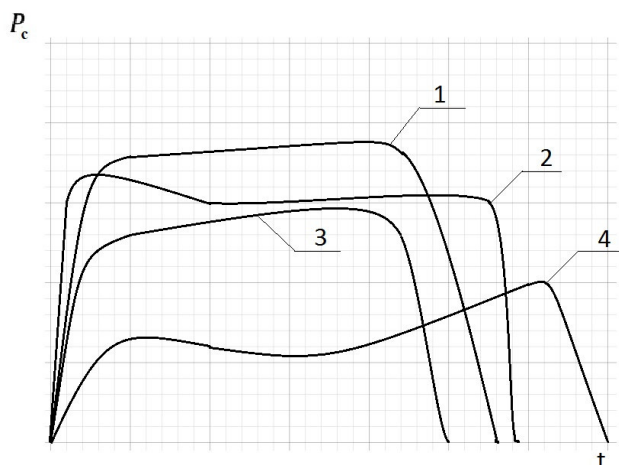


Рис. 3. Типовые зависимости давления в камере сгорания для вращающихся РДТТ:
 1 – для вращающегося РДТТ; 2 – для невращающегося РДТТ; 3 – отмечается некоторое
 увеличение установившегося давления в камере для вращающихся двигателей при $n < 10^3 \frac{\text{об}}{\text{мин}}$;
 4 – показана возможность появления второго максимума, величина которого больше первого

Fig. 3. Typical pressure dependences in the combustion chamber for rotating solid propellant rocket engines:
 1 – for a rotating solid propellant rocket engine; 2 – for a non-rotating solid propellant jet engine;
 3 – there is a slight increase in the steady-state pressure in the chamber for rotating engines at $n < 10^3 \text{ rpm/min}$;
 4 – shows the possibility of the appearance of a second maximum, the value of which is greater than the first

It should be noted that the pressure in the combustion chamber of a rotating engine can be corrected either by using an afterburning volume in its design, which increases the free volume of the combustion chamber, or by changing the thermal and hydraulic loss coefficients. The hydraulic loss coefficient can be calculated using the following formula

$$\xi = \xi_0 (1 + \text{tg} \alpha_{cr}^2)^{1.375}, \quad (6)$$

where ξ_0 is a hydraulic loss coefficient at one-dimensional gas flow through the pipe at $\alpha_{cr} = 0$.

The calculations show that α_{cr} value due to hydraulic losses to the values $\alpha_{cr} \approx 0,2$ is almost unchanged, Therefore, its reduction should be taken into account at $\alpha_{cr} > 0.3 - 0.4$, when α_{cr} is reduced by 13–35 %.

2. Switching of a rotating solid propellant jet engine to steady-state mode

When calculating the pressure-time dependence of the rotating solid-propellant engine on the steady-state mode of operation, as in the case of the flow rates of a solid propellant jet engine [3; 4], the following parameter is determined

$$a = \frac{\varphi_2 A_{rot} b f_{cr} \sqrt{\chi_{rot} R T_0} (1 - \nu)}{W_g}, \quad (7)$$

where rotation is taken into account by introducing the coefficients A_{rot} and χ_{rot} ; b and ν are coefficients in the propellant combustion law; $W_g = \rho u S_g$ is gas supply to the combustion chamber; u is a combustion rate; S_g is a combustion surface of the propellant charge.

After that, the total time for the solid propellant jet engine to reach steady-state is calculated

$$\tau_p = \frac{1}{a} \ln \frac{1 - p_b^{1-\nu}}{1 - \bar{p}^{1-\nu}}, \quad (8)$$

where $\bar{p} = 0.99$ is limit relative pressures in the combustion chamber in the process of the solid-propellant jet engine reaching the steady-state mode of operation; p_b is pressure in the chamber when the charge is ignited.

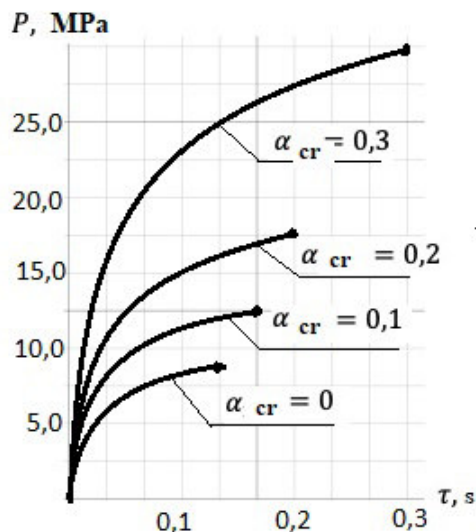


Рис. 4. Зависимость давления в камере сгорания от времени при выходе двигателя на установившийся режим

Fig. 4. Dependence of pressure in the combustion chamber on time when the engine reaches steady state

The calculations given for a 240 mm diameter rotating ground jet penetrator at swirl angles $\alpha_{cr} = 0.1; 0.2; 0.3$ showed that: 1) engine steady-state time increases by 23 % with increasing rotational speed at $\alpha_{cr} = 0.1$, by 46 % at $\alpha_{cr} = 0.2$ and by 130 % at $\alpha_{cr} = 0.3$, i.e. from 0.13 s to 0.3 s; 2) increases the steady-state pressure compared to a non-rotating engine.

In order to obtain the dependence (Fig. 4), τ_p was first defined using the formula (8), then three following values were chosen τ_1, τ_2, τ_3 , which are in the interval between τ_p and 0, and according to the value of these times the relative pressures $\bar{p}_1, \bar{p}_2, \bar{p}_3$ were determined by the formula

$$\bar{p}_i = \left[1 - (1 - p_b)^{1-\nu} e^{-a\tau_i} \right]^{\frac{1}{1-\nu}}, \quad (9)$$

Then \bar{p}_i were recalculated into real design pressures according to the dependence:

$$\bar{P}_i = P_{stot} \bar{p}_i, \quad (10)$$

where p_i is calculated up to $\bar{p} = 0.99$.

3. Calculation of pressure during the period of free flow of gases from the chamber of a solid propellant jet engine

As in the case of calculation of the after-effect period for a non-rotating engine, the end of charge combustion time is determined by the formula [3-5]

$$\tau_k = \frac{e}{u}, \quad (11)$$

where e is a burning vault thickness; for a tubular charge burning on the outer (D) and inner (d) surfaces it is, in particular, equal to

$$e = \frac{D-d}{4}. \quad (12)$$

Taking into account the dependence of the charge burning rate on the pressure in the combustion chamber, it is evident that the end of combustion time for the rotating engine will be less than the end of combustion time for the charge of the non-rotating engine, because the steady-state pressure of the rotating engine is greater than the steady-state pressure of the non-rotating engine.

The time of full flow of gases from the combustion chamber after combustion of solid propellant is calculated by the following formula

$$\tau_{fr} = \frac{1}{B} \left[\left(\frac{p_{krot}}{1.8} \right)^{0.1} - 1 \right], \quad (13)$$

where $B = \frac{K-1}{2} \frac{\varphi_2 A_{rot} f_{cr} b \sqrt{X_{rot} RT_0}}{W_{km}}$; $p_k = 1.8$ bar is the pressure in the combustion chamber up to which the supercritical flow formula is valid.

The pressure dependence on the free gas flow time is determined in the following sequence:

1) time τ_{fr} is divided into three intervals, where τ_1 , τ_2 and τ_3 are less than τ_{fr} ;

2) p_1 , p_2 and p_3 are calculated by the formula $p_i = \frac{p_{krot}}{(1 + B\tau_i)^{\frac{2k}{k-1}}}$.

The curve passing through the calculation points describes the period of free gas flow from the rotating solid propellant jet engine.

Fig. 5 shows the graph of dependence of the free flow time from the rotating engine chamber on the degree of swirl of a 240 mm diameter ground jet penetrator.

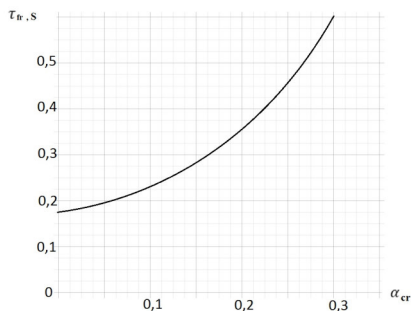


Рис. 5. Расчётная зависимость времени истечения от угла закрутки газового потока РДТТ

Fig. 5. Calculated dependence of the exhaust time on the swirl angle of the gas flow of a solid propellant jet engine

It was obtained at $\alpha_{cr} > 0$, $\tau_{fr} = 0.173$ s; at $\alpha_{cr} = 0.1$, $\alpha_{cr} = 0.2$ and $\alpha_{cr} = 0.3$, $\tau_{fr1} = 0.22$ s, $\tau_{fr2} = 0.32$ s and $\tau_{fr3} = 0.55$ s, respectively.

It can be seen from the graph (Fig. 5) that the time of free flow of gases from the combustion chamber after the end of propellant combustion increases with the increment of swirl parameters and, consequently, the number of revolutions of the jet penetrator.

Selection of linear and angular dimensions of the rotating engine nozzle

The dimensions of a single nozzle or nozzles of the nozzle block of a rotating solid propellant jet

engine are selected according to the same dependences as for a transforming engine, but taking into account the previously established dependences and coefficients.

Using dependences (5) for calculations of steady-state pressure in the chamber of a rotating engine, it is possible to find the area of the critical cross-section of the engine nozzle using the formula [1]

$$f_{cr} = \frac{s_r U_\tau \rho_\tau \sqrt{X_{rot} RT_0}}{\varphi_2 A_{rot} b p_{rot}^{1-\nu}}, \quad (14)$$

$$d_{cr} = \sqrt{\frac{4f_{cr}}{\pi n}}, \quad (15)$$

where n is the number of nozzles; $A_{rot}(\alpha_{cr})$, $X_{rot}(\alpha_{cr})$ are coefficients; p_{rot} is a design pressure at the engine chamber wall.

The comparative analysis of the calculations of the supersonic nozzle part of rotating and non-rotating engines showed that the optimum angle of the supersonic part of the rotating engine corresponds to the optimum angle of the nozzle of a non-rotating solid propellant jet engine and is equal to 20° . The experimental data presented in [1] confirm this conclusion and also show that it is necessary to choose a larger nozzle entrance angle in the presence of flow rotation than for a nozzle with one-dimensional flow.

Fig. 6 shows the experimental dependence of the single impulse J_{un} on half of the nozzle entry angle α . The graph shows that J_{un} reaches a maximum at $2\alpha = 180^\circ$, i.e., at a flat wall of the nozzle block. This effect is explained by the fact that the flat wall completely dampens the axial component of the gas flow velocity and increases its radial component, which increases the gas flow rate through the nozzle.

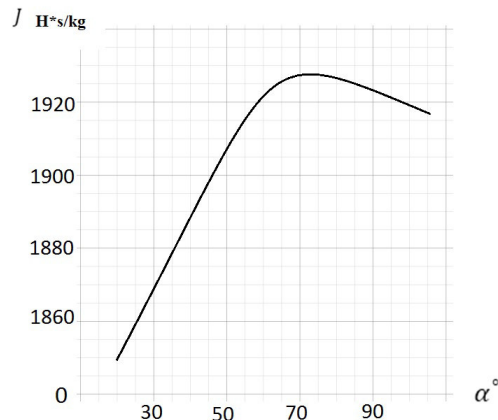


Рис. 6. Зависимость величины единичного импульса от половины угла входа в сопло двигателя

Fig. 6. Dependence of the magnitude of a unit impulse on half the angle of entry into the engine nozzle

For a single nozzle, the thrust formula can be written as follows

$$P_{rot} = K_d P_{rot} f_{cr} \varphi_1 \varphi_2 A_{rot}, \quad (16)$$

where K_d is a thrust coefficient; f_{cr} is a nozzle critical cross-sectional area; $\varphi_1 = 0.95-0.98$ is a velocity coefficient; φ_2 is a nozzle flow coefficient at gas flow without swirling; $A_{rot} = f(\alpha_{cr})$ is a flow coefficient for rotating gas flow.

Thus, knowing the laws of pressure change in the combustion chamber of a rotating a solid propellant jet engine and using the above formulae for thrust force, it is possible to graphically construct $P_{rot}(\tau)$ dependences for any type of a rotating engine [6-8].

The analysis of dependences for the thrust force of rotating ground jet vehicles allows us to state that the thrust force value of such engines will be less than that of non-rotating ones, all other conditions being equal.

The difference in thrust forces will be determined by the following ratio

$$\frac{A_0}{A_{rot}} = \left(\frac{P_{rotcr}}{P_{0cr}} \right)^{\frac{1}{1-\nu}} = \left(1 + \frac{k}{k-1} \alpha_{cr}^2 \right)^{\frac{1}{1-\nu}}, \quad (17)$$

then

$$\frac{P_0}{P_{rot}} \approx \left(1 + \frac{k}{k-1} \alpha_{cr}^2 \right)^{\frac{1}{1-\nu}}. \quad (18)$$

For real solid propellants $\nu = 0.5-0.67$ at $\alpha_{cr} = 0.1-0.15$ the value of thrust relations is within $\frac{P_0}{P_{rot}} = 1.1-1.36$, i.e. the thrust of a non-rotating engine is 10-36 % greater than that of a rotating engine [9-11].

The experimental studies of rotating solid propellant jet engines equipped with multi-ball solid propellant charges have shown that (unlike solid propellant jet engines with single-ball charges) pressure nonuniformity in the combustion chamber is observed only in the pre-nozzle chamber. Herewith, the more draughts in the charge, the less is the degree of swirl both in the channel of a single draughts and in the pre-nozzle block as a whole [12-15].

Conclusion

Within the framework of the conducted research the following tasks have been solved:

1. It has been established that the internal ballistics parameters of rotating solid propellant jet engines are mainly influenced by the coefficient of gas flow rate from the rotating engine chamber, the effect of erosive combustion of solid propellant, and the change in the heat loss coefficient.
2. The basic calculation dependences for determining the pressure in the combustion chamber of a rotating solid propellant engine are given for the periods of pressure release on the stationary mode of engine operation, engine operation on the stationary mode and during the period of free flow of gases from the chamber of a solid propellant jet engine.
3. The methodology for selecting linear and angular dimensions of the nozzle of a rotating engine is presented, which allowed a comparative analysis of the calculations of the supersonic part of the rotating and non-rotating engines.
4. An estimate of the thrust force for a single nozzle of a rotating solid propellant jet engine is given. It is found that the thrust force of rotating engines (with other identical conditions in the combustion chamber) is 1.1-1.36 times less than that of non-rotating solid propellant jet engines.
5. The conducted experiments showed a decrease in the degree of swirl of the gas flow of rotating solid propellant engines with increasing the number of propellant draughts in the engine charge.

Библиографические ссылки

1. Михайловский Ю. В. Основы теории реактивных двигателей. МО СССР, 1970, 198 с.
2. Гостинцев Ю. А. Расходные характеристики сопла при истечении винтового потока газа // Изв. АН СССР. МЖГ. 1969. № 4. С. 158-162.

3. Алемасов В. Е. Дрегалин А. Ф. Теория ракетных двигателей. М. : Машиностроение, 1969. 547 с.
4. Орлов Б. В. Мазинг Г. Ю. Термодинамические и баллистические основы проектирования РДТТ. М. : Оборонгиз, 1968. 536 с.
5. Куров В. А. Должанский Ю. М. Основы проектирования пороховых ракетных снарядов. М. : Оборонгиз, 1961. 294 с.
6. Основы проектирования ракет / Г. В. Белов и др. М. : Машиностроение, 1974, 255 с.
7. Заговорчев В. А, Пронина П. Ф., Родченко В. В. Расчет основных проектных параметров и конструкция реактивного пенетратора для движения в лунном грунте // Известия вузов. Авиационная техника. 2020. № 4. С. 126–132.
8. Заговорчев В. А., Родченко В. В. Расчет основных проектных параметров реактивного пенетратора для движения в лунном грунте // Известия вузов. Авиационная техника. 2019. № 4. С. 65–72.
9. Импульс реактивной силы пороховых ракет / Я. Б. Зельдович и др. М. : Оборонизд, 1963. 190 с.
10. Родченко В. В. Основы проектирования реактивных аппаратов для движения в грунте. М. : МАИ-Принт, 2009. 359 с.
11. Сагомоян А. Я. Проникание. М. : Изд-во Московского ун-та, 2014. 298 с.
12. Применение реактивных пенетраторов для движения в лунном грунте / В. В. Родченко, В. А. Заговорчев, Э. Р. Садретдинова, П. Ф. Пронина // Вестник Уфимского гос. авиац. технич. ун-та. 2019. Т. 23, № 1(83). С. 56–63.
13. Федоров С. В., Федорова Н. А. Влияние импульса реактивной тяги на глубину проникания исследовательского зонда в грунт планеты // Инженерный журнал: наука и инновации. 2013. № 1 (13). DOI: 10.18698/2308-60332013-1-571.
14. Возможности моделирования проникания тел в грунтовые среды / Велданов В. А., Даурских А. Ю. и др. // Инженерный журнал: наука и инновации. 2013. № 9 (21). DOI: 10.18698/2308-6033-2013-9-947.
15. Определение параметров проникания пенетраторов в грунтово-скальные преграды по различным эмпирическим зависимостям / С. В. Федоров, В. А. Велданов, А. В. Дюков, Т. А. Гущина // Инженерный журнал: наука и инновации. 2022. № 4(124). DOI 10.18698/2308-6033-2022-4-2167.

References

1. Mikhailovsky Yu. V. [Fundamentals of the theory of jet engines]. MO. USSR, 1970, 198 p.
2. Gostintsev Yu. A. [Flow characteristics of the nozzle during the expiration of a screw gas flow]. *Izvestiy Akademii Nauk USSR*. 1969, No. 4, P. 158–162 (In Russ.).
3. Alemasov V. E. Dregalin A. F. *Teoriya raketnykh dvigateley* [Theory of rocket engines]. Moscow, Mashinostroenie Publ., 1969, 547 p.
4. Orlov B. V. Mazing G. Yu. *Termodinamicheskie i ballisticheskie osnovy proektirovaniya RDTT* [Thermodynamic and ballistic principles of solid propellant rocket engine design]. Moscow, Oborongiz Publ., 1968, 536 p.
5. Kurov V. A. Dolzhansky Yu. M. *Osnovy proektirovaniya porokhovykh raketnykh snaryadov* [Fundamentals of the design of powder rocket projectiles]. Moscow, Oborongiz Publ., 1961, 294 p.
6. Belov G. V. et al. *Osnovy proektirovaniya raket* [Fundamentals of rocket design]. Moscow, Mashinostroenie Publ., 1974, 255 p.
7. Zagorovchev V. A., Pronina P. F., Rodchenko V. V. [Calculation of the main design parameters and design of a reactive penetrator for movement in lunar soil]. *Izvestiya vischih echebnih zavedeniy. Aviacionnaya tehnika*. 2020, No. 4, P. 126–132 (In Russ.).

8. Zagorovchev V. A., Rodchenko V. V. [Calculation of the main design parameters of a reactive penetrator for movement in lunar soil]. *Izvestiya vischih echebniy zavedeniy. Aviacionnaya tekhnika*. 2019, No. 4, P. 65–72 (In Russ.).
9. Zeldovich Ya. B. et al. *Impul's reaktivnoy sily porokhovyykh raket* [Impulse of the reactive force of powder rockets]. Moscow, Oborongiz Publ., 1963, 190 p.
10. Rodchenko V. V. *Osnovy proektirovaniya reaktivnykh apparatov dlya dvizheniya v grunte* [Fundamentals of designing jet vehicles for movement in the ground]. Moscow, MAI-Print Publ., 2009, 359 p.
11. Sagomonyan A. Ya. *Pronikanie* [Penetration]. Moscow, Moscow University Publ., 2014, 298 p.
12. Rodchenko V. V., Zagovorchev V. A., Sadretdinova E. R., Pronina P. F. [Application of jet penetrators for movement in lunar soil]. *Vestnik Ufimskogo gosudarstvennogo aviacionnogo tekhnicheskogo universiteta*. 2019, Vol. 23, No. 1(83), P. 56–63 (In Russ.).
13. Fedorov S. V., Fedorova N. A. [The influence of the jet thrust pulse on the depth of penetration of the research probe into the planet's soil]. *Inzhenernyi zhurnal: nauka i innovatsii*. 2013, No. 1 (13). DOI: 10.18698/2308-60332013-1-571 EDN (In Russ.).
14. Veldanov V. A., Dauriskikh A. Yu. et al. [Possibilities of modeling body penetration in soils]. *Inzhenernyi zhurnal: nauka i innovatsii*. 2013, No. 9 (21). DOI: 10.18698/2308-6033-2013-9-947 (In Russ.).
15. Fedorov S. V., Veldanov V. A., Dyukov A. V., Gushchina T. A. [Determination of parameters for penetration of penetrators into soil-rock barriers according to various empirical dependencies]. *Inzhenernyi zhurnal: nauka i innovatsii*. 2022, No. 4(124), DOI 10.18698/2308-6033-2022-4-2167 (In Russ.).

© Gusev E. V., Zagovorchev V. A., Rodchenko V. V.,
Sadretdinova E. R., Shipnevskaya E. A., 2023

Гусев Евгений Владимирович – кандидат технических наук, доцент кафедры 610 «Управление эксплуатацией ракетно-космических систем»; Московский авиационный институт (национальный исследовательский университет). E-mail: ccg-gus@mail.ru.

Заговорчев Владимир Александрович – кандидат технических наук, доцент, доцент кафедры 610 «Управление эксплуатацией ракетно-космических систем»; Московский авиационный институт (национальный исследовательский университет). E-mail: zagovorchev@mai.ru.

Родченко Владимир Викторович – доктор технических наук, профессор, профессор кафедры 610 «Управление эксплуатацией ракетно-космических систем»; Московский авиационный институт (национальный исследовательский университет). E-mail: rodchenko47@mail.ru.

Садретдинова Эльнара Рамилевна – кандидат технических наук, доцент, заместитель директора Аэрокосмического института; Московский авиационный институт (национальный исследовательский университет). E-mail: elnara-5@mail.ru.

Шипневская Елизавета Алексеевна – магистр; Московский авиационный институт (национальный исследовательский университет). E-mail: Shipnevskaya.E@gmail.com.

Gusev Evgeniy Vladimirovich – Cand. Sc., Associate Professor of Department 610 “Operation Management of Rocket and Space Systems”; Moscow Aviation Institute (National Research University). E-mail: ccg-gus@mail.ru.

Zagovorchev Vladimir Aleksandrovich – Cand. Sc., Associate Professor, Associate Professor of Department 610 “Operation Management of Rocket and Space Systems”; Moscow Aviation Institute (National Research University). E-mail: zagovorchev@mai.ru.

Rodchenko Vladimir Viktorovich – Dr. Sc., Professor, Professor of Department 610 “Operation Management of Rocket and Space Systems”; Moscow Aviation Institute (National Research University). E-mail: rodchenko47@mail.ru.

Sadretdinova Elnara Ramilevna – Cand. Sc., associate professor, deputy Director of the Aerospace Institute; Moscow Aviation Institute (National Research University). E-mail: elnara-5@mail.ru.

Shipnevskaya Elizaveta Alekseevna – master, Moscow Aviation Institute (National Research University). E-mail: Shipnevskaya.E@gmail.com.

УДК 536.2:623.5

Doi: 10.31772/2712-8970-2023-24-4-717-736

Для цитирования: Подкопаев И. А., Подкопаев А. В., Должиков В. И. Математическая модель теплофизического нагружения малокалиберного артиллерийского ствола с вариантной дискретизацией полупространственных слоев расчетной области // Сибирский аэрокосмический журнал. 2023. Т. 24, № 4. С. 717–736. Doi: 10.31772/2712-8970-2023-24-4-717-736.

For citation: Podkopaev I. A., Podkopaev A. V., Dolzhikov V. I. [Mathematical model of thermophysical loading of a small-caliber artillery barrel with variant discretization of half-integer layers of the computational domain]. *Siberian Aerospace Journal*. 2023, Vol. 24, No. 4, P. 717–736. Doi: 10.31772/2712-8970-2023-24-4-717-736.

Математическая модель теплофизического нагружения малокалиберного артиллерийского ствола с вариантной дискретизацией полупространственных слоев расчетной области

И. А. Подкопаев, А. В. Подкопаев*, В. И. Должиков

Военный учебно-научный центр Военно-воздушных сил
«Военно-воздушная академия имени профессора Н. Е. Жуковского и Ю. А. Гагарина»
Российская Федерация, 394064, г. Воронеж, ул. Старых Большевиков, 54а
*E-mail: aleksanpodkopaev@mail.ru

В условиях непрерывного финансирования программ Министерства обороны Российской Федерации особенно остро встает вопрос поиска наиболее результативных путей модернизации изделий вооружения и военной (специальной) техники, разработки в области которых максимальны и процессы их совершенствования могут занять не более нескольких лет. К таким изделиям, в частности, можно отнести авиационное артиллерийское оружие (ААО), перспективы использования которого сохраняются на весь период существования армии с вооружением обычного типа. Основным фактором, влияющим на качество функционирования ААО, считается теплофизическое нагружение малокалиберного артиллерийского ствола (далее – ствол) в процессе стрельбы. Проблема повышения точности определения температурного поля ствола вновь актуализирована ужесточением условий нанесения ударов по целям. На первый план выдвинулись вопросы, тесно связанные с интенсификацией режимов применения ААО. Это вопросы нагрева, охлаждения, прочности при нагреве, износа, живучести стволов, вопросы безопасности и эффективности стрельбы. Несмотря на методологическую очевидность аналитических и численных подходов формализации теплопередачи в стволе, их практическая реализация довольно сложна. Физико-математический смысл этой причины следующий: возможная неустойчивость решений; проявление осцилляций в областях больших градиентов; одновременное присутствие в областях решений сверхзвуковых, звуковых и дозвуковых зон; существование ламинарных, турбулентных течений и других нелинейных образований; нетривиальность постановки граничных условий; наличие термического сопротивления поверхностей и т. д. Однако практические нужды обеспечения безопасности и повышения эффективности огневой эксплуатации ААО диктуют необходимость получения близкого приближения рассматриваемой задачи к ее возможно существующему точному аналитическому решению. Целью работы установлено совершенствование математического аппарата, моделирующего температурное поле ствола на основе сочетания методов теплообмена и математической физики. Проверкой достоверности разработанной математической модели (далее – модель, если из контекста изложения материала ясно, что речь идет именно о предлагаемом инструментарии), установлены факты отсутствия методических ошибок при формировании составных блоков модели и повышения точности дефиниции теплового нагружения ствола на 9,4 %. Исходя из акцентов заявленной проблемы, аргументированы направления совершенствования модели.

Ключевые слова: режим стрельбы, теплопроводность, дифференциальное уравнение, разностное уравнение, аппроксимация, достоверность.

Mathematical model of thermophysical loading of a small-caliber artillery barrel with variant discretization of half-integer layers of the computational domain

I. A. Podkopaev, A. V. Podkopaev*, V. I. Dolzhikov

Air Force Military educational and scientific center
“Air Force academy named after professor N. E. Zhukovsky and Y. A. Gagarin”
54a, Starykh bol'shevikov St., Voronezh, 394064, Russian Federation
*E-mail: aleksanpodkopaev@mail.ru

In the conditions of continuous financing of the programs of the Ministry of defense of the Russian Federation, the question of finding the most effective ways to modernize weapons and military (special) equipment, the developments in which are maximum and the processes of their improvement can take no more than a few years, is particularly acute. Such products, in particular, include aviation artillery weapons (AAO), the prospects for the use of which remain for the entire period of the army's existence with conventional weapons. The main factor influencing the quality of the AAO functioning is considered to be the thermophysical loading of a small-caliber artillery barrel (hereinafter referred to as the barrel) during firing. The problem of increasing the accuracy of determining the temperature field of the barrel is again updated by tightening the conditions for striking targets. Issues closely related to the intensification of AAO application regimes have come to the fore. These are issues of heating, cooling, thermal strength, wear, barrel survivability, issues of safety and firing efficiency. Despite the methodological evidence of analytical and numerical approaches to formalizing heat transfer in the wellbore, their practical implementation is rather complicated. The physical and mathematical meaning of this reason is as follows: possible instability of solutions; manifestation of oscillations in areas of large gradients; simultaneous presence in the solution regions of supersonic, sonic and subsonic zones; the existence of laminar, turbulent flows and other non-linear formations; non-triviality of setting boundary conditions; the presence of thermal resistance of surfaces, etc. However, the practical needs of ensuring safety and increasing the efficiency of fire operation of AAO dictate the need to obtain a close approximation of the problem under consideration to its possibly existing exact analytical solution. The aim of the work is to improve the mathematical apparatus that simulates the temperature field of the shaft based on a combination of heat transfer methods and mathematical physics. By verifying the reliability of the developed mathematical model (hereinafter referred to as the model, if from the context of the presentation of the material it is clear that we are talking about the proposed tools), the facts of the absence of methodological errors in the formation of the constituent blocks of the model and the increase in the accuracy of determining the thermal loading of the wellbore by 9.4 % were established. Based on the accents of the stated problem, the directions for improving the model are argued.

Keywords: firing mode, thermal conductivity, differential equation, difference equation, approximation, reliability.

Introduction

An analysis of existing trends in the development of artillery convincingly shows that at present the main attention of specialists is not so much the creation of new models, but rather the optimization of the tactical and technical characteristics of serial types of AAO [1]. An important obstacle when searching for the reserve functionality of AAO is manifested in the phenomenon of heating the barrel, which is cyclically subjected to high thermomechanical loads created by firing modes. The barrel largely determines the combat properties of the AAO, since it is in the barrel that the ballistic characteristics are realized and the design of all elements of the “cartridge-barrel” system largely depends on its design. As a result, the scientific and technical task of formalizing the temperature field of the barrel seems to be a priority task of AAO research.

The physical meanings of the automatic firing process indicate the need for an indispensable description of the non-stationary heating and cooling of the barrel by solving the differential equation of

thermal conductivity and the conditions of uniqueness with variable, continuous and discontinuous coefficients [2]. However, the exact solution of the thermophysics equation is limited for a certain range of problems. Such problems include the multidimensional, nonstationary, nonlinear problem of heat transfer in a cylindrical wall with a cross section varying along its length. Without dwelling on the diverse variations of approximation schemes for the differential heat equation and uniqueness conditions in various subject areas, we note the most successful approaches developed by domestic and foreign scientists. Thus, in the articles [3–5], experimental research schemes and methods for processing output data are proposed that provide increased accuracy in determining body temperature and expanded the measurement range; the article [6] presents a unique thermal model developed based on the apparatus of probability theory; in the article [7], the temperature fields of finned walls of various configurations were determined by numerical solutions of the multidimensional heat conduction problem; the article [8] proposed tools for mathematical modeling (hereinafter referred to as modeling) of the temperature field in gas turbine units, taking into account as much as possible the set of parameters in multifactor boundary conditions of the boundary layer; in the article [9], correlation regression dependencies of the optimal extrema of loading barrels of small arms and cannon artillery weapons were obtained. Examples of works on similar topics in the field of aviation artillery science include the articles [10–13].

Despite the fact that in the analyzed works almost all of the presentation of the material, naturally, is of a purely specific nature, some ideas of colleagues turned out to be useful in achieving the goal of this work.

Formation of a model scheme for studying the temperature field of the barrel

Obtaining the desired solution to the problem posed in a non-stationary formulation, with thermo-physical coefficients depending on temperature, is carried out in a sequence that ensures step-by-step specification of dependent actions.

Since the barrel has the shape of a limited cylinder of finite length, with the structural absence of heat sources in the internal sections of the barrel, the basic equation of thermal conductivity is presented in a cylindrical coordinate system in the form [2; 14; 15]:

$$\frac{\partial T}{\partial t} = a \left(\frac{\partial^2 T}{\partial z^2} + \frac{\partial^2 T}{\partial r^2} + \frac{1}{r} \frac{\partial T}{\partial r} + \frac{1}{r^2} \frac{\partial^2 T}{\partial \theta^2} \right), \quad (1)$$

where T – barrel temperature; t – time; a – thermal diffusivity coefficient of barrel steel; z , r , θ , – radius vector, applicate and polar angle, respectively, of the cylindrical coordinate system.

Coefficient a in the equation (1) is significant for non-stationary thermal processes and characterizes the rate of change in body temperature:

$$a = \frac{\lambda}{c\rho}, \quad (2)$$

where λ , c , ρ – coefficients of thermal conductivity, specific heat capacity and density, respectively, of barrel steel.

If the thermal conductivity coefficient of barrel steel λ characterizes the ability of a material to conduct heat, then the thermal conductivity coefficient of barrel steel a is a measure of the thermal inertia properties of the body under study. The rate of temperature change at any point in the barrel will be greater, the greater the value of the coefficient a , which is revealed by the test condition when operating with formula (2), formed as a table of dependences of the thermal conductivity coefficients λ and specific heat c of the barrel steel on the barrel temperature T [16].

The most complete mathematical models of heat exchange processes occurring in various products with various configurations take into account the presence of uneven space-time fields in the desired quantities: temperatures of solids, liquids, gases, heat flows, radiation intensities, etc. [6–9]. Such mathematical models are systems of partial differential equations, integral and integrodifferential

equations. However, the solution to the problem under consideration is limited to the construction of a model based on specific assumptions, which is explained by the following reasons:

- direct implementation of complete thermal mathematical models is possible exclusively for elementary volumes under simple boundary conditions;
- the use of an absolute mathematical model of the functioning of a pulsed heat engine is complicated by the difference in the boundaries of the AAO elements and a large number of not always deterministic initial data;
- the issue of harmonizing the accuracy characteristics of physical and mathematical methods with the available characteristics of computer time, memory and bit grid involves the consistent use of more simplified, compared to the full, mathematical models that describe the thermophysical loading of the barrel with varying degrees of detail.

When solving the problem of the most complete and objective determination of the temperature field of a barrel heated by firing, the following assumptions are made that relate to the basic assumptions of the subject area of knowledge:

- the initial temperature of the barrel is approximately equal to the ambient temperature ($T_0 = T_2$) or corresponds to its distribution over the surface of the barrel; subsequent loading with shots is characterized by the presence of a very specific temperature field of the barrel before each shot;
- the material of the barrel steel ОХН2МФА is considered isotropic and homogeneous, that is, the coefficients of thermal conductivity λ and specific heat capacity c of the barrel steel do not depend on spatial coordinates;
- the contact of the cartridge case with the chamber wall is assumed to be ideal, due to the tight pressing of the cartridge case under the influence of the pressure of the powder gases (hereinafter referred to as gases) when fired;
- the cartridge is represented as a model temperature concentrator and is simulated by a concentrated heat capacity with constant thermophysical characteristics.

The first and second assumptions about the mechanism of heat transfer in the barrel allow us to assume that there are no temperature fluctuations T on the outer and inner surfaces of the barrel sections after the shot. Then the isothermal surfaces remain cylindrical, having a common axis with the pipe, and the barrel temperature T will change only in the radial and longitudinal directions, that is, $\partial T / \partial \theta = 0$ and $\partial^2 T / \partial \theta^2 = 0$ [2; 14]. Of the three coordinates written in equation (1) for the three-dimensional case, when considering the applied axisymmetric problem of determining the temperature field of the barrel, two coordinates z and r will remain. In addition, since the barrel is a body of rotation and is symmetrical about the longitudinal axis, after some transformations carried out for the convenience of data grouping, formula (1) is reduced to the equation for finding a two-dimensional temperature field of the barrel on the plane $(0, z, r)$:

$$\frac{1}{a} \frac{\partial T}{\partial t} = \frac{\partial}{\partial z} \left(\frac{\partial T}{\partial z} \right) + \frac{1}{r} \frac{\partial}{\partial r} \left(r \frac{\partial T}{\partial r} \right). \quad (3)$$

It should also be noted here that the accepting of the extreme two assumptions determines the need, discussed above, to take into account in equation (3) the dependence of the thermal conductivity coefficients λ and specific heat capacity c of barrel steel, included in formula (2), on the barrel temperature T when studying applied issues of safe placement of the next cartridge in the barrel heated by shooting.

The basic differential equation of thermophysics (3) establishes a connection between temporal and spatial changes in temperature at any point in the barrel at which the phenomenon of thermal conductivity occurs. A differential equation of the form (3) can have an infinite number of solutions. Isolating from this set a solution that reflects the conditions of thermal interaction in the barrel and specifies the problem posed was carried out by adding geometric, boundary and physical conditions of uniqueness to equation (3). The boundary conditions of uniqueness are further understood as a set of initial and boundary conditions.

When arguing the geometric conditions of unambiguity, the world's lightest 30-millimeter aircraft gun GSh-301 with a unique single-barrel automation circuit, which is in service with most modern aircraft and is planned to equip future aircraft weapons systems, was chosen. Since the barrel is a symmetrical body of rotation relative to the longitudinal axis, the introduction into consideration of a truncated region consisting of internal Γ_1 , external Γ_2 and vertical boundaries Γ_3 , Γ_4 located on one side of the longitudinal axis of the trunk is quite sufficient. Fig. 1 shows a diagram of the axial symmetry of the AAO type GSh-301 barrel in a cylindrical coordinate system $(0, z, r)$, specifying the diagram presented in article [17] by including the boundary designations $\Gamma_1 - \Gamma_4$, required for further clarifications. As before, the z axis coincides with the longitudinal axis of the barrel, and the temperature distribution in each calculated cross section of the barrel is symmetrical relative to the channel axis $T = T(r)$.

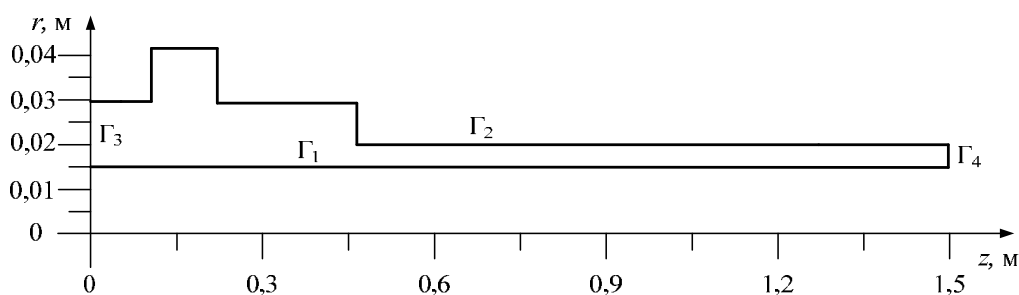


Рис. 1. Схема осевой симметрии ствола авиационной пушки ГШ-301

Fig. 1. Scheme of axial symmetry of the GSh-301 aircraft gun barrel

In the process of applying AAO, the flight of an aircraft, as a rule, is carried out in a quasi-steady mode $v_2 \approx \text{const}$ and, based on the first assumption, the initial conditions of the problem are written in the form:

$$T(z, r, 0) = T_2 = \text{const} . \quad (4)$$

The boundary conditions for the simulated process must reflect the conditions of thermal interaction between the environment and the surface of the body. In general, boundary conditions can be specified in several ways. In the theory of heat transfer, boundary conditions of four types are distinguished [2; 14]. First type boundary conditions are specified in the form of temperature distribution on the surface of bodies. A mathematical description of heat transfer by first type boundary conditions is used for given temperature changes at the boundaries of bodies or very intense thermal conductivity on surfaces, when the temperatures of the surfaces are close to each other. The range of such practical problems is limited, and first type boundary conditions are used mainly in estimation calculations. Boundary conditions of the second kind are specified by the distribution of heat flux density on the surface of the body. The physical essence of the heat exchange conditions corresponding to second type boundary conditions reflects the heating and cooling of bodies through radiation, when heat exchange occurs mainly according to the Lambert-Beer law with uniform heating of the surface of the body. Third type boundary conditions are specified in the form of a dependence of the heat flux density due to thermal conductivity from the body on the temperatures of the body surface and the environment. The mathematical description of the processes of heating and cooling a body is carried out by Newton's law. Analytical expressions for boundary conditions of the third kind have found wide application in studies of heat transfer at the boundaries of materials and substances. Fourth type boundary conditions (conjugation conditions) are specified as conditions for the continuity of the temperature field and conservation of energy on the contact surfaces of multilayer structures.

In research practices heat transfer in solid bodies flown around by gas flows, setting third type boundary conditions at the boundary between the body and the flow has found wide application. Also taking into account the fact that the barrels are not thermally insulated, when solving the problem of

determining the temperature field of the barrel of the GSh-301 aircraft gun, we will set the boundary conditions in the form of ambient temperatures and the laws of heat exchange between this environment and the surface of the barrel, depending on the design characteristics and conditions functioning.

At the inner Γ_1 and outer Γ_2 boundaries of the barrel, we will set the dependence of the thermal conductivity coefficient of the barrel steel λ on the gas temperature T_1 and air temperature T_2 , respectively.

At the inner boundary Γ_1 of the barrel, convective heat exchange will take place between hot gases and the barrel channel:

$$-\lambda_c \left. \frac{\partial T}{\partial r} \right|_{r_0} = \alpha_1 (T_1 - T), \quad (5)$$

where r_0 – inner barrel radius; α_1 – heat transfer coefficient from gases to the bore.

Here and below, the dependence of the quantities under consideration on the current time t is obvious.

We note that to calculate the boundary conditions of heat transfer in the barrel channel, it is necessary to determine the intra-ballistic parameters of gases from the solution to the main problem of internal ballistics, set out in article [18].

At the outer boundary Γ_2 of the barrel, convective heat exchange occurs between the incoming air and the outer surface of the barrel:

$$-\lambda_c \left. \frac{\partial T}{\partial r} \right|_{r_{y_j}} = \alpha_2 (T - T_2), \quad (6)$$

where r_{y_j} – thickness (outer radii) of barrel elements; α_2 – heat transfer coefficient from the outer surface of the barrel to the air.

The development of a mathematical model of heat exchange inside and in the vicinity of the barrel during near-wall flows of coolants, which makes it possible to determine the heat transfer coefficients from gases to the barrel channel α_1 and from the outer surface of the barrel to air α_2 , present in formulae (5) and (6), respectively, is the subject of the article [13].

In accordance with the second assumption, the vertical boundaries of the barrel Γ_3 and Γ_4 are considered adiabatic, that is, the heat flow through these boundaries can be neglected:

$$\left. \frac{\partial T}{\partial z} \right|_{z=0} = 0, \quad \left. \frac{\partial T}{\partial z} \right|_{z=l} = 0, \quad (7)$$

where l – barrel length.

During bursts of shots, the channel and the outer surface of the barrel have quite high temperatures, so it is necessary to take into account the design features of the AAO reference sample. Modeling of the process of functioning of the standard cooling system of the GSh-301 aircraft gun is realized by introducing a local heat transfer coefficient.

In order to increase the accuracy of modeling the temperature field of the barrel, the influence of the cartridge case located in the chamber during the shot was taken into account. Based on the third assumption, it is possible to schematize heat transfer by describing the phenomenon of thermal conductivity. Since the thickness of the shell wall is relatively small, it is assumed that it will instantly warm up to the gas temperature when firing T_1 . The boundary condition on the surface of the chamber at characteristic points of the barrel, where direct contact of the cartridge case with the wall occurs, is formulated as first type boundary condition [2; 14]:

$$T(z = 0 \dots 0,175; r = 0) = T_1. \quad (8)$$

The nonstationary temperature field of the barrel is definable with the known differential equation of the process (3) and given additional conditions (4) – (8), which completely determine the boundary value problem:

$$\left. \begin{aligned}
 & \frac{1}{a} \frac{\partial T}{\partial t} = \frac{\partial}{\partial z} \left(\frac{\partial T}{\partial z} \right) + \frac{1}{r} \frac{\partial}{\partial r} \left(r \frac{\partial T}{\partial r} \right); \\
 & -\lambda_c \frac{\partial T}{\partial r} \Big|_{r_0} = \alpha_1 (T_1 - T); \\
 & -\lambda_c \frac{\partial T}{\partial r} \Big|_{r_{y_j}} = \alpha_2 (T - T_2); \\
 & \frac{\partial T}{\partial z} \Big|_{z=0} = 0; \quad \frac{\partial T}{\partial z} \Big|_{z=l} = 0; \\
 & T(z = 0 \dots 0,175; r = 0) = T_1; \\
 & T(z, r, 0) = T_2 = \text{const.}
 \end{aligned} \right\} \quad (9)$$

Thus, with a number of simplifying assumptions, the problem of loading the barrel is formulated in a complete form. However, as noted in the papers [2; 14; 19–22], the objective lack of an exact analytical solution to direct, multidimensional, unsteady, nonlinear heat transfer problems in areas with a complex boundary configuration leads to the need to use numerical methods.

Synthesis of a finite-difference scheme for calculating the temperature field of the barrel

For most structures of complex shape, which also includes the shaft design, the system of eigenfunctions and the spectrum of eigenvalues of the corresponding homogeneous problem are not known and not tabulated [19]. Therefore, for such bodies, in this case, it is convenient to use the finite difference method as the most universal [19–22].

The area of continuous change of the argument is replaced by a discrete set of points, the intersections of which form nodes, that is, the construction of a difference grid (hereinafter referred to as the grid), as well as the reduction of the system of partial differential equations (9) to a finite-difference scheme, that is, the composition of a system of finite-difference algebraic (hereinafter referred to as difference) equations are performed by analogy with the techniques described in the publication [17]. Some of the author's duplication of information is mediated by the concentration of classical physical and mathematical meanings of the question of heating and cooling the barrel.

The area Ω_T of continuous change in the arguments of the desired value T is replaced by a certain finite set of points lying in this region. The grid points for forming the finite difference of the function of the integer argument T_{kj} along the z axis are designated by k , and similar points along the r axis are designated by j . In accordance with the specifics of the problem being solved, the region Ω_T is transformed into the area for calculating the temperature T_{kj} at kj -points of the barrel sections. In accordance with the selected coordinate system $(0, z, r)$ in the direction of the z axis, the barrel is divided into ϑ equal parts $\vartheta = l / \Delta z$, and in the direction of the r axis into ν equal parts $\nu = r_y / \Delta r$, where Δz , Δr are grid steps at the corresponding coordinates; r_y – maximum barrel thickness. To do this, $\vartheta - 1$ rays are drawn in the direction perpendicular to the z axis and $\nu - 1$ rays are directed in the direction perpendicular to the r axis, as shown in Fig. 2. As a result of this partition, we have a grid consisting of a set of internal (in Fig. 2 indicated by \blacksquare) and boundary (in Fig. 2 indicated by \bullet) nodes. Since, in the case under consideration, $\Delta z = l / \vartheta = \text{const}$ and $\Delta r = r_y / \nu = \text{const}$, then the set of nodes z_k , defined by points with numbers $k = 0, 1, 2, \dots, K_\vartheta$ and the set of nodes r_j , defined by points with numbers $j = 0, 1, 2, \dots, J_\nu$, is a uniform spatial grid in the area $\Omega_{T_{kj}}$.

Unlike the previous version [17], here we consider two possible approaches to setting geometric conditions for uniqueness when the boundary nodes of the grid do not coincide with the boundaries of the barrel. One of them is the introduction of additional nodes at points where the grid lines do not coincide with the elements of the trunk geometry. The second approach is that the geometry of the trunk is approximated by lines passing through the boundary nodes of the grid, and the geometric conditions of uniqueness are transferred to these lines. Due to the inexpediency of introducing additional nodes, which leads to a significant complication of the problem of constructing a difference

scheme, the second approach turned out to be more preferable, since it does not introduce additional difficulties in writing difference equations. The approximation of the trunk geometry is realized by conditionally dividing it into a finite number of sections, each of which is characterized by length and thickness, which are reduced to spatial grid steps Δz and Δr along the z and r axes, respectively.

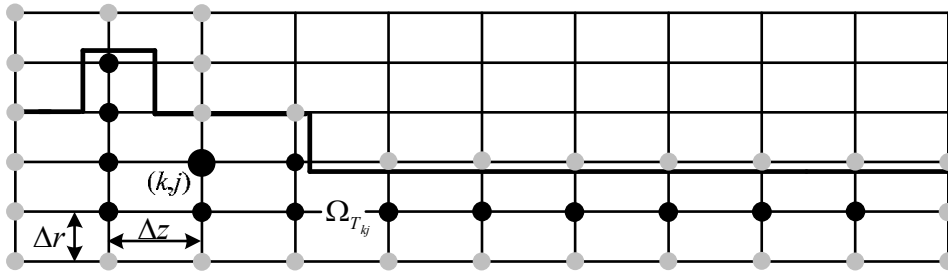


Рис. 2. Сеточная схема ствола авиационной пушки ГШ-301

Fig. 2. Grid diagram of the GSh-301 aircraft gun barrel

By analogy with the grid for the spatial domain $\Omega_{T_{kj}}$, a temporary grid of the domain Ω_{T^i} for calculating the value T^i is introduced in the set of nodes τ_i , defined by points $i = 0, 1, 2, \dots, I_0$, where i and I_0 are the current and boundary, respectively, grid points for the formation of the finite difference barrel temperature T over time t . The time grid step t is designated $\Delta \tau$.

The solution to the non-stationary problem of thermal conductivity in the barrel predetermines the unconditional intersection of one-dimensional spatial grids in each direction with a time grid in the following form:

$$\Omega_{T_k T^i} = \Omega_{T_k} \times \Omega_{T^i} = \left[\begin{array}{l} (z_k, \tau_i), z_{k+1} = z_k + \Delta z, \tau_{i+1} = \tau_i + \Delta \tau; \\ k = 0, 1, 2, \dots, K_9; i = 0, 1, 2, \dots, I_0; \\ z_0 = 0, z_{K_9} = 1, 5 \text{ м}, \tau_0 = 0, \tau_{I_0} = t. \end{array} \right]; \tag{10}$$

$$\Omega_{T_j T^i} = \Omega_{T_j} \times \Omega_{T^i} = \left[\begin{array}{l} (r_j, \tau_i), r_{j+1} = r_j + \Delta r, \tau_{i+1} = \tau_i + \Delta \tau; \\ j = 0, 1, 2, \dots, J_v; i = 0, 1, 2, \dots, I_0; \\ r_0 = 15 \cdot 10^{-3} \text{ м}, r_{J_v} = 42 \cdot 10^{-3} \text{ м}, \tau_0 = 0, \tau_{I_0} = t. \end{array} \right],$$

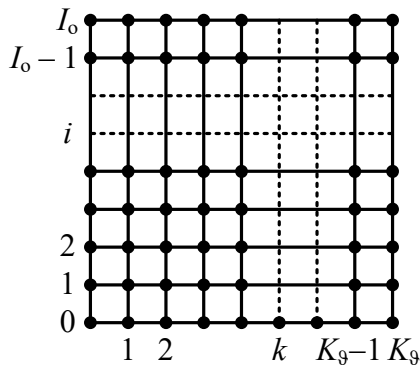


Рис. 3. К выбору пространственно-временной сетки (на примере пространственной координаты z и времени t)

Fig. 3. On the choice of a space-time grid (on the example of the spatial coordinate z and time t)

Expression (10) forms a stencil of a space-time grid, the diagram of which along the longitudinal coordinate z is shown in Fig. 3.

To construct difference analogues of differential operators of the system of equations (9), the method of formally replacing derivatives with finite-difference relations was used. This method is the most justified and applicable in problems of this class and is based on the Taylor series expansion of fairly smooth functions, which, as a rule, allows one to preserve the local properties of differential equations [15]. In addition, the method of approximating derivatives by Taylor series has two main advantages:

- when the size of the unit cell tends to zero, the difference equation is reduced to a differential equation, that is, the compatibility of the equations is ensured, which is an important criterion for stability;

– Difference equations of any degree of accuracy can be obtained by adding or removing the required number of terms in the approximating series, and if mathematical verification is necessary, the accuracy of the approximation is estimated from the discarded terms of the series.

The most natural way to replace the derivative is based on defining the derivative (for example, with respect to the z coordinate) as a limit [15; 19]:

$$\frac{\partial T}{\partial z} = \lim_{\Delta z \rightarrow 0} [T(z + \Delta z) - T(z)] \frac{1}{\Delta z}. \quad (11)$$

If we fix the step Δz in equality (11), we obtain an approximate formula for the first derivative expressed in terms of finite differences.

For the so-called right difference relation or “forward” difference:

$$\frac{\partial T}{\partial z} \approx [T(z + \Delta z) - T(z)] \frac{1}{\Delta z}. \quad (12)$$

Similarly, the left difference relation (the “backward” difference) is introduced, written in the form:

$$\frac{\partial T}{\partial z} \approx [T(z) - T(z - \Delta z)] \frac{1}{\Delta z}. \quad (13)$$

When solving heat conduction problems, it is necessary to approximate the second derivative. For the second derivative, a linear combination of relations (12) and (13) is considered:

$$\frac{\partial^2 T}{\partial z^2} \approx [T(z + \Delta z) - 2T(z) + T(z - \Delta z)] \frac{1}{\Delta z^2}. \quad (14)$$

Each transition to one step “forward” is conventionally designated by “+1”, and “backward” by “-1”. Then, for the k grid point of the formation of a finite difference in the value of T_{kj} along the z axis, the right difference relation (12) is transformed to the form:

$$\frac{\partial T}{\partial z} = (T_{k+1} - T_k) \frac{1}{\Delta z}. \quad (15)$$

The left difference relation is transformed similarly (13):

$$\frac{\partial T}{\partial z} = (T_{k+1} - T_k) \frac{1}{\Delta z}. \quad (16)$$

The difference analogue of the second derivative, corresponding to formula (14), is represented by the relation

$$\frac{\partial^2 T}{\partial z^2} = (T_{k+1} - 2T_k + T_{k-1}) \frac{1}{\Delta z^2}. \quad (17)$$

The formulas (11) – (17) and their justifications are also valid when replacing the derivative with respect to coordinate r in the system of equations (9) by difference relations. In this case, in analogue equations, instead of the variable z , the variable r will be present, and the index k will be replaced by the index j . We will keep in mind the discovered analogies further, sometimes without resorting to direct detailing of the difference scheme for the spatial variable r .

When constructing relations that approximate the time derivative $\partial T/\partial t$ in the system of equations (9), it is permissible to use temperature values at kj -points of the barrel sections at different times: $T_{k,j,i}$, $T_{k,j,i-1}$, $T_{k,j,i-2}$, However, in the practice of solving most applied problems of thermal conductivity, in the vast majority of cases, exclusively two-layer (in time t) difference schemes are used, approximating the values of the desired temperatures at the current i -th and previous ($i - 1$) time point.

Much less frequently, the temperature values at the $(i - 2)^{\text{nd}}$ moment of time are taken into $^{\text{st}}$ account by obtaining three-layer difference schemes [19–22].

When obtaining variants of two-layer difference schemes, the time derivative is approximated by the “backwards” time difference:

$$\frac{\partial T}{\partial t} = (T^i - T^{i-1}) \frac{1}{\Delta \tau}. \quad (18)$$

Spatial differential operators in a two-layer difference scheme are also approximated based on the temperature values T_{kj} at kj -points of the barrel sections at the i -th and $(i - 1)^{\text{st}}$ moments of time. In this case, two limiting cases are possible.

In the first case, only the temperature values T_{kj} at kj -points of the barrel sections for the current i moment of time are involved in the approximation. Thus, for the spatial variable z , the one-dimensional space-time approximation of the first differential operator to the system of equations (9) will have the form:

$$\frac{\partial^2 T}{\partial z^2} = (T_{k+1}^i - 2T_k^i + T_{k-1}^i) \frac{1}{\Delta z^2}. \quad (19)$$

In the second case, during approximation, only the temperature values T_{kj} at kj -points of the barrel sections for the previous time point $(i - 1)^{\text{st}}$ are used:

$$\frac{\partial^2 T}{\partial z^2} = (T_{k+1}^{i-1} - 2T_k^{i-1} + T_{k-1}^{i-1}) \frac{1}{\Delta z^2}. \quad (20)$$

In accordance with options (18) – (20), we present two types of difference equations that approximate the first equation of system (9) in a one-dimensional version:

$$\frac{1}{a} \frac{T_k^i - T_k^{i-1}}{\Delta \tau} = (T_{k+1}^i - 2T_k^i + T_{k-1}^i) \frac{1}{\Delta z^2}; \quad (21)$$

$$\frac{1}{a} \frac{T_k^i - T_k^{i-1}}{\Delta \tau} = (T_{k+1}^{i-1} - 2T_k^{i-1} + T_{k-1}^{i-1}) \frac{1}{\Delta z^2}. \quad (22)$$

A difference equation of the form (22) makes it possible to express the solution to the problem of thermal conductivity in the wellbore in explicit form on the i time layer through the known solutions on the previous $(i - 1)^{\text{st}}$ layer. Difference equation (22) forms an explicit difference scheme. Algorithms for the numerical calculation of the system of equations (9) using an explicit difference scheme are quite compact when programming, but they impose requirements on computer time.

The difference scheme specified by a difference equation of the form (21) is more complicated, since each difference equation of the form (21), in addition to the unknown solution for the k -th spatial point, includes two more sought-after solutions for the neighboring $(k - 1)$ -th and $(k + 1)$ -th spatial points. All the sought solutions turn out to be “tied” with each other into a common non-degenerate system of difference equations. Thus, in this case, at each i -th time layer, the solutions are determined not by explicit formulas of the form (22), but from the solution of the system $(K_9 - 1)$ of difference equations, as a result of which the difference scheme specified by the difference equation of the form (21) is implicit. Effective algorithms for solving the system of equations (9) using an implicit difference scheme are much more complicated than numerical algorithms using an explicit difference scheme, but the time for solving the problem can be significantly reduced by a rational choice of steps Δz , Δr and $\Delta \tau$.

The obvious difference in the behavior of the solutions obtained in cases of implementation of the template in Fig. 3 using explicit (22) and implicit (21) difference schemes, a proper physical and mathematical explanation can be given. The value of the time derivative with an explicit difference

scheme (22) is calculated from the values of the desired function at the beginning of the time interval, therefore the increment $(T_k^i - T_k^{i-1})$ does not depend on the obtained values, and the absolute value of this increment is proportional to the step. As a result, at some critical step $\Delta\tau$, new values T_k^i can be obtained that contradict the physical meaning of the problem (for example, a drop in the barrel temperature T on the i -th time layer compared to the $(i - 1)$ -th time layer with continued exposure to gas temperature T_1). In the implicit difference scheme (21), the increment $(T_k^i - T_k^{i-1})$ depends on all values T_k^i on the new time layer, that is, there is a kind of “feedback” that does not allow obtaining absurd increments of the grid function. However, the practice of solving real problems does not at all exclude the advisability of including an explicit difference scheme in the stencil shown in Fig. 3. Firstly, when describing the fast processes under study, the advantage of the implicit scheme, which consists in a more free choice of the value of the time step $\Delta\tau$, may not appear. Secondly, explicit schemes are more resource-intensive, especially when calculating on computers with several parallel processors, which are widely used nowadays.

Due to the uniformity of the grid over all spatial coordinates, the fact of difference approximation of the differential operator for the variable r for each value of z at any local point, both along an isolated coordinate r and when solving a problem with a time variable t simultaneously, can be shown in a similar way.

One of the most important achievements of computational mathematics is the development of various difference schemes for solving multidimensional partial differential equations of thermophysics [19–22]. The desire to obtain a close approximation of the problem of temperature loading of the barrel to its possibly existing exact analytical solution was facilitated by selection and some techniques for transforming the longitudinal-transverse difference scheme of the Peaceman-Rackford two-dimensional sweep method. The main advantages of the preferred explicit-implicit difference scheme include: a combination of the strengths of explicit difference schemes (low computer time consumption at the time step $\Delta\tau$) and implicit difference schemes (unconditional stability, that is, the ability to ensure the accuracy of the solution at any degree of mesh detail); possibility of application to multidimensional areas and co-occurring processes; adaptability to compiling efficient machine codes on high-speed computers with a sufficiently large amount of RAM.

The course of the two-dimensional physical process of heating and cooling the barrel at each time step $\Delta\tau$ in spatial steps Δz and Δr is delivered as a result of the sequential implementation of one-dimensional processes, each of which begins from the distribution of the temperature field of the barrel that arose after the end of the previous one-dimensional process. Based on this representation, called splitting [20; 22] modeling of one-dimensional processes is carried out implicitly, and the sequential action of processes is taken into account in an essentially explicit way. Given the given boundary conditions and the same initial temperature T_0 at all points in the region of a complex-shaped barrel, the optimal solution is achieved by reducing the multidimensional problem at each time step $\Delta\tau$ to a set of one-dimensional problems solved by the sweep method.

The specificity of the stability of the implicit approximation of locally one-dimensional problems with any division of the time step $\Delta\tau$ determined the method for increasing the accuracy of the formation of an array of barrel temperatures T . The essence of the method is to select a template on the time grid containing a half-integer layer:

$$\tau_{i+1/2} = \frac{\tau_{i+1} - \tau_i}{2} = 0,5 \cdot \Delta\tau, \quad (23)$$

as shown in fig. 4.

Then, taking into account difference equations (21) and (22), difference relation (23), as well as the discussed spatial analogies, the finite-difference approximation of the first equation of system (9) according to the longitudinal-transverse difference scheme for the direction z for any value of r will be look like:

$$\frac{1}{a} \frac{T_{kj}^{i+1/2} - T_{kj}^i}{0,5 \cdot \Delta\tau} = \frac{T_{(k+1)j}^{i+1/2} - 2T_{kj}^{i+1/2} + T_{(k-1)j}^{i+1/2}}{(\Delta z)^2} + \frac{r_j T_{k(j+1)}^i - (r_{j-1} + r_j) T_{kj}^i + r_{j-1} T_{k(j-1)}^i}{r_j (\Delta r)^2}. \quad (24)$$

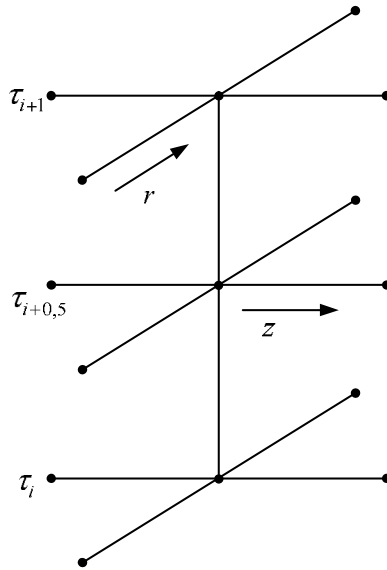


Рис. 4. К выбору временного шаблона продольно-поперечной разностной схемы методом двумерной прогонки Писмена – Рэкфорда

Fig. 4. To the choice of the time template of the longitudinal-transverse difference scheme by the method of two directions of Peaceman – Rackford

The boundary and initial conditions along the z coordinate for each fixed value of r are approximated as follows

– initial condition:

$$\left. \begin{array}{l} i = 0 \quad T_{kj}^0 = T_2, \\ i > 0 \quad T_{kj}^i = T_{kj}^{i+1}. \end{array} \right\}; \quad (25)$$

– boundary conditions:

$$\left. \begin{array}{l} T_{1j}^{i+1/2} = T_{2j}^{i+1/2}, \\ T_{K_9j}^{i+1/2} = T_{(K_9-1)j}^{i+1/2}. \end{array} \right\}. \quad (26)$$

When synthesizing a modified two-layer difference scheme, the solution to the non-stationary heat conduction problem on a separate layer can be considered as the initial condition for subsequent layers. Consequently, we write the finite-difference approximation of the first equation of system (9) for the direction r for any value of z in the following form:

$$\frac{1}{a} \frac{T_{kj}^{i+1/2} - T_{kj}^i}{0,5 \cdot \Delta\tau} = \frac{r_j T_{k(j+1)}^{i+1} - (r_j + r_{j-1}) T_{kj}^{i+1} + r_{j-1} T_{k(j-1)}^{i+1}}{r_j (\Delta r)^2} + \frac{T_{(k+1)j}^{i+1/2} - 2T_{kj}^{i+1/2} + T_{(k-1)j}^{i+1/2}}{(\Delta z)^2}. \quad (27)$$

The boundary and initial conditions along the z coordinate for each fixed value of r are approximated as follows:

– initial condition:

$$T_{kj}^{i+1} = T_{kj}^{i+1/2} + T_{kj}^{i+1/2} - \text{solution to the equation (24);} \quad (28)$$

– boundary conditions:

$$\left. \begin{aligned} -\lambda_c \frac{T_{k1}^{i+1} - T_{k2}^{i+1}}{\Delta r} &= \alpha_1 (T_{1,k}^{i+1} - T_{k1}^{i+1}), \\ -\lambda_c \frac{T_{k(J_v-1)}^{i+1} - T_{kJ_v}^{i+1}}{\Delta r} &= \alpha_2 (T_{kJ_v}^{i+1} - T_{2,k}^{i+1}). \end{aligned} \right\} \quad (29)$$

Eliminating possible discrepancies, we note that in difference relation (29) $T_{1,k}^{i+1}$ and $T_{2,k}^{i+1}$ denote, respectively, the temperatures of gases and air at the k -th spatial grid point on the $(i+1)$ -th time layer.

From equations (24), (27) it is clear that in the constructed difference scheme the transition from the i -th to the $(i+1)$ -th time layer occurs in two stages with steps of $0.5 \Delta \tau = 0.5 (\tau_{i+1} - \tau_i)$. Along with the main values of the grid function T_{kj}^i and T_{kj}^{i+1} , intermediate values $T_{kj}^{i+1/2}$, are introduced which are formally considered as the values of T_{kj} at $(\tau_{i+1} - 2\tau_{i+1/2})$. Relation (24) contains three unknown quantities $T_{(k+1)j}^{i+1/2}, T_{kj}^{i+1/2}, T_{(k-1)j}^{i+1/2}$, values $T_{k(j+1)}^i, T_{kj}^i, T_{k(j-1)}^i$ can be determined on the initial layer by integrating systems of equations of internal and intermediate ballistics [18]. That is, by relation (24) the difference scheme is classified as implicit in the z coordinate and explicit in the r coordinate. For any value of r , the numerical solution can be found by sweeping in the z direction. The desired temperature values T_{kj} at kj -points of the barrel sections are related to each other “horizontally” and “vertically”. Moreover, the unknowns of any internal horizontal straight line “interact” on the time half-layer exclusively with the unknowns of two adjacent straight lines – the upper and lower ones. Next, using relation (27), which contains three unknown quantities $T_{k(j+1)}^{i+1}, T_{kj}^{i+1}, T_{k(j-1)}^{i+1}$, (the values $T_{(k+1)j}^{i+1/2}, T_{kj}^{i+1/2}, T_{(k-1)j}^{i+1/2}$ are recorded by sweeping in the z direction at values of r), the difference scheme is translated into a form that is implicit in the r coordinate and explicit in the z coordinate. Therefore, the final distribution of temperature T_{kj} at kj -points of the barrel sections is found by sweeping in the direction r at any value of z , where the transition between time layers is also performed in half-steps in the longitudinal and transverse directions, respectively, along the rows and columns on the grid.

The problem of optimal selection of grid steps $\Delta z, \Delta r, \Delta \tau$ and thus the number of its nodes is not easy. On the one hand, the greater the accuracy required, the finer the step is desirable. On the other hand, too small a step significantly increases the requirements for the speed and memory capacity of computers. Obviously, there must be some meshes with an optimal number of nodes. We will optimize the grid based on the conditions for the best convergence of the results of the numerical calculation with the likely existing true analytical solution and borrowed experimental data.

First of all, in order to most accurately determine the temperature field of the barrel, it is advisable to solve the problem taking into account the configuration of the rifling, since their presence leads to uneven temperature distribution along the perimeter of the rifled part of the barrel bore [9; 10]. The initial requirement of incomparably small size Δr of the grid pitch along the r axis in relation to the height of the rifling field is obvious. In general, the value Δr of the grid step along the r axis is assigned according to the approximate dependence of the stationary and linear components [23]:

$$\Delta r \approx \frac{\lambda \cdot \Delta T}{\alpha_1 (T_1 - T_0 - \Delta T)},$$

where ΔT – temperature gradient on the heat exchange surface (for AAO $\Delta T \leq 323$ K).

Since the velocity of the projectile (gases) when fired v_1 in time t and along the barrel length l gradually increases, reaching the value v_n at the muzzle of the barrel, this feature does not allow constructing a uniform grid in time $\Delta \tau$, since along the barrel length l the grid step size Δz along the z axis will also increase. This, in turn, can lead to the fact that the accuracy of the solution results obtained at different points in the area of discrete changes in the arguments $\Omega_{T_{kj}}$ of the value T_{kj} will differ significantly from each other, which is unacceptable. Taking into account also the fact that calculations at

each i -th time layer are performed both on the basis of the value of the previous $(i - 1)$ -th and the previous $(i - 0.5)$ -th time layer, the error will accumulate quite quickly. In order to eliminate this event, when calculating the heating of the barrel during the time of movement of the projectile (gases) along the barrel bore $t_{\text{д}}$, it is advisable to use a variable time step $\Delta\tau \neq \text{const}$, assigned when solving the main problem of internal ballistics [18]. Further, during the aftereffect period $t_{\text{н}}$ and in the time intervals between bursts of shots Δt , a constant time step $\Delta\tau = \text{const}$ is established, assigned, in turn, for the period of intermediate ballistics:

$$\Delta\tau = \begin{cases} 0,0002 \frac{l}{v_1(l)}, & \text{if } t \leq t_{\text{д}}; \\ 0,0002 \frac{l}{v_{\text{д}}}, & \text{if } t > t_{\text{д}}. \end{cases} \quad (30)$$

In contrast to the spatial grid, the set of nodes τ_i , defined by points $i = 0, 1, 2, \dots, I_0$ is a non-uniform temporary grid in the area Ω_{T_i} .

The justification for the value Δz of the grid step along the z axis, providing the desired accuracy, of the solution was made using the stability condition for the explicit components of the difference scheme (24)–(29) [20; 22], including, among other things, the constancy of the time step $\Delta\tau$ of the lower part of formula (30):

$$\frac{(\Delta z)^2}{\Delta\tau} \geq 2a, \text{ for } \Delta\tau = \text{const}, a = \text{const}. \quad (31)$$

Formula (31) shows a strict connection between the value Δz of the grid step along the z axis and the values $\Delta\tau$ of the grid step over time t , since the accuracy of solving the problem directly depends on the correct choice of the latter. From the stability condition (31) follows a guide to action - the refinement of the spatial grid must be accompanied by the refinement of the time grid. For example, when the number of spatial nodes z_k increases by 4 times, it is necessary to increase the number of time steps t of the difference grid $\Delta\tau$ by 16 times. Previously, the need to comply with condition (31) led to the fact that when determining the step size $\Delta\tau$ in solving real non-stationary problems of thermophysics, it was not possible to proceed only from the nature of the physical process being studied. This in some cases led to unacceptable costs of machining time. In addition, with an unreasonably large number of time nodes τ_i , a rounding error was observed, which occurs during numerical calculations in calculating machines of early generations.

The stability property of the explicit part of the difference scheme (24) – (29) has also been established in practice, by ascertaining the absence of “divergent mode” of the numerical solution in the process of trial calculations.

When considering the approximation property of the formed difference scheme (24)–(29), a special concept of the so-called total approximation was introduced [20; 22] of locally one-dimensional difference schemes, which is as follows. Each of the intermediate difference equations (24) or (27) separately may not have the approximation property. However, the discrepancy arising at the first time half-step, as a rule, is compensated at the second time half-step with the correct combination of spatial steps Δz , Δr and time step $\Delta\tau$, so that in general the approximation error is obtained, tending to zero at the given degree of detail of the space-time grid.

Such a way of discretizing the computational domain should be recognized, although labor-intensive, but also the most acceptable for solving an applied problem of thermophysics.

Thus, a discrete set of grid points is characterized by coordinates and parameters:

$$\begin{aligned} z_k &= (k - 1) \cdot \Delta z, \Delta z = 0,001 \text{ м}, k = \overline{1, 151}; \\ r_j &= r_0 + (j - 1) \cdot \Delta r, \Delta r = 0,125 \cdot 10^{-3} \text{ м}, j = \overline{1, 161}; \\ \tau_i &= (i - 1) \cdot \Delta\tau, \\ \tau_{i+1/2} &= 0,5 \cdot \Delta\tau, i = 0, t. \end{aligned}$$

Thus, the resulting expressions (24)–(29) constitute a method for numerically solving the boundary value problem (9) for determining the grid temperatures of the barrel T_{jk}^i . Taking into account nonlinearity of the first kind in the numerical solution of the system of equations (9) is organized by an iterative process, in which the determination of the next approximation is carried out by including a linear solution, in which the coefficients of thermal conductivity λ and specific heat c of barrel steel are calculated from the values of barrel temperatures T found on previous iteration. The formation of a non-stationary temperature field of the GSh-301 aircraft gun barrel is generally feasible by software organization of a matrix of values T_{jk}^i when studying the application modes of AAO.

In the papers [19–22] it was proven that in the presence of approximation and stability, convergence of all types of difference schemes will always take place. However, this fact does not exclude the scientific and methodological significance of the procedure for checking the improvement in the convergence of the results of modeling the thermophysical loading of the system in comparison with the known results.

Checking the reliability of the thermophysical model of barrel loading

Applied research into the quality of AAO is preceded by checking the developed model for the adequacy of reflecting the simulated thermophysical processes occurring in a gas-dynamic pulse machine. Establishing the set of properties of the model that determine its suitability for conducting diverse numerical experiments is possible by comparing the modeling results with experimental data, as well as with the known averaged results of some theoretical works that are closest to the experimental data. This approach can significantly increase the reliability of the conclusions.

Based on these positions, the verification of the degree of objective representation by the calculation results of the actual values of the main parameter was carried out by numerical modeling of the process of heating and cooling of the barrel surface worked out at the test site during and after shooting a combat set of 75 rounds. The content of firing modes and conditions for the use of AAO are limited to the type of information that does not require further specifications. The combined results of the full-scale experiment and calculation are shown in the form of graphs of the dependence of the barrel temperature T on time t in Fig. 5.

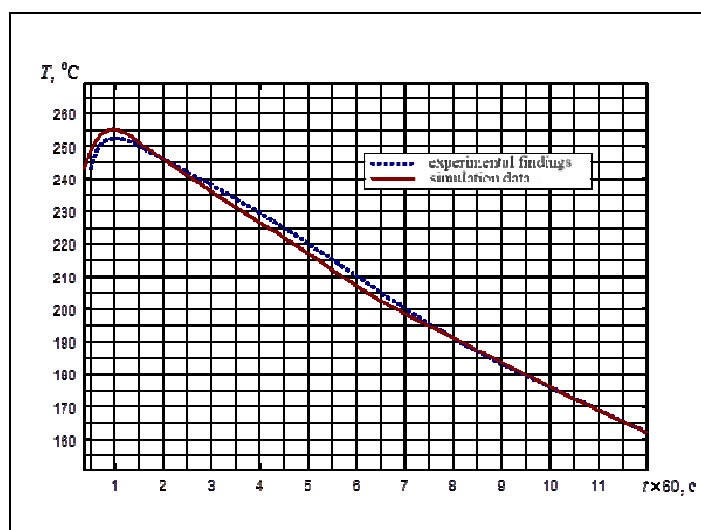


Рис. 5. Зависимость температуры ствола авиационной пушки ГШ-301 в районе компенсатора от времени при отстреле боевого комплекта в 75 патронов

Fig. 5. Dependence of the barrel temperature of the GSh-301 aircraft gun in the area of the compensator on time when firing a combat set of 75 rounds of ammunition

Analysis of the results obtained shows that there is a fairly good correlation between experiments and calculated data. Satisfactory agreement between the modeling results and the experimental data is confirmed by the fact that the averaged relative error in determining the barrel temperature T in the reference section does not exceed 0.6 %. In most works in the field of aviation artillery science, including the works of the co-author of the article, the discrepancy between this value in numerical and full-scale experiments is about 10 % [9; 11].

Thus, an increase in the accuracy of simulating thermal loading of the barrel by 9.4 % was achieved:

- taking into account the nonlinearity of the thermophysical properties of the barrel steel material $\lambda(T), c(T)$;
- choosing the values (probably close to optimal) of the grid steps $\Delta z, \Delta r$ in the corresponding coordinates z, r , as well as the size of the step Δt in time t in the thermophysical model of barrel loading;
- an effective combination of the advantages of explicit and implicit difference schemes in the constructed explicit-implicit difference scheme for finite-difference approximation of the heat transfer problem in a body with a complex geometric shape.

The formalization of thermophysical processes of heat propagation in a thermally loaded AAO element is logically completed by a package of application programs designed to calculate the thermal state of the barrel during firing and determine safe firing modes for a range of flight conditions of the carrier aircraft [24]. Algorithms for the numerical calculation of the system of equations (9) using the corresponding finite-difference scheme (24) – (29) were debugged using the Microsoft Developer Studio software product, the Fortran Power Station 4.0 environment and the FORTRAN 90 algorithmic language.

Prospects for further improvement of the model

The software organization for calculating the temperature field of the barrel when using AAO comes down to multiple (according to firing modes) solution of the system of equations (24)–(29) with the initial distribution of the barrel temperature T , which is established at the beginning of the next shot and is determined by solving the same system of equations (24)–(29) for the previous shot. The proposed tools make it possible to adequately simulate the temperature field of the barrel under various firing conditions and create a basis for the composition of the maximum effective firing modes.

At the same time, there are practical applications of medium-sized special mechanical engineering, for which some of the assumptions adopted in the paper have to be removed. Thus, when analyzing the heating of a barrel in the area of gas outlet openings of gas automatics or muzzle devices, it is necessary to take into account local heat flows in the elements connected to the barrel. Then we should move on to a much more complex three-dimensional formulation in coordinates $(0, z, r, \theta)$. The need to solve three-dimensional heat transfer problems is not excluded when analyzing the effectiveness of cooling fins or grooves, the thermal state of the rifling, and taking into account the technological variation in the thickness of the barrel. In addition, when studying the mechanism of barrel wear when analyzing the thermally stressed state of a thin surface layer of metal adjacent to the channel surface, it is inevitable to take into account the dependence of the thermophysical characteristics of the barrel steel on not only temperature, but also on spatial coordinates. In practical calculations, it is increasingly necessary to abandon the assumption of the constancy of the thermophysical characteristics of the cartridge. Calculations based on the so-called “instantaneous” values of the thermophysical characteristics of the elements of ammunition located in the barrel during breaks between automatic firing help to clarify the thermodynamic state of the “cartridge-barrel” system and more closely link it with the combat properties of the AAO.

To obtain more complete information about the accuracy characteristics of the model, it is advisable to additionally conduct a series of flight experiments that provide natural conditions for thermal loading of the barrel. Then the assessment of the averaged relative error in modeling the heating and cooling of the barrel will undoubtedly be more objective.

Conclusion

By matching the accuracy characteristics of physical and mathematical methods for solving heat transfer problems and related problems with the colossal characteristics of speed, memory and bit grid of modern computer machines, a model of increased accuracy was synthesized, which differs from the known ones by the variable selection of the pitch of the template-grid of the barrel of the GSh-301 aircraft gun. The applied significance of the model is demonstrated by the availability of methods for its adaptation to solving other problems of thermodynamics and mechanics of the strength of barrels.

Библиографические ссылки

1. Комплексы авиационного вооружения / под ред. В. А. Конуркина. М. : ВВИА им. Н. Е. Жуковского, 2005. 947 с.
2. Сапожников С. В., Китанин Л. В. Техническая термодинамика и теплопередача. СПб. : СПбГТУ, 1999. 319 с.
3. Деревянко В. А., Макуха А. В. Измерение распределения температуры с помощью трехпроводной системы датчиков на основе термисторов // Сибирский журнал науки и технологий. 2019. Т. 20, № 3. С. 334–343.
4. Анализ экспериментальных данных по плавлению и движению расплава металла по цилиндрической поверхности / П. Д. Лобанов, Э. В. Усов, А. И. Светоносов и др. // Теплофизика и аэромеханика. 2020. № 3. С. 483–490.
5. Cruz C., Marshall A. Surface and gas measurements along a film cooled wall // Thermophysics and Heat Transfer. 2007. No. 21. P. 181–189.
6. Гусев С. А., Николаев В. Н. Параметрическая идентификация теплового состояния радиоэлектронного оборудования в приборном отсеке самолета // Сибирский журнал науки и технологий. 2019. Т. 20, № 1. С. 62–67.
7. Васильев Е. Н. Расчет характеристик теплообмена оребренной стенки // Сибирский аэрокосмический журнал. 2020. Т. 21, № 2. С. 226–232.
8. Зуев А. А., Арнгольд А. А., Ходенкова Э. В. Теплоотдача в поле центробежных сил для элементов газовых турбин // Сибирский аэрокосмический журнал. 2020. Т. 21, № 3. С. 364–376.
9. Исследование термоэрозионной стойкости стволов методом планирования эксперимента / В. Ф. Захаренков, О. Г. Агошков, В. А. Девяткин и др. // Фундаментальные основы баллистического проектирования : материалы III Всерос. науч.-техн. конф. (2–6 июня 2012, г. Санкт-Петербург) : в 2 т. / Балтийский гос. техн. ун-т «Военмех». Санкт-Петербург, 2012. Т. 1. С. 79–86.
10. Ашурков А. А., Лазовик И. Н., Никитенко Ю. В. Исследование процесса износа стволов импульсных тепловых машин комплексов авиационного вооружения // Проблемы повышения боевой готовности, боевого применения, технической эксплуатации и обеспечения безопасности полетов летательных аппаратов с учетом климатических условий Сибири, Забайкалья и Дальнего Востока : материалы XIII Всерос. науч.-техн. конф. (25–27 июня 2003, г. Иркутск) : в 2 ч. / ИВАИИ. Иркутск, 2003. Ч. 1. С. 97–100.
11. Экспериментальные исследования предельных тепловых нагрузок на ствол скорострельной пушки / А. В. Подкопаев, Н. Ф. Крайнов, И. Н. Лазовик и др. // Проблемы повышения боевой готовности, боевого применения, технической эксплуатации и обеспечения безопасности полетов летательных аппаратов с учетом климатических условий Сибири, Забайкалья и Дальнего Востока : материалы XIII Всерос. науч.-техн. конф. (25–27 июня 2003, г. Иркутск) : в 2 ч. / ИВАИИ. Иркутск, 2003. Ч. 1. С. 127–129.
12. Даниленко Р. А., Подкопаев А. В. Синтез математической модели функционирования системы «оружие – патрон» на основе решения квазилинейного нестационарного уравнения теплопроводности // Академические Жуковские чтения : материалы V Всерос. науч.-практ. конф. (22–23 ноября 2017, г. Воронеж) / ВУНЦ ВВС «ВВА». Воронеж, 2018. С. 67–73.

13. Подкопаев А. В. Способ определения коэффициента теплоотдачи для расчета температурного поля ствола скорострельного артиллерийского орудия // Современное состояние и перспективы развития летательных аппаратов, их силовых установок и комплексов авиационного вооружения : материалы Всерос. науч.-практ. конф. (16–17 мая 2012, г. Воронеж) : в 12 ч. / ВУНЦ ВВС «ВВА». Воронеж, 2012. Ч. 3. С. 202–204.
14. Исаченко В. П., Осипова В. А., Сукомел А. С. Теплопередача. М. : Энергоиздат, 1981. 416 с.
15. Корн Г., Корн Т. Справочник по математике для научных работников и инженеров. М. : Наука, 1984. 832 с.
16. Справочник по авиационным материалам и технологии их применения / под ред. В. Г. Александрова. М. : Транспорт, 1979. 242 с.
17. Идентификационно-имитационная математическая модель теплофизического нагружения малокалиберного артиллерийского ствола / А. В. Подкопаев, А. Б. Бабаджанов, И. А. Подкопаев и др. // Сибирский аэрокосмический журнал. 2022. Т. 23, № 2. С 209–226.
18. Комбинированная математическая модель внутренней и промежуточной баллистики авиационного артиллерийского оружия / А. Б. Бабаджанов, И. А. Подкопаев, А. В. Подкопаев и др. // Известия Тульского государственного университета. Технические науки. 2022. Вып. 4. С. 177–185.
19. Власова Е. А., Зарубин В. С., Кувыркин Г. Н. Приближенные методы математической физики. М. : МГТУ им. Н. Э. Баумана, 2001. 700 с.
20. Дульнев Г. Н., Парфенов В. Г., Сигалов А. В. Применение электронных вычислительных машин для решения задач теплообмена. М. : Высшая школа, 1990. 207 с.
21. Зарубин В. С., Станкевич И. В. Расчет теплонапряженных конструкций. М. : Машиностроение, 2005. 352 с.
22. Самарский А. А., Николаев Е. С. Методы решения сеточных уравнений. М. : Наука, 1978. 592 с.
23. Зайцев А. С. Проектирование артиллерийских стволов. Ч. II. Специальные вопросы. М. : Изд-во ГК СССР по народному образованию, 1988. 114 с.
24. Подкопаев И. А., Подкопаев А. В. Расчет температурного поля ствола автоматической пушки во время стрельбы. М. : Роспатент. 2023. № государственной регистрации программы для ЭВМ RU 2023617444 от 10.04.2023.

References

1. *Kompleksy aviatsionnogo vooruzheniya* [Aircraft weapon systems]. Ed. by V. A. Konurkin. Moscow, AFIA named after professor N. E. Zhukovsky Publ., 2005, 947 p.
2. Sapozhnikov S. V., Kitanin L. V. *Tekhnicheskaya termodinamika i teploperedacha* [Technical thermodynamics and heat transfer]. St. Petersburg, SPbSTU Publ., 1999, 319 p.
3. Derevianko V. A., Makukha A. V. [Measuring the temperature distribution with a three-wire thermistor sensor system]. *Sibirskiy zhurnal nauki i tekhnologii*. 2019, Vol. 20, No. 3, P. 334–343 (In Russ.).
4. Lobanov P. D., Usov E. V., Svetonosov A. I., Lezhnin S. I. [Analysis of experimental data on melting and movement of a metal melt over a cylindrical surface]. *Teplofizika i aeromekhanika*. 2020. No. 3, P. 483–490 (In Russ.).
5. Cruz C., Marshall A. Surface and gas measurements along a film cooled wall. *Thermophysics and Heat Transfer*, 2007. No. 21. P. 181–189.
6. Gusev S. A., Nikolaev V. N. [Parametric identification of the thermal state of electronic equipment in the aircraft instrument compartment]. *Sibirskiy zhurnal nauki i tekhnologii*. 2019, Vol. 20, No. 1, P. 62–67 (In Russ.).

7. Vasiliev E. N. [Calculation of heat transfer characteristics of a ribbed wall]. *Sibirskiy aerokosmicheskii zhurnal*. 2020, Vol. 21, No. 2, P. 226–232 (In Russ.).
8. Zuev A. A., Arngold A. A., Khodenkova E. V. [Heat transfer in the field of centrifugal forces for elements of gas turbines]. *Sibirskiy aerokosmicheskii zhurnal*. 2020, Vol. 21, No. 3, P. 364–376 (In Russ.).
9. Zakharenkov V. F., Agoshkov O. G., Devyatkin V. A., Yurchenko N. A. [Study of the thermal erosion resistance of barrel by the method of planning an experiment]. *Materialy III Vseros. nauch.-tekhn. konf. "Fundamental'nyye osnovy ballisticheskogo proyektirovaniya"* [Materials III All-Russ. Scient. and Technic. Conf. "Fundamentals of ballistic design"]. St. Petersburg, 2012, P. 79–86 (In Russ.).
10. Ashurkov A. A., Lazovik I. N., Nikitenko Yu. V. [Study of the process of wear of barrels of pulsed heat engines of aviation weapons systems]. *Materialy XIII Vseros. nauch.-tekhn. konf. "Problemy povysheniya boyevoy gotovnosti, boyevogo primeneniya, tekhnicheskoy ekspluatatsii i obespecheniya bezopasnosti poletov letatel'nykh apparatov s uchetom klimaticheskikh usloviy Sibiri, Zabaykal'ya i Dal'nego Vostoka"* [Materials XIII All-Russ. Scient. and Technic. Conf. "Problems of increasing combat readiness, combat use, technical operation and ensuring flight safety of aircraft, taking into account the climatic conditions of Siberia, Transbaikalia and the Far East"]. Irkutsk, 2003, P. 97–100 (In Russ.).
11. Podkopaev A. V., Krainov N. F., Lazovik I. N., Morozov S. A. [Experimental studies of limiting thermal loads on the barrel of a rapid-firing gun]. *Materialy XIII Vseros. nauch.-tekhn. konf. "Problemy povysheniya boyevoy gotovnosti, boyevogo primeneniya, tekhnicheskoy ekspluatatsii i obespecheniya bezopasnosti poletov letatel'nykh apparatov s uchetom klimaticheskikh usloviy Sibiri, Zabaykal'ya i Dal'nego Vostoka"* [Materials XIII All-Russ. Scient. and Technic. Conf. "Problems of increasing combat readiness, combat use, technical operation and ensuring flight safety of aircraft, taking into account the climatic conditions of Siberia, Transbaikalia and the Far East"]. Irkutsk, 2003, P. 127–129 (In Russ.).
12. Danilenko R. A., Podkopaev A. V. [Synthesis of a mathematical model for the functioning of the "weapon-cartridge" system based on the solution of a quasi-linear non-stationary heat conduction equation]. *Materialy V Vseros. nauch.-prakt. konf. "Akademicheskkiye Zhukovskkiye chteniya"* [Materials V All-Russ. Scient. and Practic. Conf. "Academic Zhukovsky reading"]. Voronezh, 2018, P. 67–73 (In Russ.).
13. Podkopaev A. V. [Modus for determining the heat transfer coefficient for calculating the temperature field of the barrel of a rapid-firing artillery gun]. *Materialy Vseros. nauch.-prakt. konf. "Sovremennoye sostoyaniye i perspektivy razvitiya letatel'nykh apparatov, ikh silovyykh ustanovok i kompleksov aviatsionnogo vooruzheniya"* [Materials All-Russ. Scient. and Practic. Conf. "The current state and prospects for the development of aircraft, their power plants and aviation weapons systems"]. Voronezh, 2012, P. 202–204 (In Russ.).
14. Isachenko V. P., Osipova V. A., Sukomel A. S. *Teplotperedacha* [Heat transfer]. Moscow, Energoizdat Publ., 1981, 416 p.
15. Korn G., Korn T. *Spravochnik po matematike dlya nauchnykh rabotnikov i inzhenerov* [Mathematical handbook for scientists and engineers]. Moscow, Nauka Publ., 1984, 832 p.
16. *Spravochnik po aviatsionnym materialam i tekhnologii ikh primeneniya* [Handbook of aviation materials and technologies for their application]. Ed. by V. G. Alexandrov. Moscow, Transport Publ., 1979, 242 p.
17. Podkopaev A. V., Babadzhanov A. B., Podkopaev I. A., Dolzhikov V. I. [Identification and simulation mathematical model of thermo and physical loading of a small-caliber artillery barrel]. *Sibirskiy aerokosmicheskii zhurnal*. 2022, Vol. 23, No. 2, P. 209–226 (In Russ.).
18. Babadzhanov A. B., Podkopaev I. A., Podkopaev A. V., Dolzhikov V. I. [Combined mathematical model of internal and intermediate ballistics of aviation artillery weapons]. *Izvestiya Tul'skogo gosudarstvennogo universiteta. Tekhnicheskkiye nauki*. 2022, Rel. 4, P. 177–185 (In Russ.).

19. Vlasova E. A., Zarubin V. S., Kuvyrkin G. N. *Priblizhennyye metody matematicheskoy fiziki* [Approximate methods of mathematical physics]. Moscow, MSTU named after N. E. Bauman Publ., 2001, 700 p.

20. Dulnev G. N., Parfenov V. G., Sigalov A. V. *Primeneniye elektronnykh vychislitel'nykh mashin dlya resheniya zadach teploobmena* [The use of electronic computers for solving heat transfer problems]. Moscow, Vysshaya shkola Publ., 1990, 207 p.

21. Zarubin V. S., Stankevich I. V. *Raschet teplonapryazhennykh konstruktsiy* [Calculation of heat-stressed structures]. Moscow, Mashinostroyeniye Publ., 2005, 352 p.

22. Samarsky A. A., Nikolaev E. S. *Metody resheniya setochnykh uravneniy* [Methods for solving grid equations]. Moscow, Nauka Publ., 1978, 592 p.

23. Zaitsev A. S. *Proyektirovaniye artilleriyskikh stvolov. Ch. II. Spetsial'nyye voprosy* [Designing artillery barrels. P. II. Special questions]. Moscow, MC of the USSR on public education Publ., 1988, 114 p.

24. Podkopaev I. A., Podkopaev A. V. *Raschet temperaturnogo polya stvola avtomaticheskoy pushki vo vremya strel'by* [Calculation of the temperature field of the barrel of an automatic gun during firing]. Moscow, Rospatent, 2023, No. gosudarstvennoj registracii programmy dlya EVM [state registration of a computer program] RU 2023617444. (In Russ.).

© Podkopaev I. A., Podkopaev A. V., Dolzhikov V. I., 2023

Подкопаев Илья Александрович – адъюнкт; Военный учебно-научный центр Военно-воздушных сил «Военно-воздушная академия имени профессора Н. Е. Жуковского и Ю. А. Гагарина» (г. Воронеж). E-mail: ilya.podkopaev.96@bk.ru.

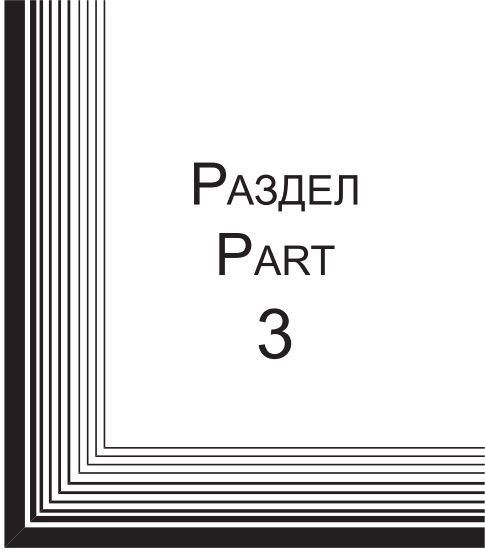
Подкопаев Александр Владимирович – кандидат технических наук, доцент, профессор кафедры эксплуатации комплексов авиационного вооружения (и прицельных систем); Военный учебно-научный центр Военно-воздушных сил «Военно-воздушная академия имени профессора Н. Е. Жуковского и Ю. А. Гагарина» (г. Воронеж). E-mail: aleksanpodkopaev@mail.ru.

Должиков Василий Иванович – кандидат технических наук, доцент, начальник кафедры эксплуатации комплексов авиационного вооружения (и прицельных систем); Военный учебно-научный центр Военно-воздушных сил «Военно-воздушная академия имени профессора Н. Е. Жуковского и Ю. А. Гагарина» (г. Воронеж). E-mail: Link707@mail.ru.

Podkopaev Ilya Aleksandrovich – adjunct; Air Force Military educational and scientific center “Air Force academy named after professor N. E. Zhukovsky and Y. A. Gagarin” (Voronezh). E-mail: ilya.podkopaev.96@bk.ru.

Podkopaev Aleksandr Vladimirovich – Cand. Sc., associate professor, professor of the department operation of aircraft weapon systems (and sighting systems); Air Force Military educational and scientific center “Air Force academy named after professor N. E. Zhukovsky and Y. A. Gagarin” (Voronezh). E-mail: aleksanpodkopaev@mail.ru.

Dolzhikov Vasily Ivanovich – Cand. Sc., associate professor, head of the department operation of aircraft weapon systems (and sighting systems); Air Force Military educational and scientific center “Air Force academy named after professor N. E. Zhukovsky and Y. A. Gagarin” (Voronezh). E-mail: Link707@mail.ru.



РАЗДЕЛ
PART
3



ТЕХНОЛОГИЧЕСКИЕ
ПРОЦЕССЫ
И МАТЕРИАЛЫ

TECHNOLOGICAL
PROCESSES
AND MATERIALS SCIENCE



УДК 621.791.722

Doi: 10.31772/2712-8970-2023-24-4-738-750

Для цитирования: Серегин Ю. Н., Мурыгин А. В., Курашкин С. О. Моделирование технологических параметров электронно-лучевой сварки для изделий ракетно-космической техники // Сибирский аэрокосмический журнал. 2023. Т. 24, № 4. С. 738–750. Doi: 10.31772/2712-8970-2023-24-4-738-750.

For citation: Seregin Yu. N., Murygin A. V., Kurashkin S. O. [Modeling of technological parameters of electron beam welding for rocket and space technology products]. *Siberian Aerospace Journal*. 2023, Vol. 24, No. 4, P. 738–750. Doi: 10.31772/2712-8970-2023-24-4-738-750.

Моделирование технологических параметров электронно-лучевой сварки для изделий ракетно-космической техники

Ю. Н. Серегин, А. В. Мурыгин, С. О. Курашкин

Сибирский государственный университет науки и технологий имени академика М. Ф. Решетнева
Российская Федерация, 660037, г. Красноярск, просп. им. газ. «Красноярский Рабочий», 31
E-mail: ius_ceregin@sibsau.ru

Статья содержит результаты научных исследований по моделированию технологических параметров электронно-лучевой сварки. При моделировании использовался материал ВТ-14 толщиной 0,16 см. Целью моделирования выбрано повышение качества сварного шва за счет оптимальной формы и отсутствие дефектов в виде пор и трещин. В расчетах применен концентрированный источник энергии, эквивалентный электронно-лучевому пучку. В ходе исследования теплового процесса нагрева материала авторами разработаны и опробованы критерии, позволяющие оптимизировать такие параметры сварки, как скорость сварки и положение фокусного пятна относительно поверхности нагреваемой детали. Авторы в своих расчетах применили оригинальный метод нахождения скорости сварки и координаты фокусного пятна по функционалам тепловой модели. Используемые математические модели позволили построить контуры зон термического влияния, соизмеримые с формами шва, полученными на образцах во время сварки с технологическими режимами, соответствующими расчетным при моделировании параметрам. Такой способ исследований позволил существенно сэкономить затраты на отработку технологического режима сварки для макетного узла. Разработанный авторами алгоритм был успешно опробован на материале АМГ-6 с толщиной 10 см. В процессе моделирования сварки для больших толщин получены результаты, которые необходимо учитывать при оптимизации параметров сварки изделий с большой толщиной. Актуальность излагаемого материала подтверждается востребованностью к качеству технологии сварки конструкций электронным пучком. Исследования авторами этого направления позволят существенно расширить возможности в применении электронно-лучевой технологии для ракетно-космической техники.

Ключевые слова: скорость сварки, фокусное расстояние электронного пучка, форма шва, мощность электронно-лучевого оборудования, погонная энергия.

Modeling of technological parameters of electron beam welding for rocket and space technology products

Yu. N. Seregin, A. V. Murygin, S. O. Kurashkin

Reshetnev Siberian State University of Science and Technology
31, Krasnoyarskii Rabochii prospekt, Krasnoyarsk, 660037, Russian Federation
E-mail: ius_ceregin@sibsau.ru

The article contains the results of scientific research on modeling the technological parameters of electron beam welding. The modeling used a material VT-14 with a thickness of 0.16 cm. The purpose of the simulation is to improve the quality of the weld due to the optimal shape and the absence of defects in the form of pores and cracks. A concentrated energy source equivalent to an electron beam is used in the calculations. During the study of the thermal process of heating the material, the authors developed and tested criteria that allow optimizing welding parameters such as welding speed and the position of the focal spot relative to the surface of the heated part. In their calculations, the authors applied an original method of finding the welding speed and the coordinates of the focal spot according to the functionals of the thermal model. The algorithm developed by the authors was successfully tested on AMG-6 material with a thickness of 10 cm. In the process of modeling welding for large thicknesses, results have been obtained that must be taken into account when optimizing the welding parameters of products with large thickness. The relevance of the presented material is confirmed by the demand for the quality of the technology of welding structures with an electron beam. Research by the authors of this direction will significantly expand the possibilities in the application of electron beam technology for rocket and space technology.

Keywords: welding speed, focal length of the electron beam, seam shape, power of electron beam equipment, linear energy.

Introduction

To create permanent connections, electron beam welding (EBW) is often used in the production of rocket and space technology. In the process of obtaining welded joints, for various reasons, defects appear that reduce the strength of a part or metal structure, violate the tightness of containers made by welding, and also contribute to a decrease in the reliability of operation of this unit as a whole.

The connection of parts requires uniformity of the heating zone of the joint, since if its heating is uneven, defects in welded joints arise. The required parameters of the welding process are usually selected using full-scale experiments. However, conducting full-scale experiments is expensive and requires a lot of time.

The research of many domestic and foreign authors is devoted to solving the issues of improving the quality of the welding process (Zuev I.V., Trushnikov D.N., Hara K., Vinogradov V.A., Sasaki S., Krivenkov V.A., Kutsan Yu.G., Anderl P. et al.) [1–4]. In his research, Rodyakina R.V. [5] develops a technique for simulating the process of passing an electron beam through a layer of evaporated metal. The authors Motasov M.I., Dovydov D.A., Alekseev V.S. [6] consider a simulation model of a beam focusing control system using the Simulink software environment, which is part of the MATLAB package. Drozd A.A. [7] in his research uses a numerical method that allows one to simulate the processes of development of thermal stresses and deformations during spot electron beam welding; the model takes into account phase transitions during heating, melting, evaporation and crystallization. V.N. Tarasova [8] developed a computer modeling method that can significantly reduce the time spent on manufacturing welded products and predict the results under predetermined conditions. The authors V.V. Melyukov and D.A. Tarabukin [9] proposed a method of mathematical and numerical modeling of the thermal welding process to determine the power of the welding source and to reduce the time and volume of a full-scale experiment when debugging the mode.

1. Application of theory of thermal processes to EBW

Most of the existing designs have a number of disadvantages: there is no ability to realize the developed methods in the production conditions due to their difficulty, narrow-focus of development, and the inability to optimize technological parameters when entering new materials into the technological process. The optimization of the technological parameters of the welding process when entering new materials requires full-scale experiments, which leads to an increase in material and labor costs. The proposed techniques and the model in this study, as well as the ACS developed by the EBW, allow you to solve the above problems, and reduce the number of defects arising from the welding project, both for existing welding modes and when commissioning a new product.

For the authors, the technology that is used for the shi-rock nomenclature of the thicknesses of the connected structures is of greatest interest. In the works [10-17], the authors propose materials on the modeling of the EBW process in order to find the optimal mode for thicknesses from 0.1 mm to 30 mm. The gained modeling experience led the authors to the idea of studying the possibility of using EBW for significantly large thicknesses of the welded products. Thus, the goal was to evaluate the possibilities of modeling the heat process of heating the material under study with a concentrated source of energy in a wide range of thickness and the use of modeling results for practical use on electron beam equipment.

When modeling the process of electron-beam welding, a classic method of presenting the process (Fig. 1) was used in the form of moving instantaneous energy sources (Fig. 2), the amount and location of which fully corresponds to a real electronic beam.

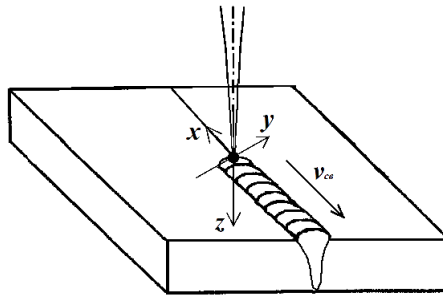


Рис. 1. Представление ЭЛС в графическом виде

Fig. 1. Representation of the EBW in graphical form

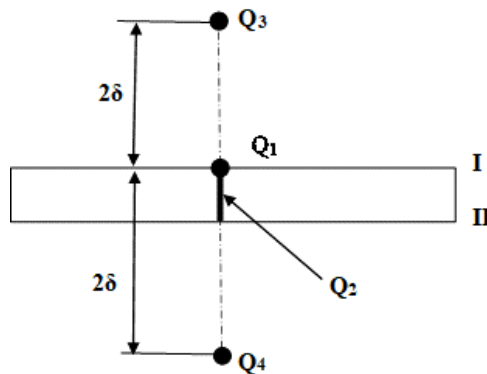


Рис. 2. Представление ЭЛС в графическом виде:
 δ – толщина детали; Q_1 – мгновенный точечный источник; Q_2 – мгновенный линейный источник; Q_3 и Q_4 – фиктивные точечные источники

Fig. 2. Representation of the EBW in graphical form:
 δ – part thickness; Q_1 – instant point source;
 Q_2 – instant linear source; Q_3 и Q_4 – fictitious point sources

The temperature of the heating of the material due to the effects of the selected sources in accordance with [18] and the principle of superposition is calculated by (1):

$$T_{\text{комп}} = \sum_{i=1}^4 T_i(x, y, z, v, t, Q_i), \quad (1)$$

where

$$T_1 = \frac{Q_1}{c\rho\sqrt{(4\pi a)^3}} e^{-\frac{vx_t}{2a}} \int_0^t \exp\left(-\frac{v^2\tau}{4a} - \frac{x^2 + y^2 + z^2}{4a\tau}\right) \frac{d\tau}{\tau^{3/2}};$$

$$T_2 = \frac{Q_2}{4\pi\lambda\delta} e^{-\frac{vx_t}{2a}} \int_0^t \exp\left(-\frac{v^2\tau}{4a} - \frac{2\lambda\tau}{c\rho\delta} - \frac{x^2 + y^2}{4a\tau}\right) \frac{d\tau}{\tau};$$

$$T_3 = \frac{Q_3}{c\rho\sqrt{(4\pi a)^3}} e^{-\frac{vx_t}{2a}} \int_0^t \exp\left(-\frac{v^2\tau}{4a} - \frac{x^2 + y^2 + (z - 2\delta)^2}{4a\tau}\right) \frac{d\tau}{\tau^{3/2}};$$

$$T_4 = \frac{Q_4}{c\rho\sqrt{(4\pi a)^3}} e^{-\frac{vx_t}{2a}} \int_0^t \exp\left(-\frac{v^2\tau}{4a} - \frac{x^2 + y^2 + (z + 2\delta)^2}{4a\tau}\right) \frac{d\tau}{\tau^{3/2}} \text{ --the temperature from expo-}$$

sure to the corresponding instantaneous sources in accordance with Fig. 2.

The used heat process model (1) was investigated and tuned for the VT-14 material with a melting thickness of 1.5 ± 0.5 mm. To compare the shape of the cross -section of the seam and the modeled zone of thermal influence, the correspondence of the ratio of the size of the width to the depth of the seam was made. In Fig. 3 shows the results of the modeling and the form of the grinding of the corresponding welding mode. The schedule of the zone of thermal influence was obtained by the number (1) and the selection of the section of the heating zone according to the coordinates corresponding to the greatest deviation of the temperature of the thermal influence (for VT-14-600 °C) from the heating exhaust position.

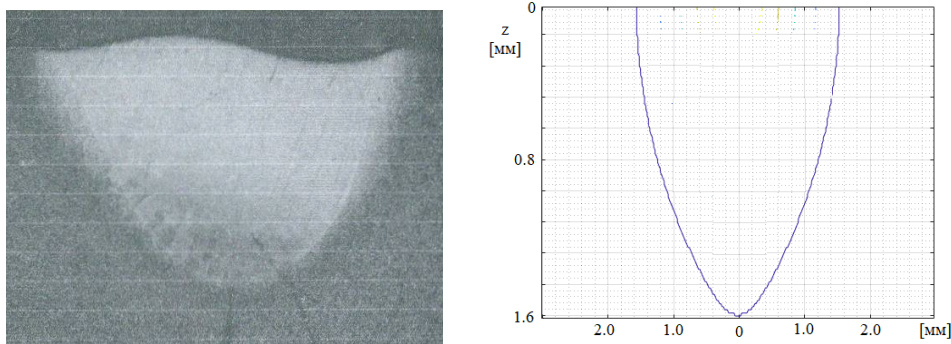


Рис. 3. Изображения формы шлифа и зоны термического влияния при глубине шва 1,6 мм и ширине 2,5 мм

Fig. 3. Images of the shape of the slot and the zone of thermal influence at a seam depth of 1.6 mm and the width is 2.5 mm

2. Development of mathematical functionality

To calculate the technological process parameters as the welding speed, the form of a fuel distance and the required EBW power, the authors have developed a model of mathematical functionality (2) (analogue of the medium-squadratic deviation), the criterion of the optimal (3) of which allows you to determine the indicated parameters of the technological process for material of any thickness.

$$J_1 = \sqrt{\frac{1}{n-1} \sum_{i=1}^n \left(T_{\text{норм}i} - \overline{T_{\text{норм}}} \right)^2}; \quad (2)$$

According to the developed criterion, the parameters of the technological process will be the solution of the system (4)

$$\begin{cases} \frac{\partial J_1}{\partial v} = 0, \\ \frac{\partial J_1}{\partial z} = 0, \\ \frac{\partial J_1}{\partial Q} = 0, \end{cases} \quad (4)$$

where v – welding speed; z – the position of the focal spot; Q – the energy of the heating source (equal to the sum of instantic point Q_1 and linear Q_2 sources).

To search for the required technological parameters of the EBW (energy, time, welding rate), an algorithm was developed, presented in the form of a block diagram in Fig. 4.

The algorithm is based on the models proposed in this study (1) - (4). After the initialization of the technological parameters, the following parameters are set: T -the temperature of the granular zone of thermal influence (from minimum to maximum), t is the time of integration, V is the speed of welding, Q is the energy of the heating sources, x -coordinates in length of the product, y - coordinates in width of the product, z - coordinates in height of the product. Further, values are co-preserved in the database for further use in future calculations. If the experiment is new, then to calculate the energy of the heating source, the values of the temperature, integration time and welding rate are set, after the heating temperature (1) with the current fictitious and real sources is calculated. Next, using Crichera optimality (2), the required energy is calculated, providing a uniform zone heating the weld. To find the integration time, the resulting energy is set and the temperature of the boundary zone of thermal influence, then the temperature of the het is calculated by variating the rest of the parameters in a certain range. Knowing the optimal values of the energy, integration time, the welding speeds are calculated, similarly to the previous stages.

Applying the specified algorithm for parts with a thickness of up to 100 mm, the authors faced with a feature that showed itself when calculating the coordinates of the focal spot of the electric beam and the distribution of energies of instant sources. With an increase in the thickness of the welded material extremum of functional (3) disappears. This is explained by the fact that the welding of large thicknesses is carried out by an electron-beam gun with a narrow focus.

The idea of a simple recharge of these parameters using the optimization criterion (3) is a task requiring large time costs, which often leads to the practical inappropriateness of work in this direction.

3. Development of physical functionality

When studying the technology of welding of structures with different thicknesses of melting, the authors faced the task of choosing specific energy values for Q_1 and Q_2 sources. What is the way to choose these values depends on the studied thicknesses of the parts. Often, during the moistening of thermal processes, researchers choose the magnitude of the energy of the point based on experimental material in order to obtain an adequate mathematical model [19–22]. The authors acted in a similar way, choosing the best correspondence in the ratio between the width of the seam and its depth.

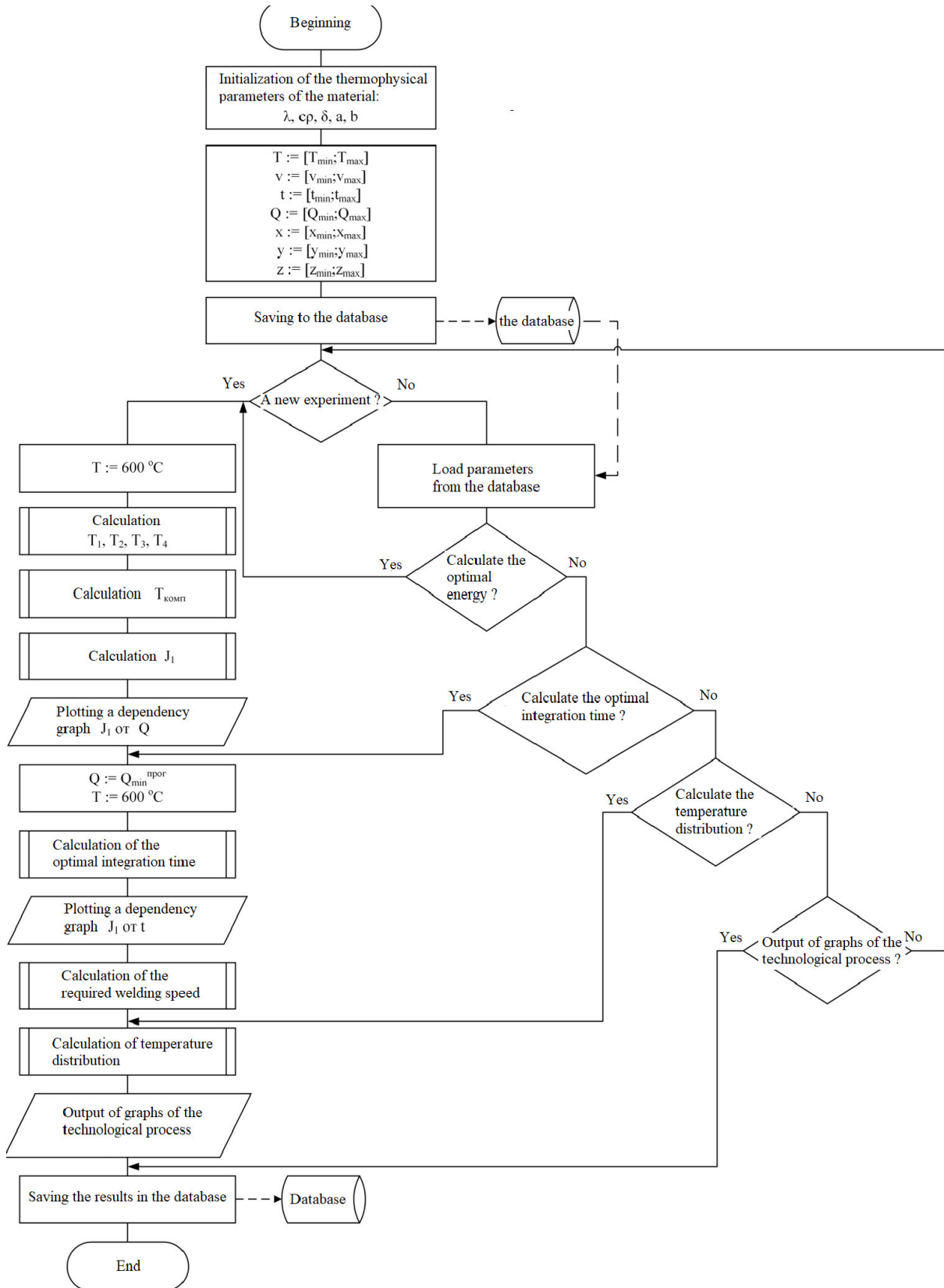


Рис. 4. Блок-схема алгоритма поиска требуемых технологических параметров процесса сварки

Fig. 4. Block diagram of the algorithm for finding the required technological parameters of the welding process

To reduce the time of searching for the specified ratio, the authors have developed physical functionality (5) and the optimization criterion for this functionality (6):

$$J_2 = \left(\left(\frac{Q}{v} \right)_{\text{норм}} - (Q \cdot t)_{\text{норм}} \right)^2; \quad (5)$$

$$J_2 = \left(\left(\frac{Q}{v} \right)_{\text{норм}} - (Q \cdot t)_{\text{норм}} \right)^2 \rightarrow \min, \quad (6)$$

where Q – the energy of the heating source, including selected sources Q_1 and Q_2 ; v – welding speed; t – the time for achieving the boundary of the zone of the thermal influence of the lower boundary of the heating zone.

Modeling the heating process during welding using both optimal criteria showed a good correlation of the developed functionals. This was the basis for combining the optimality criteria in obtaining a general solution in the search for required EBW technological parameters.

The use of physical functional when modeling the EBW process significantly reduces the computational resource, since it uses the original system of equations of the thermal process (1) in a simplified version (to determine only v - welding speed and t - time to reach the boundary of the heat-affected zone of the lower boundary heating zones).

As the starting material, the authors chose a technological mode used in production conditions. Using models (1, 3, 5), the parameters included in these equations were calculated. The calculation results are presented in the table.

Calculation results for VT-14 with a thickness of 0.16 cm

Q [Cal.]	Q ₁ [Cal.]	Q ₂ [Cal.]	Delta = 0.16 cm (f = 0)					
			J ₁	Q/v	v [cm/s]	t [s]	Q · t	J ₂
800	560	240	0.062243	484.485	1.65	0.236	188.8	0.000291516
810	567	243	0.062089	486.4865	1.665	0.2346	190.026	0.000208469
820	574	246	0.061959	488.0952	1.68	0.2332	191.224	0.00014109
830	581	249	0.061844	489.6755	1.695	0.2318	192.394	8.82512E-05
840	588	252	0.061739	491.2281	1.71	0.2304	193.536	4.88335E-05
850	595	255	0.061649	492.7536	1.725	0.229	194.65	2.17259E-05
860	602	258	0.061591	494.2529	1.74	0.2276	195.736	5.82972E-06
870	609	261	0.061522	495.7265	1.755	0.2262	196.794	6.22367E-08
880	616	264	0.061473	497.1751	1.77	0.2248	197.824	3.35895E-06
890	623	267	0.061452	498.5994	1.785	0.2234	198.826	1.46767E-05
900	630	270	0.061436	500	1.8	0.222	199.8	3.29965E-05
910	637	273	0.061431	502.7624	1.81	0.2203	200.473	1.4464E-05
920	644	276	0.061438	505.4945	1.82	0.2186	201.112	3.10314E-06
930	651	279	0.061451	508.1967	1.83	0.2169	201.717	1.45467E-07
940	658	282	0.0615	510.8696	1.84	0.2152	202.288	6.89928E-06
950	665	285	0.061547	513.5135	1.85	0.2135	202.825	2.4751E-05
960	672	288	0.061954	516.129	1.86	0.2118	203.328	5.51664E-05
970	679	291	0.062063	518.7166	1.87	0.2101	203.797	9.96923E-05
980	686	294	0.062167	521.2766	1.88	0.2084	204.232	0.000159957
990	693	297	0.06226	523.8095	1.89	0.2067	204.633	0.000237674
1000	700	300	0.062375	526.3158	1.9	0.205	205	0.000334638

Based on the results of the table, graphs for functionals (3) and (5) were constructed (Fig. 5).

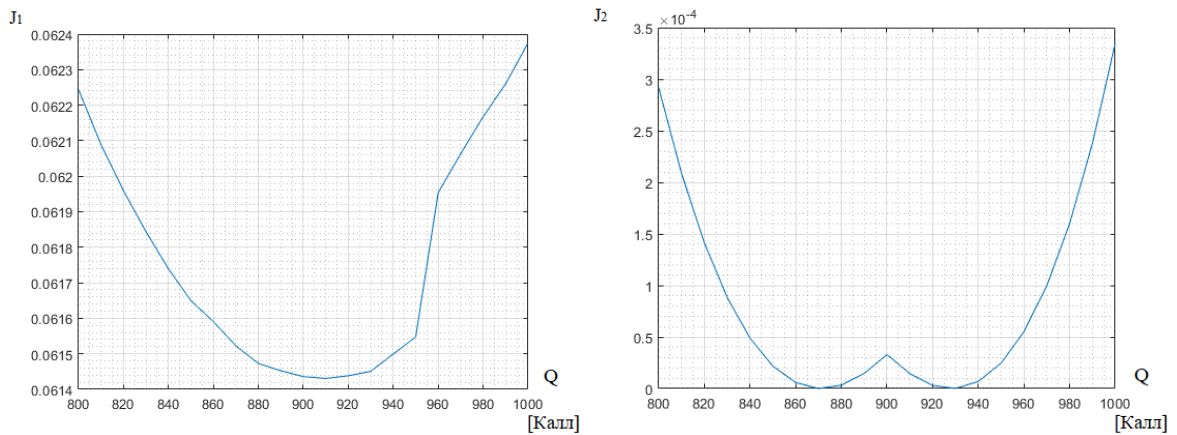


Рис. 5. Графики зависимостей функционалов

Fig. 5. Graphs of functional dependencies

We search for optimal parameters using accepted criteria (4) and (6). The coordinates where the extrema of both functionals coincide are taken as a solution.

In our case, there is some discrepancy, so the coordinate of the right extremum for the functional J_2 was chosen. The table highlights the technological mode and the one that is accepted as optimal. The dimensions of the technological mode are shown in Fig. 3. Fig. 6 shows the simulation results and the shape of the section corresponding to the selected optimal welding mode.

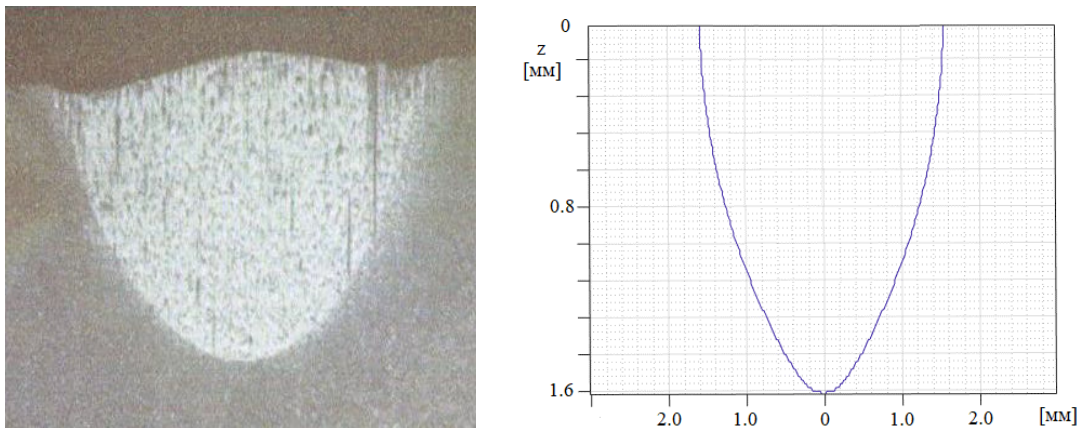


Рис. 6. Изображения формы шлифа и зоны термического влияния при глубине шва 1,6 мм и ширине 2,4 мм

Fig. 6. Images of the shape of the slot and the zone of thermal influence at a seam depth of 1.6 mm and the width is 2.4 mm

As you can see, optimization did not produce significant improvements in reducing the seam width relative to the depth. This is primarily due to the fact that the focal spot of the electron beam was on the surface of the part. The authors conducted studies on the effect of the position of the focus relative to the surface of the part on the functionality (3). It was found that the values of the functional will be the smallest in the case when the focus of the electron beam is located inside the part at approximately a depth equal to half the penetration depth (Fig. 7).

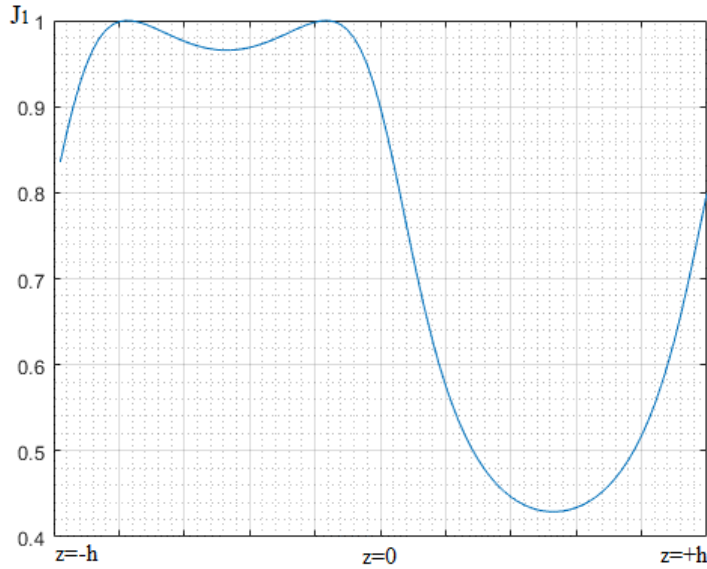


Рис. 7. График изменения функционала для толщины 0,16 см

Fig. 7. Functional change graph for 0.16 cm thickness

Taking into account the change in the focus position, the authors conducted an experiment with the previously proposed welding mode. Fig. 8 shows the simulation results and the shape of the section corresponding to the selected optimal welding mode.

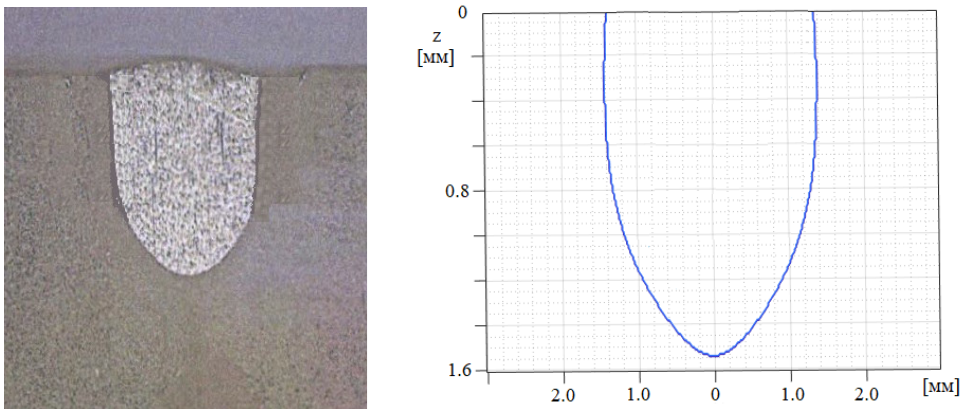


Рис. 8. Изображения формы шлифа и зоны термического влияния при глубине шва 1,6 мм и ширине 2,4 мм

Fig. 8. Images of the shape of the slot and the zone of thermal influence at a seam depth of 1.6 mm and the width is 2.4 mm

The modeling results and experimental data showed that with the use of the obtained experimental studies, the side walls of the prototype weld became more parallel, which meets the requirements for reducing residual stresses in welding parts, which significantly improves the quality indicators of the technological process.

When modeling the welding process for large thicknesses (from 3 cm or more), the authors encountered the following phenomenon: when determining the optimal focal length using the minimum of the functional (2), the extremum of the function is not observed (Fig. 9).

The authors did not have the opportunity to obtain technological parameters for samples of welds of large thicknesses. Therefore, they made the assumption that the position of the focal spot does not

affect the welding process. An explanation for this may be the ability of welding equipment to weld at such depths. As a rule, power plants equipped with electron beam guns with narrow-focus gun characteristics are used for this purpose. The authors carried out a simulation similar to that presented for the aluminum alloy AMG-6 of the predicted model of the thermal welding process of large penetration depths, which allows for an assessment of the capabilities of welding products on existing equipment or the selection of a suitable power plant for this. As can be seen from Fig. 10, in addition to the common coordinate for criteria (3) and (5), the presence of several extrema in the second functional expands the picture of the search for optimal parameters of electron beam welding, not limiting itself only to the extremum common with the first functional.

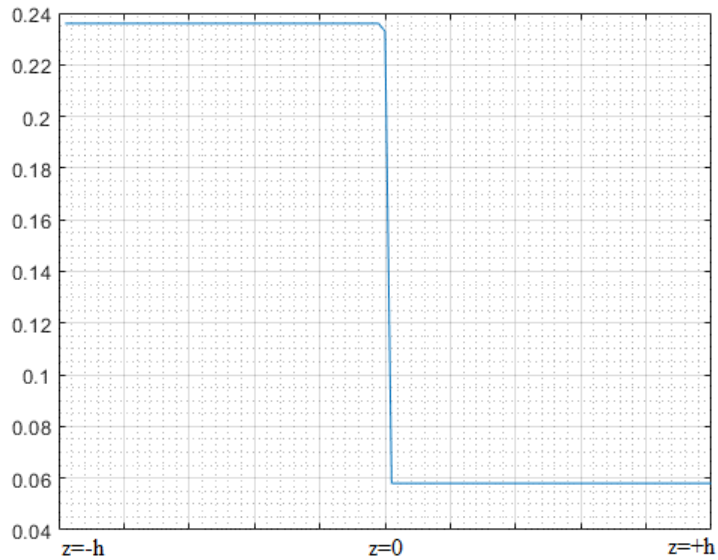


Рис. 9. График изменения функционала для толщины 10 см

Fig. 9. Functional change graph for 10 cm thickness

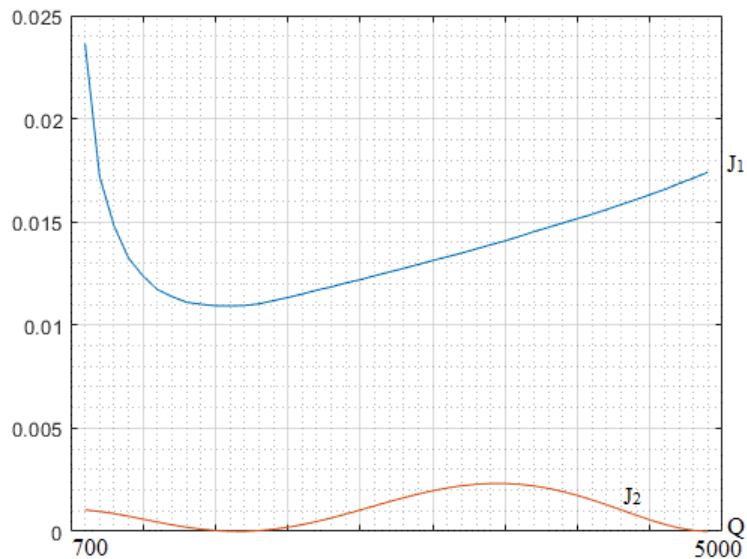


Рис. 10. Графики поведения функционалов от вводимой энергии для AMG-6 толщиной 10 см

Fig. 10. Graphs of the behavior of functionals from the input energy for AMG-6 with a thickness of 10 cm

The combined use of functionals allows for modeling to combine two physical properties of the material heating process: the temperature characteristics of the heating zone and the effective energy input of heating sources.

Conclusion

The results of scientific research carried out by the authors make it possible to theoretically determine such possible parameters of electron beam welding technology as the speed of movement of the material being welded and the required energy of the heating source for parts with a wide range of welded thicknesses. The use of electron beam technology for the manufacture of rocket and space technology products will significantly influence the quality of welded joints due to the optimal choice of the specified welding parameters.

Библиографические ссылки

1. Guoqing, Ch., Junpeng L., Xi S., Hua G. Numerical simulation of keyhole morphology and molten pool flow behavior in aluminum alloy electron-beam welding // *International Journal of Heat and Mass Transfer*. 2019. Vol. 138. P. 879–888.
2. Ziyu, Y., Yuchao F., Jingshan H. Numerical simulation of heat transfer and fluid flow during vacuum electron beam welding of 2219 aluminium girth joints // *Vacuum*. 2020. Vol. 175. P. 109–126.
3. Sanjib J., Dilip K. P. Fuzzy Inference System-Based Neuro-Fuzzy Modeling of Electron-Beam Welding // *Advances in Computational Methods in Manufacturing*. 2019. Vol. 123. P. 839–850.
4. Mathematical modeling of the electron-beam wire deposition additive manufacturing by the smoothed particle hydrodynamics method / D. N. Trushnikov, E. G. Koleva, R. P. Daviyatshi et al. // *Mechanics of Advanced Materials and Modern Processes*. 2019. Vol. 5. P. 1–14.
5. Родякина Р. В., Щербаков А. В., Гапонов Д. А. Моделирование процесса ионизации металла в ЭЛС // *Электронно-лучевая сварка и родственные технологии*. 2020. № 1. С. 129–136.
6. Мотасов М. И., Довыдов Д. А., Алексеев В. С. Автоматизация управления фокусировкой луча при электронно-лучевой сварке // *Вопросы электротехники*. 2017. № 1. С. 127–130.
7. Дрозд А. А. Численное исследование температурных полей и деформаций в процессе точечной электронно-лучевой сварки // *Прикладная математика и информатика: современные исследования в области естественных и технических наук*. 2018. № 1. С. 290–294.
8. Тарасова В. Н. Оптимизация конструкции электронно-лучевого оборудования за счет компьютерного моделирования // *Наука и современное образование. Материаловедение, машиностроение*. 2021. № 1. С. 11–13.
9. Мелюков В. В., Тарабукин Д. А. Определение параметров сварочного источника в зависимости от геометрических размеров сварочного шва // *Электронно-лучевая сварка и смежные технологии. Материаловедение*. 2017. № 1. С. 117–130.
10. Seregin Yu. N., Murygin A. V., Kurashkin S. O. Features of modeling the electron beam energy distribution for the electron beam welding process // *Siberian Journal of Science and Technology*. 2020. Vol. 21, No. 2. P. 266–273.
11. Mathematical modelling of waveguide paths by electron-beam welding / S. O. Kurashkin, A. V. Murygin, Yu. N. Seregin et al. // *3rd International Conference on Industry 4.0 and Smart Manufacturing, ISM 2021. Procedia Computer Science, Elsevier*. 2022. Vol. 200. P. 83–90.
12. Hardware Control of the Electron Beam Energy Density by the Heating Spot / S. O. Kurashkin, V. S. Tynchenko, Yu. N. Seregin et al. // *Proceedings of Sixth International Congress on Information and Communication Technology. Lecture Notes in Networks and Systems*. Springer, Singapore, 2022. P. 71–78.
13. Kurashkin S. O., Seregin Yu. N. Modeling the thermal process using the temperature functional by electron beam welding // *IOP Conference Series: Materials Science and Engineering*. IOP Publishing, 2020. Vol. 734, No. 1. P. 012003.
14. Mathematical functional for thermal distribution calculating during the electron-beam welding process / S. O. Kurashkin, Yu. N. Seregin, V. S. Tynchenko et al. // *Journal of Physics: Conference Series*. IOP Publishing, 2020. Vol. 1515, No. 5. P. 052049.

15. Analytical characteristics of the electron beam distribution density over the heated spot for optimizing the electron-beam welding process / S. O. Kurashkin, V. D. Laptенок, A. V. Murygin, Yu. N. Seregin // IOP conference series: materials science and engineering. IOP Publishing. 2019. Vol. 681, No. 1. P. 012021.
16. Свидетельство № 2021616858 Российской Федерации. Программа для моделирования плотности распределения электронного пучка с использованием различных сканирований при электронно-лучевой сварке: № 2021615834: заяв. 19.04.2021, опубл. 28.04.2021 / Курашкин С. О., Тынченко В. С., Серегин Ю. Н., Мурыгин А. В. 1 с.
17. Сертификат № 2018664000 Российской Федерации. Программа для определения скорости сварки для оптимального нагрева металла в зоне проплавления: № 2018661400: заяв. 19.10.2018; опубл. 08.11.2018 / Серегин Ю. Н., Курашкин С. О., Мурыгин А. В., Тынченко В. С. 1 с.
18. Неровный В. М. Теория сварочных процессов. М. : МГТУ им. Н. Э. Баумана, 2016. 340 с.
19. Недосека А. Я., Санченко Г. А., Ворона Г. А. Распределение температуры при воздействии концентрированного источника тепла на поверхность пластины // Автоматическая сварка. 1977. № 6. С. 1–4.
20. Недосека А. Я., Чернова О. И. Распределение температуры в пластинах с источником нагрева при сварке на разной глубине // Автоматическая сварка. 1977. № 7. С. 1–4.
21. Башенко В. В., Петров Г. Л. Формирование зоны проплавления при электронно-лучевой сварке // Автоматическая сварка. 1977. № 9. С. 23–27.
22. Михайлов В. Г., Петров П. И. Расчет тепловых процессов при электронно-лучевой сварке // Автоматическая сварка. 1988. № 5. С. 13–15.

References

1. Guoqing, Ch., Junpeng L., Xi S., Hua G. Numerical simulation of keyhole morphology and molten pool flow behavior in aluminum alloy electron-beam welding. *International Journal of Heat and Mass Transfer*. 2019, Vol. 138, P. 879–888.
2. Ziyou, Y., Yuchao F., Jingshan H. Numerical simulation of heat transfer and fluid flow during vacuum electron beam welding of 2219 aluminium girth joints. *Vacuum*. 2020, Vol. 175, P. 109–126.
3. Sanjib J., Dilip K. P. Fuzzy Inference System-Based Neuro-Fuzzy Modeling of Electron-Beam Welding. *Advances in Computational Methods in Manufacturing*. 2019, Vol. 123, P. 839–850.
4. Trushnikov D. N. Koleva E. G., Daviyatshi R. P., Gerasimov R. M., Bayandin Yu. V. Mathematical modeling of the electron-beam wire deposition additive manufacturing by the smoothed particle hydrodynamics method. *Mechanics of Advanced Materials and Modern Processes*. 2019, Vol. 5, P. 1–14.
5. Rodyakina R. V., Shcherbakov A. V., Gaponov D. A. [Modeling of the metal ionization process at EBW]. *Elektronno-luchevaya svarka i rodstvennye tekhnologii*. 2020, No. 1, P. 129–136 (In Russ.).
6. Motasov M. I., Dovyodov D. A., Alekseev V. S. [Automation of beam focusing control during electron beam welding]. *Voprosy elektrotekhniki*. 2017, No. 1, P. 127–130 (In Russ.).
7. Drozd A. A. [Numerical study of temperature fields and deformation in the process of spot electron beam welding]. *Prikladnaya matematika i informatika: sovremennye issledovaniya v oblasti estestvennykh i tekhnicheskikh nauk*. 2018, No. 1, P. 290–294 (In Russ.).
8. Tarasova V. N. [Optimization of the design of electron beam equipment due to computer modeling]. *Nauka i sovremennoe obrazovanie. Materialovedenie, mashinostroenie*. 2021, No. 1, P. 11–13 (In Russ.).
9. Melyukov V. V., Tarabukin D. A., ElectJolisch T. [Determination of welding source parameters depending on the geometric dimensions of the weld]. *Elektronno-luchevaya svarka i smezhnye tekhnologii. Materialovedenie*. 2021, Vol. 63, P. 17–28 (In Russ.).
10. Seregin Yu. N., Murygin A. V., Kurashkin S. O. Features of modeling the electron beam energy distribution for the electron beam welding process. *Siberian Journal of Science and Technology*. 2020, Vol. 21, No. 2, P. 266–273.
11. Kurashkin S. O., Murygin A. V., Seregin Yu. N., Tynchenko V. S., Lavrishev A. V. Mathematical modelling of waveguide paths by electron-beam welding. *3rd International Conference on*

Industry 4.0 and Smart Manufacturing, ISM 2021. Procedia Computer Science, Elsevier. 2022, Vol. 200, P. 83–90.

12. Kurashkin S. O., Tynchenko V. S., Seregin Yu. N., Murygin A. V., Bocharov A. N. Hardware Control of the Electron Beam Energy Density by the Heating Spot. *Proceedings of Sixth International Congress on Information and Communication Technology. Lecture Notes in Networks and Systems.* Springer, Singapore, 2022, P. 71–78.

13. Kurashkin S. O., Seregin Yu. N. Modeling the thermal process using the temperature functional by electron beam welding. *IOP Conference Series: Materials Science and Engineering.* IOP Publishing, 2020, Vol. 734, No. 1, P. 012003.

14. Kurashkin S. O., Seregin Yu. N., Tynchenko V. S., Petrenko V. E., Murygin A. V. Mathematical functional for thermal distribution calculating during the electron-beam welding process. *Journal of Physics: Conference Series.* IOP Publishing, 2020, Vol. 1515, No. 5, P. 052049.

15. Kurashkin S. O., Laptinok V. D., Murygin A. V., Seregin Yu. N. Analytical characteristics of the electron beam distribution density over the heated spot for optimizing the electron-beam welding process. *IOP conference series: materials science and engineering.* IOP Publishing, 2019, Vol. 681, No. 1, P. 012021.

16. Certificate No. 2021616858 Russian Federation. A program for modeling the electron beam distribution density using various scans during electron beam welding: No. 2021615834 : application 19.04.2021 publ. 28.04.2021 Kurashkin S.O., Tynchenko V.S., Seregin Yu.N., Murygin A.V. 1 p.

17. Certificate No. 2018664000 Russian Federation. The program for determining the welding speed for optimal heating of metal in the area of penetration: No. 2018661400 : application 19.10.2018 : publ. 08.11.2018 Seregin Yu.N., Kurashkin S.O., Murygin A.V., Tynchenko V.S. 1 p.

18. Nerovniy V. M., Konovalov A. V., Yakushin B. F. *Teoriya svarochnykh protsessov* [Theory of welding processes]. Moscow, MGTU im. N. E. Bauman Publ., 2016, 340 p.

19. Nedoseka A. Ya., Sanchenko G. A., Vorona G. A. [Temperature distribution under the action of a concentrated heat source on the plate surface]. *Avtomaticeskaya svarka.* 1977, No. 6, P. 1–4 (In Russ.).

20. Nedoseka A. Ya., Chernova O. I. [Temperature distribution in plates with a welding heating source at different depths]. *Avtomaticeskaya svarka.* 1977, No. 7, P. 1–4 (In Russ.).

21. Bashenko V. V., Petrov G. L. [Formation of the penetration zone during electron beam welding]. *Avtomaticeskaya svarka.* 1977, No. 9, P. 23–27 (In Russ.).

22. Mikhailov V. G., Petrov P. I. [Calculation of thermal processes in electron beam welding]. *Avtomaticeskaya svarka.* 1988, No. 5, P. 13–15 (In Russ.).

© Seregin Yu. N., Murygin A. V., Kurashkin S. O., 2023

Серегин Юрий Николаевич – кандидат технических наук, доцент кафедры информационно-управляющих систем; Сибирский государственный университет науки и технологий имени академика М. Ф. Решетнева. E-mail: ius_ceregin@sibsau.ru.

Мурыгин Александр Владимирович – доктор технических наук, профессор, заведующий кафедрой информационно-управляющих систем; Сибирский государственный университет науки и технологий имени академика М. Ф. Решетнева. E-mail: ius_murygin@sibsau.ru.

Курашкин Сергей Олегович – ассистент кафедры информационно-управляющих систем; Сибирский государственный университет науки и технологий имени академика М. Ф. Решетнева. E-mail: kurashkin_so@sibsau.ru.

Seregin Yuri Nikolaevich – Cand. Sc., Associate Professor of the Department of Information and Control Systems; Reshetnev Siberian State University of Science and Technology. E-mail: ius_ceregin@sibsau.ru.

Murygin Alexander Vladimirovich – Dr. Sc., Professor, Head of the Department of Information and Control Systems; Reshetnev Siberian State University of Science and Technology. E-mail: ius_murygin@sibsau.ru.

Kurashkin Sergey Olegovich – Assistant of the Department of Information and Control Systems; Reshetnev Siberian State University of Science and Technology. E-mail: kurashkin_so@sibsau.ru.

УДК 544.623.032.52

Doi: 10.31772/2712-8970-2023-24-4-751-759

Для цитирования: Трифонов С. В., Тихомиров А. А., Мuryгин А. В. Автоматизированная система очистки жидких продуктов переработки отходов для замкнутых экосистем космического назначения // Сибирский аэрокосмический журнал. 2023. Т. 24, № 4. С. 751–759. Doi: 10.31772/2712-8970-2023-24-4-751-759.

For citation: Trifonov S. V., Tikhomirov A. A., Murygin A. V. [Automated system for cleaning liquid waste products for closed ecosystems for space purposes]. *Siberian Aerospace Journal*. 2023, Vol. 24, No. 4, P. 751–759. Doi: 10.31772/2712-8970-2023-24-4-751-759.

Автоматизированная система очистки жидких продуктов переработки отходов для замкнутых экосистем космического назначения

С. В. Трифонов^{1,2*}, А. А. Тихомиров^{1,2}, А. В. Мuryгин²

¹Институт биофизики ФИЦ КНЦ СО РАН

Российская Федерация, 660036, г. Красноярск, ул. Академгородок, 50/50

²Сибирский государственный университет науки и технологий имени академика М. Ф. Решетнева
Российская Федерация, 660037, г. Красноярск, просп. им. газ. «Красноярский Рабочий», 31

*E-mail: trifonov_sergei@inbox.ru

Обеспечение жизнедеятельности человека в течение нескольких лет в изолированных условиях будущих марсианских и лунных баз представляется возможным при организации круговоротного процесса преобразования органических отходов, в том числе экзометаболитов человека (кал. урина), в необходимые ему продукты: воду, кислород и пищу. Перспективным способом организации такого круговоротного процесса является создание трехзвенной замкнутой экосистемы (ЗЭС): человек, звено получения удобрений из органических отходов и растения – где растения синтезируют необходимые человеку продукты. В работе рассмотрена оригинальная схема комплексной установки очистки жидких продуктов переработки экзометаболитов человека от загрязнителей в процессе получения питательных растворов для выращивания растений в условиях ЗЭС. Переработку экзометаболитов человека осуществляли в устройстве физико-химического окисления в водной среде перекиси водорода под действием переменного электрического тока – в реакторе «мокрого» сжигания. Подобрано периферийное оборудование для организации системы автоматического управления установкой очистки, выявлены проблемы и разработаны подходы в автоматизации технологических процессов и создании программного обеспечения для взаимодействия человека с предлагаемой установкой. Выполнены эксперименты по выращиванию растений салата, подтверждающие эффективность предлагаемых процессов очистки жидких продуктов переработки экзометаболитов человека. Сделан вывод, что созданная комплексная установка очистки, оснащенная предлагаемым программным обеспечением, может быть использована для научных исследований применительно к тематике ЗЭС, в том числе космического назначения.

Ключевые слова: управление технологическим процессом, системы жизнеобеспечения, утилизация органических отходов, обессоливание, растительное звено.

Automated system for cleaning liquid waste products for closed ecosystems for space purposes

S. V. Trifonov^{1,2*}, A. A. Tikhomirov^{1,2}, A. V. Murygin²

¹Institute of Biophysics SB RAS

50/50, Akademgorodok, Krasnoyarsk, 660036, Russian Federation

²Reshetnev Siberian State University of Science and Technology
31, Krasnoyarskii Rabochii prospekt, Krasnoyarsk, 660037, Russian Federation

*E-mail: trifonov_sergei@inbox.ru

Ensuring human life activity for several years in isolated conditions of future Martian and lunar bases is possible with the organization of a circular process of converting organic waste, including human exometabolites (feces, urine), into the products he needs: water, oxygen and food. A promising way to organize such a circular process is to create a three-link closed ecosystem (CES): a person, a link for obtaining fertilizers from organic waste and plants - where plants synthesize the products necessary for a person. The paper considers the original scheme of a complex installation for the purification of liquid products of processing of human exometabolites from pollutants in the process of obtaining nutrient solutions for growing plants in a CES. The processing of human exometabolites was carried out in a device for physicochemical oxidation of hydrogen peroxide in an aqueous medium under the action of alternating electric current – in a “wet” combustion reactor. Peripheral equipment was selected for the organization of the automatic control system of the cleaning plant, problems were identified and approaches were developed in the automation of technological processes and the creation of software for human interaction with the proposed installation. Experiments on the cultivation of lettuce plants have been carried out, confirming the effectiveness of the proposed processes of purification of liquid products of processing of human exometabolites. It is concluded that the created integrated cleaning plant, equipped with the proposed software, can be used for scientific research in relation to the subject of CES, including space purposes.

Keywords: process control, life support systems, utilization of organic waste, desalination, plant link.

Introduction

The problem of creating closed ecosystems (CES) to ensure human life during long-term space flight and stay on celestial bodies (Moon, Mars, asteroids, etc.) is currently receiving increasing attention from leading space agencies and other major research centers [1; 2]. In Russia, the Institute of Biophysics SB RAS (Siberian Branch of Russia Academy of Science) is actively engaged in the development of closed ecosystems for space purposes [3]. At the same time, much attention is paid to the creation of models of closed ecosystems. Various patterns of circular processes are worked out on their basis, which can then be the basis for the creation of full-scale closed ecosystems with humans. Future closed ecosystems should include both biological and physico-chemical methods of waste oxidation for their subsequent inclusion in cycling processes [4–17]. To ensure the effective operation of the physical and chemical processes of oxidation of organic and inorganic waste in CES, it is extremely important to create and sustainably operate a set of necessary instruments and equipment. An integral part of such equipment is an installation for the purification of liquid products of human waste processing (feces, urine), since the process of waste oxidation produces pollutants that inhibit plant growth. The Institute of Biophysics of the SB RAS is conducting research on the creation of such cleaning methods in relation to closed ecosystems. In particular, software is being developed to automate cleaning processes [17; 18].

The purpose of this work is biotesting of solutions obtained after purification and the development of a digital automated control system for the installation of physical and chemical purification of mineralized human exometabolites.

Methods and approaches

Long-term daily direct application of mineralized exometabolites into the irrigation solution will cause its salinity due to the high NaCl content in human urine [19; 20]. In addition, the “wet” combustion method is practically unable to utilize urea, which increases the risk of the development of opportunistic urobacteria in the system [21] and reduces the availability of nitrogen for the plant CES link. Therefore, the complex of physical and chemical processing of organic waste includes, in addition to “wet” combustion, several more sequential processes for purifying solutions of mineralized exometabolites, for each of which a reactor has been developed [18]: 1) decomposition of urea; 2) release of Cl_2 ; 3) synthesis of HCl; 4) release of alkali; 5) release of Na_2CO_3 ; 6) synthesis of NaCl. Together, these 6 reactors are a plant for the purification of liquid products of physical and chemical processing of human waste products.

To assess the influence of liquid products of the physicochemical oxidation of human exometabolites on plants, we used previously developed methodological approaches for preparing nutrient solutions on this basis for their subsequent use in an experimental model of a closed ecosystem, subject to regular (once every 7 days) replacement of 1/8 of the nutrient solution with water. That is, in 8 weeks there was a complete change of solution [22].

Studying the influence of possible pollutants in a nutrient solution required testing the possibility of long-term use of permanent solutions prepared on the basis of liquid products of the mineralization of human exometabolites for growing plants. The object of research was the “Moscow Greenhouse” variety lettuce. Plants in an experimental model of a closed ecosystem were grown using hydroponics on expanded clay. The technology and growing conditions are similar to those described earlier. [22; 23]. The duration of cultivation from germination to technical maturity is 21 days. In the experimental version, the solution was prepared based on liquid mineralization products. Control options – standard Knop solution: control 1 – permanent solution with correction, control 2 – every 7 days the solution was changed to a freshly prepared one. During plant growth, correction of permanent irrigation solutions was carried out with initial solutions based on the content of available forms of nitrogen.

When creating an automated control system and software for a treatment plant, a uniform approach is desirable, thanks to which the same type of process parameters and reactor programming menus will be displayed in the same way, and the same type of automatic control algorithm for all reactors will be used. This is important, since the reactors are different, and it is more convenient for the operator to control and configure them with a uniform interface display. In addition, the automation system and software being developed should be easily adaptable to connecting possible new reactors to the structure of the treatment plant. Following this logic, the automation and software must be adaptable to connecting the “wet” combustion reactor and other reactors of the physicochemical waste mineralization subsystem [17]. This seems possible, since the program interaction scheme that meets the specified requirements for the automation and software of the treatment plant is the same for the “wet” combustion reactor (Fig. 1).

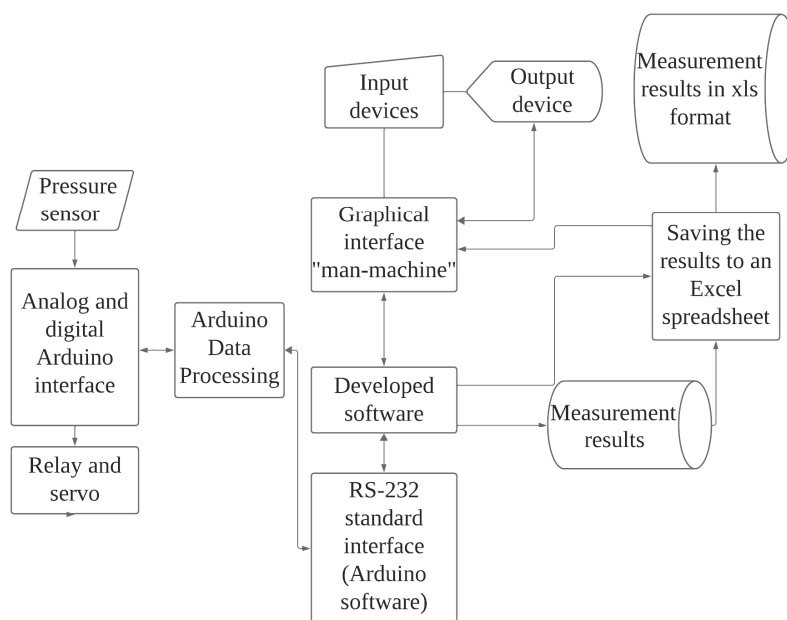


Рис. 1. Схема взаимодействия программ

Fig. 1. Scheme of program interaction

In order to ensure interaction with peripheral devices, including sensors, relays, servos and others, it was decided to use the Arduino platform due to its ease of programming, wide support for hardware

modules and sensors. The Arduino IDE development environment is chosen for Arduino programming. For software development, with a focus on creating a convenient interface for the end user, an additional development environment was added – Visual Studio using a programming language C#.

Methods and approaches

A study of the influence of pollutants in a nutrient solution showed that the biomass of lettuce plants grown in non-replaceable solutions of the experimental and control variants did not differ significantly, just as there were no significant differences from the biomass of plants grown in control solutions that were regularly replaced (see table).

Dry weight (g) per plant of lettuce variety “Moscow Greenhouse”, grown on solutions prepared on the basis of liquid products mineralization of human exometabolites

Тип питательного раствора	Общая биомасса	Биомасса листьев
Несменяемый раствор экзометаболитов	3.3±0.4	2.9±0.3
Несменяемый раствор Кнопа (контроль 1)	2.8±0.5	2.4±0.5
Сменяемый раствор Кнопа (контроль 2)	2.7±0.9	2.1±0.4

Type of nutrient solution	Total biomass	Leaf biomass
Permanent solution of exometabolites	3.3±0.4	2.9±0.3
Non-replaceable Knop solution (control 1)	2.8±0.5	2.4±0.5
Replaceable Knop solution (control 2)	2.7±0.9	2.1±0.4

Thus, the fundamental possibility of long-term use of nutrient solutions prepared on the basis of liquid products of the mineralization of human exometabolites for growing plants of the phototrophic link of a closed ecosystem has been experimentally demonstrated.

Based on the analysis of the processes of the physico-chemical unit for processing human waste, the automatic reactor control algorithm was taken as the basis for logical control [18, Fig. 2, B)], the logic of which is to maintain the parameters of the technological process conditions in the specified ranges and stop the process when the target parameter reaches the specified value. The work [18] does not disclose the operating principle of the unit for adjusting the conditions parameters, which is a problematic point when trying to create a unified structure of the automatic control algorithm for the treatment plant. This is due to the fact that the processes in the reactors of the installation are varied: they occur in the liquid and gaseous phase, have one or several stages, and may require partial operator intervention. Therefore, maintaining certain condition parameter values ultimately requires different hardware and logic solutions. As a result, despite the possibility of uniformly displaying the parameters of technological processes, the software settings for the operation of different reactors and control algorithms will differ from each other.

The need for an individual approach to settings for each reactor of a treatment plant indicates the possibility of using common software for all reactors of the physico-chemical mineralization subsystem of waste [17], including a “wet” combustion reactor, the operating algorithm of which differs from the operating algorithm of the treatment plant (Fig. 2)

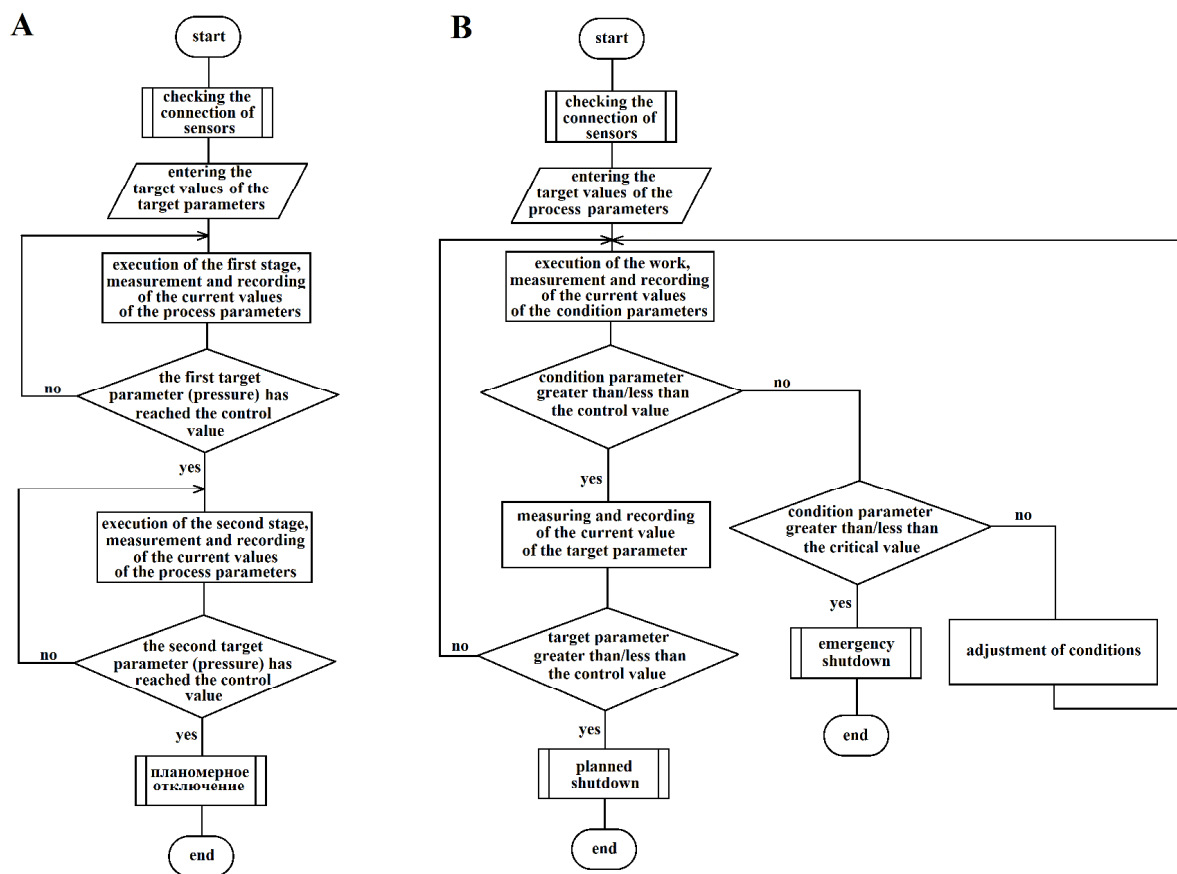


Рис. 2. Алгоритмы работы реакторов:

А – без контроля параметров условий процесса; Б – с контролем параметров условий процесса

Fig. 2. Reactor operation algorithms:

A – without control of the parameters of the process conditions; Б – with control of the parameters of the process conditions

As a result, software was developed in which, for user convenience, the operator’s workspace is divided into tabs, where each tab has its own reactor (Fig. 3). Each tab has fields for displaying indicators in text format, buttons for reactor control, fields for plotting graphs based on measurement results, as well as operating time and current date.

By pressing the “Start” button, a signal is sent to the connection port, then the Arduino begins to transmit readings of the running process. The data is displayed in the appropriate fields, and based on this data, the construction of the graphs presented in Fig. 3, where each tab corresponds to a reactor/process of physical and chemical processing of human waste products. Four-color tab marking is proposed to indicate the state of processes:

- state 1 – the process is not running, not the current tab;
- state 2 – process not running, current tab;
- state 3 – the process is running, not the current tab;
- state 4 – process running, current tab.

Reactor operation settings allow you to enter parameter values for each purification process to automatically maintain and adjust the conditions for its occurrence.

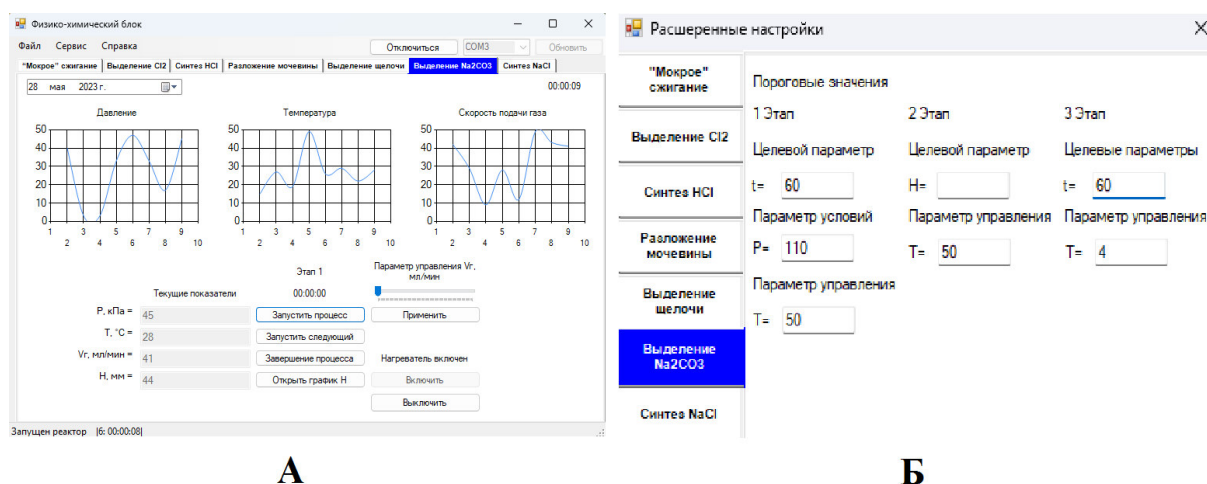


Рис. 3. Окно ПО во время работы:

А – отображение параметров текущего процесса (выделение Na_2CO_3);
 Б – отображение настроек реактора выделения Na_2CO_3

Fig. 3. The software window during operation:

A – displaying the parameters of the current process (Na_2CO_3 extraction);
 Б – displaying the settings of the Na_2CO_3 extraction reactor

When the process is started, in addition to outputting data in the current time, the data is written to a text document. All measurement results are saved in separate folders in the software directory. The file names contain the exact launch date. And the documents themselves describe the number of the launched reactor and the results of measurements over time.

Conclusion

Peripheral equipment for organizing an automatic control system was selected, problems were identified and approaches were developed to automate these processes and create software for human interaction with the proposed installation. Experiments on growing lettuce plants were carried out, confirming the effectiveness of the proposed purification processes for liquid products of the processing of human exometabolites. Thus, the created complex purification installation, equipped with the proposed software, can be used for scientific research in relation to CES topics, including space applications.

Благодарности Работы по созданию и апробации установки по очистке от поллютантов газовой среды были выполнены в рамках государственного задания Министерства науки и высшего образования РФ (проект № 121101300066-7).

Acknowledgements The study was funded by State Assignment of the Ministry of Science and Higher Education of the Russian Federation (project No. 121101300066-7).

Библиографические ссылки

1. Gitelson J. I., Lisovsky G. M., MacElroy R. D. Manmade Closed Ecological Systems. New York: Taylor and Francis, 2003. 402 p.
2. Wheeler R. M. Agriculture for space: People and places paving the way // Open agriculture, 2017. Vol. 2 (1). P. 14–32.
3. Assessment of the possibility of establishing material cycling in an experimental model of the bio-technical life support system with plant and human wastes included in mass exchange /

- A. A. Tikhomirov, S. A. Ushakova, V. V. Velichko et al. // *J. Acta Astronaut.* 2011. Vol. 68. P. 1548–1554.
4. Waste bioregeneration in life support CES: development of soil organic substrate / N. S. Manukovsky, V. S. Kovalev, V. Ye., Rygalov, I. G. Zolotukhin // *Advances In Space Research.* 1997. Vol. 10. P. 1827–1832.
 5. Wenting H., Yidong X., Hong L. A technique for preparing soil-like substrate for bioregenerative life support system // *17th IAA Humans in Space Symposium.* Moscow, 2009. P. 53.
 6. Пат. 2111939 Российская Федерация, МПК С 05 F 3/08. Способ утилизации отходов жизнедеятельности человека и несъедобной биомассы растений, приводящий к получению из них удобрений / Куденко Ю. А., Павленко Р. А. № 96114242/13 ; заявл. 10.07.96 ; опубл. 27.05.98, Бюл. № 15. 4 с.
 7. Nelson M., Dempster W. F., Allen J. P. Integration of lessons from recent research for “Earth to Mars” life support systems // *Advances in Space Research.* 2008. Vol. 41. P. 675–683.
 8. Canadian advanced life support capacities and future directions / M. Bamsey, T. Graham, M. Stasiak et al. // *Advances in Space Research,* 2009. Vol. 44. P. 151–161.
 9. Drysdale A. E., Ewert M. K., Hanford A. J. Life support approaches for Mars missions // *Advances in Space Research.* 2003. Vol. 31 (1). P. 51–61.
 10. Farges B., Poughon L., Creuly C., Cornet J.-F., Dussap C.-G., Lasseur C. Dynamic Aspects and Controllability of the MELiSSA Project: A Bioregenerative System to Provide Life Support in Space // *Applied Biochemistry and Biotechnology.* 2008. Vol. 151. P. 686–699.
 11. Progress and prospect of research on controlled ecological life support technique / S. S. Guo, R. X. Mao, L. L. Zhang et al. // *Reach,* 2017. Vol. 6. P. 1–10.
 12. Walker J., Granjou C. MELiSSA the minimal biosphere: Human life, waste and refuge in deep space // *Futures.* 2017. Vol. 92. P. 59–69.
 13. Escobar C., Nabity J. Past, present, and future of closed human life support ecosystems – a review // *47th International Conference on Environmental Systems.* Charleston, 2017. P. 18.
 14. Putnam D. F. Composition and Concentrative Properties of Human Urine. NASA contract report. Washington, 1971. 107 p.
 15. Kudenko Yu. A., Gribovskaya I. A., Zolotukhin I. G. Physical-chemical treatment of wastes: A way to close turnover of elements in LSS // *Acta Astronautica,* 2000. Vol. 46. P. 585–589.
 16. Kudenko Yu. A., Gribovskaya I. A., Pavlenko R. A. Mineralization of wastes of human vital activity and plants to be used in a life support system // *Acta Astronautica.* 1997. Vol. 41. P. 193–196.
 17. Подсистема физико-химических реакторов минерализации отходов для биолого-технических систем жизнеобеспечения космического назначения / Е. А. Морозов, С. В. Трифонов, Салтыков М. Ю. и др. // *Сибирский журнал науки и технологии.* 2017. Т. 18, № 3. С. 585–591.
 18. Разработка принципов управления блоком обессоливания для замкнутых систем жизнеобеспечения космического назначения / А. А. Тихомиров, С. В. Трифонов, Е. А. Морозов, А. В. Мурыгин // *Сибирский аэрокосмический журнал.* 2022. Т. 23, № 3. С. 551–560.
 19. Effect of NaCl concentration on productivity and mineral composition of *Salicornia europaea* as a potential crop for utilization NaCl in LSS / S. A. Ushakova, N. P. Kovaleva, I. V. Gribovskaya et al. // *Adv. Space Res.* 2005. Vol. 36. (7). P. 1349–1353.
 20. Effect of NaCl concentration on productivity and mineral composition of *Salicornia europaea* as a potential crop for utilization NaCl in LSS / S. A. Ushakova, N. P. Kovaleva, I. V. Gribovskaya et al. // *Advances in Space Research.* 2005. Vol. 36. P. 1349–1353.
 21. Mobley H., Mendz G., Hazell S. *Helicobacter pylori: Physiology and Genetics.* ASM Press, 2001. 626 p.
 22. A biological method of including mineralized human liquid and solid wastes into the mass exchange of bio-technical life support systems / S. A. Ushakova, A. A. Tikhomirov, N. A. Tikho-

mirova et al. // *Advances In Space Research*. 2012. Vol. 50, No. 7. P. 932–940. DOI: 10.1016/j.asr.2012.05.023.

23. Автоматическая система контроля концентраций O_2 и H_2 в технологических газовых контурах биотехнических систем жизнеобеспечения космического назначения / Е. А. Морозов, Трифонов С. В., Мурыгин А. В. и др. // *Сибирский журнал науки и технологии*. 2018. Т. 19, № 4. С. 691–697.

References

1. Gitelson J. I., Lisovsky G. M., MacElroy R. D. *Manmade Closed Ecological Systems*. New York, Taylor and Francis, 2003, 402 p.

2. Wheeler R. M. Agriculture for space: People and places paving the way. *Open agriculture*. 2017, Vol. 2 (1), P. 14–32.

3. Tikhomirov A. A., Ushakova S. A., Velichko V. V., Tikhomirova N. A., Kudenko Yu. A., Gribovskaya I. V., Gros J.-B., Lasseur Ch. Assessment of the possibility of establishing material cycling in an experimental model of the bio-technical life support system with plant and human wastes included in mass exchange. *J. Acta Astronaut*. 2011, Vol. 68, P. 1548–1554.

4. Manukovsky N. S., Kovalev V. S., Rygalov V. Ye., Zolotukhin I. G. Waste bioregeneration in life support CES: development of soil organic substrate. *Advances In Space Research*. 1997, Vol. 10, P. 1827–1832.

5. Wenting H., Yidong X., Hong L. A technique for preparing soil-like substrate for bioregenerative life support system. *17th IAA Humans in Space Symposium*. Moscow, 2009, P. 53.

6. Kudenko Yu. A., Pavlenko R. A. *Sposob utilizatsii otkhodov zhiznedeyatel'nosti cheloveka i nesjedobnoy biomassy rasteniy, privodyashhiy k polucheniyu iz nih udobreniy* [Way of utilization of human wastes and inedible plant biomass, gaining hydroponic fertilizer]. Patent RF, no. 2111939, 1998.

7. Nelson M., Dempster W. F., Allen J. P. Integration of lessons from recent research for Earth to Mars life support systems. *Advances in Space Research*. 2008, Vol. 41, P. 675–683.

8. Bamsey M., Graham T., Stasiak M. et al. Canadian advanced life support capacities and future directions. *Advances in Space Research*. 2009, Vol. 44, P. 151–161.

9. Drysdale A. E., Ewert M. K., Hanford A. J. Life support approaches for Mars missions. *Advances in Space Research*. 2003, Vol. 31, P. 51–61.

10. Farges B., Poughon L., Creuly C. et al. Dynamic Aspects and Controllability of the MELiSSA Project: A Bioregenerative System to Provide Life Support in Space. *Applied Biochemistry and Biotechnology*. 2008, Vol. 151, P. 686–699.

11. Guo S. S., Mao R. X., Zhang L. L. et al. Progress and prospect of research on controlled ecological life support technique. *Reach*. 2017, Vol. 6, P. 1–10.

12. Walker J., Granjou C. MELiSSA the minimal biosphere: Human life, waste and refuge in deep space. *Futures*. 2017, Vol. 92, P. 59–69.

13. Escobar C., Nabity J. Past, present, and future of closed human life support ecosystems – a review. *47th International Conference on Environmental Systems*. Charleston, 2017, P. 18.

14. Putnam D. F. *Composition and Concentrative Properties of Human Urine*. NASA contract report. Washington, 1971, 107 p.

15. Kudenko Yu. A., Gribovskaya I. A., Zolotukhin I. G. Physical-chemical treatment of wastes: A way to close turnover of elements in LSS. *Acta Astronautica*. 2000, Vol. 46, P. 585–589.

16. Kudenko Yu. A., Gribovskaya I. A., Pavlenko R. A. Mineralization of wastes of human vital activity and plants to be used in a life support system. *Acta Astronautica*. 1997, Vol. 41, P. 193–196.

17. Morozov Ye. A., Trifonov S. V., Saltykov M. Yu. et al. [Physico-chemical waste mineralization reactors subsystem for closed bio technical life support systems for space application]. *Siberian Journal of Science and Technology*. 2017, No. 3, P. 585–591 (In Russ.).

18. Tikhomirov A. A., Trifonov S. V., Morozov Ye. A., Murygin A. V. [Development of control principles for the desalination unit for closed life support systems for space purposes]. *Siberian Aerospace Journal*. 2022, Vol. 23, No. 3, P. 551–560 (In Russ.).
19. Ushakova S. A., Kovaleva N. P., Gribovskaya I. V. et al. Effect of NaCl concentration on productivity and mineral composition of *Salicornia europaea* as a potential crop for utilization NaCl in LSS. *Adv. Space Res.* 2005, Vol. 36 (7), P. 1349–1353.
20. Ushakova S. A., Kovaleva N. P., Gribovskaya I. V., Dolgushev V. A., Tikhomirova N. A. Effect of NaCl concentration on productivity and mineral composition of *Salicornia europaea* as a potential crop for utilization NaCl in LSS. *Advances in Space Research*. 2005, Vol. 36, P. 1349–1353.
21. Mobley H., Mendz G., Hazell S. *Helicobacter pylori: Physiology and Genetics*. ASM Press, 2001, 626 p.
22. Ushakova S. A., Tikhomirov A. A., Tikhomirova N. A. et al. A biological method of including mineralized human liquid and solid wastes into the mass exchange of bio-technical life support systems *Advances In Space Research*. 2012, Vol. 50, No. 7, P. 932–940. DOI: 10.1016/j.asr.2012.05.023.
23. Morozov Ye. A., Trifonov S. V., Murygin A. V., Tikhomirov A. A. [Automatic Control System of O₂ and H₂ Concentrations in Technological Gas Circuits of BTLSS Space Application]. *Siberian Journal of Science and Technology*. 2018, Vol. 19, No. 4, P. 691–697 (In Russ.).

© Trifonov S. V., Tikhomirov A. A., Murygin A. V., 2023

Тихомиров Александр Аполлинариевич – доктор биологических наук, профессор, заведующий лабораторией управления биосинтезом фототрофов, Институт биофизики Сибирского отделения Российской академии наук; заведующий кафедрой замкнутых экосистем, Сибирский государственный университет науки и технологий имени академика М. Ф. Решетнева. E-mail: alex-tikhomirov@yandex.ru.

Трифонов Сергей Викторович – кандидат биологических наук, заведующий лабораторией проблем создания круговоротных процессов искусственных экосистем, Институт биофизики Сибирского отделения Российской Академии наук; доцент кафедры замкнутых экосистем, Сибирский государственный университет науки и технологий имени академика М. Ф. Решетнева. E-mail: trifonov_sergei@inbox.ru.

Мурыгин Александр Владимирович – доктор технических наук, профессор, заведующий кафедрой информационно-управляющих систем; Сибирский государственный университет науки и технологий имени академика М. Ф. Решетнева. E-mail: avm514@mail.ru.

Tikhomirov Alexander Apollinariievich – Dr. Sc., professor, Head of laboratory of Phototrophic Biosynthesis Control, Institute of Biophysics Siberian Branch of Russian Academy of Sciences; Head of chair of Closed EcoSystems, Reshetnev Siberian State University of Science and Technology. E-mail: alex-tikhomirov@yandex.ru.

Trifonov Sergei Viktorovich – Ph. D., head of Laboratory for Problems of Establishing Cycling Processes of Artificial Ecosystems, Institute of Biophysics Siberian Branch of Russian Academy of Sciences; Associate Professor, Department of Closed Ecosystems, Reshetnev Siberian State University of Science and Technology. E-mail: trifonov_sergei@inbox.ru.

Murygin Alexander Vladimirovich – Dr. Sc., professor, Head of chair of Information and Management Systems; Reshetnev Siberian State University of Science and Technology. E-mail: avm514@mail.ru.

УДК 621.9.048

Doi: 10.31772/2712-8970-2023-24-4-760-767

Для цитирования: Удельные энергозатраты электро-контактно-химической обработки металлов вибрирующим инструментом в электролите / И. Я. Шестаков, В. И. Шестаков, И. В. Трифанов, И. А. Ремизов // Сибирский аэрокосмический журнал. 2023. Т. 24, № 4. С. 760–767. Doi: 10.31772/2712-8970-2023-24-4-760-767.

For citation: Shestakov I. Ya., Shestakov V. I., Trifanov I. V., Remizov I. A. [Specific energy consumption of electro-contact-chemical treatment of metals with a vibrating tool in the electrolyte]. *Siberian Aerospace Journal*. 2023, Vol. 24, No. 4, P. 760–767. Doi: 10.31772/2712-8970-2023-24-4-760-767.

Удельные энергозатраты электро-контактно-химической обработки металлов вибрирующим инструментом в электролите

И. Я. Шестаков^{1*}, В. И. Шестаков¹, И. В. Трифанов¹, И. А. Ремизов²

¹Сибирский государственный университет науки и технологий имени академика М. Ф. Решетнева
Российская Федерация, 660037, г. Красноярск, просп. им. газ. «Красноярский Рабочий», 31

²Сибирский федеральный университет
Российская Федерация, 660041, г. Красноярск, просп. Свободный, 79,

*E-mail: yakovlevish@mail.ru

По удельному расходу энергии процессы формообразования располагаются в трёх энергетических уровнях. Электрофизические и электрохимические методы обработки металлов находятся на третьем уровне, где удельные энергозатраты составляют более $6 \cdot 10^4$ Дж/см³. Анализ литературных данных показал противоречивость удельных затрат некоторых авторов. Удельные энергозатраты электроконтактной обработки никак не могут быть соизмеримы с затратами при электрохимической обработке из-за разных размеров удаляемых частиц с поверхности обрабатываемой детали. Литературные данные по удельным энергозатратам электро-контактно-химической обработки металлов вибрирующим инструментом в электролите отсутствуют, поэтому проведены эксперименты с фиксацией осциллограмм тока, напряжения и межэлектродного зазора. Приведена методика расчёта удельных энергозатрат по осциллограммам процесса. Рассчитаны затраты энергии на вибрацию электрода-инструмента, которые на порядок меньше на электро-контактно-химическую обработку. При уменьшении амплитуды вибрации или увеличении напряжения на электродах процесс в межэлектродном зазоре переходит в размерную обработку дугой. При электро-контактно-химической обработке металлов вибрирующим инструментом в воде удельные энергозатраты равны $(3,5-3,8) \cdot 10^5$ Дж/см³, что соответствует электроконтактной обработке. Предполагается, что использование водных растворов нейтральных солей приведёт к снижению затрат энергии.

Ключевые слова: удельные энергозатраты, электро-контактно-химическая обработка, вибрация, амплитуда, частота, осциллограмма, расчёт.

Specific energy consumption of electro-contact-chemical treatment of metals with a vibrating tool in the electrolyte

I. Ya. Shestakov^{1*}, V. I. Shestakov¹, I. V. Trifanov¹, I. A. Remizov²

¹Reshetnev Siberian State University of Science and Technology
31, Krasnoyarskii Rabochii prospekt, Krasnoyarsk, 660037, Russian Federation

²Siberian Federal University
79, Svobodnyi Av., Krasnoyarsk, 660041, Russian Federation

*E-mail: yakovlevish@mail.ru

According to the specific energy consumption, the shaping processes are arranged in three energy levels. Electrophysical and electrochemical methods of metal processing are at the third level, where the specific energy consumption is more than $6 \cdot 10^4 \text{ J/cm}^3$. The analysis of the literature data showed the inconsistency of the specific costs of some authors. The specific energy consumption of electrical contact processing cannot be commensurate with the costs of electrochemical processing due to the different sizes of the particles removed from the surface of the workpiece. There are no literature data on the specific energy consumption of electro-contact-chemical treatment of metals with a vibrating instrument in the electrolyte, therefore, experiments have been carried out with the fixation of current, voltage and interelectrode gap oscillograms. The method of calculation of specific energy consumption according to the oscillograms of the process is given. The energy costs for vibration of the electrode-tool are calculated, which are an order of magnitude less for electro-contact-chemical treatment. When the vibration amplitude decreases or the voltage on the electrodes increases, the process in the interelectrode gap turns into dimensional arc processing. When electro-contact-chemical treatment of metals with a vibrating tool in water, the specific energy consumption is equal to $(3.5\text{--}3.8) \cdot 10^5 \text{ J/cm}^3$, which corresponds to electrocontact treatment. It is assumed that the use of aqueous solutions of neutral salts will lead to a reduction in energy costs.

Keywords: specific energy consumption, electro-contact-chemical treatment, vibration, amplitude, frequency, oscillogram, calculation.

Introduction

Specific energy consumption is one of the important indicators affecting the economic efficiency of the molding process. Specific energy consumption is defined in kWh/kg, J/cm^3 . In [1; 2] it is recommended to determine the properties of metals per unit volume when revealing the regularities of metal behavior under various physical processes.

According to this characteristic, all the forming processes are arranged in three energy levels. The first level includes the processes that require a minimum of energy to break the bonding forces between only a part of atoms or molecules of the body. This level extends up to the melting energy of metals (Table 1), i.e., approximately up to 10^4 J/cm^3 [3].

The second level includes processes that require energy inputs to break the bonds between all atoms and molecules of the body. Casting is a characteristic process for this condition. It is not clear why reaming and grinding are located in this level, because there is no breaking of bonds between all atoms and molecules. Metal removal occurs in the form of chips [4]. The second energy level is located between the melting energy of 10^4 J/cm^3 and the vaporization energy of metals $6 \cdot 10^4 \text{ J/cm}^3$.

Table 1

Energy levels of shaping processes

Energy level	Shaping method	Specific energy consumption, J/cm^3
I	Cold deformation	$1 \cdot 10^1\text{--}4 \cdot 10^1$
	Stamping	$2 \cdot 10^1\text{--}6.5 \cdot 10^1$
	Cold extrusion	$5.5 \cdot 10^2\text{--}8.5 \cdot 10^2$
	Turning	$1.7 \cdot 10^3\text{--}2.5 \cdot 10^3$
	Broaching	$2.5 \cdot 10^3\text{--}3.7 \cdot 10^3$
	Milling	$5 \cdot 10^3\text{--}7.5 \cdot 10^3$
II	Hot deformation	$9 \cdot 10^3\text{--}3.4 \cdot 10^4$
	Casting	$1.4 \cdot 10^4\text{--}2.5 \cdot 10^4$
	Reaming	$1.2 \cdot 10^4\text{--}3 \cdot 10^4$
	Grinding	$5.5 \cdot 10^4\text{--}7 \cdot 10^4$

Energy level	Shaping method	Specific energy consumption, J/cm ³
III	Dimensional electrochemical treatment	4.25·10 ⁵ –4.35·10 ⁵
	Treatment:	
	anodic mechanical	1.7·10 ⁵ –5.2·10 ⁵
	electrocontact	2.3·10 ⁵ –4.6·10 ⁵
	electropulse	3.5·10 ⁵ –7.1·10 ⁵
	electrospark	1.1·10 ⁶ –2.9·10 ⁶
	ultrasonic	6·10 ⁵ –3.6·10 ⁶
	light-beam	2.8·10 ⁷ –4.7·10 ⁷

In the third energy level there are processes, which require energy for complete destruction of bonding forces between all atoms or molecules of the body. Characteristic for this level are dimensional electrochemical treatment, electrospark and electro-pulse treatments, treatment with electron and light beams. This level is located above the vaporization energy of metals, i.e. above 6·10⁴ J/cm³.

As the hardness and strength of materials increase, energy consumption increases (Fig. 1) [4] and treatment productivity decreases. Modern metals and alloys have a tensile strength of more than 200 MPa, so high energy consumption of electro-treatment is quite justified, as other shaping methods become uncompetitive in terms of productivity.

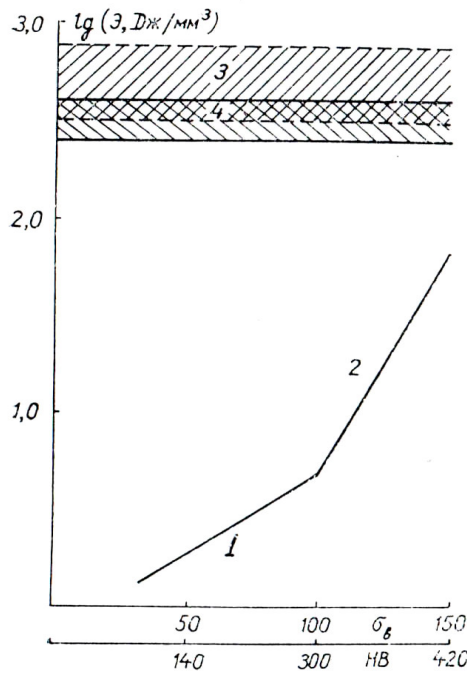


Рис. 1. Энергоёмкость некоторых видов обработки:
 1 – обработка лезвийным инструментом; 2 – шлифование;
 3 – электроимпульсная; 4 – ЭХО

Fig. 1. Energy intensity of some types of processing
 1 – blade tool processing; 2 – grinding; 3 – electric pulse; 4 – electrochemical treatment

Analysis

The data given in [4-6] and Tables 1-3 do not agree with the values of specific energy consumption during electrochemical processing presented by the authors [7; 8] (Table 4). According to these authors,

the costs at electrochemical treatment are 9–40 times higher than at electrocontact treatment. Tables 1 and 2 show that the specific energy consumption of electrocontact and electrochemical treatments are commensurable, which does not correspond to reality because the removal of metal from the treated surface occurs with different particle sizes, in the first case in the form of molten metal droplets, in the second case in the form of metal ions.

Detailed indicators of varieties of electrophysical treatment methods are given in the reference book [6] Table 3.

Table 2

Specific energy consumption of electric methods of treatment

№	Treatment	Specific energy consumption, J/cm ³
1	Electrospark	11–29
2	Electropulse	3.5–7.1
3	Electrochemical	4–6
4	Electrocontact	2.3–4.6

Table 3

Main properties of electrophysical methods of metal processing

Treatment method	Average specific productivity, cm ³ /s	Average specific energy consumption, J/cm ³
Electrospark: rough finishing precision	9.3 · 10 ⁻³ –1 · 10 ⁻² 8 · 10 ⁻⁴ –1.6 · 10 ⁻³ 1.7 · 10 ⁻⁶ –1.7 · 10 ⁻⁵	(4.3–7.2) · 10 ⁵ (1.4–2.0) · 10 ⁶ (2.0–2.5) · 10 ⁶
Electroimpulse: rough finishing	1.7 · 10 ⁻² –1.8 · 10 ⁻¹ 8 · 10 ⁻⁴ –8 · 10 ⁻³	(3.5–7.1) · 10 ⁵ (2.6–5.8) · 10 ⁵
Electrocontact: cutting turning skinning piercing	1.6 · 10 ⁻² –1.3 · 10 ⁻¹ 1.6 · 10 ⁻² –6.5 · 10 ⁻¹ 15–17 8.3 · 10 ⁻³ –2.5 · 10 ⁻²	(0.3–1.2) · 10 ⁵ (1.2–1.4) · 10 ⁵ (2.3–4.6) · 10 ⁵ (0.12–5.8) · 10 ⁴

In Table 3, the specific energy consumption for electrical contact piercing of holes is questionable, which is an order of magnitude lower than for other types of this processing. The removal of erosion products from the holes is difficult during electrocontact piercing, so additional energy consumption is required.

Table 4

Specific energy consumption of certain electrochemical methods of treatment

№ п/п	Treatment	Specific energy consumption, J/cm ³ *10 ⁵
1	Electrochemical	2.52–5.61[5]; 5.61–11.2[6]
2	Electrical discharge	1.68–3.36
3	Electrocontact	0.28–0.56

More data on electrochemical treatment specific energy consumption in kWh/kg are available in the reference book [9]. Taking into consideration the density of metals the calculation of energy consumption per volume item of material being processed was fulfilled. Table 5 shows the results of this calculation for some metals.

Table 5

Specific energy consumption of electrochemical dimensional treatment of metals in aqueous solutions of neutral salts, $J/cm^3 \cdot 10^5$

Metal	25%NaCl	30%NaNO ₃	15%Na ₂ SO ₄
Steel U10	1.96	6.44	70.84
Steel 35HGS	3.28	3.84	28.03
Steel 4H5V2FS	3.12	4.37	34
Aluminium	1.55	1.94	65.5
Nickel	2.14	22.3	39.2
Titanium alloy BT8	3.49	5.33	258

Table 5 shows that the lowest specific energy consumption is characteristic of electrochemical treatment in aqueous sodium chloride solution. This is explained by the presence of activating chlorine anion in the electrolyte which favours the formation of intermediate complex compounds [10]. During electrochemical treatment in aqueous sodium sulphate specific energy consumption increases by 10-15 times the reason for which is passivation of the anode [11]. This phenomenon is especially characteristic of titanium alloy BT8 since titanium is an active metal, its standard electrode potential is 1.2 V [12] and its surface always has an oxide film.

Methodology

Experimental studies were carried out on an electro-treatment unit with a linear electrodynamic motor described in the scientific journal [13]. To fix the electrode tool a fixture was made to ensure the flow of water (weak electrolyte) through the interelectrode gap. The methodology of experimental studies is described in [14]. The treated metal is HVG steel. However this paper doesn't provide a methodology for calculating the specific energy consumption of electro-contact-chemical treatment of metals in the electrolyte based on oscillograms of the process.

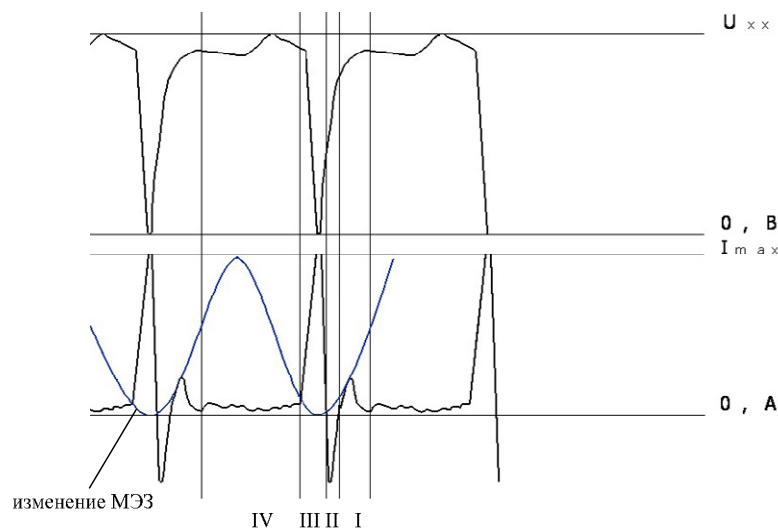


Рис. 2. Осциллограмма напряжения и тока ЭКХО

Fig. 2. Oscillogram of the voltage and current of the electro-contact-chemical treatment

Calculation of specific energy consumption based on the oscillogram. Typical oscillogram of current, voltage and interelectrode gap during electro-contact chemical treatment with vibrating electrode-tool in water is shown in Fig. 9. The data were obtained at an average electrode voltage of 16.7 V and a tool oscillation amplitude of 0.75 mm. At the oscillation amplitude of 0.25 mm and the average velocity of water flow in the interelectrode gap of 1 m/s and less, the current and voltage oscillogram characteristic of dimensional arc machining is observed [15; 16].

The oscillogram is divided into sections I, II, III, IV. Section I is the pre-breakdown period - the time of streamer formation - the discharge channel. Section II - breakdown of the interelectrode gap, III - contact of electrodes, IV - period when the current is caused by anodic dissolution of the treated metal (electrochemical treatment). The square of each triangle is determined, thus the amount of electricity passed in each period (sections I - IV) will be known. Next, the average voltage value at each section is determined from the oscillogram data.

For section I we have

$$q_I = \frac{1}{2} h_I a_I M_I M_\tau,$$

Where h_I is the height of the triangle of section I; a_I is the length of the base of the triangle of section I; M_I is the current scale, $M_I = 2.5$ A/mm; M_τ is the time scale, $M_\tau = 0.48$ ms/mm.

After calculating the amount of electricity for all sections we get

$$q_I = 56,25 \cdot 10^{-3} \text{ Кл}; \quad q_{II} = 76,6 \cdot 10^{-3} \text{ Кл};$$

$$q_{III} = 600 \cdot 10^{-3} \text{ Кл}; \quad q_{IV} = 162 \cdot 10^{-3} \text{ Кл}.$$

Average voltage at the sections is

$$U_I = 24,3 \text{ В}; \quad U_{II} = 17,5 \text{ В}; \quad U_{III} = 11,3 \text{ В}; \quad U_{IV} = 25,7 \text{ В}.$$

Pulse energy at the sections is

$$Q_I = 1,351 \text{ Дж}; \quad Q_{II} = 1,348 \text{ Дж}; \quad Q_{III} = 6,78 \text{ Дж}; \quad Q_{IV} = 4,155 \text{ Дж}.$$

Taking into account the frequency of oscillation of the electrode-tool (50 Hz), processing time and the volume of removed metal, the specific energy consumption is determined as follows

$$W = [(Q_1 + Q_2 + Q_3 + Q_4) * f * t] / V,$$

where f is the oscillation frequency, s^{-1} ; t is the treatment time, s; V is the volume of removed metal, cm^3 .

Specific energy consumption is $W = (3.5-3.8) \cdot 10^5 \text{ J/cm}^3$.

In addition to the electrical energy consumed for the electro-machining process, it is necessary to take into account the energy consumption for the vibration of the electrode-tool. This energy is determined by the well-known formula

$$W_B = m * f^2 * A^2,$$

where m is the mass of the electrode-tool with the device for its fixing, kg; A is the amplitude of vibration of the electrode-tool, m. After substituting the data into the above formula it turns out that the energy consumption for the vibration of the tool electrode is an order of magnitude less than for the processes of electro-contact-chemical treatment.

Conclusion

Specific energy consumption is an important indicator when selecting a method of treatment of metals and alloys. For materials difficult to be machined by mechanical methods, the alternative is the methods of electrical treatment. The analysis of literature data has shown that indicators on specific energy consumption are contradictory, and for the combined electro-contact-chemical method of processing by vibrating electrode in water this characteristic is practically absent. Calculation by oscillograms of the process shows that specific energy consumption of electro-contact-chemical treatment by vibrating electrode in water corresponds to electro discharge treatment and electrochemical treatment in aqueous solution of sodium chloride or sodium nitrate. At electro-contact-chemical treatment in aqueous solution of the above mentioned salts it is necessary to expect decrease of specific energy

consumption as energy losses on heating of electrolyte decrease due to decrease of its electrical resistance, and chlorine and nitrate ions reduce activation energy of the treated metal.

Библиографические ссылки

1. Верхотуров А. Д., Шпилёв А. М., Евстигнеев А. И. Основы материаловедения : монография. Т. 1. Владивосток : Дальнаука, 2012. 270 с.
2. Николенко С. В., Верхотуров А. Д. Новые электродные материалы для электроискрового легирования. Владивосток : Дальнаука, 2005. 219 с.
3. Смоленцев Е. В. Проектирование электрических и комбинированных методов обработки. М. : Машиностроение, 2005. 511 с.
4. Зубарев Ю., Приемышев А. Теория и практика повышения эффективности шлифования материалов. М. : Лань, 2010. 304 с.
5. Физико-химические методы в производстве газотурбинных двигателей / Ю. С. Елисеев, В. В. Крылов, Б. П. Саушкин и др. ; под ред. Саушкина Б. П. М. : Форум, 2013. 456 с.
6. Справочник технолога-машиностроителя. В 2 т. Т. 2 / под ред. А. М. Дальского, А. Г. Сулова, А. Г. Косиловой, Р. К. Мещерякова. 5-е изд., испр. М. : Машиностроение, 2003. 944 с.
7. Теоретическое обоснование рациональных параметров режима электроконтактной обработки проволочным инструментом / М. Г. Киселев, А. В. Дроздов, А. В. Москаленко, П. С. Богдан // Вестник Гомельского гос. техн. ун-та им. П. О. Сухого. 2012. № 3. С. 3–11.
8. Орлов В. Ф., Чугунов Б. И. Электрохимическое формообразование. М. : Машиностроение, 1990. 240 с.
9. Справочник по электрофизическим и электрохимическим методам обработки / Г. Л. Ами-тан и др. ; под общ. ред. В. А. Волосатого Л. : Машиностроение, 1988. 719 с.
10. Житников В. П., Зайцев А. Н. Импульсная электрохимическая размерная обработка. М. : Машиностроение, 2008. 413 с.
11. Саушкин Б. П., Сычков Г. А., Атанасянц А. Г. Современное состояние и перспективы развития электрохимической размерной обработки // Металлообработка. 2002. № 6. С. 9–17.
12. Справочник по электрохимии / под ред. А. М. Сухотина. Л. : Химия, 1981. 488 с.
13. Совершенствование системы управления установки электрообработки металлов на базе линейного электродинамического двигателя / И. Я. Шестаков, В. И. Шестаков, А. А. Фадеев, Н. А. Швалева // Сибирский аэрокосмический журнал. 2021. Т. 22, № 3. С. 543–549.
14. Шестаков И. Я., Стрюк А. И., Цуканов А. В. Импульсная электро-обработка вибрирующим электродом-инструментом // Вестник СибГАУ. 2004. Вып. 5. С. 253–258.
15. Носуленко В. И. Размерная обработка металлов электрической дугой // Электронная обработка материалов. 2006. № 1. С. 1–10.
16. Саушкин Б. П. Электрический разряд в жидких и газовых средах основа нового поколения методов и технологий машиностроительного производства // Электронная обработка материалов. 2004. № 1. С. 1–14.

References

1. Verkhoturov A. D., Shpil'jov A. M., Evstigneev A. I. *Osnovy materialologii* [Fundamentals of Materialology]. Vol. 1. Vladivostok, Dal'nauka Publ., 2012, 270 p.
2. Nikolenko S. V., Verkhoturov A. D. *Novye elektrodnye materialy dlya elektroiskrovogo legirovaniya*. [New electrode materials for electric spark alloying]. Vladivostok, Dal'nauka Publ., 2005, 219 p.
3. Smolentsev E. V. *Proektirovanie elektricheskikh i kombinirovannykh metodov obrabotki*. [Design of electrical and combined processing methods]. Moscow, Mechanical Engineering Publ., 2005, 511 p.
4. Zubarev Yu., Priemyshev A. *Teoriya i praktika povysheniya effektivnosti shlifovaniya materialov* [Theory and practice of improving the efficiency of grinding materials]. Moscow, Lan Publ., 2010, 304 p.

5. Eliseev Ju. S., Krylov V. V., Saushkin B. P. *Fiziko-himicheskie metody v proizvodstve gazoturbinnykh dvigateley* [Physico-chemical methods in the production of gas turbine engines]. Moscow, Forum Publ., 2013, 456 p.
6. *Spravochnik tehnologa-mashinostroytelya* [Handbook of a mechanical engineer]. Moscow, Mashinostroyeniye Publ., 2003, 944 p.
7. Kiselev M. G., Drozdov A.V., Moskalenko A.V., Bogdan P. S. [Theoretical substantiation of rational parameters of the mode of electrocontact processing with a wire tool]. *Vestnik Gomel'skogo gos. tekhn. un-ta im. P. O. Sukhogo*. 2012, No. 3, P. 3–11 (In Russ.).
8. Orlov V. F., Chugunov B. I. *Elektrokhimicheskoe formoobrazovanie* [Electrochemical shaping]. Moscow, Mashinostroyeniye Publ., 1990, 240 p.
9. *Spravochnik po elektrofizicheskim i elektrokhimicheskim metodam obrabotki* [Handbook of electrophysical and electrochemical processing methods]. Moscow, Mashinostroyeniye Publ., 1988, 719 p.
10. Zhitnikov V. P., Zaitsev A. N. *Impul'snaya jelektrokhimicheskaja razmernaja obrabotka* [Pulsed electrochemical dimensional processing]. Moscow, Mashinostroyeniye Publ., 2008, 413 p.
11. Saushkin B. P., Suchkov G. A., Atanasyants A. G. [Current state and prospects of development of electrochemical dimensional processing]. *Metallobrabotka*. 2002, No. 6, P. 9–17 (In Russ.).
12. *Spravochnik po elektrokhimii* [Handbook of Electrochemistry]. Leningrad, Khimiya Publ., 1981, 488 p.
13. Shestakov I. Ya., Stryuk A. I., Bez'yazykov S. A. [Electrical treatment plant with linear electrodynamic motor]. *Siberian Aerospace Journal*. 2021, Vol. 22, No. 3, P. 543–549 (In Russ.).
14. Shestakov I. Ya., Stryuk A. I., Tsukanov A. V. [Impul'snaya elektroobrabotka vibriruyushchim elektrodom-instrumentom]. *Vestnik SibGAU*. 2004, No. 5, P. 253–258 (In Russ.).
15. Nosulenko V. I. [Dimensional processing of metals by electric arc]. *Elektronnaya obrabotka materialov*. 2006, No. 1, P. 1–10 (In Russ.).
16. Saushkin B.P. [Electric discharge in liquid and gas media is the basis of a new generation of methods and technologies of machine-building production]. *Elektronnaya obrabotka materialov*. 2004, No. 1, P. 1–14 (In Russ.).

© Shestakov I. Ya., Shestakov V. I., Trifanov I. V., Remizov I. A., 2023

Шестаков Иван Яковлевич – доктор технических наук, доцент, профессор кафедры электронной техники и телекоммуникаций; Сибирский государственный университет науки и технологий имени академика М. Ф. Решетнева. E-mail: yakovlevish@mail.ru.

Шестаков Владислав Иванович – аспирант кафедры технического регулирования и метрологии; Сибирский государственный университет науки и технологий имени академика М. Ф. Решетнева. E-mail: pn3vm4t@gmail.com.

Трифанов Иван Васильевич – доктор технических наук, профессор, заведующий кафедрой технического регулирования и метрологии; Сибирский государственный университет науки и технологий имени академика М. Ф. Решетнева. E-mail: sibgau-uks@mail.ru.

Ремизов Игорь Анатольевич – кандидат физико-математических наук, доцент кафедры технической механики; Сибирский федеральный университет. E-mail: 2remizov@mail.ru.

Shestakov Ivan Yakovlevich – Dr. Sc., Associate Professor, Professor of the Department of Electronic Engineering and Telecommunications; Reshetnev Siberian State University of Science and Technology. E-mail: yakovlevish@mail.ru.

Shestakov Vladislav Ivanovich – graduate student of the Department of Technical Regulation and Metrology; Reshetnev Siberian State University of Science and Technology. E-mail: pn3vm4t@gmail.com.

Trifanov Ivan Vasilievich – Dr. Sc., Professor, Head of the Department of Technical Regulation and Metrology; Reshetnev Siberian State University of Science and Technology. E-mail: sibgau-uks@mail.ru.

Remizov Igor Anatolyevich – Cand. Sc., associate professor of the department of technical mechanics; Siberian Federal University. E-mail: 2remizov@mail.ru.

ИНФОРМАЦИЯ ДЛЯ АВТОРОВ

ТРЕБОВАНИЯ К ОФОРМЛЕНИЮ СТАТЕЙ

Файлы со статьями принимаются по электронной почте vestnik@sibsau.ru.

Электронная копия. Статья набирается в программе Microsoft Office Word 2003 (**расширение имени файла DOC!**)

Объем статьи: 5–20 страниц (включая рисунки, таблицы и библиографические ссылки), краткое сообщение – 4–5 страниц, обзорная статья – до 20 страниц.

Параметры страницы. Формат А4 (210×297). Поля: правое и левое – 2 см, верхнее и нижнее – 2,5 см.

Текст. Шрифт Times New Roman 11. Подзаголовки: шрифт Times New Roman 11 bold.

Межстрочный интервал – одинарный, межбуквенный и междусловный интервал – нормальный, перенос слов не допускается.

Абзацный отступ равен 0,5 см.

Не допускается (!) набирать тексты прописными (заглавными) буквами и жирным шрифтом (кроме названия), а также размещать все указанные элементы в рамках и имитировать оформления набора, выполняемого в журнале.

Статья должна содержать предмет, тему, цель работы; метод или методологию проведения работы; результаты работы; область применения результатов; выводы.

Страницы не нумеруются.

СТРУКТУРА СТАТЬИ:

1) **Индекс УДК** предшествует названию статьи, соответствует заявленной теме и проставляется в верхнем левом углу листа.

2) **Название статьи:** не более 15 слов. Аббревиатуры и сокращения в названии не допускаются.

3) **Авторы.** Инициалы и фамилия. Количество авторов одной статьи не более пяти. Автор имеет право публиковаться в выпуске один раз, второй в соавторстве.

4) **Аффилиация автора при публикации:** название и адрес организации, а также электронная почта автора-корреспондента. Если авторов несколько, у каждой фамилии и соответствующей организации проставляется цифровой верхний индекс. Если все авторы статьи работают в одной организации, она указывается один раз;

5) **Аннотация:** минимум 230–250 слов (следует ориентироваться на объем англоязычной аннотации). Структура аннотации: цель исследования, методы, результаты, заключение. Курсивом.

6) **Ключевые слова:** не более 5–7 слов или словосочетаний. Курсивом.

7) **Название статьи** на английском языке.

8) **Авторы** на английском языке.

9) **Аффилиация автора** на английском языке.

10) **Аннотация** на английском языке.

11) **Ключевые слова** (Keywords) на английском языке.

12) **Основной текст** строится по следующей схеме и содержит обязательные подзаголовки:

– Введение

– Тематические подзаголовки по основной части текста.

– Заключение.

13) **Благодарности** (если есть указание на источники финансирования, гранты).

14) **Acknowledgements** (Благодарности дублируются на английском языке).

15) **Библиографические ссылки.** Библиографические ссылки должны содержать не менее 15 источников! Библиографические ссылки оформляются на русском языке по ГОСТ Р 7.0.5-2008. Ссылки на источники расставляются по тексту в квадратных скобках в порядке нумерации по мере цитирования.

16) **References.** Библиографические ссылки в романском алфавите оформляются по требованиям, представленным на сайте. Используется система транслитерации BGN (translit.net)

17) **Сведения об авторах на русском и английском языках.** сведения указывается ФИО автора, ученая степень, ученое звание, должность, название организации. Например:

Сенашов Сергей Иванович – доктор физико-математических наук, профессор, заведующий кафедрой ИЭС; Сибирский государственный университет науки и технологий имени академика М. Ф. Решетнева. E-mail: sen@sibsau.ru.

Senashov Sergei Ivanovich – Dr. Sc, Professor, Head of the Department of IES; Siberian State University of Science and Technology. E-mail: sen@sibsau.ru.

